# The twilight zone : how mixed-input bipolar cells process rod and cone signals

Joselevitch, C.

**Publication date**
2005
**Document Version**
Final published version

## The Author

Christina Joselevitch was born in São Paulo, Brazil, on February 24th, 1972. She graduated at the end of 1988 from the *Escola Americana e Colégio Mackenzie*, in São Paulo. After studying History for two years at the *Faculdade de Letras e Ciências Humanas* of the University of São Paulo (FFLCH-USP), she enrolled the Veterinary Medicine School (*Faculdade de Medicina Veterinária e Zootecnia,* FMVZ-USP) of the same University in 1992.

From early on, she started doing undergraduate research with the goldfish eye, moving from gross anatomy to histology, immunocytochemistry and electron microscopy, under the supervision of Dr. Arani Nanci Bomfim Mariana (FMVZ-USP), Dr. Wagner Intelizano (FMVZ-USP), and Dr. Ricardo L. Smith (*Escola Paulista de Medicina*, EPM-UFESP). All these studies were supported by personal grants from FAPESP (the Foundation for Research Support of the State of São Paulo).

Her last undergraduate project, regarding the study of the aqueous humor outflow in the eye of standard and Black Moor goldfish, won the first prize at the X Science Week of the FMVZ-USP in 1996. This gave her the opportunity to present her work abroad for the first time, at the ARVO Annual Meeting of 1997.

After graduating as a veterinarian in December 1996, she won a scholarship from the *Deutsche Forschungsgemeinschaft* for a two-month traineeship in neuroethological techniques at the University of Konstanz, under supervision of Dr. Juan Delius (*Allgemeine Fachgruppe Psychologie, Sozialwissenschäftliche Fakultät*).

She returned to São Paulo in March 1997 and started doing electrophysiological research in the goldfish retina at the Psychology Institute of the University of São Paulo (IP-USP, with Dr. Dora S. F. Ventura and Dr. John Manuel de Souza). This work was also funded by FAPESP, and enabled her to obtain her Master's Degree in Neurosciences and Behavior at the University of São Paulo in September 1999.

In October 1999 she started her Ph.D. project at the Netherlands Ophthalmic Research Institute (NORI), with a scholarship from CNPq (the National Research Council of Brazil) and complementary funding from the NORI. During this period she extended her expertise in retinal physiology, electrophysiological techniques and mathematical modeling under the supervision of Dr. Maarten Kamermans. The result of this work is presented in this thesis.

The Twilight Zone

Christina Joselevitch

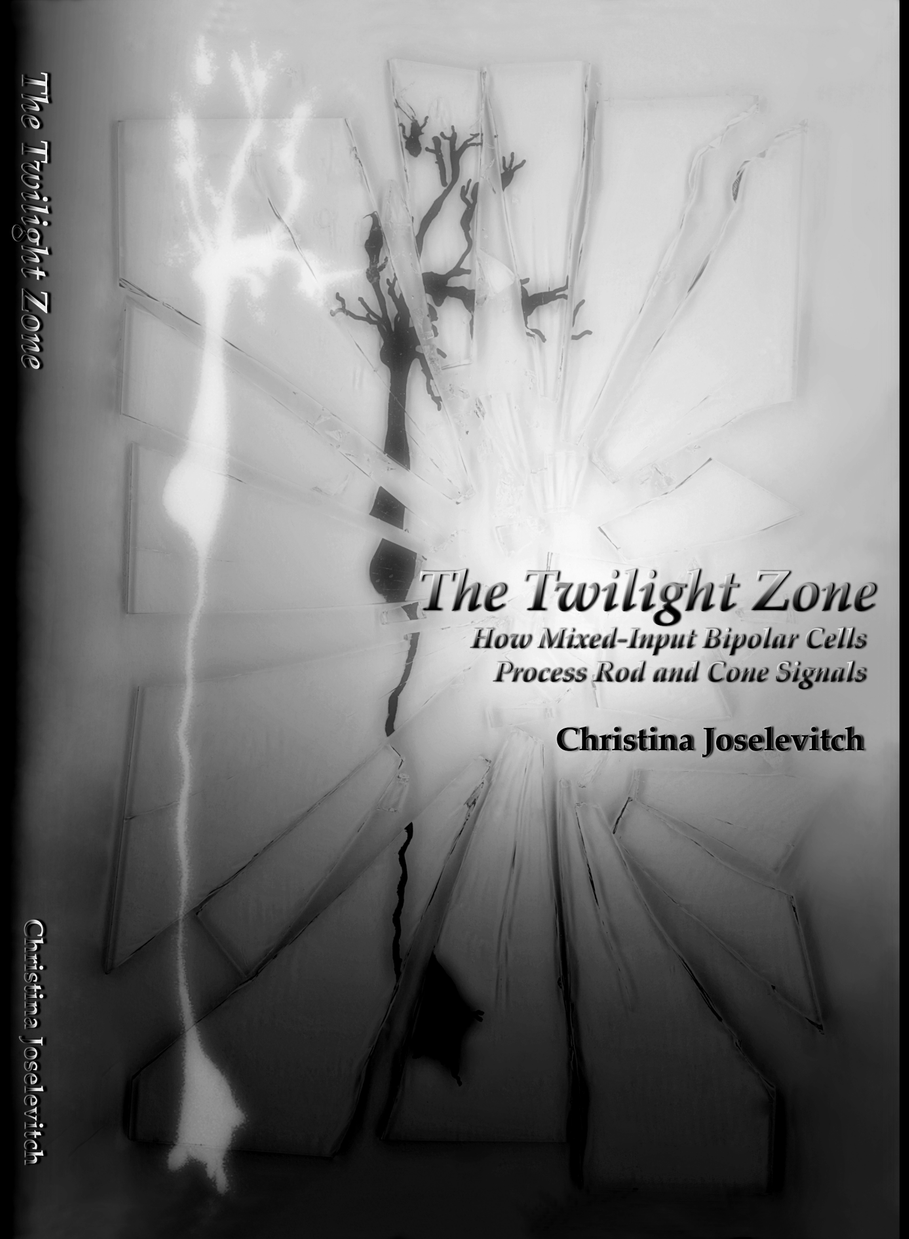

# The Twilight Zone

## How Mixed-Input Bipolar Cells Process Rod and Cone Signals

**Christina Joselevitch**

*You unlock this door*
*with the key of imagination.*
*Beyond it is another dimension —*
*a dimension of sound,*
*a dimension of sight,*
*a dimension of mind.*
*You're moving into a land*
*of both shadow and substance,*
*of things and ideas.*
*You've just crossed over*
*into the Twilight Zone.*

*Rod Serling*

# *The Twilight Zone*

*How Mixed-Input Bipolar Cells*
*Process Rod and Cone Signals*

ACADEMISCH PROEFSCHRIFT

Ter verkrijging van de graad van doctor
aan de Universiteit van Amsterdam,
op gezag van de Rector Magnificus prof. mr. P.F. van der Heijden,
ten overstaan van een door het college voor promoties ingestelde comissie,
in het openbaar te verdedigen in de Aula der Universiteit
(Oude Lutherse Kerk, ingang Singel 411, hoek Spui)

op dinsdag 11 oktober 2005, te 14:00 uur

door

Christina Joselevitch

geboren te São Paulo, Brazilië

## Promotiecommissie

| | |
|---|---|
| Promotor: | prof. dr. ir. Henk Spekreijse |
| Co-promotor: | dr. Maarten Kamermans |
| Overige leden: | dr. Willem Kamphuis<br>prof. dr. Fernando H. Lopes da Silva<br>prof. dr. Doekele G. Stavenga<br>prof. dr. Dora S. F. Ventura<br>prof. dr. Wytse J. Wadman |

Faculteit der Geneeskunde

The research described in this thesis was carried out in the Research Unit Retinal Signal Processing of the Netherlands Ophthalmic Research Institute from The Dutch Royal Academy of Arts and Sciences (KNAW), and was supported by the Conselho Nacional de Pesquisa (CNPq, Brazil), and by the KNAW.

Printed by Febodruk B.V.
ISBN-10: 9090198911
ISBN-13: 9789090198910

Cover: Carol Leticia Quaini Sousa

*In the particular*
*is contained*
*the universal*

*James Joyce*

# Contents

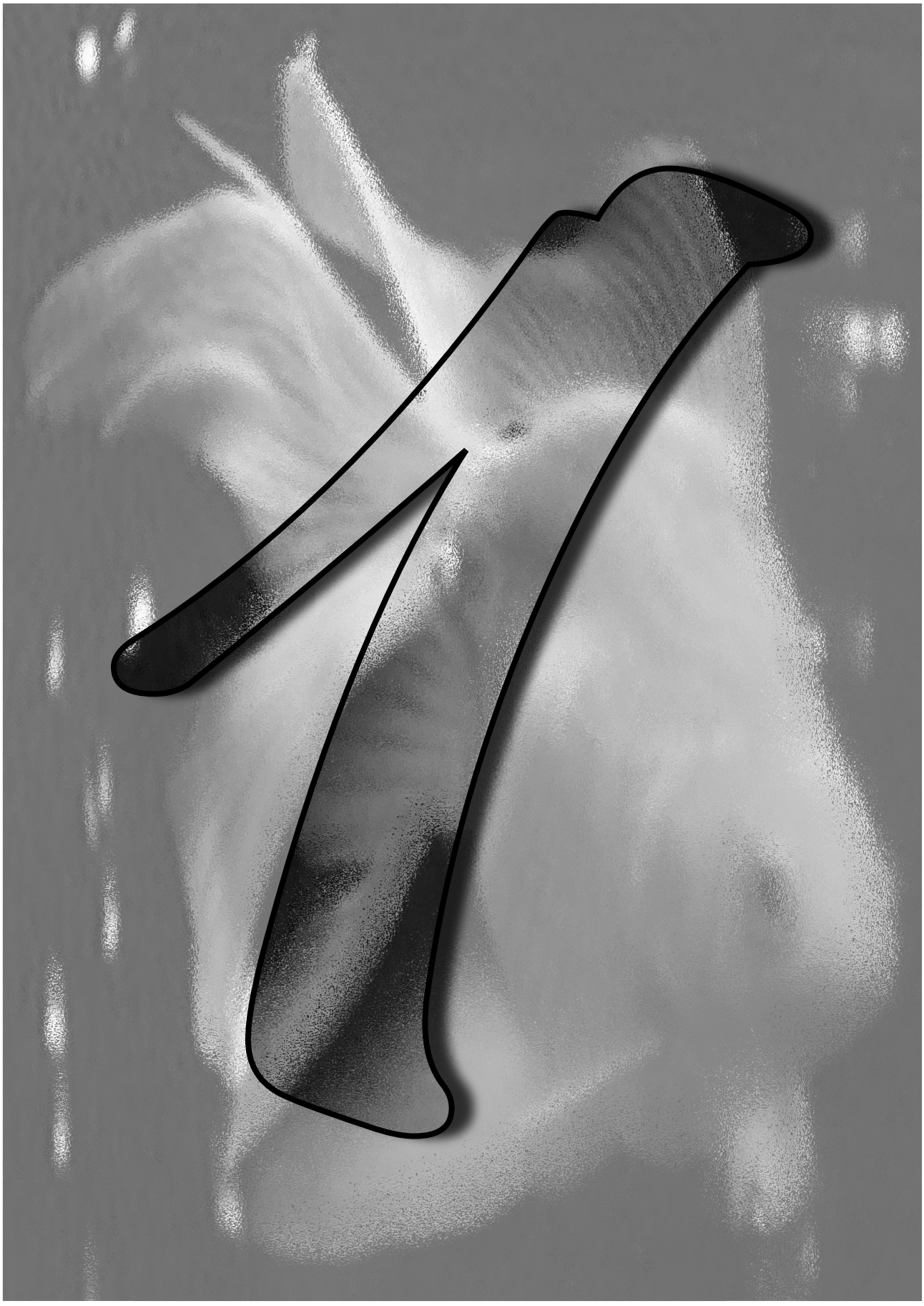

# Chapter 1

# General Introduction

This thesis is mainly concerned with how mixed-input bipolar cells gather and transmit photoreceptor signals to the forthcoming neurons. The first Chapter comprises a general overview of the retina and different bipolar cell types, with emphasis on the visual tasks mixed-input bipolar cells have to cope with. It also presents the questions addressed in the remaining Chapters of this thesis.

## 1.1 The Retina

The retina of the goldfish (*Carassius auratus*) is organized in a way that resembles closely that of higher vertebrates. It has a laminated structure, with nuclear layers that contain the cell bodies and interplexiform layers or neuropil, where the processes of these cells make contacts. As shown in Figure 1.1, there are three nuclear layers (outer nuclear layer or ONL, inner nuclear layer or INL, and ganglion cell layer or GCL) and two plexiform laminas (outer plexiform layer or OPL and inner plexiform layer or IPL).

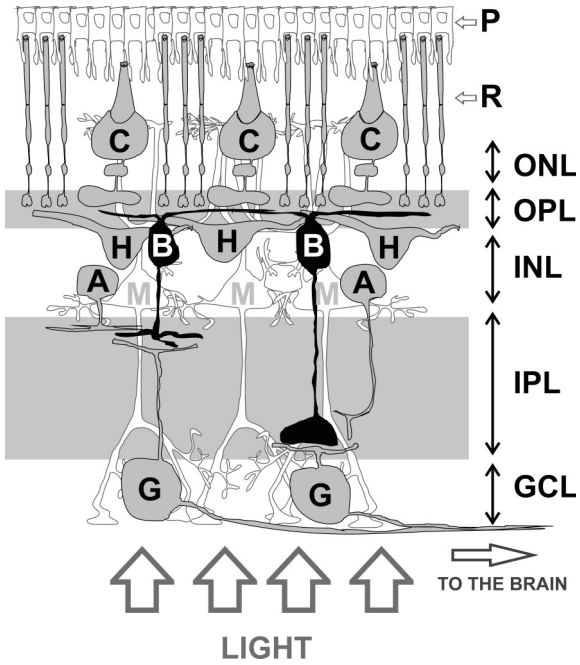


**Figure 1.1:** A schematic representation of the vertebrate retina. P: pigment epithelium; R: rod; C: cone; H: horizontal cell; B: bipolar cell; A: amacrine cell; G: ganglion cell; M: Müller cell. ONL: outer nuclear layer; OPL: outer plexiform layer; INL: inner nuclear layer; IPL: inner plexiform layer; GCL: ganglion cell layer. Light enters the eye from the ganglion cell side. Visual information is transmitted from the photoreceptor side and leaves the eye via the ganglion cell axons, which form the optic nerve.

The ONL contains the cell bodies of the photoreceptors, whose outer segments (their photosensitive part) are wrapped in a protective layer of pigmented epithelial cells. The somas of three types of retinal second-order neurons are localized in the INL: horizontal cells (HCs), bipolar cells (BCs), and amacrine cells (ACs). HCs and BCs contact the photoreceptors in arrangements called “triads” in the OPL (Figure 1.2); ACs, BCs and ganglion cells (GCs) make contacts called “diads” at different levels (also called *sublaminas*) of the IPL. Müller cells are glial elements that provide support for the neuronal structures and help removing neurotransmitter from the extracellular space (Dowling, 1987).

There are two main types of photosensitive transducers in the retina, rods and cones. They are classified as being different types of photoreceptors on morphological grounds: their outer segments differ in shape and in the way photosensitive pigments are packed within these segments. The kinds of photopigments and the phototransduction cascade are also distinct in rods and

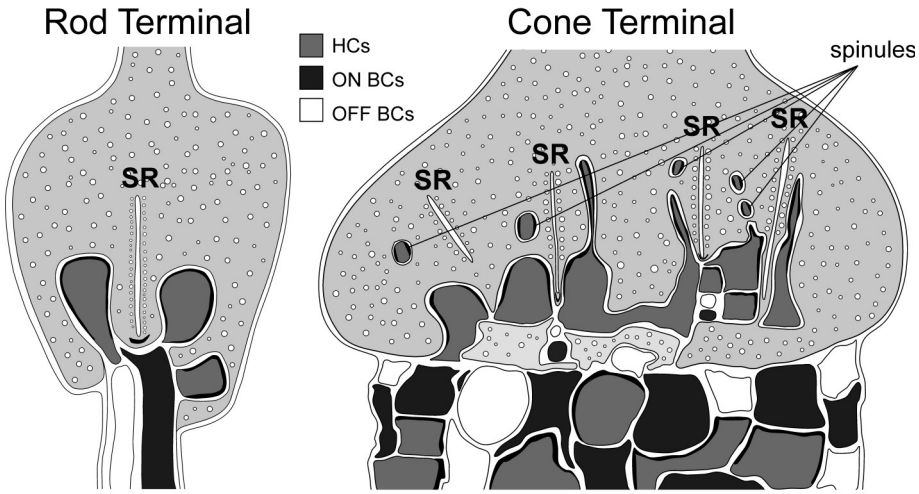


**Figure 1.2:** Triads. Left: at the rod spherule, three post-synaptic processes are arranged in the vicinity of the release site, the synaptic ribbon or ridge (SR); two lateral structures belonging to rod-driven horizontal cells (gray), and a central element belonging to an ON BC (dark gray). OFF BCs (white) also invaginate into the terminal, but do not directly contact the ribbon. Rather, they are found along ON BC processes, at some distance from the synaptic rigde. Right: at the cone pedicle, three post-synaptic elements surround each synaptic ribbon (SR). Either all of them belong to cone-driven HCs (gray), or only the lateral processes. In this case, the central element is the dendrite of an OFF BC (in white). ON BC dendrites (dark gray) are generally localized directly beneath OFF BC processes. Outside the pedicle, dendrites of HCs, ON and OFF BCs are also found. HC and BC processes can be distinguished from each other based on ultrastructural features: in EM pictures, the cytoplasm of HCs is light in appearance and has some electrondense vesicles, and there is accumulation of electrondense material (also called “fussy undercoating”) right under the cell membrane. BC processes tend to be thinner, darker, and richer in cytoplasmic vesicles. In the light-adapted retina, fish HC dendrites send expansions into the cone pedicles called spinules. Drawing modified from Klooster et al. (2004), after descriptions from Stell (1976), Saito et al. (1983/1985) and Weiler and Wagner (1984).

cones. Altogether, these differences have a number of consequences for visual function, the most important being sensitivity: rods are considerably more sensitive to light than cones (for a review, see Pugh and Lamb, 1990 and Ebrey and Koutalos, 2001).

In addition to light sensitivity, rods and cones also differ in their responses to monochromatic stimuli (Figure 1.3). Goldfish rods have their maximal sensitivity around 520 nm (Tsin et al., 1981; Mooij and Van den Berg, 1983), whereas cones are divided in four distinct types according to the wavelength of peak absorption ($\lambda_{max}$): UV-sensitive cones, ($\lambda_{max}$ = 360 nm), short wavelength-sensitive cones (S-cones, $\lambda_{max}$ = 450 nm), middle wavelength-sensitive cones (M-cones, $\lambda_{max}$ = 530 nm), and long wavelength-sensitive cones (L-cones, $\lambda_{max}$ = 625 nm) (Harosi and MacNichol, 1974; Harosi, 1976; Stell and Harosi, 1976; Tsin et al., 1981; Palacios et al., 1998).

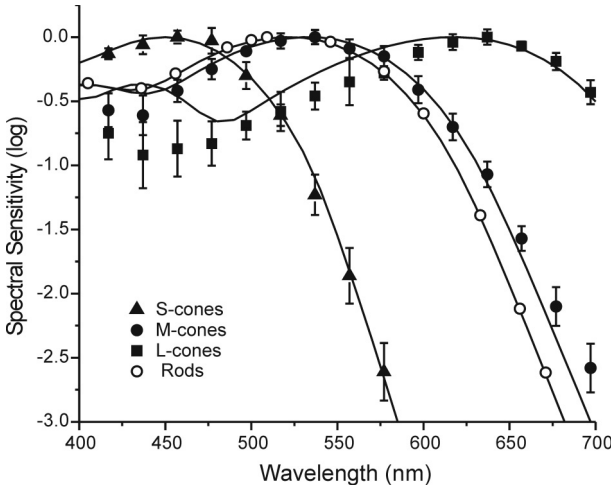


**Figure 1.3:** Spectral sensitivity of the goldfish photoreceptors. Cone data points replotted after Palacios et al. (1998); rod data points and fits after Mooij and Van den Berg (1983). UV cones were omitted.

The dynamic range of a photoreceptor can be determined as a function of photon capture rates (for continuous illumination) or flash intensities. Whatever the measurement applied, although there is a very big difference in the absolute threshold of the different kinds of photoreceptors, the dynamic ranges of both rods and cones are about 2 log units (Baylor and Fuortes, 1970; Grabowski et al., 1972; Schneeweis and Schnapf, 1995) and overlap in great part (Figure 1.4).

After light is captured at the photoreceptor outer segments, it is transformed into electrical signals that are in turn transmitted to the forthcoming neurons via a change in the rate of neurotransmitter (glutamate) released by the photoreceptors. It is this modulation of the glutamate concentration in the OPL that is sensed by glutamate receptors on BC and HC dendrites (Murakami et al., 1972; Cervetto and MacNichol, 1972; Kaneko and Shimazaki, 1976).

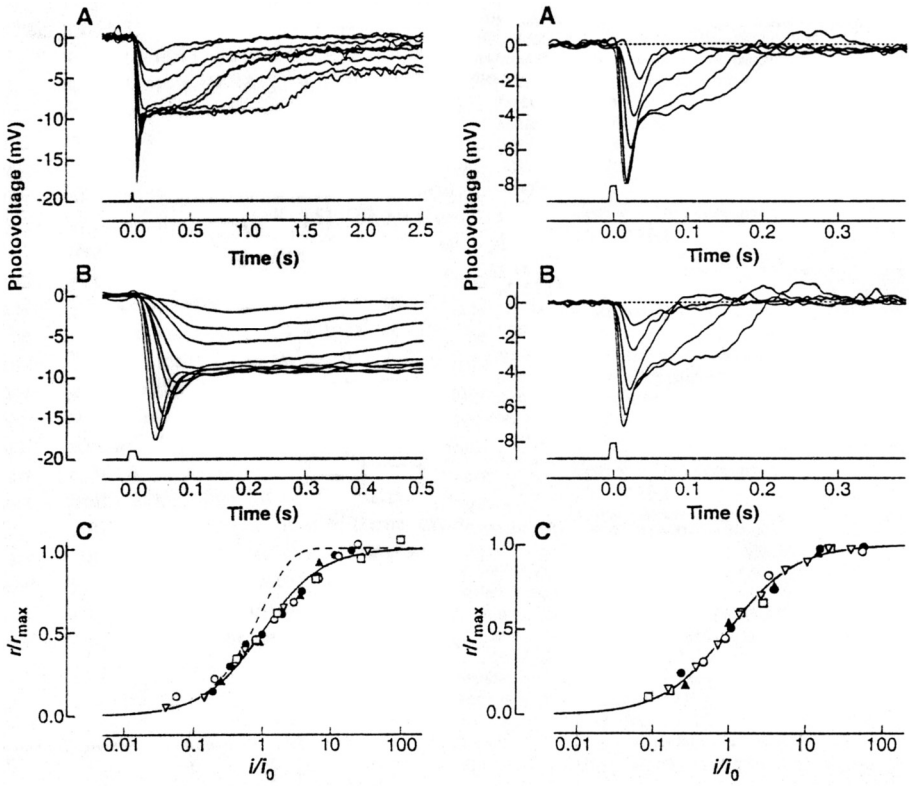


**Figure 1.4:** Photoreceptor dynamic range. Examples of light responses of a rod of the macaque monkey retina to 500 nm stimulation on two time scales (left, A and B) and of a red cone of the macaque monkey retina to stimulation at 500 or 660 nm (right, A and B) at increasing intensities. In C, the intensity-response relations of 5 rods (left) and 5 cones (right) are fitted with a Hill function (solid lines). Although there are differences in their response dynamics, amplitude and waveform, both photoreceptor types have a similar dynamic range: their light responses follow a sigmoidal function and saturate after about 2 log units. After Schneeweis and Schnapf (1995).

The laminated organization of the retina generates two streams of visual information: a main or vertical flow, from the photoreceptors to BCs and from BCs to GCs, and a secondary lateral flow, comprising local feedback circuits from HCs back to photoreceptors (Stell et al., 1975; Byzov et al., 1977; Kamermans et al., 2001), and from ACs back to BCs (Kaneko and Tachibana, 1987; Tachibana and Kaneko, 1987; Yazulla et al., 1987). These lateral circuits adjust the gain of the pre-synaptic cells, in order to optimize signal transmission.

Until visual information reaches GCs and leaves the eye, a number of calculations has already taken place in both plexiform layers. Since BCs form the connection between the outer and the inner retina, they are the ideal place to study the steps in information coding that precede inner retinal processing. By studying

the transformations the photoreceptor signals undergo at the BC level, one can understand how GC responses (and ultimately the output of the retina to the brain) are generated.

## 1.2 Bipolar Cells

Photoreceptors, HCs and BCs respond to light with sustained, graded membrane potential changes (Figure 1.5). This may be so because these neurons have short processes and do not need to transmit information over long distances: passive spread of potential along the cell membrane is enough for information to be transmitted from one end of the cell to the other. A second possible reason could be that such graded potentials are capable of discriminating a wider range of signals than all-or-none action potentials (Dowling, 1987). The first action potentials observed in the retina are those generated by ACs followed by GCs.

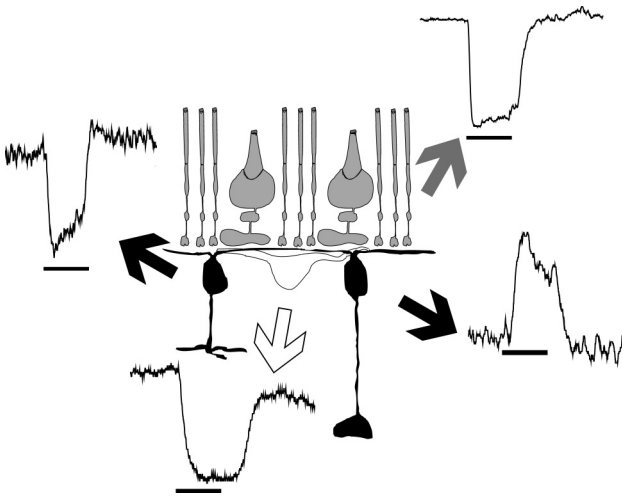

**Figure 1.5:** Outer retinal neurons respond to light with sustained membrane potential changes. Examples of light responses of a goldfish cone (top right), an ON BC (bottom right), a cone-driven monophasic HC (bottom) and an OFF BC (left) are depicted.

Although photoreceptors only hyperpolarize to light stimulation, at the BC level this signal is split into two main streams of information: one BC type hyperpolarizes when small white spots are presented in the center of its receptive field and another one depolarizes under same stimulus conditions. The former are called *hyperpolarizing* or *OFF BCs*, and the latter are called *depolarizing* or *ON BCs* (Kaneko and Hashimoto, 1969; Werblin and Dowling, 1969; Kaneko, 1970).

The receptive fields of these cells are concentrically arranged into antagonistic zones (Figure 1.6): illumination of the surround decreases or fully antagonizes the response to illumination at the center of the receptive field (Kaneko, 1973; Werblin, 1974). While the center is a result of direct photoreceptor input, the

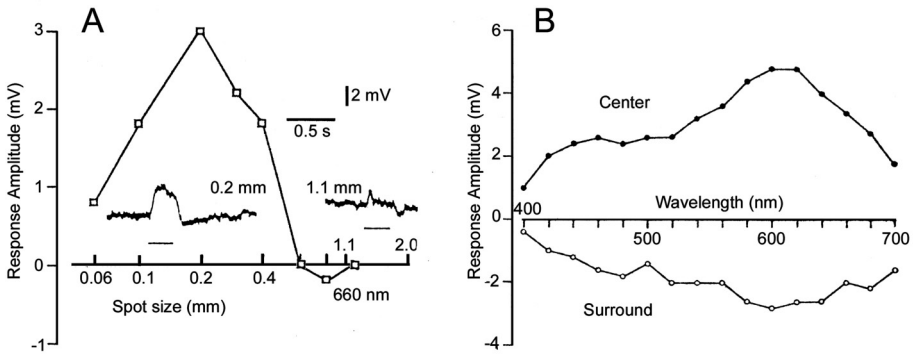


**Figure 1.6:** Center-surround organization of BC receptive fields. A: Spatial summation curve. Upon stimulation with light spots of increasing sizes, BC light response amplitudes initially increase. The size of their receptive field center is considered equivalent to the stimulus diameter that elicits the largest response (in this case, 0.2 mm). If the size of the stimulus is increased beyond this diameter, the amplitudes decrease due to concomitant activation of the inhibitory surround (compare 0.2 mm and 1.1 mm). B: Spectral response curves. Response amplitudes of the same ON BC to a small spot of light (which activates only the center of its receptive field), and to a light annulus (which solely stimulates the surround) at different wavelengths. Although both center and surround-mediated responses are most sensitive to light around 600 nm, their response polarity is not the same. Source: Kaneko, 1973.

surround is presumably generated by the feedback system between HCs (that spatially integrate over the almost the whole retina) and photoreceptors (Werblin, 1974; Marchiafava, 1978; Toyoda and Tonosaki, 1978).

There seems to be some correlation between the polarity of the BC light responses to white light and the position of its dendrites in the triads (Figure 1.2), as well as the stratification level of its axon terminal at the IPL (Figure 1.7). The axons of OFF BCs terminate in the most distal stratum (*sublamina a*), whereas those of ON BCs terminate more proximally, in the so-callled *sublamina b* (Famiglietti and Kolb, 1976; Famiglietti et al., 1977). Differences in the synaptic contacts made between the dendrites of ON- and OFF BCs and photoreceptors at the OPL were also reported (Stell et al., 1977; Stell, 1978; Ishida et al., 1980; Stell, 1980), although this classification does not seem to hold strictly (Saito et al., 1983; Saito et al., 1985; Calkins et al., 1996; Hopkins and Boycott, 1997).

In the goldfish retina, at least 15 different types of morphologically distinct BCs (depicted in Figure 1.8) have been described (Sherry and Yazulla, 1993). These morphological types are arranged in two major classes: mixed input cells that receive both rod and cone inputs (6 types), and cone-driven BCs (9 types) that receive inputs exclusively from cones. Mixed input BC axon terminals stratify roughly at one of the two main sublaminas, whereas some cone-driven BCs present, in addition, characteristic patterns of multilaminar spread of terminals in the IPL. BCs with terminations in both sublaminas of the IPL were also identified in other species (Scholes and Morris, 1973; Scholes, 1975; Mariani, 1983; Wu et al., 2000; Connaughton and Nelson, 2000), but their response properties have not been thoroughly investigated.

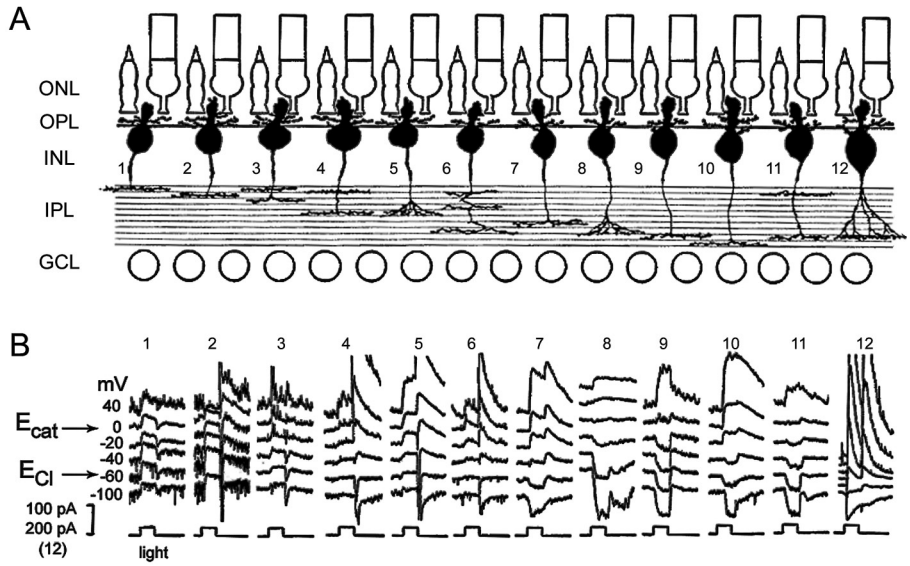


**Figure 1.7:** BC stratification patterns at the IPL. A) Morphology of 12 different BC types of the salamander retina, classified according to the level of the IPL in which their axons terminate. Cells were injected with Lucifer Yellow after patch-clamp recordings in the retinal slice preparation and sketched by hand. B) Light-evoked current responses of these cells to a 500 nm stimulus. The polarity of the light responses is correlated to the stratification pattern: OFF BCs comprise cells terminating at the first (distal) half of the IPL (BCs 1 to 6), and ON BCs include cells terminating at the second (proximal) half of the IPL (BCs 7 to 12). After Wu et al. (2000).

Unfortunately, there is still no strict correlation between the morphological and physiological BC types of the teleost retina. Most of what we know in terms of BC physiology comes from experiments in which the morphology of the cells recorded from was not known. Therefore it is hard to say how photoreceptors and HCs shape BC responses and how these might give rise to AC and GC responses, which also have center-surround organization (Daw, 1968; Beauchamp and Daw, 1972; Daw and Beauchamp, 1972; Raynauld, 1972).

Since the retinal slice preparation enables one to visually choose the cells to record from, we limited our studies to one class of BC of the goldfish retina, namely the mixed-input BCs. In the next sections the main characteristics of these cells and the tasks they have to perform will be addressed.

### 1.3 Mixed-Input Bipolar Cells

As previously mentioned, mixed-input BCs receive input from both rods and cones, and can be roughly divided in ON- and OFF-types according to their stratification pattern, although spectral opponency was also reported to be present in these cells

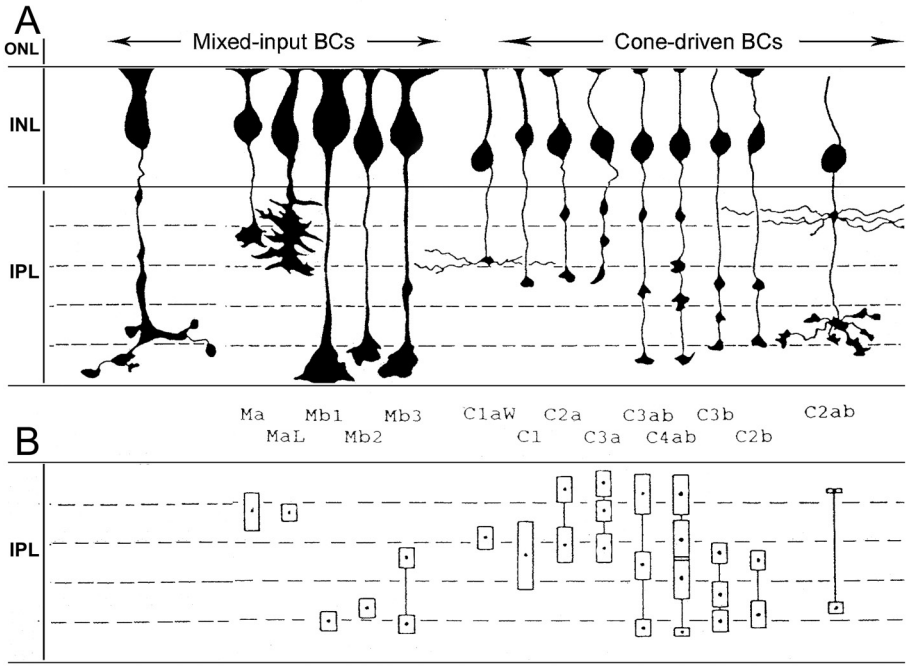


**Figure 1.8:** Goldfish BC types. A) Schematic drawing of Golgi-impregnated material. The 5 large BCs to the left are mixed-input BCs; the 9 small types are exclusively cone-driven. B) Summary of the stratification pattern at the IPL and nomenclature of the 15 types illustrated in A. The mean terminal midpoint is represented by a dot and the standard deviation by the height of the box around the dot. The first cell in A has no representation in B because it was seen only once. Ma: mixed-input BC terminating in the sublamina a; Mb: mixed-input BC terminating in sublamina b; Ca: cone-driven BC terminating in sublamina a; Cb: cone-driven BC terminating in sublamina b; Cab: multistratified cone-driven BC. After Sherry & Yazulla (1993).

(Shimbo et al., 2000). Their spectral coding seems to originate in selective contacts with different spectral types of cones at the OPL: in the goldfish, some mixed-input BCs (mb1, both ON- and OFF types) contact rods and L-cones and others (mb2 and mb3, also ON- and OFF types) contact in addition M-cones (Stell, 1978/1980; Ishida et al., 1980).

Mixed-input BCs were originally identified morphologically in the teleost retina (Stell, 1967; Scholes, 1975; Stell, 1976/1978; Ishida et al., 1980), but reports of BCs contacting both rods and cones in mammalian species appeared in the literature recently (Hack et al., 1999; Fyk-Kolodziej et al., 2003; Li et al., 2004).

The scarcity of physiological data on fish and mammalian BCs reflects mostly the difficulty in recording from these cells, and not their abundance. Independently from being either a peculiarity of the fish visual system or a more general characteristic of the vertebrate retina, mixed-input BCs have a very complex task to perform: the integration of rod- and cone-driven signals.

Although this might sound simple, such a function involves a number of unsolved issues, such as segregation of the photoreceptor signals into ON- and OFF pathways, chromatic processing, light-dark adaptation, spatial integration and receptive field formation. Even their glutamate receptor makeup (which allows them to tackle these jobs) is to a large extent unknown. Some of the issues dealt with during our studies will be introduced below, and discussed in more depth in the remaining Chapters of this thesis.

### 1.4 The ON and OFF Pathways

The dualistic idea of ON- and OFF- pathways started with the observation that optic nerve units of the frog, when recorded extracellularly, responded to light with either an increase or a decrease in basal activity (Hartline, 1938). These responses were then called ON- and OFF-types, respectively. Later, Kaneko and Hashimoto (1969) and Werblin and Dowling (1969) recorded intracellularly from inner retinal neurons in the mudpuppy and carp and found that ON and OFF response types were already present in the outer retina.

Subsequently, Kolb and Famiglietti (1976) and Famiglietti et al. (1977) injected intracellularly recorded neurons of the cat and goldfish with a fluorescent dye and realized that ON and OFF neurons terminated in different sublaminas of the inner plexiform layer. OFF cells would terminate in the most distal stratum (sublamina a), whereas ON cells would have their axons in the most proximal inner plexiform layer (sublamina b). This relation seemed to hold not only for sustained responding neurons, but also for GCs. In the primate, the ON and OFF channels supposedly remain largely segregated in the geniculostriate system until they reach the cortex, where they converge upon single cells (Schiller, 1992).

However, the existence of BCs with multilaminar axonal terminations, as already discussed, is an indication that the classification of retinal neurons into ON and OFF types is somewhat inexact. This scheme also bypasses spectral coding. In addition to ON and OFF response types, cells with wavelength-dependent responses (that is, ON responses to short wavelengths and OFF responses to long wavelengths and vice-versa) were described in the retina LGN (Wiesel and Hubel, 1966) and in areas of the visual cortex (for a review, see Gegenfurtner, 2001).

These spectral opponent responses are however not a privilege of higher brain areas: when stimulated with monochromatic lights, BCs of the teleost retina present a complex range of responses, which can be summarized as follows (Figure 1.9): 1) non-spectrally coded cells – center and surround responses have the same sensitivity peak (Sakakibara and Mitarai, 1982); 2) spectrally opponent cells - center and surround responses have either different sensitivity peaks (Kaneko, 1973) or there is spectral opponency in one of the components of the receptive field (Sakakibara and Mitarai, 1982); 3) double-opponent cells – center and surround

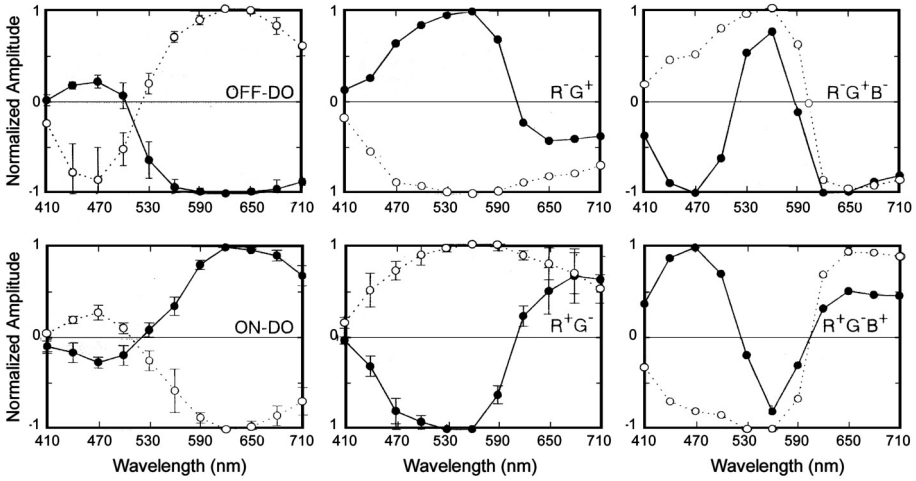


**Figure 1.9:** Spectrally opponent mixed-input BCs of the carp retina. Spectral curves of 6 types of opponent mixed-input BCs to stimulation with a small spot (dark symbols) or with an annulus (open symbols) of different wavelengths under diffuse background illumination. In these cells, center and surround responses do not have the same spectral sensitivity, and in some cases the surround is also spectrally opponent. Upper row: cells with hyperpolarizing (OFF) center responses to long wavelength stimuli. Bottom row: cells with depolarizing (ON) center responses to long wavelength stimulation. OFF-DO: double-opponent (OFF type); $R^-G^+$: hyperpolarizing to red light, depolarizing to green light; $R^-G^+B^-$: hyperpolarizing to red and blue lights, depolarizing to green light; ON-DO: double-opponent (ON type); $R^+G^-$: depolarizing to red light, hyperpolarizing to green light; $R^+G^-B^+$: depolarizing to red and blue lights, hyperpolarizing to green light. After Shimbo et al. (2000).

responses are spectrally coded (Kaneko and Tachibana, 1981/1983; Shimbo et al., 2000).

There is some indication that most of the spectrally opponent BCs of the fish retina (the types 2 and 3 of the previous paragraph) are light-adapted mixed-input BCs (Shimbo et al., 2000). These cells, when stimulated solely by rods, respond to light with either ON or OFF responses (Saito et al., 1979; Saito and Kaneko, 1983; Shimbo et al., 2000). Upon light adaptation, their response patterns change dramatically (Saito et al., 1979; Shimbo et al., 2000). This means that, under different adaptive conditions, mixed-input BCs might perform different tasks.

## 1.5 Chromatic Processing

A second dichotomy largely spread in literature is that there are separate, parallel retinal channels for the processing of “brightness” and “color” (for a review, see Calkins and Sterling, 1999 and Calkins, 2004). The ON- and OFF pathways would be part of a “broadband” channel, and spectrally coded cells would form a second channel devoted exclusively to the processing of color information (Schiller et al.,

1990a/b; Schiller, 1991). Before we go on examining this idea, it is important here to make a distinction between “color” and “wavelength”: color is a psychophysical term that describes a *sensation*; wavelength is a physical property of light.

The color of an object depends strongly upon the emitted/reflected spectral light distribution. The fact that we reliably use different names for certain sets of colors necessarily means that we can discriminate between them. However, the converse is not true. That is, there are many sets of wavelengths that are easily discriminable to the normal human observer, but which are given the same color name (lights of 530 and 550 nm are both called “green”). In other words, we do not have a distinct name for each discriminable set of wavelengths.

A primary question of interest to vision researchers relates to the underlying discriminations among wavelengths, and how those discriminations are made. Without such discriminations, different color names could not reliably be used to describe different wavelengths and mixture of wavelengths. Therefore, *wavelength discrimination underlies color vision*. And although color vision involves processing in higher brain areas, wavelength discrimination starts in the retina (Cornsweet, 1970).

A photoreceptor is per se “color blind”, that is, it hyperpolarizes to light of all wavelengths. It is the convergence of the activity of different photoreceptor types at some point in the visual system that leads to wavelength discrimination and color perception. Since this convergence happens already at the photoreceptor-BC synapse, it is expected that BCs carry information about color. The question arising next is whether the spectral opponency found in fish mixed-input BCs have chromatic processing as their main goal.

The idea of opponent or antagonistic processes as the basic physiological substrate of our ability to perceive colors was originally developed by Hering (1964). According to this theory, color channels are organized in an opponent way: red/green, blue/yellow and white/black (Hurvich and Jameson, 1957). A basic premise of this notion is that the members of an opponent pair of colors are mutually exclusive. Red and green on one hand and blue and yellow on the other hand are never seen simultaneously in the same place at the same time in a color. The psychophysical cancellation experiments are based on this premise (Hurvich, 1985).

At the retinal level, therefore, one expects that spectrally opponent neurons carry at least some information about the spectral properties (i.e. wavelength composition) of the visual scene. However, the fact that lower vertebrates possess spectrally opponent neurons whose response properties resemble the human opponent process (such as some BCs in Figure 1.9 and the cone-driven HCs in Figure 1.10) does not mean that color vision in these species is *per se* an opponent process. Despite the abundance of studies about spectral sensitivity (Yager, 1967/1968/1969; Beauchamp et al., 1979; Neumeyer, 1984/1985; Hawryshyn and Beauchamp, 1985; Neumeyer, 1986) and wavelength discrimination in the goldfish (Neumeyer and Arnold, 1989; Hawryshyn, 1991; Fratzer et al., 1994), to date there is

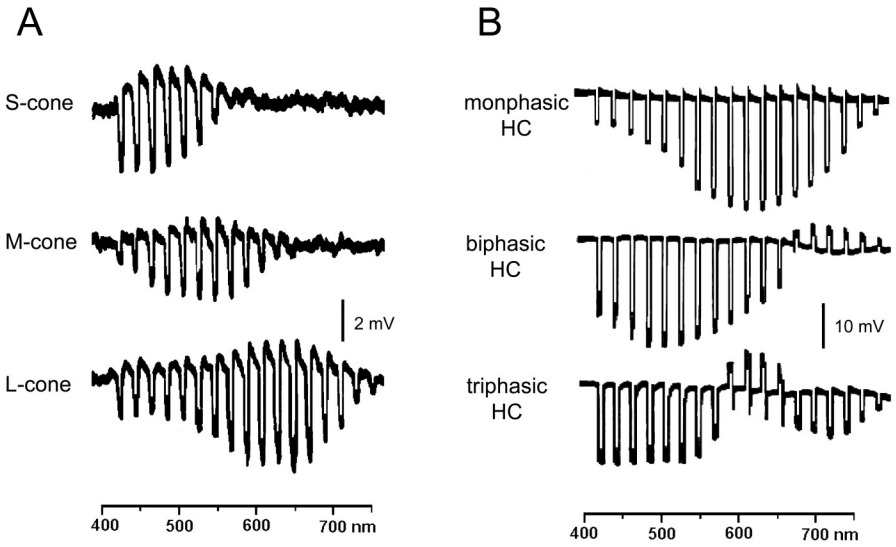


**Figure 1.10:** Coding strategies of second-order neurons in the fish retina. Although the different spectral types of cones only hyperpolarize to light of all wavelengths, some cone-driven HCs hyperpolarize to certain wavelengths and depolarize to others. A) Light responses of an S-cone (upper row), and M-cone (middle row) and an L-cone (bottom row) from the carp, *Cyprinus carpio.* Source: Kaneko, 1971. B) Light responses of a monophasic (upper row), biphasic (middle row), and a triphasic (bottom row) cone-driven HC of the goldfish, *Carassius auratus*. Source: Kaneko (1987).

no data available on color categorization for fish, that is, which are the “pure” colors they see and how fish color channels are organized.

One hopes that it is possible to draw analogies between color vision among species, and therefore the goldfish and related cyprinids as the carp have been widely used as animal models for color vision experiments. But it is still to be shown what role each sort of spectrally opponent neuron plays in the color processing of these species and if this role also holds for human color perception.

The emerging picture in literature is that spectrally coded neurons do not have a unique role in the transmission of chromatic information, but in the simultaneous codification of many aspects of the visual world (Schiller, 1996; Gegenfurtner and Kiper, 2003). The spectral coding of some cone-driven HCs of the fish retina (reviewed in Kamermans and Spekreijse, 1995 and shown in Figure 1.10), for instance, seems to be a strategy to avoid redundancy (Buchsbaum and Gottschalk, 1983).

As for fish mixed-input BCs, some authors ascribed to the double-opponent BCs a role in simultaneous color contrast (Kaneko and Tachibana, 1981/1983; Kolb and Lipetz, 1991; Dorr and Neumeyer, 1997). It seems however more likely that these cells use the same coding tactics as cone-driven HCs to transmit information to the inner retina without at this stage making a distinction about the kind of information being transmitted.

To which extent their spectrally opponent responses reflect a mechanism for chromatic processing is still to be determined. Further, how the interactions between rods and cones shape these responses, which glutamate receptors underlie their spectral coding and which tasks these cells perform in the light and dark-adapted retina remain for a large part unknown.

## 1.6 Light-Dark Adaptation

The third duality in vision research relates to the rod- and cone-driven pathways. Although our visual world at one particular moment of the day presents us with only about one log unit in contrast, during the whole day our light environment changes in range with a magnitude of 9 to 10 log units (Rodieck, 1998). In order to deal with such a huge range of light intensities, the visual system has developed rods and cones.

The first researcher to come up with this idea Schultze (1866). By comparing retinas of nocturnal and diurnal animals he observed that the former had more rods. Since nocturnal animals have to cope with dimmer visual environments, he realized that rods should then subserve vision at low light levels, the cones being responsible for vision at high intensities.

Visual function was then divided in “scotopic” (from the Greek “*scotos*”, dark) and “photopic” (from the Greek “*photos*”, light) systems, and Schultze’s theory was named the *duplex theory of vision*. This theory (whose main features are presented in Table 1.1 and discussed subsequently in the text) has been proven correct by a number of psychophysical, morphological, biochemical and electrophysiological experiments, and retinas containing both rods and cones are still referred to as “duplex retinas”.

According to the duplex theory of vision, rods and cones should be active in different intensity ranges (darkness or “scotopic range” for rods, light or “photopic range” for cones), as one would expect from their absolute sensitivity thresholds,

| Feature | Scotopic Vision | Photopic Vision |
|---|---|---|
| *Photic environment* | Dark | Light |
| *Photoreceptor type* | Rods | Cones |
| *Spectral sensitivity* | ~ 500 nm | Shifts to longer λ |
| *Absolute sensitivity* | High | Low |
| *Speed of response* | Slow | Fast |
| *Visual acuity* | Low | High |
| *Rate of dark adaptation* | Slow | Fast |
| *Saturation (photochemical adaptation)* | Yes | Little |
| *Cellular adaptation* | Little | Yes |
| *Visual pigment* | “Rod-like” | “Cone-like” |
| *Wavelength discrimination* | No | Yes |

**Table 1.1:** Characteristics of photopic and scotopic systems. After Ebrey and Koutalos (2001).

and that the overlap between their dynamic ranges (the so-called “mesopic range”) should be minimal.

When the retina light adapts, a transition from rod-dominated to cone-dominated vision takes place. This transition was documented both psychophysically and electrophysiologically. As light intensity (or ambient illumination) is increased, one observes the so-called “Purkinje shift” (Figure 1.11): under photopic conditions, the human spectral sensitivity function peaks at longer wavelengths, reflecting the combined activity of the different cone types (Purkinje, 1825).

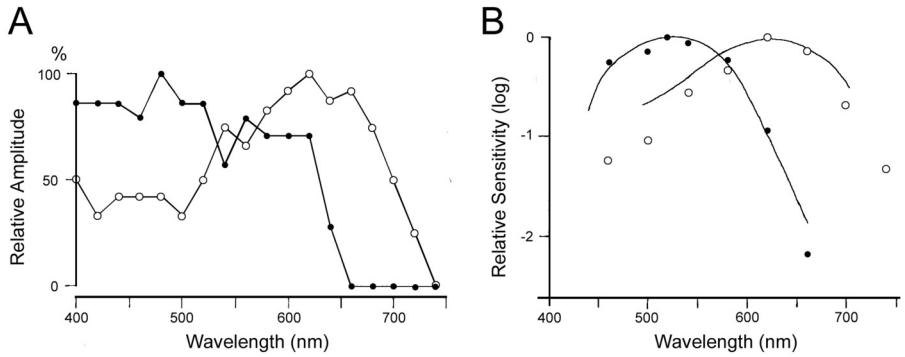


**Figure 1.11:** Purkinje shift. A) Spectral responses of an OFF BC of the carp to a small stimulus in the dark-adapted retina (dark symbols) and 15 minutes after switching on a diffuse white background illumination to light-adapt the retina (open symbols). The sensitivity of the cell shifted towards longer wavelengths as the retina light-adapted. B) Spectral sensitivity plot of an ON BC in the dark-adapted (dark symbols) and light-adapted conditions (open symbols). The solid lines are the absorption spectra of the rods and L-cones. The agreement between the data points and the photoreceptor curves indicates that the spectral sensitivity of this cell shifted from rod-dominated to cone-dominated as the background light was switched on. Source: Kaneko & Tachibana (1978).

The first to record such a Purkinje shift in retinal neurons were Barlow et al. (1957). Later on, both Beauchamp and Daw (1972) and Raynauld (1972), when measuring from goldfish optic nerve fibers in different adaptive states noticed that, although the receptive field arrangement of those GCs remains the same in the dark- and light- adapted retinas (i.e. the sizes of receptive field center and surround), their spectral sensitivity does not. Namely, cells that are in the dark-adapted retina “green ON” become “red ON/green OFF” in photopic conditions. The same holds for “green OFF” cells: in the light-adapted retina, they become “red OFF/green ON”.

An important result of those pioneer experiments that would influence the thinking about rod and cone convergence up to our days is that in the course of light- and dark-adaptation *rods and L-cones seem to share the same retinal pathways*. In order to investigate at which retinal level this convergence takes place, Kaneko and Tachibana (1978) recorded intracellularly from mixed-input BCs in the carp retina and realized that this Purkinje shift already happens at the BC level (Figure

1.11). Again, the response polarities to inputs from rods and L-cones had the same polarity, in both ON- and OFF- BCs. Similar results were also reported by Saito et al. (1978).

But what do the terms “light-adapted” and “dark-adapted” mean? These expressions were created in the early stages of visual research after the observation that the visual system behaves differently after prolonged exposure to light or darkness. It is a common experience to be almost blind when first entering a movie theater, but to be able to see quite a lot after 5 or 10 minutes. This phenomenon is dark adaptation.

This is possible in part because the photon catching ability of the photoreceptors is varied through bleaching and regeneration of the photopigment in the photoreceptor outer segment, allowing vision to adapt to large variations in illumination. Dark adaptation has predominantly been studied by determining the threshold for vision at increasing time in the dark after shutting off a pre-adaptation light, which supposedly bleaches all the photopigment available (Figure 1.12).

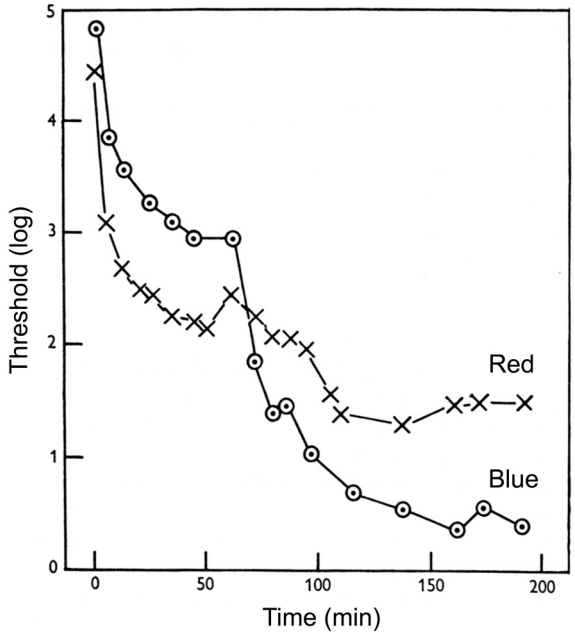


**Figure 1.12:** Dark-adaptation curve. Thresholds from a cat ON GC for a blue and for a red stimulus were measured after 30 minutes of light adaptation. With increasing time in darkness, thresholds decrease, that is, the eye becomes more sensitive to light. During the first hour in darkness, vision is cone-dominated; thresholds for red light are lower than for blue light (i.e. the animal is more sensitive to red light than to blue light). The first plateau represents therefore cone dark-adaptation. After this plateau is reached, thresholds start decreasing again. This time, thresholds to blue light decrease much more than those to red light, due to rod dark-adaptation. This is a consequence of the Purkinje shift that happens when vision switches from cone-dominated to rod-dominated. Taken from Barlow et al. (1957).

The retinas we studied are called “dark-adapted” because they were kept in darkness for at least 40 minutes before the beginning of an experiment. Under this condition, one expects the retina to be rod-dominated and the dynamic range of rods and cones to be almost non-overlapping. Nonetheless, it is the intensity of

the stimulus used that ultimately determines which photoreceptor type is mostly stimulated.

Most of the differences in adaptive properties between rods and cones are intrinsic to the photoreceptors themselves (Picones and Korenbrot, 1995; Rebrik and Korenbrot, 1998/2004). In addition to the modulation of the phototransduction cascade (as reviewed in Miller et al., 1994), the number of synaptic ribbons in the photoreceptor terminals seems to be modulated in the course of dark-adaptation (Vollrath and Spiwoks-Becker, 1996; Adly et al., 1999).

There are also network adaptive changes that modify the properties of the visual system at each adaptive state. For instance, at the outer retinal level, fish HCs develop the so-called “spinules” in the light-adapted retina (Weiler and Wagner, 1984; Weiler, 1994). These are dendritic processes that increase their contact area with the photoreceptors, and their appearance seems to be under dopaminergic control. In the dark-adapted retina, the number of synaptic ribbons changes (Wagner, 1973; Schmitz et al., 1989), spinules disappear (Wagner, 1980), the electrical coupling between HCs decreases (Mangel and Dowling, 1985; Tornqvist et al., 1988) and feedback strength is diminished (Weiler and Wagner, 1984; Fahrenfort et al., 1999). Other retinal adaptive changes include spinule formation at the mixed-input BC axon terminals (Yazulla and Studholme, 1992; Behrens and Wagner, 1996; Behrens et al., 1998), and changes in the receptive field properties of BCs (Shimbo et al., 2000) and GCs (Beauchamp and Daw, 1972; Raynauld, 1972).

How these changes in the receptive field properties of retinal neurons are triggered by a rod-cone switch is not completely understood. Since mixed-input BCs are the first place in the retina where rod and cone inputs converge, they are the ideal place to investigate what happens to the glutamate release of each photoreceptor type in different adaptive conditions.

### 1.7 The Glutamate Receptors of Mixed-Input BCs

The fourth dualism in outer retinal physiology refers to the glutamate receptor make up of BCs. In both lower vertebrates and mammals, AMPA/KA receptors mediate the light responses of hyperpolarizing BCs (zebrafish: Connaughton and Nelson, 2000; salamander: Hensley et al., 1993; cat: Sasaki and Kaneko, 1996; ground squirrel: DeVries and Schwartz, 1999; DeVries, 2000; rat: Euler et al., 1996), whereas depolarizing light responses are generated via a glutamate receptor sensitive to L-AP4, an agonist for metabotropic receptors of the group III (dogfish: Shiells et al., 1981; goldfish: Nawy and Copenhagen, 1987; hybrid bass: Grant and Dowling, 1996; mudpuppy: Slaughter and Miller, 1981; Thoreson and Miller, 1993; tiger salamander: Tian and Slaughter, 1995; rat: Yamashita and Wässle, 1991, Nakajima et al., 1993; Euler et al., 1996). Immunocytochemical studies indicate that this receptor might be mGluR6, since it is preferentially expressed in the retina (Nakajima et al., 1993), and

is present on BC dendrites in various species (rat: Nomura et al., 1994; Vardi and Morigiwa, 1997; monkey: Vardi et al., 1998/2000).

In the fish retina, it was postulated that rod and cones drive different glutamate receptors in mixed-input BCs, based on changes in light response properties after cell polarization and on membrane resistance changes upon light stimulation (Saito et al., 1978/1979/1981; Kaneko and Saito, 1983; Saito and Kaneko, 1983; Saito et al., 1984). Subsequent studies tried to characterize pharmacologically the cone-driven receptors (Grant and Dowling, 1995/1996; Wong et al., 2005a/b), but a thorough study on the properties of rod- and cone-driven light responses in mixed-input BCs has not yet been done, probably due to technical difficulties.

Such a study is however of uttermost importance in order to understand how photoreceptors shape the light responses of mixed-input BCs in the dark-adapted and light-adapted retina, how these inputs interact in the mesopic range, and how spectral opponency comes about.

### 1.8 Thesis Outline

**Chapter 2** is concerned with the immunocytochemical localization of metabotropic glutamate receptors in the goldfish retina, as a substrate for the generation of rod- and cone- driven light responses in mixed-input BCs;

**Chapter 3** deals with the characteristics of goldfish mixed-input BC receptive field organization and its consequences for information processing;

**Chapter 4** addresses the origin and function of spectral coding in mixed-input BCs of the goldfish retina;

**Chapter 5** describes a mechanism in mixed-input ON BCs that could underlie a switch between rod-dominated and cone-dominated modes in different adaptive states;

**Chapter 6** contains a general discussion of the data and topics dealt with in this thesis, as well as some open issues.

# Chapter 2

# Localization of Metabotropic Glutamate Receptors in the Outer Plexiform Layer of the Goldfish Retina

*Christina Joselevitch, Jan Klooster and Maarten Kamermans*
*(To be submitted)*

## 2.1 Abstract

We studied the localization of group I (mGluR1$\alpha$ and mGluR5), group II (mGluR2/3) and group III (mGluR4, mGluR6, mGluR7 and mGluR8) mGluRs at light- and electron microscopical level in the OPL of the goldfish. Double-labeling with antibodies against the ON BC markers PKC$\alpha$ and Go$\alpha$ was performed to investigate the mGluR composition of mixed-input ON BCs. The ultrastructural localization of PKC$\alpha$ and Go$\alpha$ was used as reference for the identification of ON BC processes in the rod and cone terminals. Both mGluR1$\alpha$ and mGluR6 co-localized with PKC$\alpha$ and Go$\alpha$. Ultrastructurally, the antibodies labeled dendritic processes at the position of BC dendrites invaginating into the rod spherules. Occasionally, mGluR1$\alpha$ and mGluR6 were also found in structures whose position in the rod spherule and cytology are consistent with rod-driven HCs. No double-labeling was found with mGluR5, mGluR2/3 and mGluR4, although in all three cases there was some staining at the OPL. Immunolabeling for mGluR5 and mGluR4 was localized pre-synaptically to Go$\alpha$ and PKC$\alpha$-positive cells; at the EM level, mGluR4 was found within the rod terminals. In cone pedicles, the mGluR1$\alpha$, mGluR2/3 and mGluR6 antibodies labeled cone-driven HC dendrites: mGluR2/3 was found in both central and lateral elements of the triad, whereas mGluR1$\alpha$ labeled lateral processes and spinules, and mGluR6 central processes and spinules. The antibodies against mGLuR7 and mGluR8 yielded diffuse labeling at the inner margin of the INL, IPL and GCL. The pre-synaptic localization of mGluR4 and the existence of mGluR6 in HC dendrites raise the possibility that the group III agonists and antagonists used to study ON BCs have multi-synaptic effects. The presence of mGluR1$\alpha$ in the dendrites of mixed-input ON BCs indicates that either these cells possess a second G-protein that subserves mGluR1$\alpha$ signaling, or that mGluR6 and mGluR1$\alpha$ share at least part of the same machinery. Finally, the organized pattern of mGluR localization in cone-driven HCs suggest that the expression of an mGluR is restricted to certain populations of HCs. The G-protein coupled to these receptors is unknown.

## 2.2 Introduction

L-glutamate is the major excitatory neurotransmitter in the central nervous system. In the retina, photoreceptors release L-glutamate in the dark, and this release is decreased by light stimulation (Cervetto and MacNichol, 1972; Murakami et al., 1972; Kaneko and Shimazaki, 1976). The modulation of the glutamate concentration in the OPL is sensed by glutamate receptors localized in the dendrites of second-order neurons (BCs and HCs), and this leads to transmission of visual signals to the next cells.

Glutamate receptors can be roughly divided in ionotropic and metabotropic (Eccles and McGeer, 1979). Ionotropic receptors (iGluRs) form an integral ion channel, whereas metabotropic receptors (mGluRs) mediate responses through indirect mechanisms involving intracellular chemical reactions. Although many of these responses are a result of activation of G-proteins that functionally couple mGluRs (Rodbell, 1980), there is also evidence for G-protein-independent mGluR signaling (Heuss and Gerber, 2000).

Whereas different iGluR types (subdivided into AMPA, kainate and NMDA) can be unambiguously identified through pharmacological experiments, mGluRs cannot. So far, 8 different mGluRs have been cloned and classified into three groups based on their sequence similarities, second-messenger cascade, and pharmacology: group I comprises mGluR1 (Masu et al., 1991; Houamed et al., 1991) and mGluR5 (Abe et al., 1992) and their splice variants (1a-d and 5a-b); group II contains mGluR2 and mGluR3 (Tanabe et al., 1992/1993); and group III includes mGluR4 (Tanabe et al., 1992/1993), mGluR6 (Nakajima et al., 1993), mGluR7 (Okamoto et al., 1994; Saugstad et al., 1994) and mGluR8 (Duvoisin et al., 1995) and their splice variants (4a-b, 7a-b, 6a-b and 8a-b). The lack of specific pharmacological tools to distinguish between mGluRs within a group makes it difficult to identify the mGluR mediating a certain response (for reviews, see Thoreson and Ulphani, 1995, or Schoepp et al., 1999). Furthermore, these drugs can generate multi-synaptic effects if a given mGluR (or other mGluRs to which the drug also show affinity) is expressed in cells localized pre-synaptically to the one studied.

Light responses in ON BCs of a number of species are sensitive to substances that target group III mGluRs (Shiells et al., 1981; Slaughter and Miller, 1981; Thoreson and Miller, 1993). There is compelling evidence that the receptor activated by these drugs is mGluR6 (Nakajima et al., 1993; Akazawa et al., 1994; Masu et al., 1995; Ueda et al., 1997; Vardi and Morigiwa, 1997; Laurie et al., 1997; Vardi et al., 2000), and that this receptor couples to Go$\alpha$ (Vardi, 1998; Nawy, 1999; Dhingra et al., 2000/2002). However, effects of group III agonists were also reported in cone terminals of fish, amphibians and mammals (Koulen et al., 1999; Hirasawa et al., 2002;Hosoi et al., 2005) and in goldfish HCs (Nawy et al., 1989; Takahashi and Copenhagen, 1992), raising the possibility that group III mGluRs are expressed in other cells than mixed-input ON BCs in the goldfish. However, a thorough study

on the localization of mGluRs in the goldfish retina has not yet been done; the only data available was obtained from other species. All mGluRs, with the exception of mGluR3, were identified by immunohistochemistry and in situ hybridization in the vertebrate retina, although the distributions vary according to the species (Nomura et al., 1994; Koulen et al., 1996/1997; Vardi and Morigiwa, 1997; Brandstätter et al., 1998; Gafka et al., 1999; Cai and Pourcho, 1999; Vardi et al., 2000).

In order to identify which mGluRs could be involved pre-and post-synaptically in the generation of light responses in mixed-input ON BCs of the goldfish retina, we investigated the localization of mGluR1α, mGluR2/3, mGluR4 mGluR5, mGluR6, mGluR7 and mGluR8 at light- and electron microscopy level. For light microscopy, double-labeling studies with the ON BC markers Goα (Vardi, 1998) and PKCα (Negishi et al., 1988; Suzuki and Kaneko, 1990; Yazulla and Studholme, 1992) were performed when there was evidence of OPL staining. The results will be presented and discussed in the following sections.

## 2.3 Material and Methods

*Preparation*

Goldfish (*Carassius auratus*), 12-15 cm standard body length, were obtained from a commercial supplier and maintained at 18 °C in aerated tanks filled with tap water circulating through a biological filter system. The fish were fed and kept on a 12 h / 12 h light-dark cycle. All animal experiments were carried out under the responsibility of the ethical committee of the Royal Netherlands Academy of Arts and Sciences acting in accordance with the European Communities Council Directive of 24 November 1986 (86/609/EEC).

Light-adapted fish were transected cervically; all dissections took place at room light. The cornea and lens were removed and eyecups were cut in half along the dorsal-ventral axis. Half eyecups were placed vitreous side down on a Millipore filter (13 mm diameter, 8 μm pore size, Millipore BV, The Netherlands) that was placed on a filter holder. Suction was used to remove the vitreous; the sclera and retinal pigment epithelium were peeled away.

*Immunochemicals*

Polyclonal antibodies against the C-terminus of rat mGluR1α (which recognizes only the splice variant mGluR1a), mGluR2 (mGluR2/3), mGluR5, rabbit mGluR6, rat and human mGluR8, as well as the mouse monoclonal against bovine Goα were purchased from Chemicon International (Temecula, CA). A polyclonal antibody against the C-terminus of rat mGluR4 (specific for the mGluR4a splice variant) was obtained from Zymed laboratories Inc. (San Francisco, CA), and a polyclonal against the C-terminus of human mGluR7 was purchased from Upstate (Lake Placid, NY). The mouse monoclonal antibody against PKCα was acquired from Sigma-Aldrich

Inc. (St. Louis, MO). Goat anti-mouse Alexa was obtained from Molecular Probes (Breda, The Netherlands), and goat anti-rabbit Cy3 from Jackson ImmunoResearch Lab (West Grove, PA).

*Light Microscopy*

Retinas were fixed for 10 min at room temperature in 0.1 M phosphate-buffered (pH 6.5) 4% paraformaldehyde, followed by fixation in a 0.1 M sodium carbonate-buffered 4% paraformaldehyde (pH 10.4) solution for 10 min. After rinsing in 0.1 M phosphate buffer (PB) pH 7.4, tissue was cryoprotected at room temperature in PB containing 12% sucrose for 30 min, and 25% sucrose for 2 hours. The pieces of retina, still attached to the filter, were embedded in Tissue Tek (Sakura Finetek Europe B.V., Zouterwoude, The Netherlands) in an aluminum boat and frozen in liquid nitrogen.

Sections, 8-10 μm thick, were mounted on poly-L-lysine coated slides (Menzel-Gläser, Germany), dried and stored in a non-frost-free freezer at –20° C. Retinal sections were washed in PBS for 10 min (2x), and blocked in 2% normal goat serum (NGS, Jackson ImmunoResearch Lab, West Grove, PA) in PBS for 20 min. Sections were then incubated overnight with primary antibody at 4° C in PBS (mGluR1α 1:100, mGluR5 1:100, mGluR2/3 1:100, mGluR4 1:100, mGluR6 1:100, , mGluR7 1:500, mGluR8 1:500, Goα 1:2000, PKCα 1:500) containing 0.3% Triton X-100 and 5% NGS. After washing (15 min, 3x, in PBS), sections were incubated in the secondary antibodies for 30 min (Cy3: 1:500, Alexa: 1:600).

Controls were performed by omitting the primary antibody, which eliminated all staining. Sections were cover-slipped with Vectashield (Vector Labs, Burlingame, CA) and stored at –20 °C. Slides were observed on a Leica DMRD (Leica, Germany) fluorescence microscope equipped with filter sets that were designed for FITC and Cy3. Sections of double-label experiments were observed on an inverted Zeiss Axiovert 100 M microscope equipped with the LSM 510 META laser scanning confocal module (Zeiss, Germany).

*Electron Microscopy*

The same fixation and cryoprotection procedures were used as described above for light microscopy. The retinas were peeled off the filter and embedded in 4% agar in PB, containing 10% glycerol and 20% sucrose in an aluminum boat. The boat was frozen in liquid nitrogen. Frozen sections, 30-40 μm thick were obtained on a freezing microtome and collected in PB.

The retinal sections were incubated 72 hours with diluted antisera (mGluR1α 1:100, mGluR5 1:100, mGluR2/3 1:100, mGluR4 1:100, mGluR6 1:100, Goα 1:1000, PKCα 1:400). After rinsing, the tissue was incubated in a Poly-HRP-Goat anti-rabbit IgG (PowerVision, ImmunoVision Technologies Co, Daly City, CA). To visualize the peroxidase, the material was incubated in a Tris-HCl diaminobenzidine (DAB, 0.05%) solution containing 0.03% $H_2O_2$. Subsequently, the DAB reaction product

was intensified by the gold-substituted silver peroxidase method (Van den Pol and Gorcs, 1988). Sections were rinsed in sodium cacodylate buffer 0.1 M (pH 7.4) and post-fixed for 20 min in 1% $OsO_4$ supplemented with 1.5 % potassium ferricyanide in sodium cacodylate buffer 0.1M (pH 7.4). After rinsing in the sodium cacodylate buffer, the material was dehydrated and embedded in epoxy resin. Ultrathin sections were observed and photographed in a Philips 201 electron microscope (Philips, Eindhoven, The Netherlands) and/or Technai (CM)12 electron microscope (FEI, Eindhoven, The Netherlands).

*Production of Photomicrographs*
Light micrographs were acquired as TIFF files directly from the Leica microscope using a Leica 350 F digital B/W camera at 1284x1028 1.3 Mpixels. Light micrographs of the double-label experiments were acquired as TIFF files from the inverted Zeiss Axiovert 100M equipped with LSM 510 META laser scanning confocal module. Electron micrographs were first printed from the negatives for analysis. The negatives of the prints that were selected for publication were scanned on a sprint scan 4000 scanner (Polaroid, Breda, The Netherlands) and acquired as TIFF files at 600 dpi. All TIFF files were optimized for brightness and contrast using Photoshop software, version 7.0 (Adobe Systems, San Jose, CA).

## 2.4 Results

Results will be described according to the mGluR groups. For every experiment described in the next sections, results were obtained from retinas of at least three animals. Whenever the single-labeling experiment revealed OPL staining, double-labeling with antibodies against the ON BC markers PKC$\alpha$ and Go$\alpha$ was performed and studied at the light microscopical level, in order to find out whether any of the mGluRs studied are co-localized with mixed-input ON BCs. The exact localization of the mGluRs in the OPL was further investigated at EM level. The ultrastructural localization of PKC$\alpha$ and Go$\alpha$ was also studied to serve as a standard for the identification of mixed-input ON BC dendrites in both rod and cone synaptic terminals. A description of the cytology and position of HC and BC dendrites in rod and cone terminals is provided in Figure 1.2 of this thesis.

*PKC$\alpha$ and Go$\alpha$*
In the goldfish retina, immunostaining for the $\alpha$ species of PKC (Figure 2.1a) was described to label two populations of ON BCs at the light microscopical level (Negishi et al., 1988; Suzuki and Kaneko, 1990; Cuenca et al., 1993; Yazulla et al., 2000): cells with small somata (arrowheads) in the middle of the INL and small axonal terminations, and BCs with large flask-shaped somas (asterisks) and bulbous axon terminals. The first type comprises cone-driven ON BCs, and the second corresponds

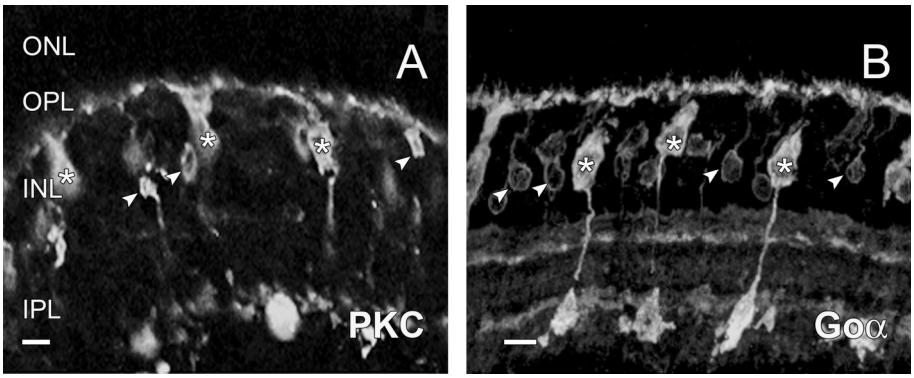


**Figure 2.1:** Immunostaining for ON BC markers. A) Distribution of PKCα-IR in the goldfish retina, visualized with Alexa. Two populations of ON BCs are positively labeled: large cells with flask-shaped somas (asterisks) and bulbous axon terminals, and smaller cells (arrowheads) with little axonal terminations. Scale bar = 10 µm. B) Distribution of Goα-IR in the goldfish retinal slice, visualized with Alexa. Also here two populations of ON BCs can be distinguished: large mixed-input BCs are strongly and uniformly stained (asterisks), and a faint Goα-IR appears to ring the somas of smaller BCs (arrowheads). In the IPL, two strongly immunoreactive bands can be seen. Scale bar = 10 µm.

to mixed-input ON BCs (Stell, 1967; Scholes, 1975; Sherry and Yazulla, 1993). The antibody against Goα yields a similar pattern of immunoreactivity (Figure 2.1b): two BC populations seem to be labeled. This is different from what happens in the rat retina, where only rod-driven ON BCs are positive for PKCα and Goα (Greferath et al., 1990; Kamphuis et al., 2003), but similar to monkey and cat, in which Goα labels both rod- and cone-driven ON BC dendrites (Vardi, 1998). Contrary to what was reported in the latter, however, the antibody against Goα also stains heavily the axon terminals of goldfish ON BCs, plus two immunoreactive bands in the IPL; comparable results were reported in the tiger salamander (Zhang and Wu, 2003). The differences in the axonal termination shapes of the mixed-input BCs in Figures 2.1a and b can be attributed to small differences between the adaptive state of the retinas studied: dark-adaptation induces the formation of spinule-like protrusions in these terminals, whereas in light-adapted animals mixed-input BC axon terminals are fairly round and without appendages (Yazulla and Studholme, 1992; Behrens and Wagner, 1996).

The ultrastructural localization of PKCα (Figure 2.2a-c) and Goα (Figure 2.3a and c) in the rod spherule was described in a number of species (PKC: Greferath et al., 1990; Kolb et al., 1993; Klooster et al., 2001; Goα: Vardi, 1998). Briefly, both antibodies label invaginating dendrites, which form the central element of the synapse, and immunostaining can also be found at some distance from the ribbon. The labeled processes resemble in position and appearance the dendrites of mixed-input ON BCs (Stell, 1967). Lateral processes immediately adjacent to the pre-synaptic ridge, previously classified as dendrites of rod-driven HCs (Stell, 1967;

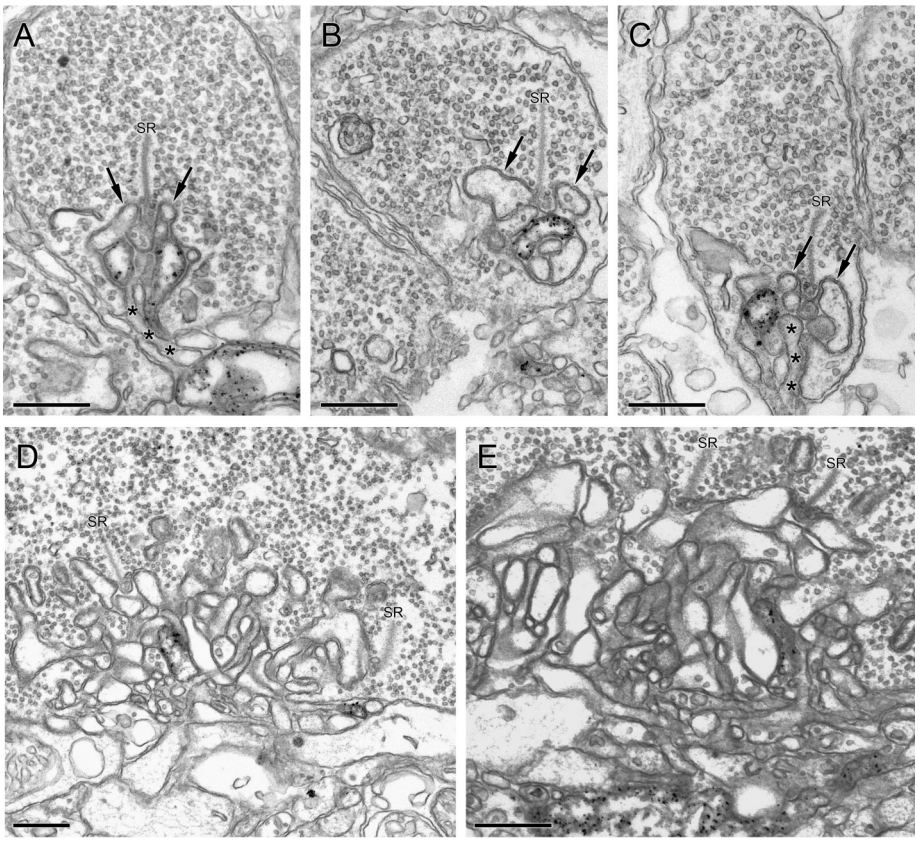


**Figure 2.2:** Ultrastructural localization of PKCα-IR in the OPL. In the rod spherules (A, B and C), invaginating structures are positively labeled. These elements can be elongated (A) or u-shaped (B), and are found either in close apposition to the pre-synaptic ridge (A and B) or a little away from it (C). The lateral elements of the triad are unlabeled (arrows), as well as some invaginating processes (asterisks). In the cone pedicles (D and E), PKC-IR was observed in small invaginating profiles at the base of the pedicles. These structures were never associated with the synaptic ribbons (SR). Scale bars = 0.5 µm.

Scholes, 1975; Stell, 1976) were not labeled (arrows). Some invaginating processes were not labeled (asterisks); their position and cytology, in combination with the lack of staining, lead us to the conclusion that they are the dendrites of mixed-input OFF BCs (Stell, 1967/ 1976; Saito et al., 1983/1985).

In the cone terminal, however, PKCα (Figure 2.2d and e) and Goα (Figure 2.3d-f) immunostaining yielded somewhat distinct patterns. PKCα-immunoreactive structures were very rarely observed. When present, these positively labeled structures were never associated to the synaptic ribbon, but were instead localized at the base of the cone pedicle. In the post-synaptic elements of the cone pedicle, only the Goα-IR was observed in a small profile at the apex of synaptic ribbon. There

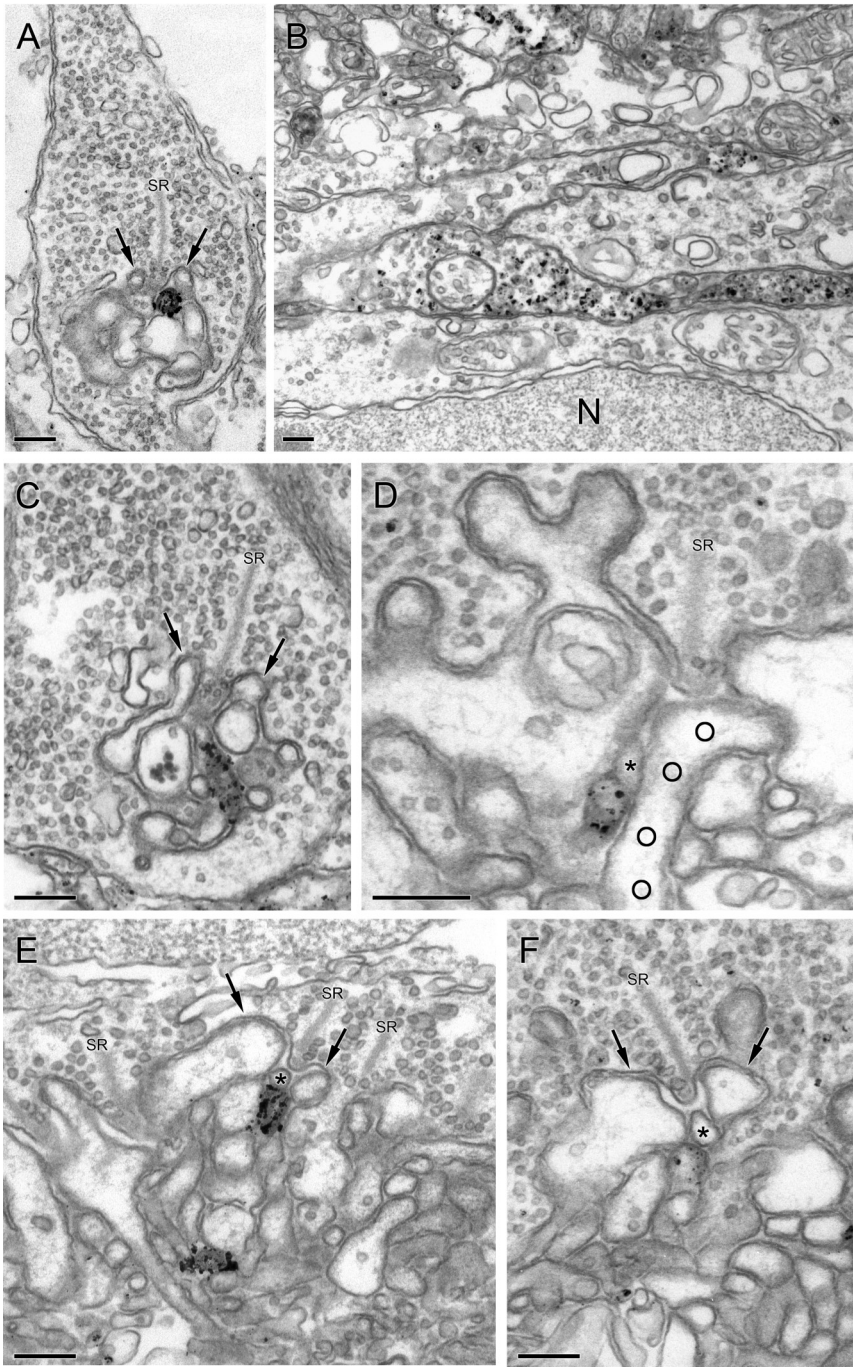
A
SR
B
N
C
SR
D
SR
*
E
SR
SR
SR
*
F
SR
*

**Figure 2.3 (opposite page):** Ultrastructural localization of Goα-IR in the OPL. In the rod terminals (A and C), invaginating structures closely associated with the pre-synaptic ridge were positively stained. The lateral elements of the synaptic complex were unlabeled (arrows). In the cone pedicles (D, E and F), staining was found in small invaginating profiles in the proximity of the synaptic ribbon; a central element positioned between the labeled dendrite and the apex of the pre-synaptic ridge was always unlabeled (asterisk), as well as the lateral processes of the triad (arrows). When the central element of the synapse was an HC dendrite (D, open circles), the two small profiles could also be seen beside it. In the neuropil (B), Goα-IR was observed in tangentially oriented processes rich in vesicles. SR: synaptic ribbon. Scale bars = 0.25 µm.

were always two small profiles; one was labeled and the other not (asterisk). The non-labeled profile was always facing the apex of the synaptic ribbon; the labeled one was just below it. The structure facing the pre-synaptic ridge was described as belonging to cone-driven OFF BCs, and the profile just below it to cone-driven ON BCs in the catfish (Sakai and Naka, 1983) and carp (Saito et al., 1983; Saito et al., 1985). When the central process had a cytology consistent with that of an HC dendrite (Stell, 1976), it was unlabeled (circles in Figure 2.3d); the two small profiles were also present along the unlabeled HC dendrite that ran to be the central element. Also in this case, the structure at the position of the ON BC dendrite showed Goα-IR. Lateral elements, classified in previous studies as belonging to cone-driven HC dendrites (Stell, 1967; Scholes, 1975; Stell, 1976) were never Goα-positive (arrows).

*Group I mGluRs (mGluR1α and mGluR5)*

Distribution of mGluR1α-IR yielded in a diffuse staining of the OPL, INL, IPL and some sparse staining in the GCL (not shown). Double-labeling with the PKCα-IR (Figure 2.4a and b) was strongest in the OPL (arrowheads), with sparse labeling of mixed-input ON BC somata (asterisks). Double-labeling with Goα (Figure 2.2c and d) resulted in colocalization with the mGluR1α-IR of the mixed-input ON BC somata in the INL (asterisks), and some diffuse labeling in the OPL (arrowheads). Colocalization was mainly at the proximal site of the soma, in contrast to the distribution obtained with PKCα. Occasionally, the mGluR1α antibody labeled structures (presumably AC somata) in the inner border of the INL that were not Goα-positive (Figure 2.4d, arrows). In neither double-labeling experiments were cone-driven ON BCs positive for mGluR1α, and there was no complete overlap between the mGluR1α-IR and the ON BC markers on the dendrites located in the OPL.

To examine the precise localization of mGluR1α in the OPL, a study was performed at the EM level (Figure 2.5). The main characteristic of the mGluR1α-IR at the ultrastructural level is the labeling of the central element or an invaginating dendrite in the rod spherule (Figure 2.5a-d), which can be elongated (Figure 2.5a) or ellipsoid (Figure 2.5b). Based on their position within the spherule and cytology, and in agreement with previous studies (Scholes, 1975; Stell, 1976; Saito et al., 1985; Yazulla et al., 2001; Klooster et al., 2001) we conclude that these mGluR1α-positive elements are mixed-input ON BC dendrites. We also observed mGluR1α-IR in goblet-shaped dendrites surrounding the synaptic ribbon in the rod spherule

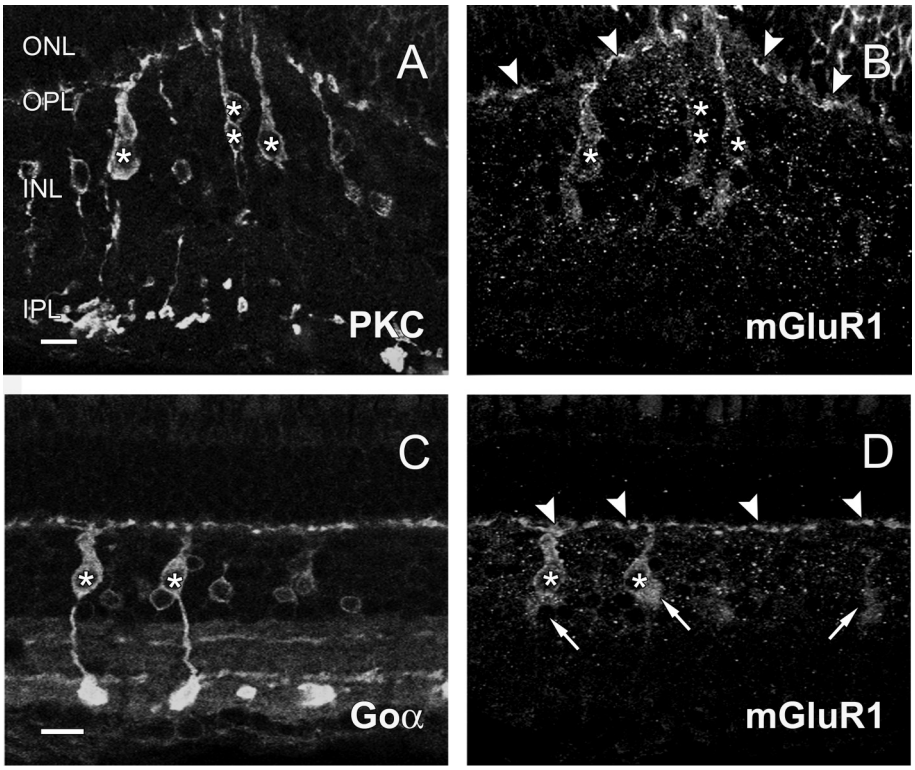


**Figure 2.4:** Immunostaining for mGluR1α. Green- (A) and red- (B) channel images (presented in black and white) of the same tissue section that was double-labeled with the antibodies against PKCα (Alexa, A) and mGluR1α (Cy3, B). In addition to diffuse mGluR1α-IR in the INL, the distal part of the large BC somas (asterisks) was positively labeled. In the OPL, a band of mGluR1α-IR could be seen (arrowheads), which partially overlapped with the dendritic processes of PKCα-positive cells. In C) and D), similar results are presented for a double-label experiment with the Goα antibody. Arrows in D point to structures positive for mGluR1α that were not labeled for Goα. Scale bars = 10 µm.

**Figure 2.5 (opposite page):** Ultrastructural localization of mGluR1α in the OPL. In the rod terminals (A, B, and C), invaginating processes at the summit of the synaptic ribbon were positively labeled. These processes could be elongated (A), ellipsoid (B) or goblet-shaped (C). Some invaginating processes were not labeled (asterisks); these are probably dendrites of mixed-input OFF BCs. In most cases, the lateral elements of the synapse were unlabeled (arrows), although at times a laterally positioned dendrite showed mGluR1α-IR (D). In the cone pedicles (E and F), mGluR1α-IR was found in small invaginating profiles at the base of the pedicles, which were not associated to the ribbons. In addition, one of the lateral elements of the triads was positively labeled (E), while the other lateral element was unlabeled (arrows). The antibody also stained structures resembling HC spinules in the cone terminals (F). SR: synaptic ribbon. Scale bar = 0.25 µm.

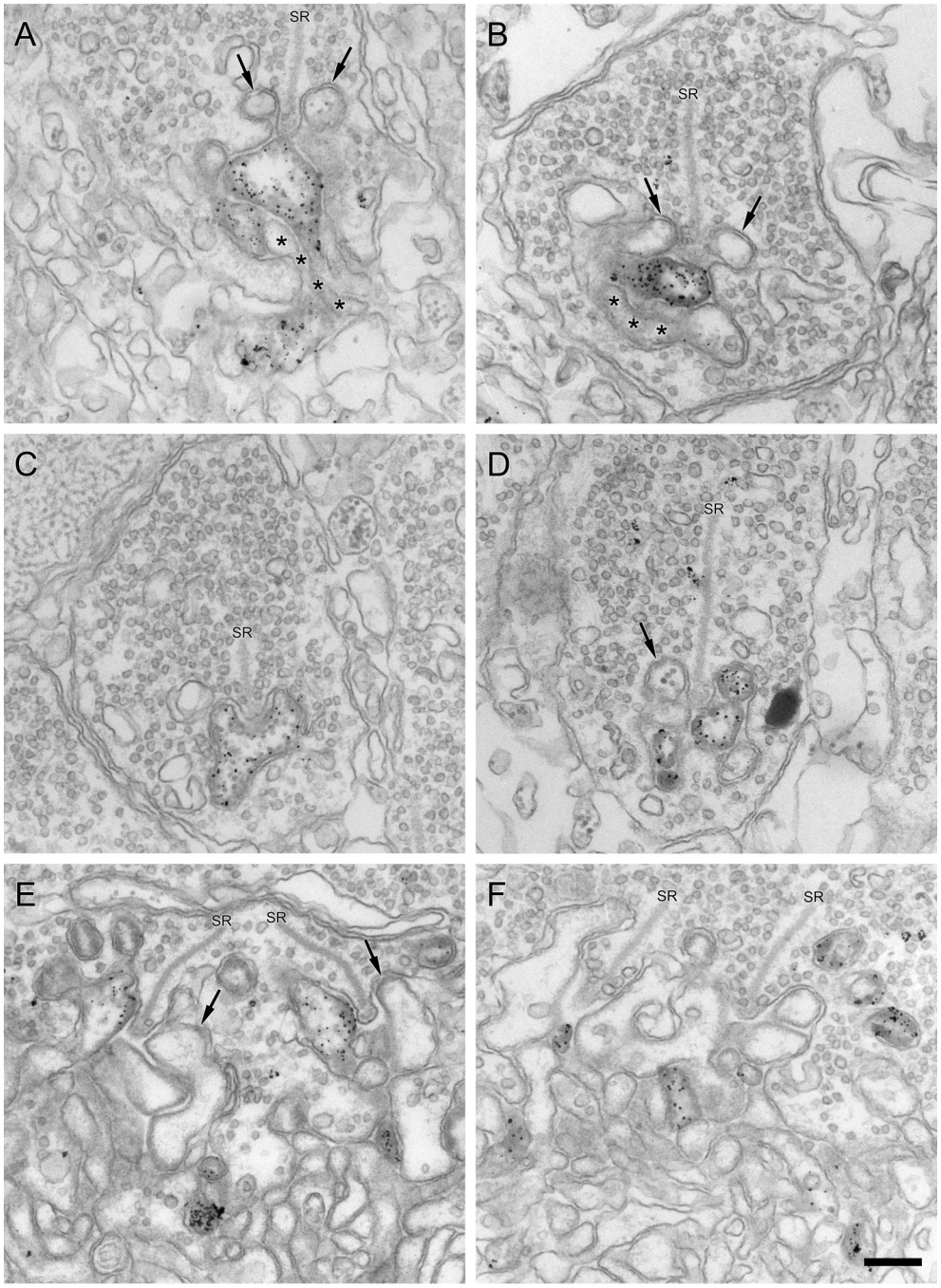
A
SR
B
SR
C
SR
D
SR
E
SR
SR
F
SR
SR

(Figure 2.5c). In a previous study, we showed that this particular structure could be the dendrite of a mixed-input ON BC (Klooster et al., 2001). In a few spherules mGluR1α-IR was also found in one lateral element facing the synaptic ribbon (Figure 2.5d). Such elements were classified as belonging to rod HC dendrites (Stell, 1967/1976). In the spherules in which this pattern was found, only one lateral HC dendrite showed mGluR1α-IR; the other lateral element was unlabeled (arrow).

The localization of mGluR1α-positive structures in the cone terminals was somewhat surprising. In addition to small processes not associated with the synaptic ribbons we found in some pedicles mGluR1α-IR at one lateral dendrite of the cone triad (Figure 2.5e). The position and cytology of these dendrites identify them as belonging to cone-driven HCs (Stell, 1967/1976; Sakai and Naka, 1983). When one lateral HC dendrite showed mGluR1α-IR, the opposite HC dendrite was not positive (arrows). We do not have clear evidence of labeling of a central element in a cone triad. In light-adapted retinas, a few structures that resemble HC spinules in terms of location and appearance (Wagner, 1980) exhibited mGluR1α-IR (Figure 2.5f).

In double-labeling experiments, mGluR5-IR was found at the level of the photoreceptor terminals and diffusely at the IPL and OPL (Figure 2.6). Some HC bodies seemed to be positively labeled at the outer margin of the INL (not shown). There was no colocalization with PKCα or Goα. The labeling shows a fine grain character in vertical bands at the ONL (arrowheads). It is not clear from these pictures whether mGluR5 is in the photoreceptor terminals or in surrounding Müller cells. At the EM level, mGluR5-IR is seen in longitudinally oriented structures localized between photoreceptor terminals, consistent with Müller cells (not shown).

*Group II mGluRs (mGluR2/3)*

In single-labeling experiments at the light microscopical level, mGluR2/3-IR appeared to give smooth labeling in the INL; clearly stained somata could not be distinguished (compare Figures 2.7a and b). Tiny immunoreactive bands were visible in the OPL (arrowheads). Experiments with the PKCα and Goα antibodies (not sown) resulted in no double-labeling, suggesting that mixed-input ON BCs do not contain mGluR2/3. Nonetheless, also in these experiments the immunoreactivity at the OPL could be seen.

To elucidate which elements in the OPL display mGluR2/3-IR, we performed immunocytochemistry at the ultrastructural level. In the rod spherule, no immunoreactive structures could be identified. In the cone pedicles, mGluR2/3-IR was very rarely found on the lateral elements of the cone triads, at the position corresponding to cone-driven HC dendrites (Figure 2.8). Central elements were also labeled; the cytology of these central processes is consistent with that of HC dendrites as well (Stell, 1967; Scholes, 1975; Stell, 1976). Only in a few cone pedicles these labeled structures could be seen. No mGluR2/3-IR was seen in structures resembling BC dendrites, consistent with our light microscopy findings.

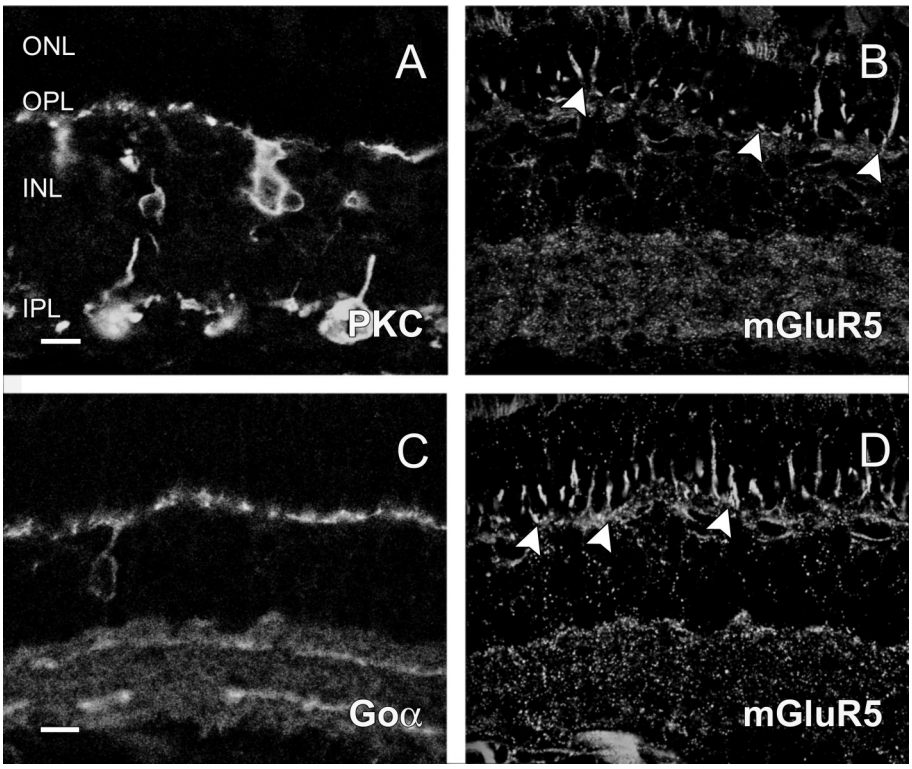


**Figure 2.6:** Immunostaining for mGluR5. Green- (A) and red- (B) channel images (presented in black and white) of the same tissue section that was double-labeled with the antibodies against PKCα (Alexa, A) and mGluR5 (Cy3, B), showing that there was no colocalization. The mGluR5 antibody yielded diffuse labeling of the IPL, and some vertical bands in the ONL (arrowheads). In C) and D), similar results are presented for a double-label experiment with the Goα antibody. Scale bars = 10 µm.

*Group III mGluRs (mGluR4, mGluR6, mGluR7 and mGluR8)*

Light microscopically, mGluR4-IR was found at the level of the photoreceptor terminals (Figure 2.9, arrowheads). It is not clear from these experiments if all photoreceptors terminals were labeled. Double-labeling with PKCα and Goα antibodies did not give evidence of localization in BCs. At the EM level, labeling was found only in the rod spherules (approximately four in every five rods were mGluR4-positive); the plasma membrane was intensely labeled (Figure 2.10).

The main feature of the mGluR6-IR at the light microscopical level is a diffuse labeling in the OPL, INL and IPL (Figure 2.11b and d). In the INL, cells at the position of the BCs and HCs showed mGluR6-IR; PKCα- and Goα- positive BCs were double-labeled for mGluR6 (asterisks). Double-labeling was found in the synaptic terminals of mixed-input BCs in the IPL, in the somata in the INL and in the dendrites in the OPL.

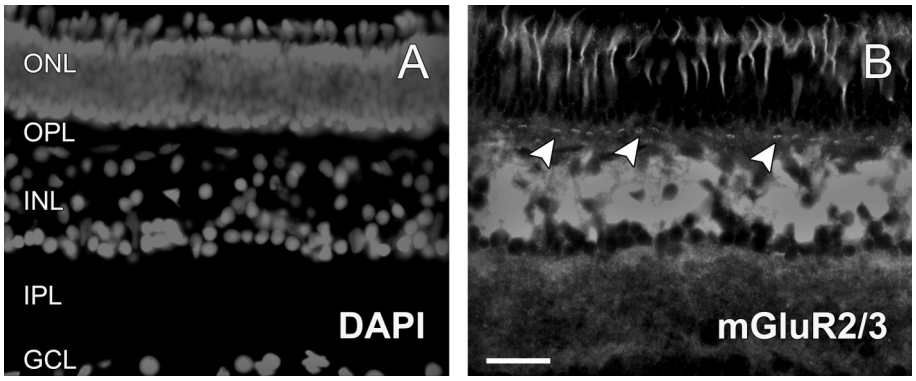


**Figure 2.7:** Immunostaining for mGluR2/3. Blue- (A) and red- (B) channel images (presented in black and white) of the same tissue section that was double-labeled with the nuclear stain DAPI (A) and the mGluR1α antibody (Cy3, B). In addition to smooth mGluR1α-IR in the INL, tiny immunoreactive bands in the OPL could be distinguished (arrowheads). Scale bar = 10 µm.

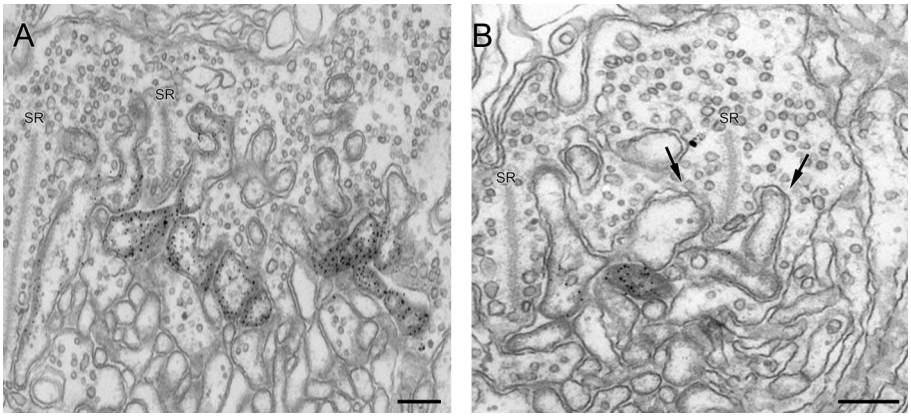


**Figure 2.8:** Ultrastructural localization of mGluR2/3 in the OPL. In some cone pedicles, mGluR2/3-IR was found in central and lateral elements of the cone triad. Their position, large size and cytology are consistent with HC dendrites. These labeled structures were only rarely found (compare the two active zones in B). SR: synaptic ribbon. Scale bars = 0.5 µm.

At the ultrastructural level, mGluR6-IR was observed in structures with cytology and position compatible with mixed-input ON BC dendrites invaginating into the rod spherule (Figure 2.12a-d). The pattern is similar to the one already described for PKCα, Goα and mGluR1α: the labeled structures can have an elongated (Figure 2.12 a) or an ellipsoid form (Figure 2.12b), and are localized either directly opposing the synaptic ribbon (Figure 2.12c) or somewhat away from it (Figure 2.12d). Unlabeled invaginating processes, as previously described, presumably belong to mixed-input OFF BCs (asterisks). Most frequently, the lateral

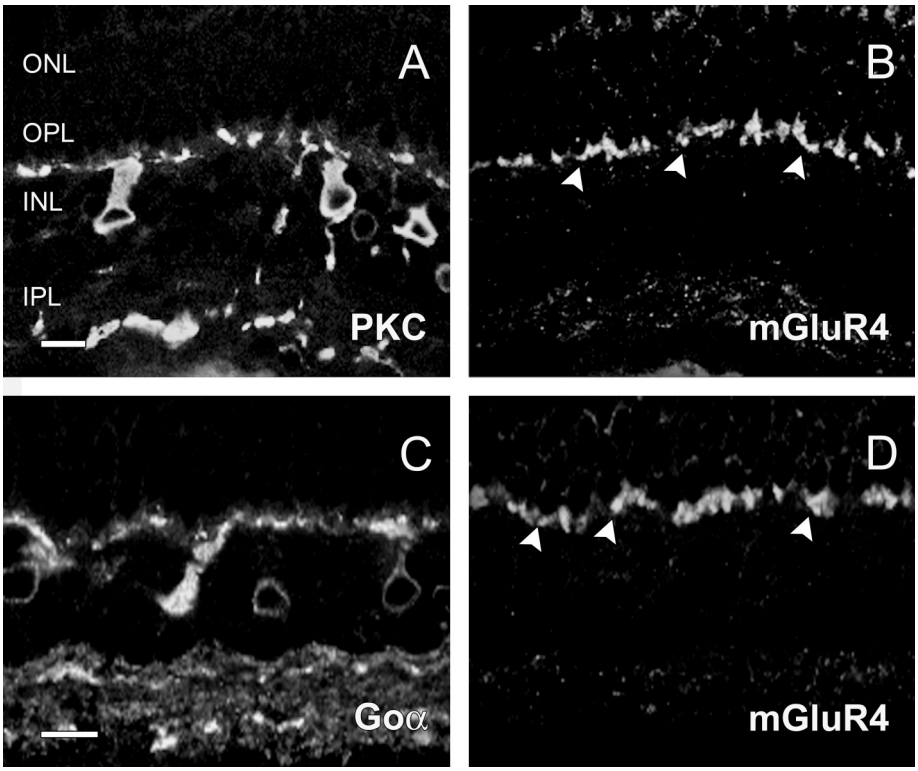


**Figure 2.9:** Immunostaining for mGluR4. Green- (A) and red- (B) channel images (presented in black and white) of the same tissue section that was double-labeled with the antibodies against PKCα (Alexa, A) and mGluR4 (Cy3, B), showing no colocalization. Immunolabeling for mGluR4 is restricted to the ONL (arrowheads). In C) and D), similar results are presented for a double-label experiment with the Goα antibody. Scale bars = 10 µm.

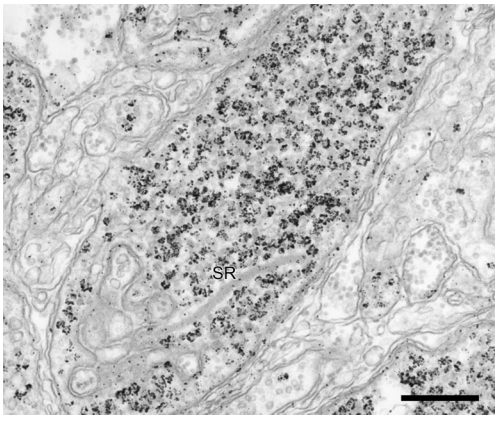


**Figure 2.10:** Ultrastructural localization of mGluR4 in the ONL. Intense mGluR4-IR was found in the cytoplasm of rod spherules. No post-synaptic structures were labeled. Scale bar = 0.25 µm.

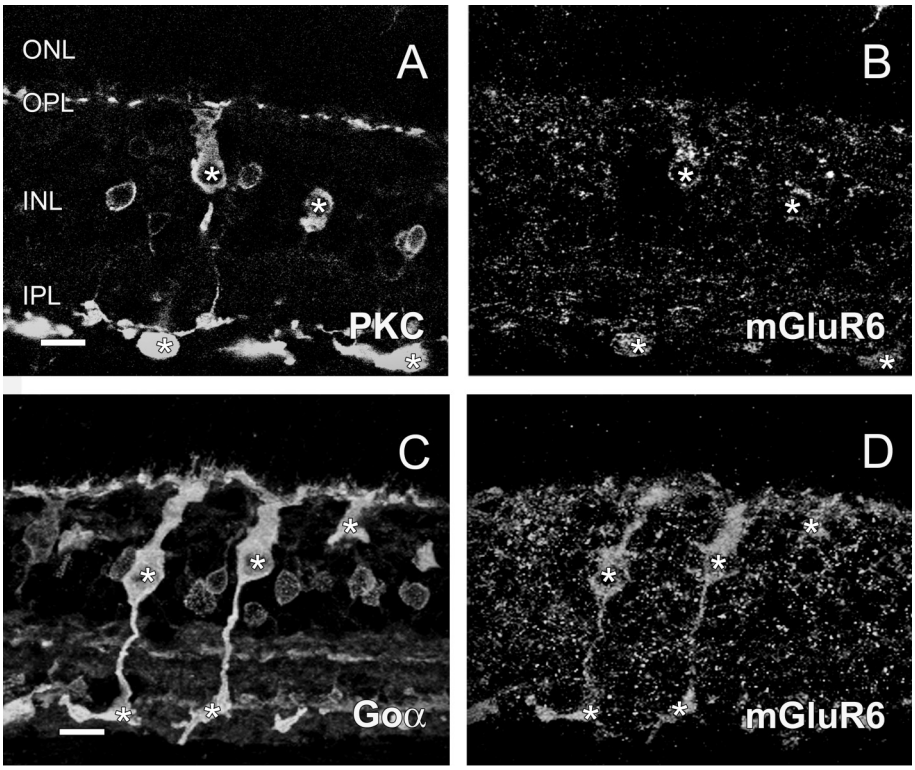


**Figure 2.11:** Immunostaining for mGluR6. Green- (A) and red- (B) channel images (presented in black and white) of the same tissue section that was double-labeled with the antibodies against PKCα (Alexa, A) and mGluR6 (Cy3, B). In addition to diffuse mGluR6-IR in the INL and IPL, the large BC somas and axon terminals (asterisks) were positively labeled for both antibodies. In C) and D), similar results are presented for a double-label experiment with the Goα antibody. Scale bars = 10 µm.

elements of the synapse were unlabeled (arrows); only in a few oblique sections mGluR6-IR was found in an element directly adjacent to the pre-synaptic ridge, in the position ascribed to the dendrites of rod-driven HCs (compare Figures 2.12e and f, see also Figure 2.12h). In a few sections, structures whose cytology resembles that of spinules were labeled (Figure 2.12g).

In the cone pedicles, mGluR6-IR was located at the central element of the cone triad (Figure 2.13a and b). According to previous descriptions, this type of central element belongs to cone-driven HCs, since it possesses cytology similar to the lateral elements (large dimensions as compared to BC dendrites, cytoplasm devoid of organelles, some electron-dense amorphous material applied to the cytoplasmic surface, and a wide cleft separating it from the synaptic ridge, after Stell, 1976). In contrast to what was found for mGluR1α and mGluR2/3, we never found mGluR6-IR in the lateral processes of the cone triads. Spinules were sometimes

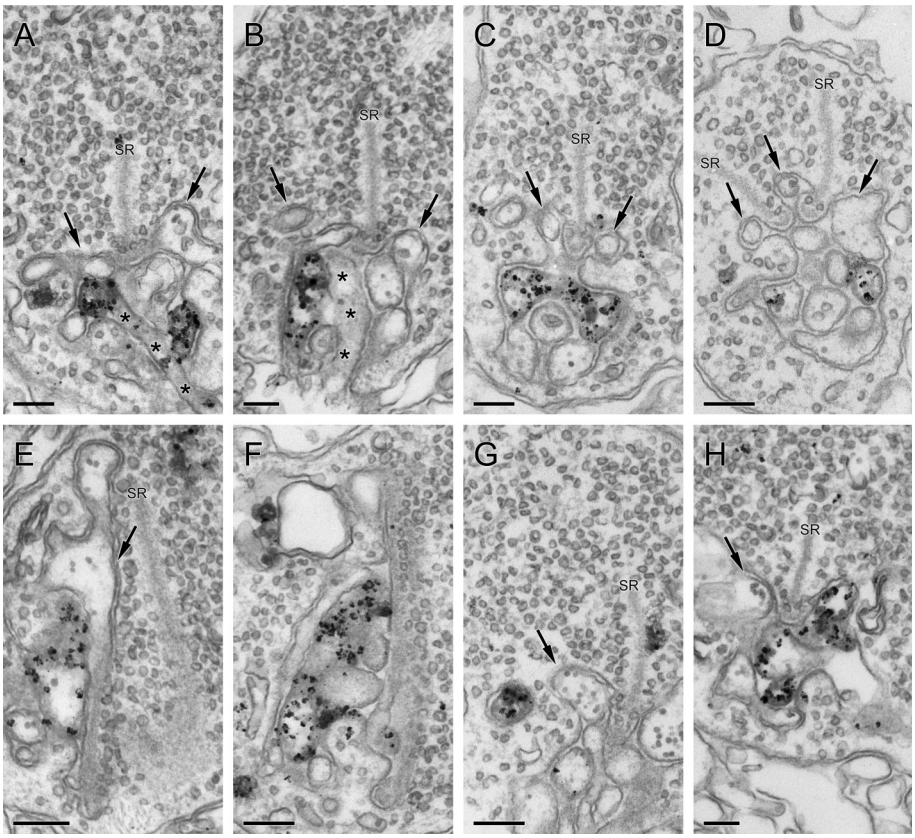


**Figure 2.12:** Ultrastructural localization of mGluR6 in the rod spherule. A,B,C) mGluR6-IR was found mainly in invaginating structures closely related to the synaptic ribbon, or a little away from it (D); these could be elongated (A), ellipsoid (B) or butterfly-shaped (C). Unlabeled invaginating dendrites were also present (asterisks), probably belonging to mixed-input OFF BCs. In most cases, the lateral elements of the synapse did not show staining (arrows). In some oblique sections, however, labeling was found in processes directly adjacent to the synaptic ribbons (compare E and F, see also H). In some sections, structures similar to spinules also displayed mGluR6-IR (G). SR: synaptic ribbon. Scale bars = 0.25 µm.

labeled (Figure 2.13c). In the neuropil of the OPL, HC profiles at the base of the cone pedicle showed strong mGluR6-IR (Figure 2.13d). Profiles belonging to this structure run into the cone pedicle. Based on their horizontal position we conclude that the mGluR6 reactive profiles belong to cone-driven HCs. No structures with cytology consistent with ON BC dendrites were labeled in the vicinity of the cone terminals.

Single-labeling experiments with the mGluR7 and mGluR8 antibodies (Figure 2.14) yielded some diffuse staining in the IPL. Occasionally, ACs and GCs were labeled (asterisks), but in both cases the OPL was devoid of labeling (arrowheads, compare with DAPI staining).

## 2.5 Discussion

*Appropriateness of the Antibodies*

For the kind of study presented here, techniques such as single-cell RT-PCR are more appropriate to determine protein expression in specific cell types. Unfortunately, however, sequence information for goldfish mGluRs is not available. We therefore performed Western blots of goldfish brain and retina and compared the results with those obtained in rat cerebrum (not shown). Although the antibodies did recognize bands at the right positions in goldfish brain and rat cerebrum, the bands obtained in goldfish retina were not comparable to them. This is probably due to the sensitivity of the technique: the concentration of these proteins in the fish retina is very low and confined to some hot spots; when homogenizing the whole retina, the signal is lost, and the final concentration in the gel is too low to yield a reliable result.

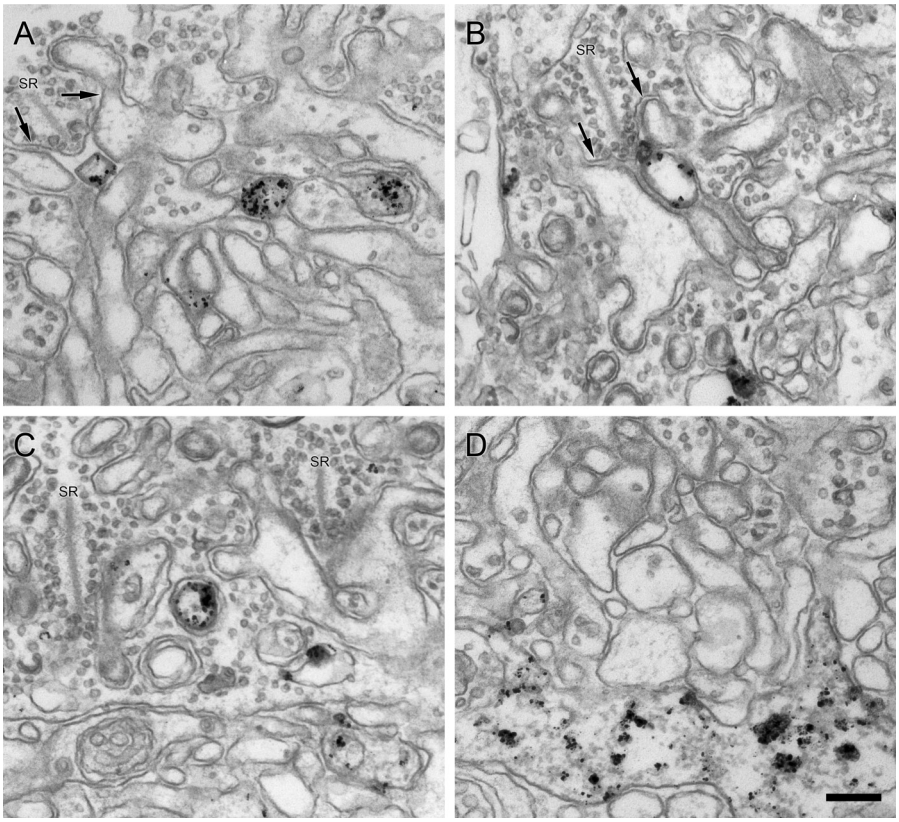


**Figure 2.13:** Ultrastructural localization of mGluR6 in the cone pedicle. A, B) Central elements with cytology consistent with HC dendrites were positive. Lateral processes were not labeled (arrows). C) A spinule showing mGluR6-IR. D) Processes in the neuropil with cytology similar to HC dendrites also displayed mGluR6-IR. SR: synaptic ribbon. Scale bar = 0.25 µm.

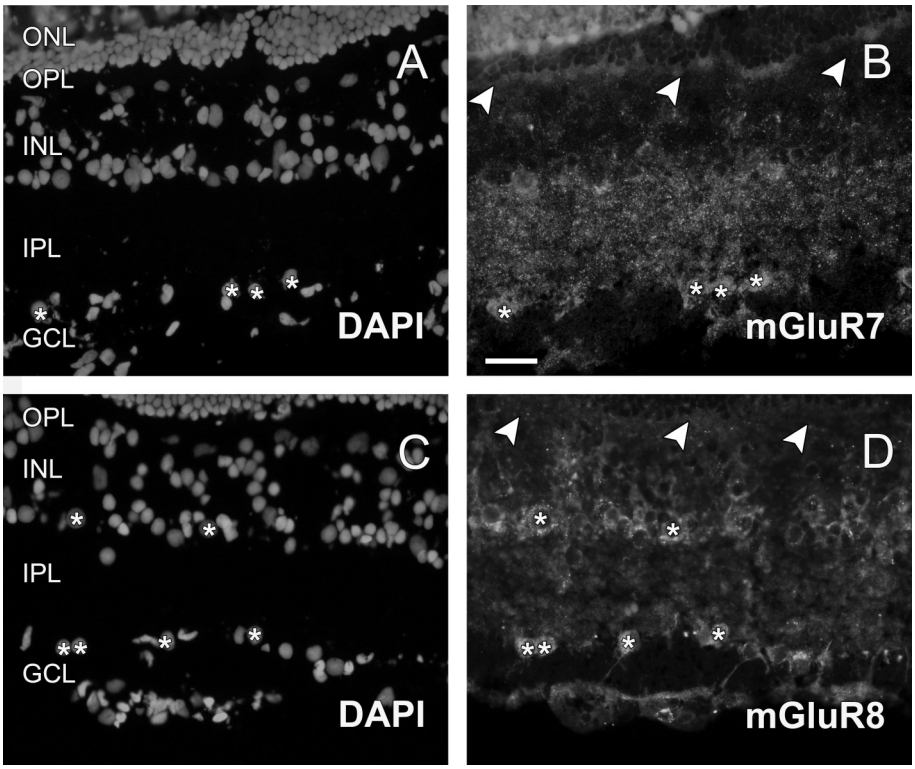


**Figure 2.14:** Immunoreactivity for mGluR7 and mGluR8. Blue- (A) and red- (B) channel images (presented in black and white) of the same tissue section that was double-labeled with the nuclear stain DAPI (A) and the mGluR7 antibody (Cy3, B). In addition to smooth mGluR7-IR in the IPL, some GC somata were faintly outlined (asterisks). The OPL was devoid of labeling (arrowheads). In (C) and (D), a similar pattern was found with the mGluR8 antibody. In addition to IPL and GC labeling, some AC somas were stained (asterisks). Scale bar = 10 µm.

Nonetheless, the very specific localization we found for the different mGluRs at light- and EM levels, combined with information obtained from other studies (i.e. Go$\alpha$ and mGluR6 colocalization in ON BCs: Zhang and Wu, 2003; PKC$\alpha$ and mGluR1$\alpha$ in mixed-input ON BCs of the goldfish: Klooster et al., 2001; evidence for a group III mGluRs in photoreceptor terminals: Koulen et al., 1999; Hirasawa et al., 2002; Hosoi et al., 2005) make us feel confident about the specificity of the antibodies used.

*Summarizing Scheme*

Figure 2.15 sums up the main findings of this Chapter. Briefly, both PKC$\alpha$ and Go$\alpha$ labeled invaginating dendrites of putative mixed-input ON BCs in he rod spherule. The mGluR1$\alpha$ and mGluR6 antibodies labeled similar structures; lateral elements

were also occasionally labeled. In the cone pedicles, PKCα labeled structures at the base of the terminal, whereas the Goα antibody labeled both invaginating dendrites and processes in the neuropil. Spinules were positive for mGluR1α and mGluR6, and lateral elements were labeled by the mGluR1α and mGluR2/3 antibodies. Finally, HC central elements were positive for mGluR2/3 and mGluR6. No structures resembling BC processes were stained with the mGluR antibodies in the cone pedicle.

*ON BC Markers*

The uniform labeling of mixed-input ON BCs yielded by the Goα antibody is in contrast to the restricted localization reported in mammals (Vardi, 1998). This homogeneous intracellular distribution might be a consequence of Goα subserving more than one function at different locations within the labeled cells. The immunoreactive bands in the IPL indicate that Goα is used by other cell types as well in the goldfish retina (probably ACs), in agreement with the descriptions in mammals (Vardi, 1998).

Although in the goldfish the antibodies against PKCα and Goα seem to label the same two cell populations at the light microscopical level (mixed-input and cone-driven ON BCs), there were unexpected differences in their ultrastructural localization in the cone pedicles. These discrepancies can be explained in two ways. The first possibility is that these antibodies are not labeling the same cell types. In fact, previous studies have shown that there are many different subtypes of mixed-input and cone-driven ON BCs in the goldfish (Stell, 1976/1978; Sherry and Yazulla, 1993), which are not readily discriminable in our preparations. The second possibility is that PKCα may have a more compartmentalized localization within the labeled cells as compared to Goα, which would give rise to the different patterns seen at the EM level. PKC is known to be transported to different locations of the mixed-input BCs of the goldfish (Vaquero et al., 1997) and rod BCs of the rabbit and rat retinas (Osborne et al., 1991), depending on the adaptive state of the retina (Vaquero et al., 1997).

*mGluRs of ON BCs*

The staining of BCs by the mGluR6 antibody at the light microscopical level is in agreement with work on the catfish (Gafka et al., 1999) and mammalian retinas (Masu et al., 1995; Vardi et al., 2000). In the latter, however, mGluR6 is concentrated in the dendritic compartment and somatic labeling is fainter (Kamphuis et al., 2003). The presence of mGluR6 also in the axon terminals of mixed-input ON BCs raises the possibility that mGluR6 has multiple functions in these cells. At least in the salamander retina, group III mGluRs were implicated in modulating the glutamate release of ON BCs (Awatramani and Slaughter, 2001; but see Higgs et al., 2002). That Goα is also found at the axon terminal indicates that it may couple to mGluR6 in this compartment as well.

The localization of mGluR6 to the dendrites of mixed-input ON BCs in the rod spherules of the goldfish retina was already expected, given the data on the

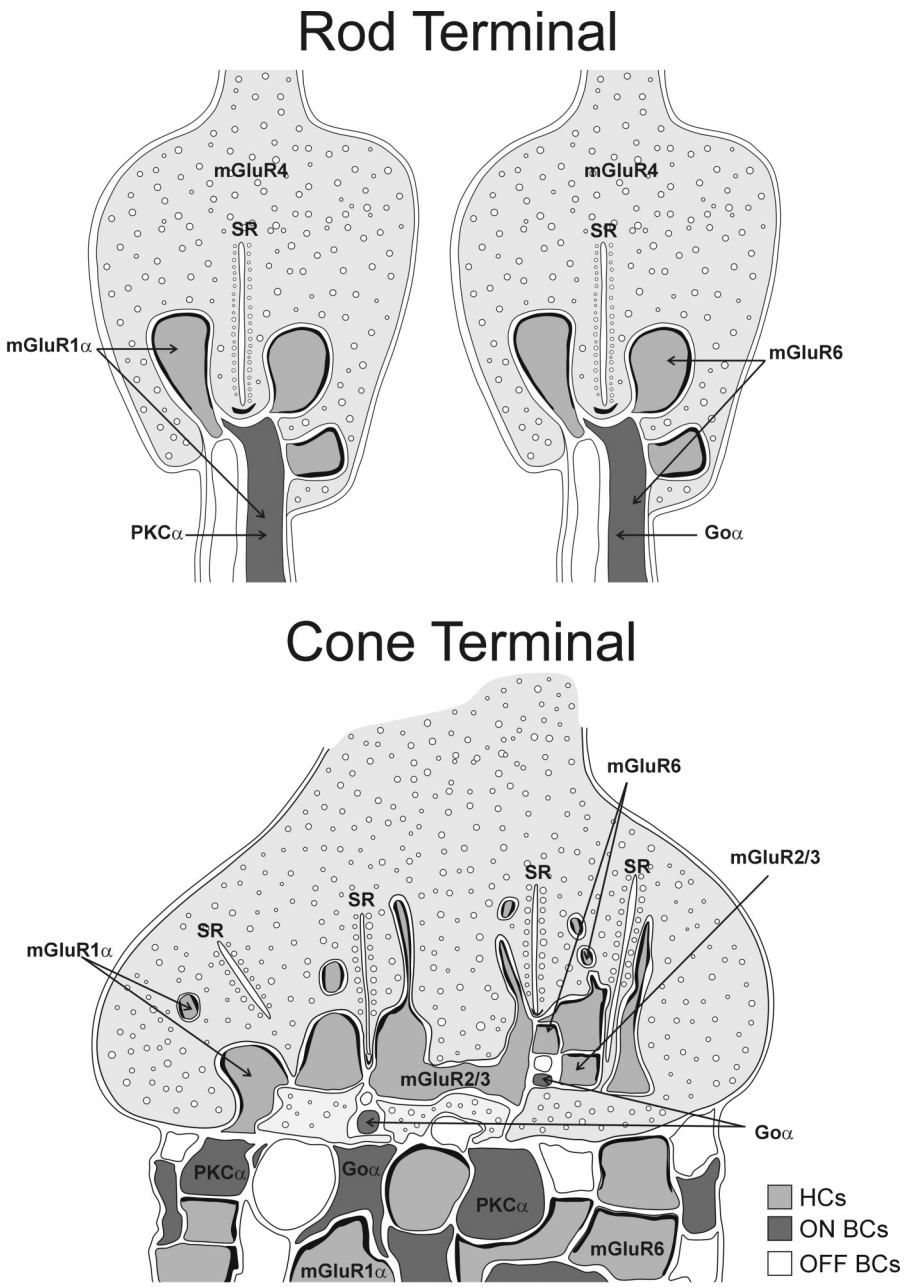


**Figure 2.15:** Summary diagram of a rod spherule and of a cone pedicle, depicting the localization of PKCa, Goα, and the different mGluRs found in the photoreceptor terminals (mGluR1α, mGluR2/3, mGluR4 and mGluR6).

involvement of a group III mGluR in the generation of rod-driven light responses of ON BCs in fish (Shiells et al., 1981; Nawy and Copenhagen, 1987; Nawy et al., 1989; Wong et al., 2005b; this thesis, Chapters 3 and 5) and the localization of mGluR6 in rod-driven BCs of a number of species (Nakajima et al., 1993; Akazawa et al., 1994; Masu et al., 1995; Laurie et al., 1997; Ueda et al., 1997; Vardi and Morigiwa, 1997; Vardi et al., 2000).

Since the light-driven mGluR6 cascade in ON BCs seems to be linked to Go$\alpha$ (Vardi, 1998; Nawy, 1999; Dhingra et al., 2000/2002), we had expected that the mGluR6 antibody would yield a similar pattern of immunoreactivity as Go$\alpha$ in the cone pedicle, and label dendrites of cone-driven ON BCs. That this was not the case indicates that the post-synaptic Go$\alpha$ immunolabeling in the cone pedicle may not be directly related to the depolarizing light responses of these BCs. Cone-driven light responses in both mixed-input and cone-driven ON BCs of fish are thought to be driven by another type of receptor, which modulates a conductance carried by either $K^+$ or $Cl^-$ (Saito et al., 1978/1979/1981; Grant and Dowling, 1995/1996; this thesis, Chapters 3 and 5). Since we did not find evidence for any of the mGluRs tested (mGluR1$\alpha$, mGluR2/3, mGluR4, mGluR5, mGluR6, mGluR7 and mGluR8) in the dendrites of cone-driven ON BCs, the question remains as to which receptor is linked to Go$\alpha$ in these cells and what is its function.

The labeling of mixed-input ON BC processes in the rod spherule with the antibody against mGluR1$\alpha$ corroborates previous findings in the rat (Koulen et al., 1997; Cai and Pourcho, 1999), catfish (Gafka et al., 1999) and goldfish (Klooster et al., 2001). This pattern is somewhat distinct from the one described for cat retina, in which mGluR1$\alpha$ is pre-synaptic to rod-driven BCs (Cai and Pourcho, 1999). Since there is as yet no evidence for a participation of mGluR1$\alpha$ in the generation of the light responses of ON BCs, one can only speculate that mGluR1$\alpha$ might play a modulatory role in the light-driven conductance.

Nonetheless, the presence of mGluR1$\alpha$ in mixed-input ON BCs of the goldfish indicates that either these cells possess a second G-protein that subserves mGluR1$\alpha$ signaling, or that both mGluR6 and mGluR1$\alpha$ signal through Go$\alpha$. To date, the only G protein found immunocytochemically in ON BCs is Go$\alpha$ (Vardi et al., 1993), but this does not mean that it is the only one. Alternatively, mGluR1$\alpha$ could signal through a G-protein-independent pathway (Brakeman et al., 1997; Kato et al., 1998; Tu et al., 1998; Heuss and Gerber, 2000). Further studies on the localization of other putative mGluR-binding proteins in the retina are necessary to test these possibilities.

*mGluRs of HCs*

Here we show that rod and cone-driven HCs of the goldfish present a myriad of mGluRs, although the exact mGluR composition of these cells differs somewhat from reports in other species (i.e. no mGluR1$\alpha$ in cat HCs: Cai and Pourcho, 1999; no mGluR2/3 in catfish HCs: Gafka et al., 1999; no mGluR6 in rat or monkey HCs: Vardi et al., 1998).

Rod-driven HCs were positively labeled for both mGluR1α and mGluR6, although the labeling was quite rare. In the cone pedicle, mGluRs seemed to be expressed in a non-random manner. Group I receptors (mGluR1α) tended to be localized to dendrites occupying the lateral position in the cone triad and to spinules; group II receptors (mGluR2/3) were found at both lateral and central processes directly opposing the synaptic ribbon, and group III receptors (mGluR6) were most frequently associated to spinules and central elements.

This highly organized pattern indicates that either a single cone-driven HC type expresses distinct mGluRs in different dendrites, or that the expression of a given mGluR is restricted to a certain population of HCs. In some cyprinid retinae, three physiological and morphological HC types were described (MacNichol and Svaetichin, 1958; Norton et al., 1968); one could easily imagine that each HC class could express only one or two mGluRs at their dendritic tips. In this case, this type-specific expression would be reflected in the selectivity of mGluR-IR observed at the EM level. This seems plausible, given the fact that rod-driven HCs, which comprise a single cell class (Stell, 1967; Kaneko, 1987), express only two types of mGluR (mGluR1α and mGluR6). Nonetheless, the possibility of selective expression of mGluRs in different dendrites of the same cell cannot be completely ruled out. As shown in the case of rod-driven HCs processes, immunoreactivity for mGluR1α and mGluR6 (when present) was confined to one lateral process only, indicating that these cells do not express mGluRs in all of their dendrites arbitrarily.

The absence of labeling for Goα in HC dendrites indicates that other G-proteins (or other mGluR-binding molecules, as discussed previously) may couple these receptors to their intracellular targets. Since the light responses of HCs are mediated by AMPA/KA receptors (Lasater and Dowling, 1982; Slaughter and Miller, 1983; Zhou et al., 1993) and are not abolished by mGluR agonists or antagonists (Yang and Wu, 1989, Luo and Liang, 2003, this thesis, Chapter 6), it is likely that these mGluRs are involved in the modulation of other aspects of HC physiology. Agonists for mGluRs were shown to modify HC electrical coupling (Dong and McReynolds, 1989; Djamgoz et al., 1998), as well as the light-modulated (Nawy et al., 1989; Takahashi and Copenhagen, 1992) and voltage-gated conductances (Gafka et al., 1999; Linn and Gafka, 1999).

*mGluRs In Photoreceptor Terminals*

The pre-synaptic localization of a group III mGluR is not surprising. In many parts of the central nervous system, mGluRs are involved in pre-synaptic modulation of neurotransmitter release (Takahashi et al., 1996; Wu and Saggau, 1997; Cochilla and Alford, 1998; Anwyl, 1999). In the cerebellum, pre-synaptic modulation of glutamate release via mGluR4 was found (Daniel and Crepel, 2001). In the rat retina, activation of mGluR8 at the cone pedicles leads to a decrease in glutamate release (Brandstätter et al., 1998; Koulen et al., 1999). A similar mechanism was reported in the carp (Hirasawa et al., 2002) and in the newt (Hosoi et al., 2005)

retinas, although the identity of the pre-synaptic group III mGluR is not known. We only found mGluR4 at the rod spherule, where it could also be modulating glutamate release (but see General Discussion). Since we did not investigate the localization of all group III mGluRs, the system described by the later group in cyprinid cones might be subserved by either mGluR7 or mGluR8. In any case, also here the G-protein linked to these receptors is unknown.

*Consequences for the Interpretation of Pharmacological Experiments*
Much of what we know about outer retinal physiology comes from pharmacological studies. However, the specificity of the available drugs imposes serious constraints to the investigation of mGluR function. The findings described here indicate that drugs that act on either mGluRs or their G-proteins may yield results of difficult interpretation, due to the widespread localization of group I, II and III mGluRs in the outer retina. With the exception of specific group II agonists or antagonists (which will only act at cone-driven HCs) extracellular application of any substance directed against mGluRs or G protein function will act at more than one level.

Intracellularly targeting these molecules might also produce confusing outcomes, since in a given cell type the same mGluR might play distinct roles at different compartments (i.e. mGluR6 at the dendrites and axon terminals of mixed-input ON BCs), or different mGluRs might share the same compartment and perhaps even part of the same intracellular cascade (i.e. mGluR1$\alpha$ and mGluR6 at the dendrites of mixed-input BCs). Before the physiological roles of the distinct mGluR types in outer retinal neurons can be pharmacologically disentangled, there needs to be substantial improvement in the pharmacological tools and molecular biological information available to perform such a task. Until then, the combination of morphological, biophysical and pharmacological experiments, as presented in this thesis, is indispensable to understand the function of these receptors.

**Acknowledgements**

The authors would like to thank Dr. Willem Kamphuis for reading an early version of this manuscript, Dr. Stephen Yazulla and Dr. Keith Studholme for helpful comments on the figures, Dr. Bob Nunes-Cardozo for the confocal pictures and Ton Put for preparing the photographs.

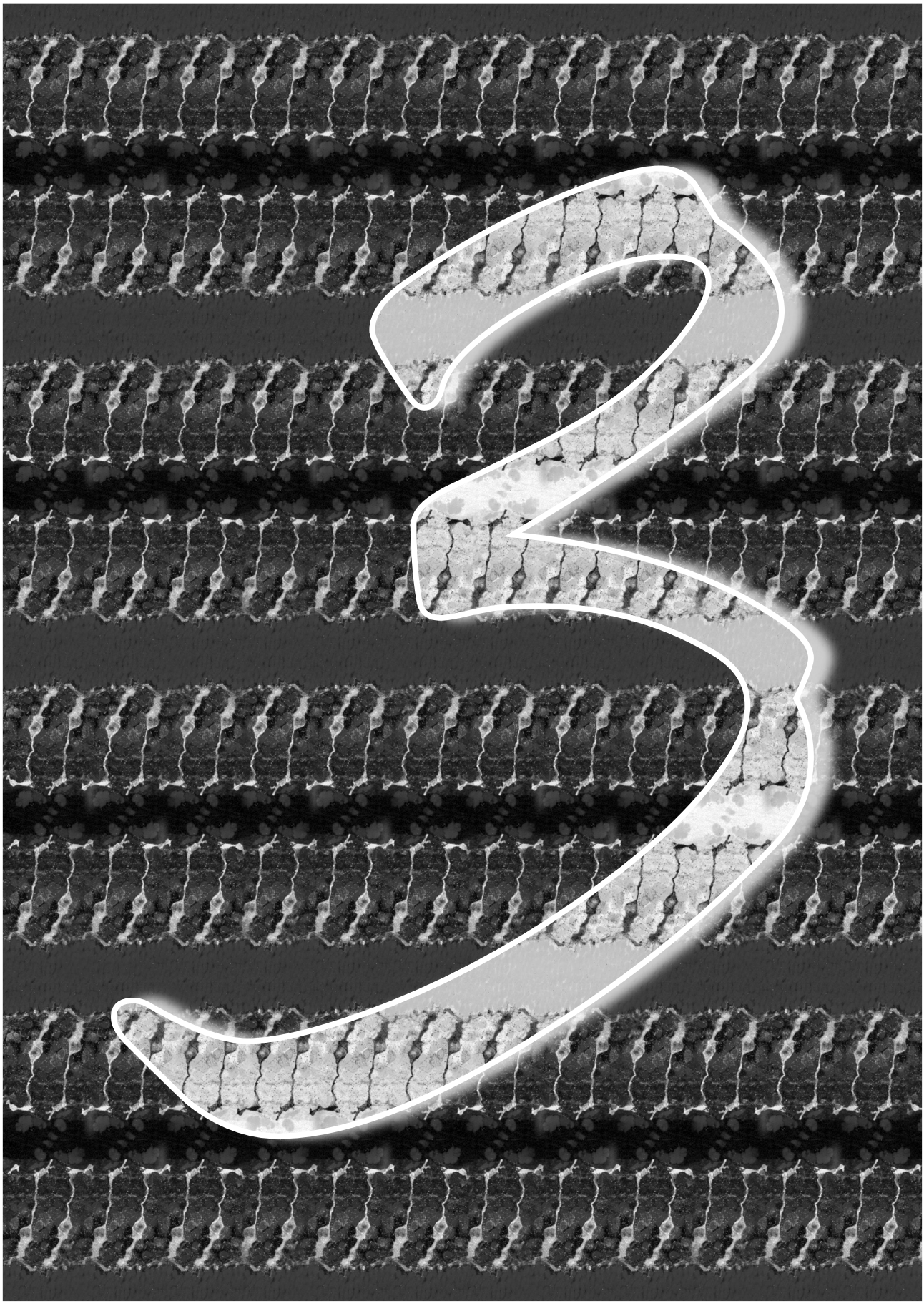

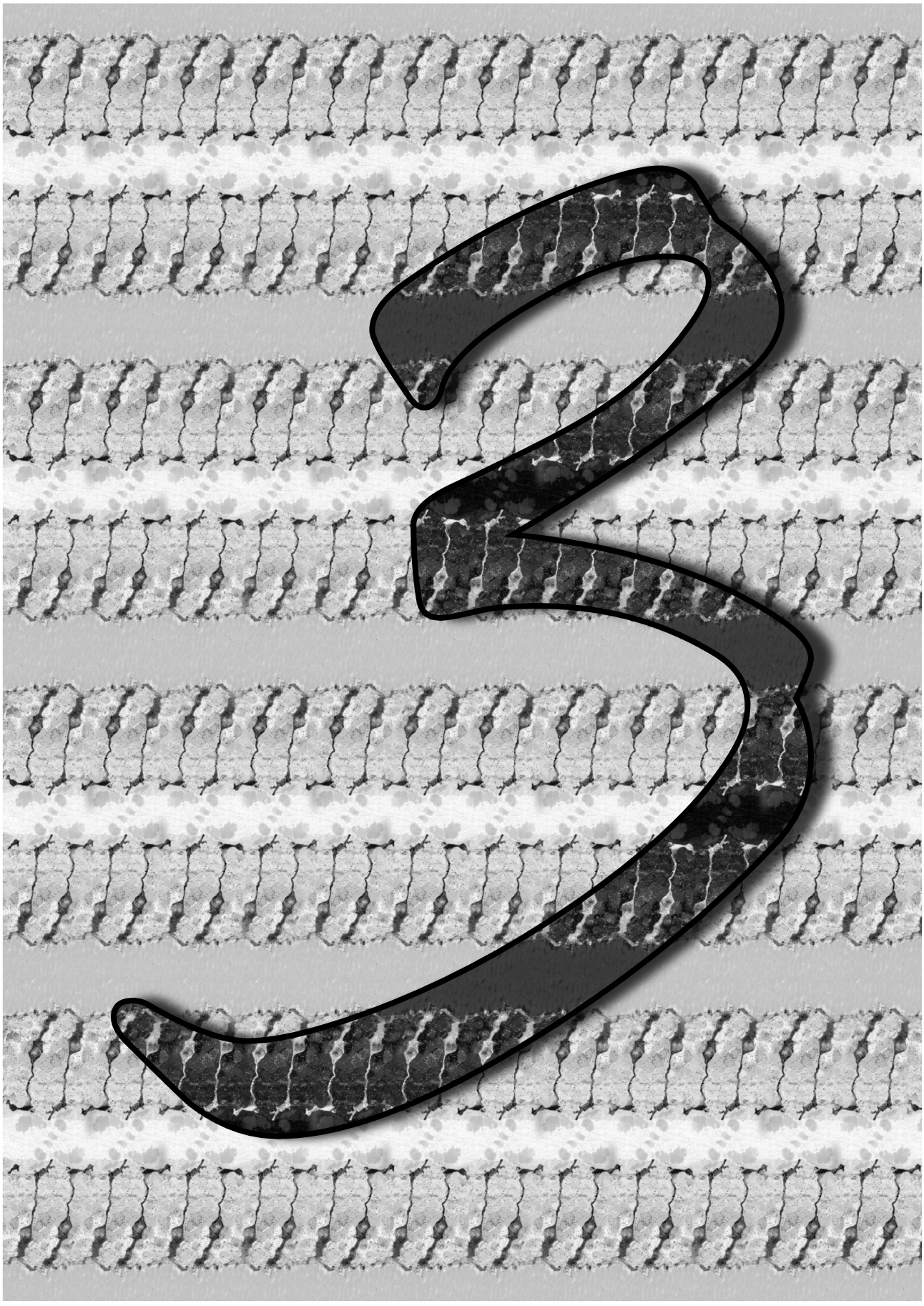

# Chapter 3

# Properties of the Mixed-Input Bipolar Cell Syncytium in the Goldfish Retinal Slice

*Christina Joselevitch and Maarten Kamermans*
*(To be submitted)*

## 3.1 Abstract

In the dark-adapted retina, mixed-input ON and OFF BCs of the goldfish lack a pronounced center-surround organization. Instead, their receptive fields present considerable spatial summation, which cannot be explained by lateral integration at the photoreceptor layer. Here we show by means of current- and voltage-clamp recordings under different pharmacological conditions that the large receptive field centers of these cells are a result of electrical coupling between neighboring BCs. As a consequence of this coupling, both rod- and cone-driven light responses are less sensitive to spatially small stimulation that does not cover the whole receptive field center than to full-field stimuli. Additionally, electrical coupling decreases the input resistance ($R_{in}$) of the cells, limits dialysis with the pipette solution and shifts the measured reversal potentials of synaptic conductances. The site of coupling is probably the dendrites, since similar results were obtained from intact and axotomized cells. Our results show that the gap junctions between BCs are not permeable to Lucifer Yellow and do not seem to be affected by commonly used gap junction blockers, which rules out some connexin types. Signal spread in the BC layer diminishes sensitivity to small stimuli, but increases signal-to-noise ratio. Since photoreceptor convergence to fish BCs is one order of magnitude larger than in mammalian retinas, syncytial integration at the BC level could help retain light sensitivity gained through convergence by removing the noise amplification generated by the sum of converging inputs.

## 3.2 Introduction

Bipolar cells are the link between the outer and the inner retina. Because their input forms the receptive field centers of GCs, their organization, glutamate receptor composition and response properties are critical for shaping the output of the eye. The receptive fields of BCs in the light-adapted retina comprise two concentric circles: a central zone, which originates from direct photoreceptor inputs (Werblin and Dowling, 1969; Kaneko, 1970,1973), and a much larger inhibitory zone,

which arises from interactions between the HC syncytium and the photoreceptors (Naka and Nye, 1971; Naka and Witkovsky, 1972; Werblin, 1974).

In the dark-adapted retina, the receptive field of BCs was reported to lack such an inhibitory surround in many species (Ashmore and Falk, 1980; Borges and Wilson, 1987; Belgum and Copenhagen, 1988; Yamada and Saito, 1997). A main difference between the light- and dark-adapted states resides in changes in the dopamine concentration; dopamine levels are supposed to be higher in the light-adapted state (Dowling and Ehinger, 1978; Dowling, 1986; Weiler et al., 1989; Dong and McReynolds, 1991). However, there is also evidence that in the OPL dopamine levels are high in the dark-adapted state (Tornqvist et al., 1988; Yang et al., 1988a/b). Dopamine was shown to abolish the antagonistic surround of BC receptive fields (Hedden and Dowling, 1978; Yamada and Saito, 1988), indicating that its levels may change locally in physiological conditions, or that bath application of dopamine might have different effects according to the adaptive state of the retina.

The center of the BC receptive field is assumed to have the diameter of the light spot that elicits the biggest light response, as shown in Figure 1.6a (Kaneko, 1973; Saito and Kujiraoka, 1982,1988). Estimates of its size by physiological methods, however, yield values up to an order of magnitude larger than the diameter of the dendritic BC arbors determined morphologically (Kaneko, 1973; Saito and Kujiraoka, 1982; Borges and Wilson, 1987; Saito and Kujiraoka, 1988; Yamada and Saito, 1988; Hare and Owen, 1990).

This discrepancy was attributed to electrical coupling between homologous BC types in the carp (Kujiraoka and Saito, 1986; Umino et al., 1994; Yamada and Saito, 1997), dace (Umino et al., 1994) and salamander (Borges and Wilson, 1987; Hare and Owen, 1990), since signal spread in the photoreceptor layer is not large enough to produce such wide receptive field centers (Baylor and Fuortes, 1970; Baylor et al., 1971; Copenhagen and Owen, 1976; Fain et al., 1976; Detwiler and Hodgkin, 1979; Witkovsky et al., 1979). The finding of tracer coupling (Saito and Kujiraoka, 1988; Umino et al., 1994) and the direct observation of gap junctions between BC dendrites in the OPL of the carp (Cuenca et al., 1993) confirmed that electrical coupling plays a prominent role in determining the size of BC receptive field centers.

While dopamine changes electrical coupling in some HC types (Teranishi et al., 1983; Piccolino et al., 1984; Lasater and Dowling, 1985; Mangel and Dowling, 1985) and photoreceptors (Copenhagen and Green, 1987; Krizaj et al., 1998; Ribelayga et al., 2002), it has no effect on the length constant of BC receptive field centers (Hedden and Dowling, 1978; Yamada and Saito, 1988). This indicates that the gap junctions between BCs are of a different nature than those responsible for electrotonic communication within the photoreceptor and HC networks, and that electrical coupling determines the size of BC receptive field centers.

The aim of the present study was to investigate whether mixed-input BCs in the dark-adapted goldfish retinal slice are also electrically coupled, to which extent

this electrical coupling determines their response properties, and which connexins could be forming gap junctions between goldfish mixed-input BCs. We will show that electrical coupling causes an apparent decrease in sensitivity to spatially small stimulation when there is stray light, decreases the input resistance of BCs recorded *in situ*, reduces the efficiency of dialysis by the pipette solution, and leads to a small shift in the measured reversal potential of the light responses. The electrical coupling between BCs does not seem to be changed by commonly used gap junction modulators, indicating that the connexins involved in this process might be of a special kind.

### 3.3 Material and Methods

*Preparation*
All animal experiments were carried out under the responsibility of the ethical committee of the Royal Netherlands Academy of Arts and Sciences, acting in accordance with the European Communities Council Directive of 24 November 1986 (86/609/EEC). Goldfish (*Carassius auratus)* of 10-15 cm standard body length were kept in aquaria at 18 °C in a 12 h / 12 h light-dark period. The technique used to prepare retinal slices is a modification of the method described elsewhere (Werblin, 1978). Animals in the light phase of their circadian rhythm were dark-adapted for 5-10 minutes prior to decapitation, and one eye was enucleated under infrared illumination ($\lambda$ > 850 nm). The anterior segment of the eye was removed; the retina was peeled off the pigment epithelium and sclera, and placed receptor-side-up onto a piece of filter paper (Millipore, 13 mm diameter, 8 $\mu$m pore size). Vacuum was applied to the other side of the filter, in order to suck away the vitreous and attach the isolated retina firmly to the paper. The retina and the filter were cut in slices (100-150 µm thick) that were subsequently positioned on vaseline tracks in a superfusion chamber.

*Solutions*
The composition of the Ringer's solution was (in mM): 102 NaCl, 2.6 KCl, 1 $CaCl_2$, 1 $MgCl_2$, 28 $NaHCO_3$ and 5 glucose (bubbled continuously with 2.5% $CO_2$ and 97.5% $O_2$ for a pH of 7.8, approx. 248 mOsm). In some experiments, bicuculline methobromide (BIC), picrotoxin (PTX), strychnine (STRY) or 6,7-dinitroquinoxaline-2,3(1H,4H)-dione (DNQX) were added to the control solution in order to block all GABAergic and glycinergic inputs to the BCs. The drug content of the Ringer's solution and the composition of the intracellular solution are given in Table 3.1. Junction potentials for each pipette solution were calculated after Barry and Lynch (1991) and Ng and Barry (1995), and subtracted from the nominal voltage command values before correction for series resistance (see *Data Analysis* section). All chemicals were supplied by Sigma (The Netherlands).

| | Figures | | | | | | | | | | | |
|---|---|---|---|---|---|---|---|---|---|---|---|---|
| | **3.1a** | **3.1b** | **3.2** | **3.3a** | **3.3b** | **3.3b** | **3.3c** | **3.3d** | **3.4** | **3.7b** | **3.8** | **3.9** |
| **Solutions** | ON BC | OFF BC | ON BC | Cone | Rod HC | Cone HC | ON BC | OFF BC | ON BC | ON BC | ON BC | ON BC |
| *KOH* | 18 | 17 | 17 | 12 | | | 16 | 17 | 17 | | | |
| *CsOH* | | | | | 19 | 18 | | | | 24 | 20 | 16 |
| *NaCl* | | | | | 35 | | 34 | | | | | 34 |
| *KCl* | 15 | 10 | 46 | 11 | | | | 10 | 50 | | | |
| *CsCl* | | | | | 5 | 93 | 5 | | | 47 | 15 | 5 |
| *KGlu* | | | | 95 | | | | 60 | | | | |
| $CH_3O_3SCs$ | | | | | | | | | | 8 | | |
| *KF* | 55 | 55 | 24 | | | | | | 20 | | | |
| $MgCl_2$ | | | 1 | 1 | | | | | | 1 | | |
| $CaCl_2$ | | | 0.1 | | 0.1 | | 0.1 | | | 0.1 | | 0.1 |
| *TEACl* | | | | | 20 | | 20 | | | | 25 | 20 |
| *EGTA* | | | | 5 | | | | | | | | |
| *HEPES* | | | | 5 | | | | | | 10 | 10 | |
| *ATP-Mg* | | | | | | | | | | | 10 | |
| $ATP\text{-}Na_2$ | | | | | 10 | | 10 | | | | | 10 |
| $ATP\text{-}K_2$ | 10 | 10 | 10 | 4 | | 10 | | 10 | 10 | 10 | | |
| $BAPTA\text{-}Na_4$ | | | | | 10 | | 10 | | | | | 10 |
| $BAPTA\text{-}k_4$ | 10 | 10 | 10 | | | 10 | | 5 | 10 | 10 | 10 | |
| *GTP-Na* | 1 | 1 | 1 | 1 | 1 | 2 | 1 | 1 | 1 | 2 | 1 | 1 |
| *cAMP* | | | | | | | | 1 | | 1 | | |
| *cGMP-Na* | 1 | 1 | 1 | 0.2 | 1 | 1 | 1 | 2 | 1 | 1 | 1 | 1 |
| $PC\text{-}Na_2$ | | | | 20 | | | | | 40 | | | |
| *CK* | | | | 494 U | | | | | 989 U | | | |
| $LY\text{-}K_2$ | 1 | 1 | 1 | | 1 | 1 | 1 | 1 | 1 | 1 | 1 | 1 |
| *[mOsm]* | 223 | 187 | 218 | 284 | 208 | 266 | 200 | 205 | 316 | 222 | 175 | 200 |
| *BIC* | | | | | | 200 | | | | 200 | | |
| *PTX* | | | | | 500 | 500 | 500 | 500 | 100 | 500 | 500 | 500 |
| *STRY* | | | | | 18 | 5 | 18 | 5 | 5 | 5 | 10 | 18 |
| *DNQX* | 50 | | | | | | 50 | | | | 100 | 50 |
| *DL-AP4* | | | | | 250 | | | | 20 | 250 | | |

**Table 3.1:** Composition (in mM) and osmolarity (in mOsm) of the intracellular solutions used to record from the cells shown in the different Figures, as well as drug content of the Ringer's solution (in μM) in each experiment. KGlu:D-gluconic acid; TEA: tetraethylammonium; PC: phosphocreatine; CK: creatine phosphokinase; LY: Lucifer Yellow; PTX: picrotoxin; BIC: bicuculline methobromide; STRY: strychnine; DNQX: 6,7-dinitroquinoxaline-2,3(1H,4H)-dione; DL-AP4: (±)-2-amino-4-phosphonobutyric acid.

*Optical Stimulator*

The superfusion chamber was mounted on a microscope equipped with infrared ($\lambda$ > 800 nm) differential interference contrast optics (NIKON Eclipse E600-FN, Japan) and the preparation was viewed in a TV monitor by means a 60 x water-immersion objective (N.A. 1.0) and a CCD camera (Philips, The Netherlands).

Two light beams originated from one xenon arc and were separated with a beam splitter (Starna, UK). All set-up configurations were calibrated carefully with a radiometer (Tektronix, 50-245, irradiance head J1812, UK), and later with a photodiode (Siemens BPW34, Germany) and by means of measurements of cone light responses to stimulation originating from both channels. Both light beams passed through a series of neutral density filters (Schott, Germany), double interference filters (Melles Griot, The Netherlands, peak transmission $\lambda_s$ = 400, 450, 500, 550, 600, 650, 700 nm, 8 nm bandwidth), and circular neutral density wedges (Barr & Strout, UK).

Light stimuli were cast onto the retina via two different optical paths: one light channel was focused through the objective by means of mirrors and lenses and could project small stimuli (slits of 50, 100 and 250 $\mu$m interposed on the optical path) onto the preparation; the second channel projected a 3.5 cm field (referred to from now on as “full field”) through the microscope condensor. In the isolated retina, one uses spots of light to test the receptive field center of cells with center-surround organization. In slice preparations, light slits directed perpendicularly to the orientation of the slice are equivalent to light spots projected on the photoreceptor side of the retina. The width of the slit on a slice preparation is thus equivalent to the diameter of a spot onto an isolated retina. Given the dimensions of the preparation, the effective diameter of the full field was equivalent to the width of the slices (3-6 mm). Absolute intensity values are given throughout the paper in log quanta$\cdot\mu m^{-2}\cdot s^{-1}$.

*Electrodes and Recording Set-up*

Patch pipettes were pulled from borosilicate capillaries (Harvard Apparatus Ltd., UK) with a Brown Flaming Puller (Sutter Instruments, Novato, California) and had impedances between 5 and 15 M$\Omega$ when filled with pipette solution and measured in Ringer’s solution. Series resistances ranged from 6 to 33 M$\Omega$ and were corrected for offline (see next section).

Electrodes were placed in a PCS-5000 micromanipulator (Burleigh Instruments, Inc., Fishers, New York) and connected to an Axopatch 200 Patch Clamp (Axon Instruments, Inc., Union City, California). Data acquisition and control of the optical stimulator were made by means of a CED 1401 AD/DA converter (Cambridge Electronic Design Limited, UK) and an MS-DOS-based computer system.

Recordings were done in both current-clamp and voltage-clamp modes. For current-clamp measurements, $I_{hold}$ = 0 pA, and for voltage-clamp recordings, $V_{hold}$ = -50 mV, unless otherwise stated.

*Data Analysis*

Analyses of current transients were used to calculate the series resistances and the input resistances of the cells. Current relaxations to -10 mV voltage steps from a holding potential of -70 mV for 80 ms were subtracted from the holding current and fit by biexponential functions of the form

$$A_{(t)} = A_0 + A_1 \cdot e^{-t/\tau_1} + A_2 \cdot e^{-t/\tau_2},$$

where $A_0$ is the amplitude of the steady-state current at the end of the voltage step, $A_1$ and $A_2$ are the amplitudes of the two exponentials at the instant of voltage change, and $\tau_1$ and $\tau_2$ are the corresponding time constants of the current decay towards $A_0$. This approach was used because the current relaxations did not follow a monoexponential course (for a detailed explanation of the method and its application, see Mennerick et al., 1997, and Nadeau and Lester, 2000). Fits begun 35-45 µs after the voltage change to avoid contamination by residual system filtering, and extrapolated back to the onset of the voltage step in order to estimate the instantaneous current ($A_0$+$A_1$+$A_2$). The calculated curves were subtracted from the data and the residual plots were used to control the quality of the fits (Ellis and Duggleby, 1978; Mennerick et al., 1997).

Series resistances were then calculated using the equation (Nadeau and Lester, 2000)

$$R_{\text{series}} = \left( \frac{V_{\text{step}}}{A_0 + A_1 + A_2} \right),$$

where $R_{\text{series}}$ is the series resistance, and $V_{\text{step}}$ is the applied voltage clamp step. The voltage error for each recording was calculated offline according to the formula

$$V_{\text{error}} = R_{\text{series}} \cdot A_0,$$

and subtracted from the nominal command voltages subsequently. Input resistances were estimated using the equation

$$R_{\text{in}} = \left( \frac{V_{\text{step}}}{A_0} \right) - R_{\text{series}}.$$

Light responses were measured at the peak. Response amplitudes were plotted against stimulus intensity (intensity-response relations). Data points were fitted with Hill functions,

$$Y = Y_{\text{max}} \cdot \left( \frac{X^n}{X^n + K^n} \right),$$

where $Y$ is the response amplitude, $Y_{\text{max}}$ is the maximal response amplitude, $X$ is the stimulus intensity, $K$ is the stimulus intensity needed to generate a response with half-maximal amplitude, and $n$ is the slope factor.

The sensitivity of a cell was defined as the inverse of the intensity needed

for a half-maximal response amplitude (log $K^{-1}$). To isolate rod and cone inputs, BC light and spectral sensitivities were determined by comparing the log *K* values of the intensity-response relations to stimulation at 450, 550 and 650 nm. Statistical analysis (ANOVA and two-tailed Student's t-tests) was performed on raw data, and the results are expressed as mean ± SD.

## 3.4 Results

Mixed-input BCs were visually selected based on their characteristic morphology and position in the outer part of the INL (Stell, 1976). Cell type was confirmed by filling the cells with the fluorescent dye Lucifer Yellow (LY) and observing the fluorescence immediately after the experiment. Data from both intact and axotomized neurons were used. Unless otherwise stated, at least three cells yielded similar results for each experiment reported in the following sections.

*Receptive Fields Centers of Mixed-Input BCs are Large*

Although we never observed dye coupling in any of the mixed-input BCs we recorded from, their light responses to full-field stimulation are always larger than the responses to small stimuli (Figure 3.1). Since the dendritic trees of the different kinds of mixed-input BCs of the goldfish were reported to be much smaller than the stimuli we used (measurements of the dendritic properties of goldfish mixed-input BCs are given in Table 3.2), one can explain their large receptive field centers by either electrical coupling at the photoreceptor level or by coupling between BCs themselves.

In order to get an estimate of the size of the BC receptive field centers in the dark-adapted goldfish retinal slice, we tested ON BCs with stimuli of increasing diameters (an example is given in Figure 3.2 for stimulation at 450 nm, 550 nm

| BC type | Average dendritic field dimensions (µm) | Average number of receptors per BC | | | Total rod-BC junctional area (µm² per BC) |
|---|---|---|---|---|---|
| | | L-cones | M-cones | Rods | |
| *Ma1* | 65x23 | 11.4 | 0 | 25 | 1.3. |
| *Ma2* | 43x36 | 7.3 | 4.8 | 20 | 0.4 |
| *Mb1* | 41x30 | 8.3 | 0 | 218 | 139.0 |
| *Mb2* | 55x48 | 9.7 | 8.0 | 223 | 306 |
| *Mb3* | 104x71 | 35.0 | 22.5 | 100 | 1.8 |

**Table 3.2:** Dendritic properties of mixed-input BCs in the goldfish retina. The dendritic arbors of mixed-input BCs in the goldfish retina are much smaller than some of our stimuli, even when one corrects for 10-20 % linear shrinkage. Ma: mixed-input BC terminating in *sublamina a* of the IPL (putative OFF BC); Mb: mixed-input BC terminating in *sublamina b* of the IPL (putative ON BC). Source: Stell (1978).

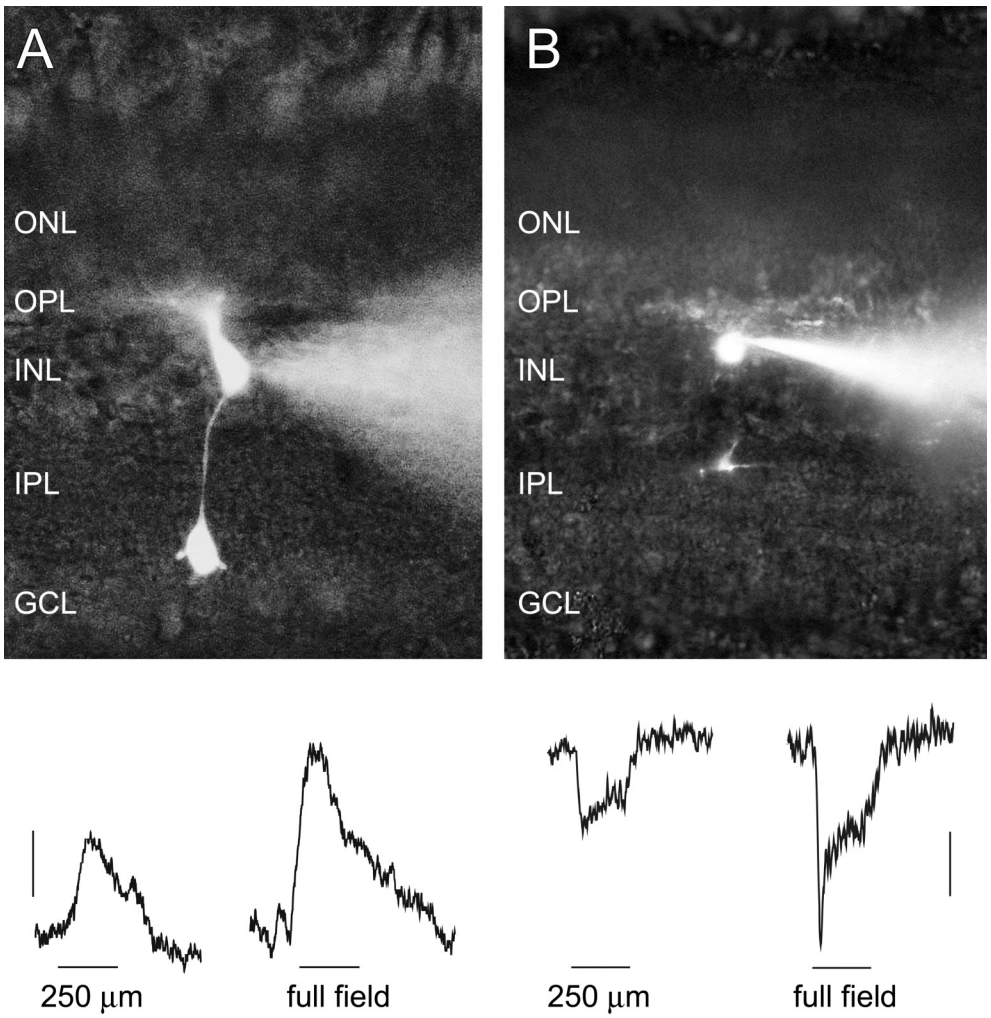


**Figure 3.1:** Mixed-Input BCs of the goldfish show no dye coupling, but have large receptive field centers. A) Top: Fluorescence micrograph of a recorded mixed-input ON BC filled with LY, still attached to the patch pipette. The dye did not diffuse to neighboring cells, indicating that either this cell is not electrically coupled, or that the gap junctions between this BC and its neighbors are not permeable to LY. Bottom: Light responses of the same cell to a 250 µm slit and to a full field at 550 nm and similar intensities (-0.44 and -0.68 log, respectively). The response to full-field stimulation is bigger, indicating that the receptive field center of this cell is larger than 250 µm. Horizontal bars indicate stimulus timing (500 ms), vertical bar = 2 mV. B) Top: Fluorescence micrograph of a recorded mixed-input OFF BC filled with LY and still attached to the recording electrode. Also in this case there was no dye coupling. Bottom: Light responses of the same cell to a 250 µm slit and to a full field at 550 nm and similar intensities (-0.11 log and -0.01 log, respectively). The response to full-field stimulation is bigger, indicating that the receptive field center of this cell is larger than 250 µm. Horizontal bars indicate stimulus timing (500 ms), vertical bar = 4 mV. ONL: outer nuclear layer; OPL: outer plexiform layer; INL: inner nuclear layer; IPL: inner plexiform layer; GCL: ganglion cell layer.

and 650 nm). With this stimulus paradigm, light responses increased linearly with stimulus size up to about 250 µm, but tended to level off for full-field stimulation. This indicates that the receptive field centers are not as large as the maximum stimulus diameter, although considerable spatial summation takes place. We did not find evidence of a center-surround organization in our stimulus conditions (compare Figure 3.2 with Figure 1.6a).

Although length constants measured in retinal slices cannot be directly compared to those in isolated retinas due to the fact that the slicing procedure removes part of the receptive fields of the cells measured, they do serve as an indication of the extent of receptive field in this preparation. Exponential fits to the spatial summation curves of two mixed-input ON BCs tested with non-saturating light stimuli yielded length constants between 0.6 and 0.8 mm, which is significantly larger than their dendritic trees.

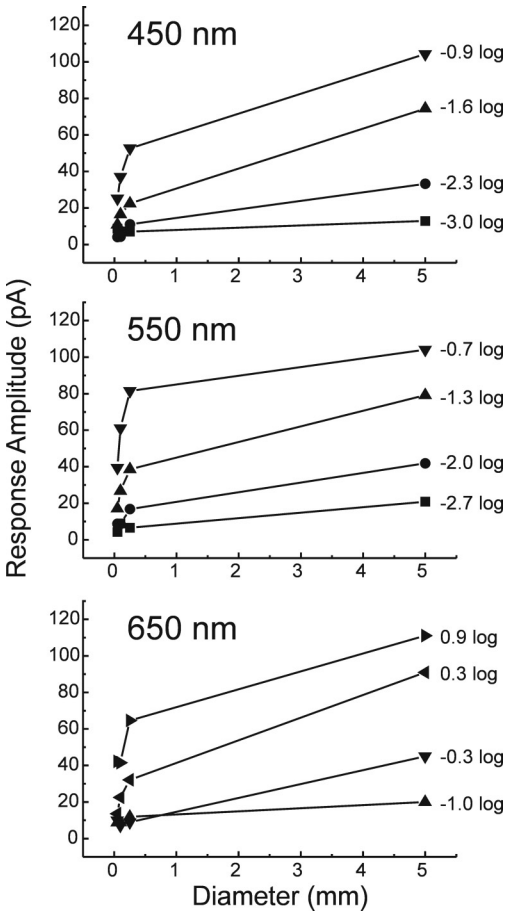


**Figure 3.2:** Spatial characteristics of BC receptive fields. Spatial summation curves of a mixed-input ON BC for 450 nm (top graph), 550 nm (middle graph) and 650 nm (bottom graph) stimuli of increasing diameters (50 µm, 100 µm, 250 µm and full field) at different intensities (intensity values depicted to the right of each curve). Response amplitudes increase linearly with small stimuli, but seem to reach a plateau between 250 µm and 5 mm (width of the slice from which recordings were made), indicating that the size of the receptive field center lies within these values.

From this experiment one can conclude that the receptive field centers of mixed-input ON BCs and OFF BCs of the goldfish (data not shown, but see next section) are larger than their dendritic fields, suggestive of electrical coupling either pre- or post-synaptically, and that the receptive field of these BCs in the dark-adapted goldfish retina lack an inhibitory surround. A more accurate measurement of the receptive field properties of these cells in retinal slices was not possible because of the characteristics of the optical stimulator and the fact that the slicing procedure eliminates part of the receptive fields.

*Electrical Coupling Changes BC Sensitivity to Small Stimuli*

To be able to demonstrate whether photoreceptor coupling contributes to the large receptive field centers of mixed-input BCs in the dark-adapted retinal slice of the goldfish, we investigated the effects of coupling on the overall sensitivity of retinal neurons. Insight in this phenomenon is essential, because the photoreceptor input to the BCs will be classified on the basis of sensitivity throughout this thesis. We cannot record directly from goldfish rods due to their diminutive dimensions.

Electrically coupled cells show an apparent decrease in sensitivity to small stimuli that do not cover their whole receptive field center (Norton et al., 1968; Dowling and Ripps, 1971; Naka, 1972; Marchiafava and Pasino, 1973; Copenhagen and Owen, 1976; Fain et al., 1976). On the other hand, the concomitant activity of center- and surround-mediated processes at the BC and GC level can lead to a decrease in the sensitivity of the light response to full-field stimulation, as shown in Figure 1.6a (Kaneko, 1973; Werblin, 1974).

Figure 3.3a depicts the intensity-response relations of an M-cone to stimulation at 550 nm with a 100 μm slit (filled squares) and a full field (open circles). Cone response amplitudes do not change with these stimulus sizes and can be fitted by a single Hill function (solid line). This means that cones are not extensively coupled in our experimental conditions, and that the light responses to both spatially small and large stimuli yield a good estimate of their sensitivity. This is in agreement with previous work in the goldfish (Hedden and Dowling, 1978), carp (Tomita, 1965), and turtle (Baylor and Fuortes, 1970; Detwiler and Hodgkin, 1979).

At the HC level, however, only full-field stimuli can be used for this purpose, due to the large size of their receptive field centers. In Figure 3.3b the intensity-response relations of a rod-driven HC (left panel) and of a cone-driven monophasic HC (right panel) are depicted for stimulation at 550 nm with a 100 μm slit (solid squares) and a full field (open circles). The relations could be fitted by two Hill functions (continuous lines) that differed in slope ($n$) and in their $K$ values. HCs are more sensitive when stimulated with full-field stimuli than with small stimuli.

The lower sensitivity to spatially small stimuli can be accounted for as follows (Naka, 1972): electrical coupling decreases the maximal response amplitude to slit stimulation at all intensities, leaving $K$ and $n$ unchanged. As the intensity of the slit is increased, light starts scattering onto regions of the receptive field center not

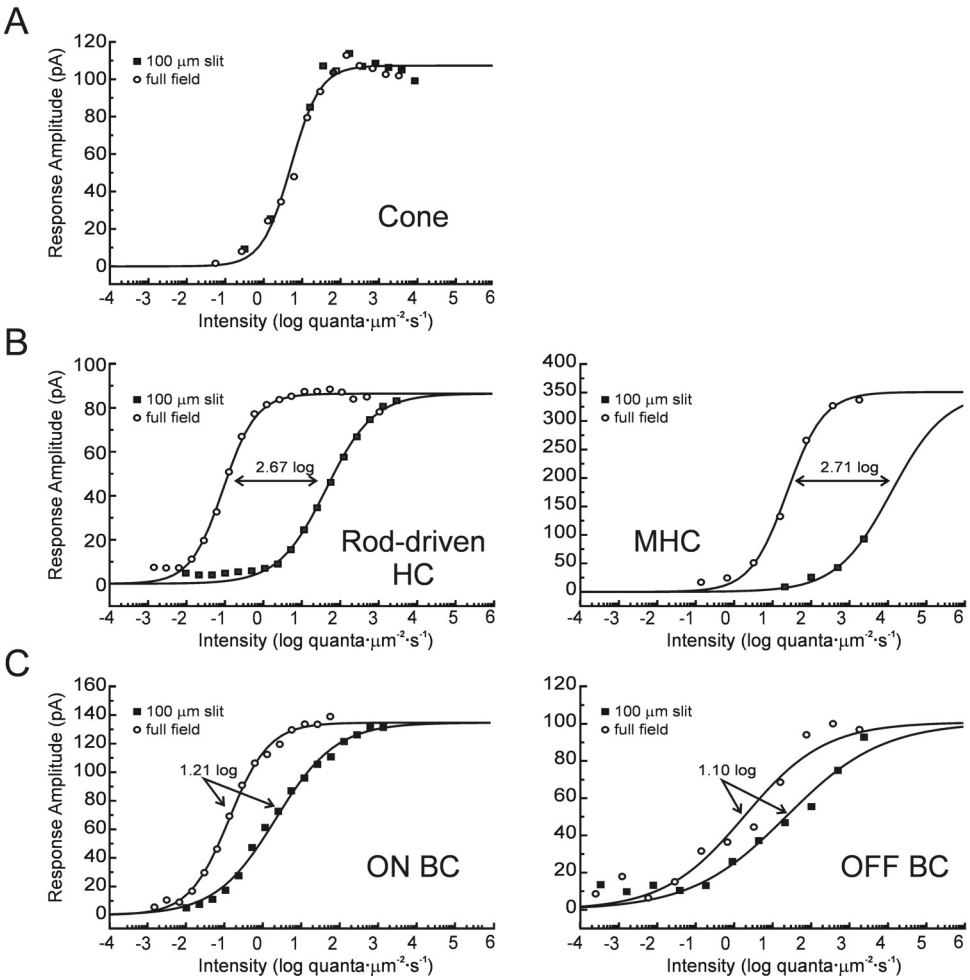


**Figure 3.3:** Sensitivity changes with stimulus size. A) Intensity-response relations of an M-cone to stimulation at 550 nm with a 100 μm slit (filled squares) and a full field (open circles). Both sets of data could be fit by a single Hill function (continuous line), indicating that the stimulus size does not influence the response amplitude of the photoreceptors. B) Intensity-response relations of a rod-driven HC (left, $V_{hold}$ = -70 mV) and a cone-driven monophasic HC (MHC, right) to stimulation at 550 nm with a 100 μm slit (filled squares) and a full field (open circles). In both cases, the data points were fit by two Hill functions (continuous lines) that differed in slope and in their *K* values by more than 2 log. The shallower slope and reduced sensitivity of the responses to a slit of light are a consequence of the tight electrical coupling between HCs in the goldfish retina, combined with light scatter. C) Intensity-response relations of a mixed-input non-opponent ON BC (left) and a mixed-input non-opponent OFF BC (right) to stimulation at 550 nm with a 100 μm slit (filled squares) and a full field (open circles). The data points were fit by two Hill functions (continuous lines) that differed in their *K* values by more than 1 log. As in (B), the intensity-response relations to slit stimulation have a shallower slope and reduced sensitivity as compared to the intensity-response relations for full-field stimulation, also as a consequence of electrical coupling and stray light. The fit parameters are listed in Appendix A.

covered by the slit originally, and weakly stimulate a larger area. As a consequence, the responses to the slit stimulus continue to increase and become actually larger than they would if there were no scatter. Eventually, the amplitude generated by a very intense slit of light will approach the maximal amplitude for full-field stimuli. The result is a reduction in the slope of the intensity-response relation and an increase in the *K* value. This illustrates that when one wants to determine the sensitivity of the inputs to the HCs, full-field stimulation must be used.

The same phenomenon is observed at the BC level in the dark-adapted goldfish retina. Figure 3.3c shows the intensity-response relations of a mixed-input ON BC (left panel) and OFF BC (right panel) to stimulation at 550 nm with a 100 μm slit (filled squares) and a full field (open circles), fitted with two Hill functions (continuous lines). As in the case of HCs, illumination with a small slit yields a relationship with a shallower slope than to full field. The combined effects of stray light and electrical coupling lead to an apparent sensitivity shift of 1.21 and 1.10 log, respectively. The parameters used to fit the intensity-response relations of this figure are given in Appendix A. On average, the difference in *K* values between the light responses of mixed-input BCs to a 100 μm slit and to full-field stimulation at 550 nm was 1.06 ± 0.43 log for ON BCs ($p<0.001$, n = 37 cells) and 1.18 ± 0.50 for OFF BCs ($p<0.001$, n = 8 cells). The slope (*n*) strongly varied between the distinct BC types. This will be addressed in Chapter 4.

Taken together, these results indicate that a) cones are not extensively coupled in our experimental conditions and cannot therefore be the reason for the large receptive field centers of mixed-input BCs; b) electrical coupling (either in the rod network or between neighboring BCs) decreases BC sensitivity to spatially small stimulation that does not cover the entire receptive field center; c) the receptive field centers of OFF BCs and ON BCs seem to have similar properties in the retinal slice, since the sensitivity shift observed in both cell types was not significantly different ($p>0.05$, but see next sections); d) mixed-input BCs seem to be less extensively coupled than HCs, as one can infer from the difference in the sensitivity shifts in BCs and HCs; and e) to estimate photoreceptor inputs to HCs and BCs one has to use full-field stimulation. Next, we investigated whether rod-rod coupling could explain the response properties of mixed-input BCs.

*Large Receptive Field Centers are Not a Result of Rod-Rod Coupling*

Evidence for the post-synaptic localization of the site of electrical coupling responsible for the spatial properties of the BC receptive fields is presented in Figure 3.4. We tested mixed-input ON BCs in control Ringer's (left panels) and in Ringer's containing DL-AP4 (right panels), an agonist for group III metabotropic glutamate receptors. In the fish retina, this drug abolishes rod-driven light responses in mixed-input ON BCs and leaves the cone-driven pathway intact, presumably because these photoreceptors drive different glutamate receptors post-synaptically (Nawy and Copenhagen, 1987; Grant and Dowling, 1996; Wong et al., 2005a/b; this thesis,

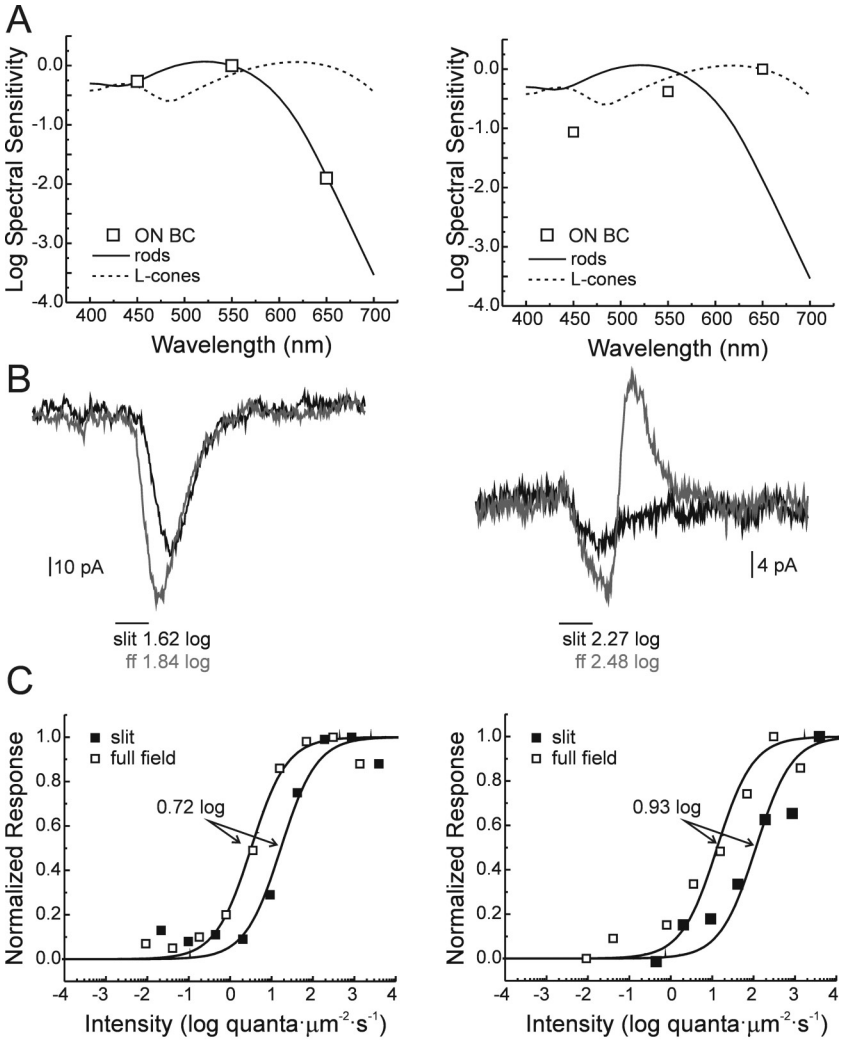


**Figure 3.4:** Rod- and cone-driven light responses have large receptive field centers. A) Spectral sensitivity of a mixed-input ON BC recorded in control Ringer's (left) and in Ringer's containing DL-AP4 (right) to suppress rod-driven light responses. In control, the cell follows the rod absorption spectrum, suggesting that in this situation it is predominantly driven by rods. Upon bath application of DL-AP4 the rod input is suppressed and a Purkinje shift can be observed: the BC is now predominantly cone-driven. Photoreceptor absorption spectra after Mooij and Van den Berg (1983). B) Light responses of the same BC to a 100 µm slit (in black) and a full field (in grey) at 650 nm and similar intensities (intensity values depicted in the figure) in control Ringer's (left) and in DL-AP4 (right). In both cases, light responses to full-field illumination are larger. C) Intensity-response relations of this mixed-input BC to 650 nm stimulation in control (left) and DL-AP4. The light sensitivity of the cell decreased, as can be inferred by the log *K* values for full-field stimulation (0.50 log in control and 1.12 log in DL-AP4), indicating that the rod input was efficiently suppressed by DL-AP4. The apparent sensitivity shift due to a small stimulus is however similar in both cases (values depicted in the figure), indicating that rod-rod coupling is not responsible for the spatial summation of mixed-input BC receptive field centers.

Chapters 4 and 5). If the sensitivity difference in the light responses for spatially small stimuli is entirely due to rod-rod coupling, it should disappear when the BCs are tested in DL-AP4.

As can be seen in Figure 3.4a, the spectral sensitivity of mixed-input ON BCs in the dark-adapted retina follows the rod absorption spectrum (left). Upon superfusion of the slice with DL-AP4, the spectral sensitivity shifts to longer wavelengths (a Purkinje shift, described in detail in the Introduction: Purkinje, 1825), indicating that the rod input was efficiently suppressed and that cones now drive the cell. Even so, BC light responses are still larger for full-field stimulation than to small light slits (Figure 3.4b). When one compares the intensity-response relations of these cells in both conditions (Figure 3.4c), the overall light sensitivity of the cell is decreased (*K* value is 0.62 log units larger in DL-AP4), as one expects if the rod input is abolished. Nonetheless, the apparent sensitivity shift due to spatially small stimulation (as discussed in the previous section) is still present and has roughly the same magnitude.

Figure 3.5 summarizes the results obtained in 14 cells in control Ringer's (left) and 4 of the same group in DL-AP4 (right). The larger standard deviations in the DL-AP4 group are a result of noise; some cone-driven responses were very small. Nonetheless, responses to full-field light stimuli were always larger than responses to light slits. The sensitivity difference between responses for small and large stimuli in both cases was significantly different from zero for all wavelengths

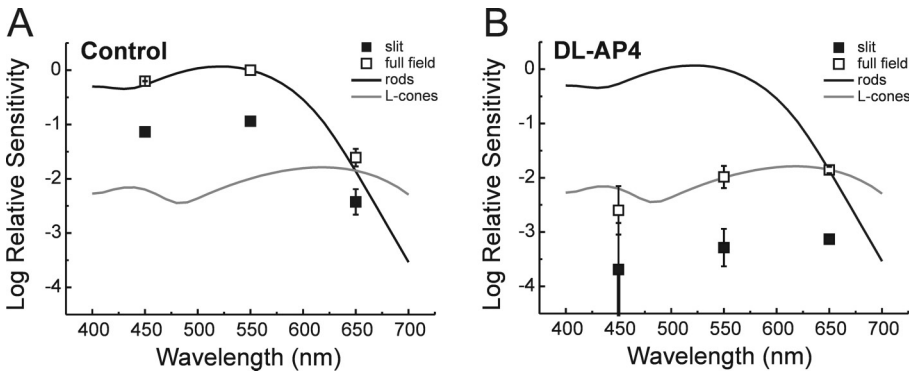


**Figure 3.5:** Sensitivity shift due to spatial properties of stimulus remains when rod input is suppressed. A) Relative sensitivity of mixed-input ON BCs recorded in control Ringer's (n=14). The cells follow the rod absorption spectrum (black line), suggesting that in this situation they are predominantly driven by rods. For all wavelengths tested, light responses to full-field stimulation (open symbols) are always more sensitive than light responses to 100 µm slits (closed symbols). B) Relative sensitivity of 4 mixed-input ON BCs from (A) recorded in Ringer's containing DL-AP4 to suppress rod-driven light responses. Data was normalized to the maximal sensitivity in (A). The cells are now less sensitive and follow the absorption spectrum of the L-cones (black line), indicating that they are now predominantly cone-driven. For all wavelength tested, light responses to full-field stimulation (open symbols) are always more sensitive than light responses to 100 µm slits (closed symbols). Photoreceptor absorption spectra after Mooij and Van den Berg (1983).

tested ($p<0.001$) and similar in magnitude ($p>0.3$) within a group (i.e. 450 nm control compared to 650 nm in control) and in between groups (i.e. 450 nm control compared to 450 nm in DL-AP4). One can conclude from these data that the large receptive field centers of mixed-input BCs in both situations is not due to spread of signals in the photoreceptor layer, but that it results predominantly from electrical coupling at the BC level.

*Mixed-Input BCs in the Slice Preparation Have Very Low Input Resistances*
Further evidence for electrical coupling at the BC level can be found in their whole-cell current-voltage (*IV*) relations. Mixed-input BCs in the goldfish retinal slice have input resistances ($R_{in}$) about ten times lower than the ones reported for isolated cells (Heidelberger and Matthews, 1992; Burrone and Lagnado, 1997). It is highly unlikely that this low $R_{in}$ comes from technical artifacts (i.e. a low resistance of the seal between the patch pipette and the cell membrane, $R_{seal}$, which would shunt part of the current applied via the pipette), for a number of reasons listed below.

First, the resting membrane potentials ($V_{rest}$) that we record from these cells in the slice preparation (-41±11 mV for ON BCs, n = 95, and -40±13 mV for OFF BCs, n = 15) are very similar to the ones reported for both isolated mixed-input BCs of the goldfish (-32±10 mV: Kaneko and Tachibana, 1985; -46.2±9.9 mV: Zenisek and Matthews, 1997), as well as for mixed-input BCs recorded in the intact goldfish retina (around -40 mV, Kaneko, 1970), carp retina (37±8 mV: Saito et al., 1979; Saito and Kaneko, 1983; Saito and Kujiraoka, 1982) and rod-driven BCs in the intact dogfish retina (-45.4±8.2 mV: Ashmore and Falk, 1980). Second, if the leakiness in our cells would be the result of an artifact, one would expect a larger variation in $R_{in}$ values. As we will discuss in the following sections, $R_{in}$ in mixed-input ON BCs is fairly constant, although mixed-input OFF BCs show a somewhat broader distribution. Third, low $R_{in}$ values in mixed-input BCs of the goldfish recorded *in situ* were also reported by other researchers (Palmer et al., 2003a/b), and are routinely used as a means to distinguish between intact cells (which have low $R_{in}$) and isolated axon terminals (which are electrotonically very compact) in their preparations.

Figure 3.6a illustrates that mixed-input ON BCs recorded with different intracellular solutions ($K^+$-, $Na^+$- or $Cs^+$-based, exact salt composition of the solutions is given in Table 3.3) have roughly the same $R_{in}$ values (in the range of 150-250 MΩ). Although mixed-input OFF BCs tend to be slightly more compact than ON BCs (Figure 3.6b), their $R_{in}$ is still extremely low if compared to the values given in literature for isolated cells, which are in the GΩ range.

Since low $R_{in}$ values are not observed in isolated cells, it is very likely that their cause be localized to the dendrites or axonal terminations, which are partially damaged in the isolation procedure (Attwell et al., 1987; Zenisek and Matthews, 1997; Schultz et al. 2001). One could argue that this leakiness might then arise from the synaptic input itself. Open glutamate- or GABA-gated channels in the BC membrane *in situ* would indeed contribute to a smaller $R_{in}$ as compared to isolated

| Ion | Pipette Solution 1 | Pipette Solution 2 | Pipette Solution 3 | Pipette Solution 4 |
|---|---|---|---|---|
| $Na^+$ | 2.0 | 2.0 | 1.0 | 97.3 |
| **$K^+$** | **148.0** | **41.2** | **41.2** | **1.0** |
| $Cl^-$ | 47.9 | 39.3 | 49.3 | 6.7 |
| $F^-$ | 23.9 | - | - | - |
| $Ca^{2+}$ | 0.1 | - | 0.1 | - |
| $Mg^{2+}$ | 1.0 | 9.8 | 10.8 | 10.5 |
| **$Cs^+$** | **-** | **33.4** | **75.6** | **45.8** |
| $TEA^+$ | - | 24.5 | - | - |
| $Li^-$ | - | - | 1.0 | - |
| $H_2PO_4^-$ | - | - | - | 54.5 |
| $CH_3O_3S^-$ | - | - | 9.8 | - |

**Table 3.3:** Composition of the pipette solutions used in Figure 3.6 to record from mixed-input ON BCs.

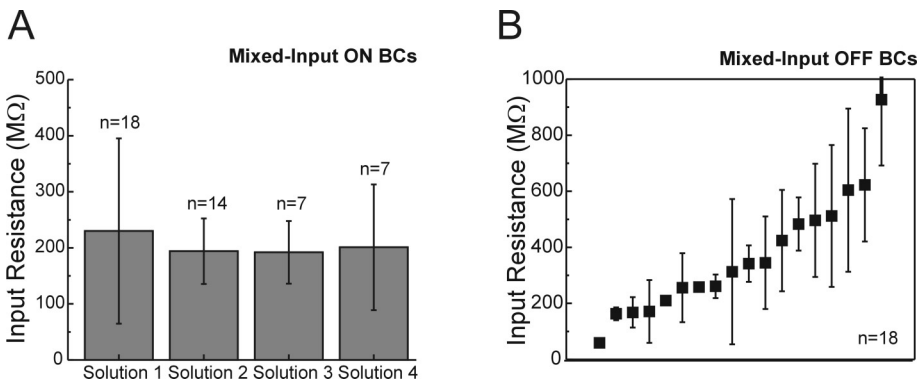


**Figure 3.6:** Mixed-input BCs have low input resistances. A) Comparison of the input resistances of mixed-input ON BCs recorded with pipettes containing different concentrations of $K^+$, $Na^+$ and $Cs^+$ (the composition of each solution is given in Table 3.3). In all groups input resistances were low and not significantly different ($p>0.5$). B) Mean input resistances of 18 mixed-input OFF BCs recorded in the goldfish retinal slice. Although OFF BCs tend to be more compact than ON BCs ($p=0.0052$), their input resistances can also be very low.

BCs in which the tonic synaptic input is absent. The contribution of inner retinal inputs is however negligible, since we routinely recorded with PTX+STRY in the bath. Furthermore, the $R_{in}$ of axotomized BCs is not significantly higher than that of intact cells (not shown). Figure 3.7a shows that pharmacological suppression of the rod-driven input with DL-AP4 or ACPT-I and of residual inputs with DNQX

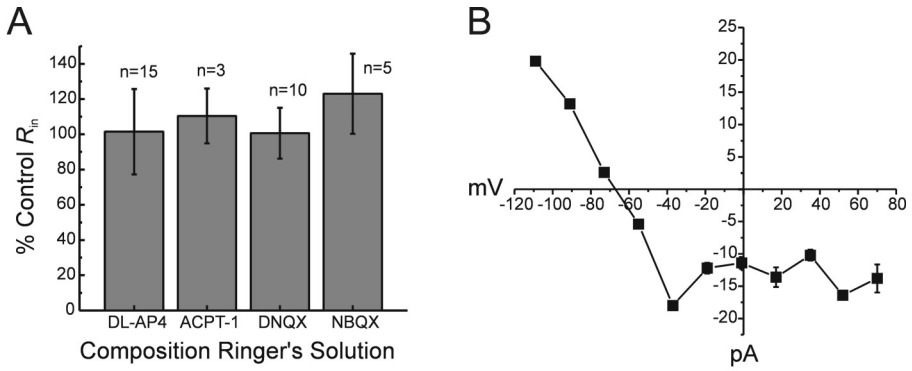


**Figure 3.7:** Low $R_{in}$ in mixed-input BCs is not due to synaptic inputs. A) Comparison of the change in $R_{in}$ of mixed-input ON BCs bathed in Ringer's solutions containing DL-AP4, ACPT-I, DNQX or NBQX in addition to PTX and STRY (which were already present in the control solutions). In all groups $R_{in}$ did not change significantly in relation to control ($p>0.08$), indicating that glutamatergic and GABAergic synaptic inputs do not contribute substantially to the low $R_{in}$ values of these cells. B) *IV* relation of the light-driven conductance of a mixed-input ON BC recorded in Ringer's containing DL-AP4, PTX, BIC and STRY to isolate the cone-driven input. The cell was stepped from -70 mV to different potentials and stimulated with saturating light flashes (550 nm, 3.38 log, 100 µm). The cone-driven conductance is too small (it induces a maximum current of about only 20 pA in most cells recorded from so far) to be responsible for the low $R_{in}$ of mixed-input ON BCs (in this cell, $R_{in}$ = 165 MΩ). Note that at positive potentials the *IV* relation rectifies – this issue will be addressed in Chapter 5.

or 1,2,3,4-tetrahydro-6-nitro-2,3-dioxo-benzo[f]quinoxaline-7-sulfonamide (NBQX) did not significantly change $R_{in}$ values of mixed-input ON BCs recorded in the slice. The remaining cone-driven conductance, which is open in darkness, is too small to account for this leak (Figure 3.7b). Similar results were also obtained for mixed-input OFF BCs (not shown).

Taken together, these results indicate that the low $R_{in}$ values of mixed-input BCs in the retinal slice preparation do not originate in synaptic conductances, leaving electrical coupling between neighboring BCs as a likely source.

*Gap Junction Blockers/Modulators Are Ineffective*

Even though we know that mixed-input BCs are electrically coupled, what we do not know is to what extent this electrical coupling can interfere with our voltage-clamp measurements of glutamatergic conductances. Low $R_{in}$ values can lead to a considerable shift in the reversal potential of remote synaptic conductances due to voltage escape at the leaky dendrites (Spruston et al., 1993; Hausser and Roth, 1997). In order to get an estimate of the contribution of electrical coupling to the low $R_{in}$ of mixed-input BCs, we tried to directly block these gap junctions in mixed-input ON BCs. These experiments were not performed in OFF BCs because we could not record from these cells stably for long periods of time (which is a requirement for such studies, due to the difficulty in obtaining washouts).

Bath application of the non-specific gap junction blocker carbenoxolone

(CBX, 100 µM) in two mixed-input ON BCs led to depolarization and complete disappearance of the light responses (Figure 3.8a), probably due to pre-synaptic effects of the drug that can impair synaptic transmission (Kamermans et al., 2001). The elimination of light responses made it impossible to judge changes in receptive field sizes of the BCs tested with CBX. Figure 3.8b shows that the ratio between light response amplitudes to spatially small and large stimuli was not significantly altered either in the first minutes of treatment (before disappearance of the light responses) or during the washout. Noise levels were also not increased during the treatment (compare the traces in Figure 3.8a), suggesting that coupling was not

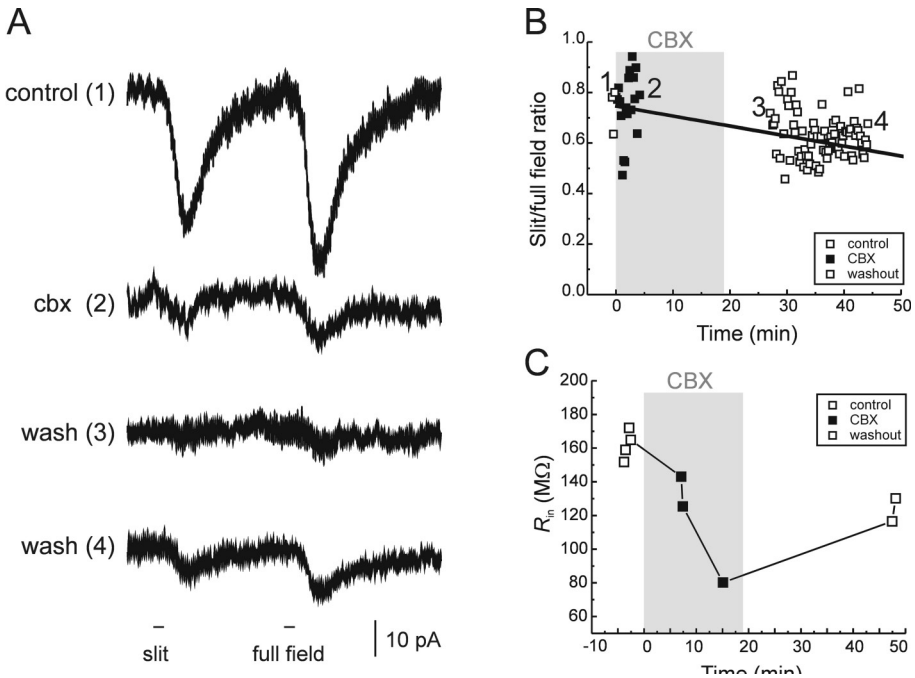


**Figure 3.8:** Effects of the gap junction blocker carbenoxolone (CBX) in mixed-input ON BCs. A) Light responses of a mixed-input ON BC to spatially small (100 µm slit) and large (full field) stimulation of similar intensities at 550 nm (-0.64 log and -0.88 log, respectively) in control Ringer's (top trace), during bath application of CBX (trace in the second row), and during early and late washout (bottom traces). Although light responses were greatly suppressed and a complete washout was not achieved (compare response amplitudes of the bottom traces with those in control), one can see that neither were noise levels increased (which one would expect if coupling were suppressed) nor was the relation between the amplitudes to both sorts of stimuli altered. B) Ratio between the response amplitudes to slit and full field before (open squares), during (solid squares) and after (open squares) application of CBX in the same cell, showing that responses to small stimuli were always smaller than those to large stimulation. The numbers in this graph refer to the traces in (A). A linear regression was fit to the data points in order to demonstrate that treatment with CBX even led to a decrease in the slit/ff ratio. C) $R_{in}$ of this BC as a function of time. During treatment with CBX, $R_{in}$ decreased to approximately half of its control value, which is the opposite of what one would expect if electrical coupling were substantially suppressed.

significantly altered. Additionally, $R_{in}$ values decreased slightly (Figure 3.8b), which further indicates that at this concentration CBX is not able to eliminate BC coupling, and that most of its effect is due to a modulation of the photoreceptor glutamate release.

Replacement of some of the $Cl^-$ ions in the bath by acetate (25 and 50 mM) to induce intracellular acidification and close gap junctions did not significantly change $R_{in}$ of the cells tested, and the sensitivity difference between light responses to small or large stimuli was unaffected (Figure 3.9). In all cells tested with this protocol (n = 6), acetate induced a hyperpolarization and a reduction in light response amplitudes to both kinds of stimuli (compare the scales of the graphs in Figure 3.9b and c).

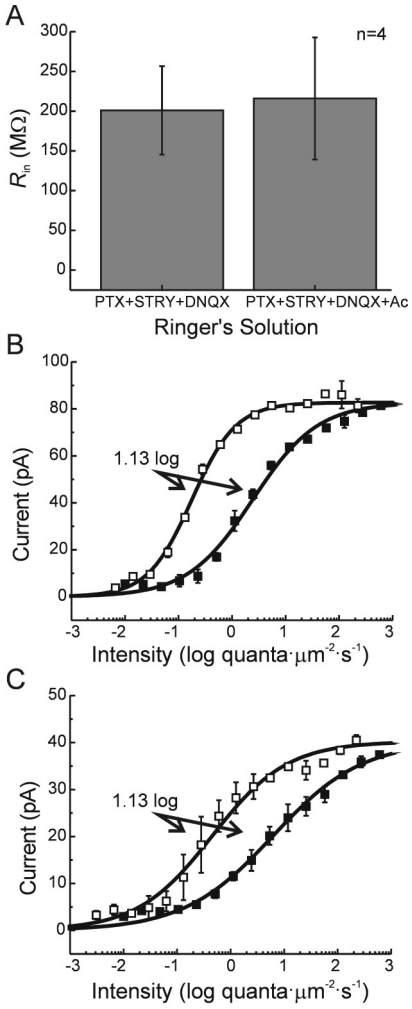


**Figure 3.9:** Effects of intracellular acidification in mixed-input ON BCs. A) Mean input resistances of 4 mixed-input ON BCs in control Ringer's (contaning PTX, STRY and DNQX), and with the replacement of part of the $Cl^-$ ions of the control solution by acetate. There was no significant change in $R_{in}$ values (p=0.34). B) Intensity-response relations of a mixed-input ON BC to stimulation at 550 nm with a full field (open symbols) and a 100 µm slit (closed symbols) in control Ringer's. Data points are means of two flashes at each intensity. The resulting relations were fitted by two Hill functions (solid lines) whose *K* values differ by 1.13 log. C) Intensity-response relations of the same cell in (B) to similar stimulation in acetate Ringer's. Data points are means of two flashes at each intensity. Although light responses became substantially smaller (compare the scales in B and C), the difference between the Hill fits (solid lines) for both relations is still 1.13 log.

We tested a number of other substances reported to act on gap junctional coupling in different cell types, without any success: high intracellular cAMP (5-10 mM, Miyachi and Murakami, 1989; Bevans and Harris, 1999); intracellular potassium fluoride (PKA inhibitor, also tested in 12 mixed-input OFF BCs with no result, Vargas et al., 1999); intracellular cGMP (0.2-1 mM, Burt and Spray, 1988; Miyachi and Murakami, 1991; Bevans and Harris, 1999), extracellular PMA (PKC activator, 1 mM, Kwak et al., 1995). In all cases, cells had still low $R_{in}$ values, whole cell *IV* relations were linear, and the difference in sensitivity between spatially large and small was stimulation still present.

*Electrical Coupling Shifts Measured Reversal Potentials*

Since the direct approach failed, we tried to estimate the magnitude of the shift in reversal potential ($V_{rev}$) of cone-driven light responses in BCs caused by BC electrical coupling. Cone-driven light responses in fish mixed-input ON BCs are a conductance decrease with a negative $V_{rev}$. This conductance was shown to be predominantly carried by $Cl^-$ ions in other fish species (Grant and Dowling, 1995/ 1996; Connaughton and Nelson, 2000; Wong et al., 2005b) because its reversal potential follows $E_{Cl}$ closely in these animals. The difference between the calculated $E_{Cl}$ and the $V_{rev}$ of the cone-driven light responses of mixed-input ON BCs of the goldfish would be a direct measure of the amount of coupling between ON BCs.

However, this set of experiments yielded unexpected results. We could not find a strict correlation between $E_{Cl}$ and the $V_{rev}$ of cone-driven light responses (Figure 3.10). The values obtained were always more negative than the calculated

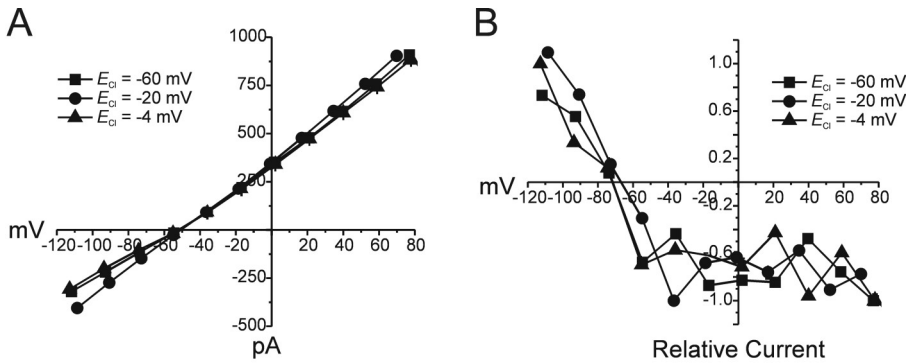


**Figure 3.10:** Electrical coupling shifts $V_{rev}$ of cone-driven light responses. A) Whole-cell *IV* relations of three mixed-input ON BCs with different calculated values for $E_{Cl}$ (-60 mV, -20 mV and -4 mV, respectively) bathed in PTX, STRY, BIC and DL-AP4 to block inner retinal contributions and the rod input. In this condition, cells rest at approximately -55 mV and still exhibit large whole-cell currents. $V_{hold}$ = -70 mV. B) Relative *IV* relations of the light-driven conductance of the BCs shown in (A). The most negative current values were scaled to -1 for comparison. Cells were stepped from -70 mV to different potentials and stimulated with a 100 µm light slit at saturating intensities ($E_{Cl}$ -60 mV and -20 mV: 550 nm, 3.38 log; $E_{Cl}$ -4 mV: 450 nm, 3.48 log). In all cases, light responses reversed at around -70 mV, independent of the calculated $E_{Cl}$ values.

$E_{Cl}$. Even when $E_{Cl}$ was set more positive than the resting membrane potential ($V_{rest}$) of the cells (around -50 mV in DL-AP4, Figure 3.10a), which should yield a shift in the opposite direction, cone-driven light responses still reversed at quite negative potentials (Figure 3.10b).

The failure to shift $V_{rev}$ towards values more positive than $V_{rest}$ can be explained by intercellular diffusion of ions. Since BCs are electrically coupled, it seems likely that neighboring cells would act as a source of $Cl^-$, $K^+$ and other ions for the BC recorded from, keeping $E_{Cl}$ at more negative values than our calculated $E_{Cl}$ and more negative than $V_{rest}$. Nonetheless, given that cone-driven light responses in mixed-input ON BCs reversed between -90 and -60 mV (n = 12), this indicates a shift of 10 to 40 mV in relation to $V_{rest}$. If we assume that the $E_{Cl}$ in these cells is more negative than $V_{rest}$ (Satoh et al., 2001; Billups and Attwell, 2002), then the shift in $V_{rev}$ due to electrical coupling would not exceed 35 mV. This notion is of crucial importance for Chapter 5, in which we will investigate the interaction between rod- and cone-driven conductances in mixed-input ON BCs.

## 3.5 Discussion

In this Chapter, we show that both ON and OFF mixed-input BCs in the dark-adapted goldfish retinal slice are electrically coupled, and that this electrical coupling determines a number of features of the physiology of these cells. The receptive fields of these BCs are larger than their dendritic trees, and extensive spatial summation of photoreceptor inputs takes place at the BC level. Not only are inputs shared among neighboring cells, but also intracellular constituents, and this imposes constraints to voltage-clamp measurements of synaptic currents. Since we could not modulate the gap junctional conductance in mixed-input ON BCs with a number of standard physiological manipulations, the connexins involved in forming the gap junctions between these cells must follow some criteria such as low sensitivity to pH changes and phosphorylation. In the following sections we will discuss each of these topics, and elaborate on the function of such syncytial integration at the BC level.

*Spatial Summation in the Dark-Adapted Retina*

The absence of surround-mediated responses in BCs in the dark-adapted retina was described previously in the dogfish (Ashmore and Falk, 1980), salamander (Borges and Wilson, 1987), toad (Belgum and Copenhagen, 1988) and in the carp retina (Saito and Kujiraoka, 1988; Yamada and Saito, 1997). Receptive field centers of carp mixed-input BCs were shown to be up to an order of magnitude larger than their dendritic trees (Saito and Kujiraoka, 1988).

Here we show that this is also the case in the dark-adapted goldfish retina, and that, similarly to what happens in the carp, the reason for such large receptive

fields lies in electrical communication between BCs. Although we did not perform a systematic study of receptive field profiles of ON and OFF BCs due to the limitations of the technique, there seems to be little variation in receptive field sizes and amount of coupling. OFF BCs tend to have higher $R_{in}$ values than ON BCs, although they present similar shifts in light sensitivity due to spatially small stimulation.

The site of electrical coupling is probably the dendrites, because in our experiments axotomized cells had receptive fields with similar spatial properties as intact ones. Furthermore, as shown in Chapter 2, the dendrites of mixed-input ON BCs in the outer retina show contiguity in histological preparations, but their axon terminals do not (i.e. Figures 2.1, 2.11c). This result corroborates data from the carp retina, in which dendrites of simultaneously recorded cell pairs were shown to make contact, but not their axon terminals (Kujiraoka and Saito, 1986; Saito and Kujiraoka, 1988).

*Low Input Resistance of Bipolar Cells in Situ*

Gap junctional coupling reduces the input resistance and increases the electrotonic length of cells (Getting, 1974;Rorig et al., 1996; Poznanski, 1999). Although isolated mixed-input BCs of the goldfish have a high $R_{in}$ as can be inferred by the small amplitudes of their whole-cell currents (Kaneko and Tachibana, 1985; Kaneko et al., 1991; Heidelberger and Matthews, 1992; Mennerick et al., 1997), intact cells recorded in the retinal slice display much lower values (Palmer et al., 2003a/b). In the intact retina, $R_{in}$ of BCs can be extremely low – values ranging from 10 to 44 MΩ were reported in the dogfish (Ashmore and Falk, 1980), and as low as 45 MΩ in the goldfish (Nawy and Copenhagen, 1987).

The same difference in $R_{in}$ of dissociated cells as compared to BCs recorded in the slice preparation was described for the axolotl, *Ambystoma mexicanum* (Attwell et al., 1987; Tessier-Lavigne et al., 1988). In these papers, the $R_{in}$ of BCs recorded in the slice was reported to be ten times smaller than in isolated BCs. The conclusion drawn by the authors is that either synaptic inputs or electrical coupling between BCs (both absent in isolated cells) would be responsible for the discrepancy. Here we show that tonic synaptic inputs cannot account for the low $R_{in}$ measured in the retinal slice, since blocking these with a number of pharmacological agents known to interfere with synaptic transmission did not increase $R_{in}$ significantly.

Calculations done in previous studies indicate that this low $R_{in}$ measured in the dark represents largely properties of the dendrites (Ashmore and Falk, 1980). Voltage-gated currents are also unlikely to be the source, because $R_{in}$ values in this study were determined in a voltage range in which these currents are not active in mixed-input BCs (-70 to -80 mV). Furthermore, intracellular and extracellular application of $K^+$ channel blockers such as $Cs^+$ and TEA and 4-AP did not increase $R_{in}$ (not shown). One must assume therefore that the low $R_{in}$ of mixed-input BCs of the goldfish retina is due to gap junctional coupling, and that the site of coupling is at the dendrites. Intact mixed-input BCs in the goldfish retinal slice were reported

to have much lower $R_{in}$ (<0.5 GΩ) than their isolated axon terminals (Palmer et al., 2003a/b), which provides further evidence for electrical coupling as the source of this low resistance, and the site of coupling being in the soma and/or dendrites.

Both gap junctional and membrane resistance determine the strength of electrical coupling. Voltage-dependent changes in coupling have been reported for HCs (Itzhaki and Perlman, 1987). In our experimental conditions, however, synaptic input hardly modifies $R_{in}$, indicating that BC receptive field properties are unlikely to change with stimulus parameters or with the adaptive state of the retina.

*Which Connexins Are Involved in BC Coupling?*

That we could not effectively modulate $R_{in}$ by means of substances that interfere with gap junctional communication sets a number of criteria that the connexins forming these gap junctions have to follow. Information about the pharmacological properties of fish connexins is however scarce: most experiments regarding connexin permeability and modulation were performed in mammalian cells expressing mammalian connexins. So far there are about 20 mouse connexins cloned (Willecke et al., 2002; Sohl and Willecke, 2004), from which some fish orthologues were found; yet, the homology is not complete, and characteristics such as expression, permeability and modulation might change from mammalian to fish connexins or even between the same connexin gene expressed in different fish species.

Skate connexin 35 (Cx35), for instance, lacks a PKA phosphorylation consensus that is present in perch Cx35. As a result, the latter is a target for PKA-cAMP-dependent phosphorylation, whereas the first is not (Mitropoulou and Bruzzone, 2003; O'Brien et al., 2004). In our experimental conditions, high concentrations of cAMP or KF did not modulate coupling, suggesting that the gap junctions in ON and OFF mixed-input BCs of the goldfish are not targets for phosphorylation and related dopaminergic modulation, which is consistent with literature reports on the (lack of) dopamine effects on mixed-input ON BC receptive field centers (Hedden and Dowling, 1978; Yamada and Saito, 1988). Since nanomolar concentrations of cAMP and cGMP effectively shut gap junctional channels formed by connexin 26 (Cx26) and 32 (Cx32) (Bevans and Harris, 1999; Goldberg et al., 2004), it is highly unlikely that these connexins are involved in BC coupling as well.

Gap junctional permeability is not a simple function of molecule size, but is also affected by other parameters such as charge (Goldberg et al., 2004). Different connexins have different permeability properties for endogenous compounds. Whereas all gap junctions are indistinctly permeable for monovalent cations, the same is not true for anions and a number of other molecules (Suchyna et al., 1999; Nicholson et al., 2000; Goldberg et al., 2004). The fact that we failed to control $E_{Cl}$ in our experiments suggests that the coupling between BCs allow $Cl^-$ ions to pass from one cell to the other.

Although the gap junctions in ON and OFF BCs might differ, they have at least one characteristic in common: impermeability to LY, a negatively charged and

relatively heavy molecule (mass 443 D) if compared to tracers such as neurobiotin (287 D), which was reported to pass readily through gap junctions between BCs in the black bass retina (Umino et al., 1994). In most cases in which LY was shown to permeate gap junctions between BCs in the cyprinid retina, it was forced through via current injections (Kujiraoka and Saito, 1986; Saito and Kujiraoka, 1988), and even so dye coupling occurred very rarely. According to studies in cultured cells, only certain combinations of (mouse) connexins are permeable to LY (Elfgang et al., 1995). Channels formed between $\alpha$- (Cx37, Cx40, Cx43 and Cx45) and $\beta$- (Cx26, Cx31 and Cx32) connexins are impermeable to LY, as well as homotypic Cx31, Cx40 and Cx45 transfectants. Cx43 was reported to be highly permeable to LY (Steinberg et al., 1994), which indicates that this connexin might not be involved in gap junctional coupling between BCs.

The molecular mechanism through which glycyrrhizic acid metabolites such as carbenoxolone uncouple cells is to date unknown (Dhein, 2004), although a direct interaction with the connexin plaque was suggested (Goldberg et al., 1996). However, not all connexin types seem to respond well to the concentration of CBX we used in this study. That we could not modulate coupling with 100 µM CBX is consistent with another report in turtle retina, in which 200 µM CBX were not enough to alter electrical coupling between some HC types (Pottek et al., 2003). We did not try higher doses because our main interest was to evaluate the effect of electrical coupling on light responses, and CBX suppressed these already at 100 µM.

The suppression of light responses in mixed-input ON BCs due to CBX application can be explained in different ways. By closing hemichannels in the tip of HC dendrites, CBX was shown to bring the $Ca^{2+}$ current of the photoreceptors out of their operating range (Kamermans et al., 2001). This effect alone can lead to a drastic reduction in synaptic transmission and abolishment of light responses in second-order neurons (Kamermans et al., 2001; Xia and Nawy, 2003). Additionally, there are a number of options unrelated to gap junctional coupling that together can also account for the depolarization and loss of light responses in goldfish mixed-input ON BCs: CBX was reported to directly inhibit $Ca^{2+}$ channels of the photoreceptors, decrease cone sensitivity 6 fold without significantly altering responses to saturating light (Verweij et al., 2003), have effects in gene expression and activation of MAPK pathways (Uyama et al., 2003), functionally enhance NO activity (Chaytor et al., 2000), and directly suppress neuronal activity (Rouach et al., 2003). Whatever might be the explanation for the effects we observed, CBX effectively uncouples cardiac cells containing Cx40 or Cx43 (de Groot et al., 2003) and ictal cells expressing Cx32 (Szente et al., 2002) at lower concentrations than used here, which indicates that these connexins are not involved in coupling between mixed-input ON BCs.

An alternative method to modulate gap junctional coupling is intracellular acidification. The approach used in this Chapter (bath application of weak acids such as acetate) leads to intracellular acidification due to the release of protons after membrane permeation (Dixon et al., 1993; Takahashi et al., 1993). Most connexins

are sensitive to pH changes, although the magnitude of the effect varies strongly with cell and connexin types (Rorig et al., 1996; Dhein, 1998; Trexler et al., 1999; Peracchia, 2004). Paradoxically, the connexins ruled out in the last paragraphs (Cx32, Cx40 and Cx43) were shown to have the lowest sensitivity to pH regulation when compared to other connexins. The order of decreasing sensitivity of eight murine connexins based on pKa was Cx50>Cx46>Cx45>Cx26>Cx37>Cx43>Cx40>Cx32 (Stergiopoulos et al., 1999). However, heterotypic combinations can lead to a decreased (or increased) pH sensitivity (Francis et al., 1999). Further, the type of connexin is not the only determinant of sensitivity: similar cytosolic acidifications obtained by different methods yield distinct results (Peracchia, 2004).

Since we could not perform these experiments in OFF BCs, we cannot extend our conclusions to this cell type based on the CBX and acetate experiments only, but the Cx43 permeability to LY and Cx32 sensitivity to high cAMP concentrations indicate that these connexins are not expressed by mixed-input OFF BCs as well.

*Why Couple BCs?*

Voltage changes in rods absorbing a few photons are minimal (Fain, 1975; Copenhagen and Owen, 1976), and this voltage signal is even further attenuated by electrical coupling between rods (Fain, 1975; Fain et al., 1976). To improve threshold sensitivity in second-order neurons, considerable signal amplification takes place at the first retinal synapse (Capovilla et al., 1987; Copenhagen et al., 1990). To accomplish such a task, many gain control mechanisms are placed at the photoreceptor-BC synapse (reviewed in Falk, 1988, Shiells, 1994 and Field et al., 2005): non-linearities of transmitter release, convergence of multiple inputs, number and properties of channels driven by the post-synaptic glutamatergic receptors, and amplification through second-messenger pathways in the case of ON BCs. However beneficial, this amplification can at the same time compromise signal transmission by increasing noise levels considerably (Taylor and Smith, 2004).

To eliminate part of this synaptic noise, one useful strategy is to couple post-synaptic neurons. Electrical coupling increases signal-to-noise ratio by averaging out uncorrelated noise (Lamb and Simon, 1976; Laughlin, 2002). The price paid by such spatial summation in the retina is loss of sensitivity and decrease in response amplitude to spatially small stimulation, as we have shown in Figure 3.3. Therefore, the balance between amplification and electrical coupling is of uttermost importance to set the sensitivity of the eye. Both kinds of gain control happen in different stages of the visual system, with some interspecies variations on the sites in which they occur.

In mammalian retinas, there is no evidence for electrical coupling between BCs (Berntson and Taylor, 2000), but lateral integration takes place between photoreceptors (Wu and Yang, 1988; Schneeweis and Schnapf, 1999; Tsukamoto et al., 2001; DeVries et al., 2002; Armstrong-Gold and Rieke, 2003) and at the AC level (Vaney, 1991; Bloomfield and Dacheux, 2001). Together with a thresholding

mechanism at the photoreceptor-BC synapse, where considerable convergence occurs, such a system enables elimination of synaptic noise without damping completely single-photon signals (Rossum and Smith, 1998; Field and Rieke, 2002).

A second good reason for coupling BCs is an improvement of temporal resolution. This reasoning was used when describing syncytial integration in rod networks (Detwiler et al., 1978; Attwell and Wilson, 1980), but might as well be used for coupling between second-order neurons. Due to the activation of voltage-gated currents (induced by hyperpolarization in the case of OFF BCs, and by depolarization in the case of ON BCs), the voltage response of a given BC could speed up as it spreads throughout the coupled network (see Chapter 5). Such a filtering is especially interesting in the transmission of rod-driven signals, which are characteristically slow (Falk, 1988).

Finally, little is known about spatial summation in cone-driven BCs, and how signals from these BCs are transmitted to GCs. Depending on the hardwiring of the retinal network, differences in rod- and cone-driven pathways might compensate for the loss of sensitivity generated by electrical coupling between mixed-input BCs.

**Acknowledgements**

The authors thank Drs. Marjelle van Leeuwen, Colleen Shields, Robert G. Smith and Tom van den Berg for useful discussions.

## Appendix A

| | full field | | | slit | | | |
|---|---|---|---|---|---|---|---|
| **Cell Type** | $Y_{max}$ | $n$ | log $K^{(1)}$ | $Y_{max}$ | $n$ | log $K^{(2)}$ | log $K^{(2)}$ - log $K^{(1)}$ |
| *Cone* | 108.06 | 1.12 | 0.71 | 108.06 | 1.12 | 0.71 | 0.00 |
| *Rod-Driven HC* | 86.40 | 1.02 | -1.03 | 86.40 | 0.70 | 1.65 | 2.67 |
| *Cone-Driven HC* | 350.85 | 0.91 | 1.38 | 350.85 | 0.61 | 4.10 | 2.71 |
| *ON BC* | 134.67 | 0.84 | -0.88 | 134.67 | 0.56 | 0.33 | 1.21 |
| *OFF BC* | 100.80 | 0.41 | 0.27 | 100.80 | 0.35 | 1.36 | 1.10 |

Hill fit parameters used for the intensity-response relations in Figure 3.3. $Y_{max}$ values are in pA.

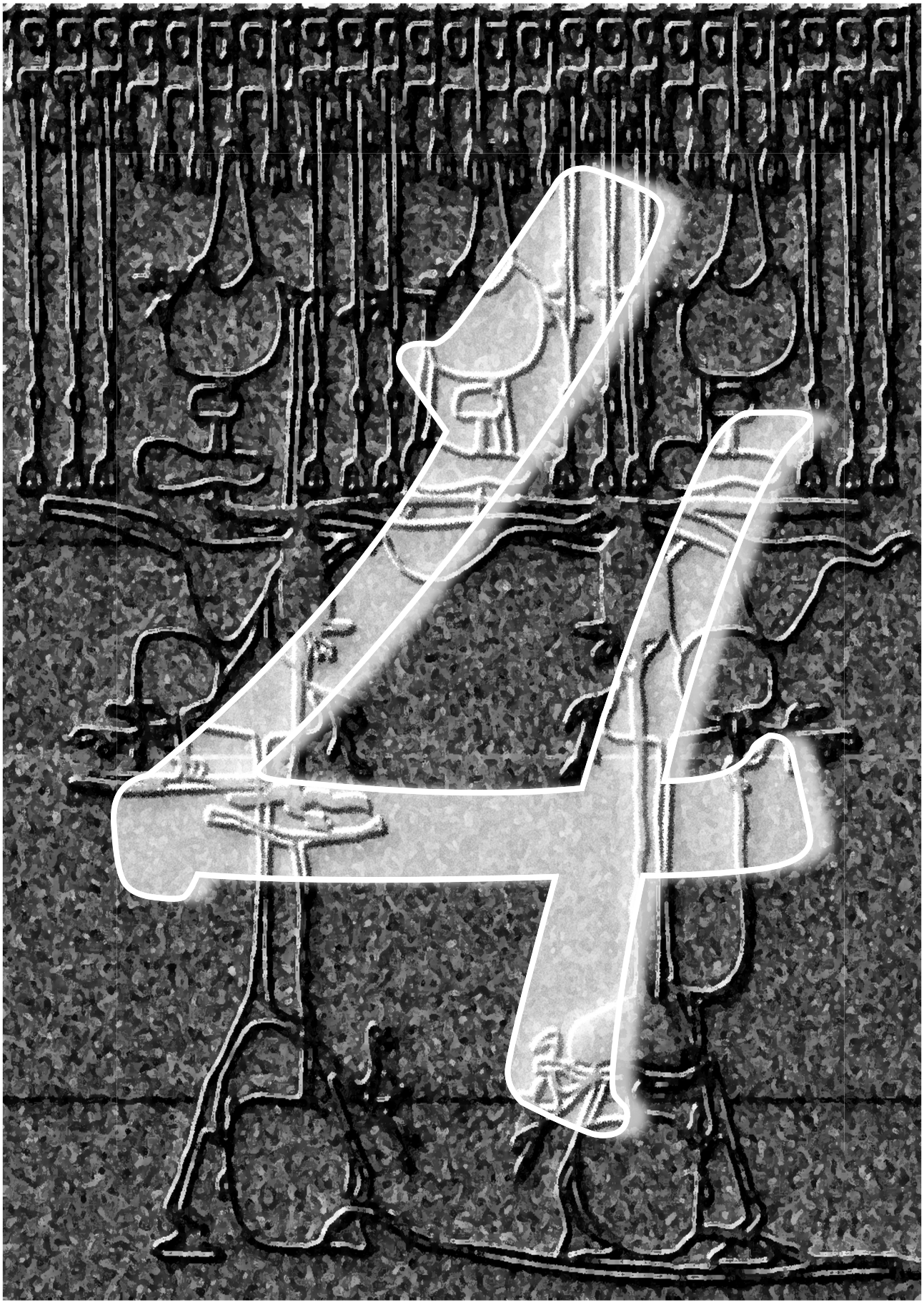

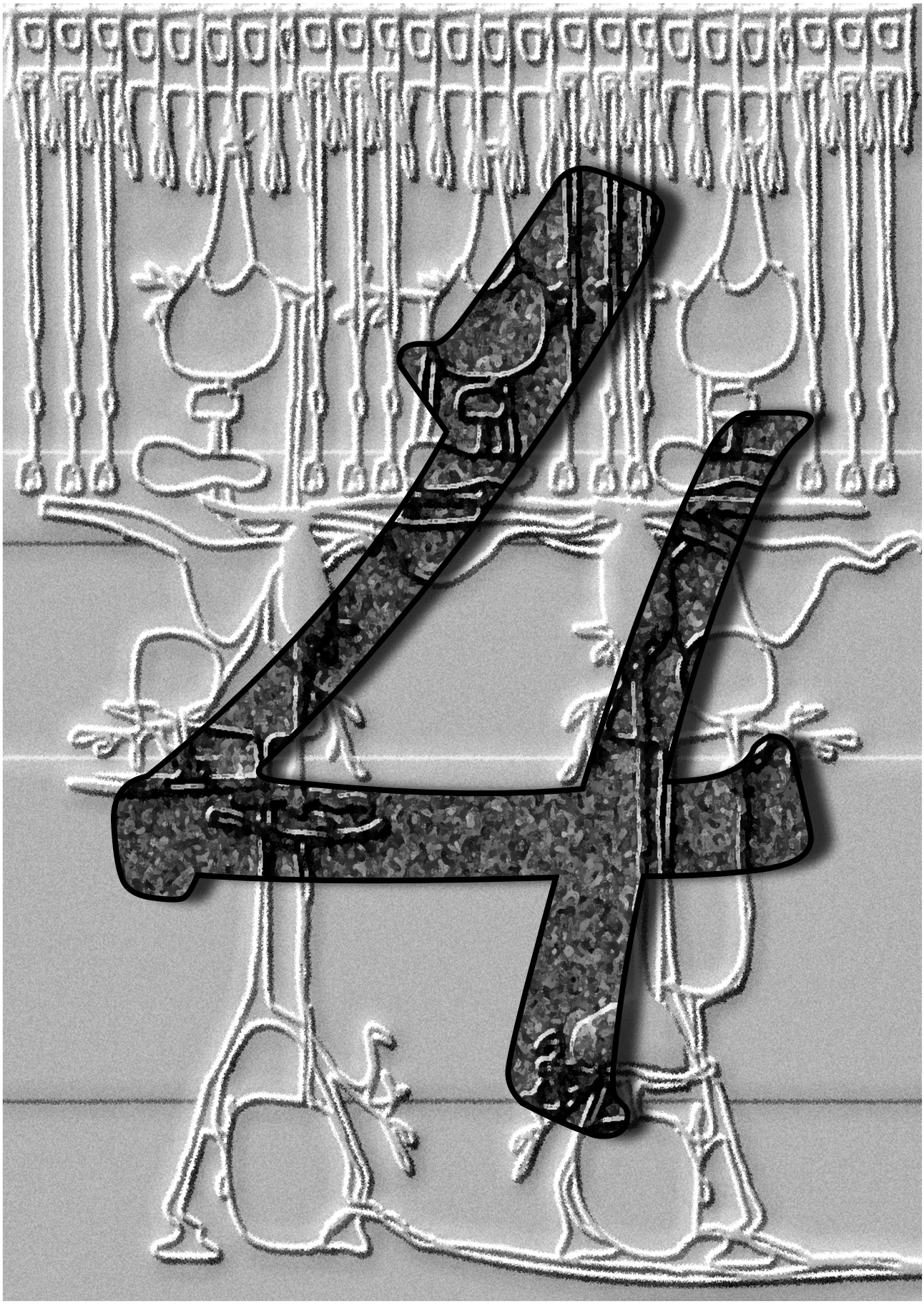

# Chapter 4

# The Physiological Role of Opponency in Goldfish Bipolar Cells

*Christina Joselevitch and Maarten Kamermans*
*(Submitted)*

## 4.1 Abstract

Since color vision is an opponent process, spectrally opponent neurons in the visual system are thought to underlie color vision. We recorded light responses of mixed-input BCs in the dark-adapted retinal slice of goldfish, and found that spectrally opponent BCs have an intensity-dependent nature: the sign of their center response reverses when the stimulus intensity is increased. We show that this intensity-dependent behavior can be generated by antagonistic inputs from rods and cones, or by inputs originating in distinct spectral types of cones. The antagonistic interactions cause opponent BCs to have a much steeper intensity-response relation than any of their inputs. This BC type becomes as a result an ideal intensity change detector: small changes in stimulus intensity evoke a large change in response amplitude. The results presented in this Chapter show that goldfish BCs seem to use the same coding scheme as cone-driven HCs to compress information, via a non-opponent, broadband channel, and spectrally opponent channels. Segregation into ON and OFF pathways is therefore not complete at the first retinal synapse.

## 4.2 Introduction

The segregation of visual information into the so-called ON- and OFF pathways generally happens at the BC level (Stell et al., 1977; Famiglietti et al., 1977). In the OPL, the OFF pathway is mediated by ionotropic glutamate receptors (Attwell et al., 1987; DeVries and Schwartz, 1999), whereas the ON pathway is mediated by mGluR6, a metabotropic glutamate receptor of the group III (Shiells et al., 1981; Slaughter and Miller, 1981; Nakajima et al., 1993; Vardi and Morigiwa, 1997). This separation of ON and OFF information pathways seems to remain present throughout the retina, as can be inferred by the ON/OFF stratification of the INL (Kolb and Famiglietti, 1976). There are, however, deviations from this general rule (for a review, see Boycott and Wässle, 1999), as will be illustrated in the following sections.

Spectrally opponent neurons generate ON responses (depolarizing

responses) to stimulation at a certain wavelength, and OFF (hyperpolarizing) responses when stimulated with another wavelength. Such cells are found at many different levels of the mammalian central nervous system (Wiesel and Hubel, 1966; DeValois et al., 1967; Land et al., 1983; Zeki, 1983a/b). Already in the retina, spectrally opponent HCs (MacNichol and Svaetichin, 1958; Norton et al., 1968; Fuortes and Simon, 1974), BCs (Kaneko, 1973; Yazulla, 1976; Mitarai et al., 1978; Sakakibara and Mitarai, 1982) and GCs (Daw, 1967/1968; de Monasterio et al., 1975b) are present in a number of species.

Specialized tasks have been associated to spectrally coded neurons. Since color vision is an opponent process (Hering, 1964; Hurvich, 1985) it was argued that opponent cells underlie wavelength discrimination. However, this role of opponency is still a matter of debate. As an alternative, it has been proposed that the spectral coding of teleost HCs, for instance, plays a role in color constancy (Kamermans et al., 1998) and represents an efficient way of information coding (Buchsbaum and Gottschalk, 1983). The aim of this study is to evaluate the opponent coding of mixed-input BCs.

We show that spectral opponency in BCs of the goldfish retina originates in antagonistic interactions between rods and cones at the photoreceptor-BC synapse, or between distinct spectral types of cones. The intensity-dependent behavior of spectrally opponent BCs arises due to sensitivity differences between the photoreceptor types at certain wavelengths. As a result, these BCs are spectrally coded in a restricted intensity range. Although spectrally opponent BCs might carry some information about the spectral composition of the stimulus, their spectral coding changes with stimulus intensity, making them unsuitable as absolute wavelength detectors. Our data indicate that rather than being directly linked to color vision, spectrally opponent BCs seem to act as intensity change detectors. The implications of these results for GC function and our current understanding of retinal ON and OFF pathways are discussed.

## 4.3 Material and Methods

*Preparation*

All animal experiments were carried out under the responsibility of the ethical committee of the Royal Netherlands Academy of Arts and Sciences, acting in accordance with the European Communities Council Directive of 24 November 1986 (86/609/EEC). Goldfish (*Carassius auratus)* of 10-15 cm standard body length were kept in aquaria at 18 °C in a 12 h / 12 h light-dark period. The technique used to prepare retinal slices is a modification of the method described elsewhere (Werblin, 1978). Animals in the light phase of their circadian rhythm were dark-adapted for 5-10 minutes prior to decapitation, and one eye was enucleated under infrared illumination ($\lambda$ > 850 nm). The anterior segment of the eye was removed; the retina

was peeled off the pigment epithelium and sclera, and placed receptor-side-up onto a piece of filter paper (Millipore, 13 mm diameter, 8 μm pore size). Vacuum was applied to the other side of the filter, in order to suck away the vitreous and attach the isolated retina firmly to the paper. The retina and the filter were cut in slices (100-150 μm thick) that were subsequently positioned on vaseline tracks in a superfusion chamber.

*Solutions*

The composition of the Ringer's solution was (in mM): 102 NaCl, 2.6 KCl, 1 $CaCl_2$, 1 $MgCl_2$, 28 $NaHCO_3$ and 5 glucose (bubbled continuously with 2.5% $CO_2$ and 97.5% $O_2$ for a pH of 7.8, approx. 248 mOsm). In some experiments, bicuculline methobromide (BIC, 200 μM), picrotoxin (PTX, 500 μM) and strychnine (STRY, 5-10 μM) were added to the control solution in order to block all GABAergic and glycinergic inputs to the BCs. The drug content of the Ringer's solution and the composition of the intracellular solution are given in Table 4.1. All chemicals were supplied by Sigma (The Netherlands).

*Optical Stimulator*

The superfusion chamber was mounted on a microscope equipped with infrared ($\lambda$ > 800 nm) differential interference contrast optics (NIKON Eclipse E600-FN, Japan) and the preparation was viewed in a TV monitor by means a 60 x water-immersion objective (N.A. 1.0) and a CCD camera (Philips, The Netherlands).

The light sources were initially a 450 W xenon arc (Osram, Germany) for the first channel and the halogen lamp of the microscope (Philips 7724, 12 V, 1000 W, The Netherlands) for the second channel. In later experiments, both light beams originated from the same xenon arc and were separated with a beam splitter (Starna, UK). All set-up configurations were calibrated carefully with a radiometer (Tektronix, 50-245, irradiance head J1812, UK), and later with a photodiode (Siemens BPW34, Germany) and by means of measurements of cone light responses to stimulation originating from both channels. Both light beams passed through a series of neutral density filters (Schott, Germany), double interference filters (Melles Griot, The Netherlands, peak transmission $\lambda$s = 400, 450, 500, 550, 600, 650, 700 nm, $\pm$ 8 nm bandwidth), and circular neutral density wedges (Barr & Strout, UK).

Light stimuli were cast onto the retina via two different optical paths: one light channel was focused through the objective by means of mirrors and lenses and could project small stimuli (slits of 50, 100 and 250 μm interposed on the optical path) onto the preparation; the second channel projected a 3.5 cm field (referred to from now on as "full field") through the microscope condensor. In the isolated retina, one uses spots of light to test the receptive field center of cells with center-surround organization. In slice preparations, light slits directed perpendicularly to the orientation of the slice are equivalent to light spots projected on the photoreceptor side of the retina. The width of the slit on a slice preparation is thus equivalent to the

| | Figures | | | | | | | |
|---|---|---|---|---|---|---|---|---|
| **Solutions** | **4.1a** ON BC | **4.1b** OFF BC | **4.2, 4.3, 4.9** Opponent BCs | **4.4a** Rod-HC | **4.4a** Cone-HC | **4.4b** ON BC | **4.4b** OFF BC | **4.7, 4.8** ON BC, Opponent BC |
| *NaCl* | | | | 35 | | 34 | | |
| *KCl* | 30 | 15 | 15 | | | | 46 | 50 |
| *KF* | 80 | 55 | 94 | | | | 24 | 20 |
| *CsCl* | | | | 5 | 93 | 5 | | |
| *TEACl* | | | | 20 | | 20 | | |
| $MgCl_2$ | | | | | | | 1 | |
| $CaCl_2$ | | | | 0.1 | | 0.1 | 0.1 | |
| *BAPTA-*$Na_4$ | | | | 10 | | 10 | | |
| *BAPTA-*$K_4$ | | 10 | 5 | | 10 | | 10 | 10 |
| *ATP-*$Na_2$ | | | | | | 10 | | |
| *ATP-*$K_2$ | 10 | 10 | 10 | 10 | 10 | | 10 | 10 |
| *GTP-Na* | | 1 | | 1 | 2 | 1 | 1 | 1 |
| *cAMP* | | | | | | | | 1 |
| *cGMP-Na* | | 1 | | 1 | 1 | 1 | 1 | 1 |
| *KOH* | | 18 | 18 | | | | 17 | 17 |
| *CsOH* | | | | 18 | 18 | 16 | | |
| *[mOsm]* | 255 | 223 | 273 | 204 | 243 | 200 | 224 | 222 |
| *PTX* | | | | 500 | 500 | 500 | 500 | 500 |
| *BIC* | | | | | 200 | | | |
| *STRY* | | | | 10 | 5 | 10 | 10 | 10 |
| *DNQX* | | | | | | 50 | | |
| *DL-AP4* | | | | 250 | | | | |

**Table 4.1:** Composition (in mM) and osmolarity (in mOsm) of the intracellular solutions used to record from the cells shown in the different Figures, as well as drug content of the Ringer's solution (in μM) in each experiment. PC: phosphocreatine; CK: creatine phosphokinase; PTX: picrotoxin; BIC: bicuculline methobromide; STRY: strychnine; DNQX: 6,7-dinitroquinoxaline-2,3(1H,4H)-dione; DL-AP4: (±)-2-amino-4-phosphonobutyric acid.

diameter of a spot onto an isolated retina. Given the dimensions of the preparation, the effective diameter of the full field was equivalent to the width of the slices (3-6 mm). Absolute intensity values are given throughout the paper in log quanta·$\mu m^{-2}$·$s^{-1}$.

*Electrodes and Recording Set-up*

Patch pipettes were pulled from borosilicate capillaries (Harvard Apparatus Ltd., UK) with a Brown Flaming Puller (Sutter Instruments, Novato, California) and had impedances between 5 and 15 MΩ when filled with pipette solution and measured in Ringer's solution. Series resistances ranged from 6 to 33 MΩ and were not corrected for.

The electrodes were placed in a PCS-5000 micromanipulator (Burleigh Instruments, Inc., Fishers, New York) and connected to an Axopatch 200 Patch Clamp (Axon Instruments, Inc., Union City, California). Data acquisition and control of the optical stimulator were made by means of a CED 1401 AD/DA converter (Cambridge Electronic Design Limited, UK) and an MS-DOS-based computer system.

Recordings were done in both current-clamp and voltage-clamp modes. For current-clamp measurements, $I_{hold}$ = 0 pA, and for voltage-clamp recordings, $V_{hold}$ = -50 mV.

*Data Analysis*

Light responses were measured either at the peak (for cones, HCs and non-opponent mixed-input BCs) or averaged within 100-150 ms after stimulus onset. The latter method was only applied to opponent mixed-input BCs, since the complexity of their response waveforms made it sometimes difficult to determine peaks. Response amplitudes were plotted against stimulus intensity (intensity-response relations). Data points were fitted with Hill functions,

$$Y = Y_{\max} \cdot \left( \frac{X^n}{X^n + K^n} \right),$$

where $Y$ is the response amplitude, $Y_{max}$ is the maximal response amplitude, $X$ is the stimulus intensity, $K$ is the stimulus intensity needed to generate a response with half-maximal amplitude, and $n$ is the slope factor.

The sensitivity of a cell was defined as the inverse of the intensity needed for a half maximal response (log $K^{-1}$). Light and spectral sensitivities were determined by comparing the log $K$ values of the intensity-response relations to stimulation at 450, 550 and 650 nm. This way, rod and cone inputs to the BCs recorded from could be isolated. Statistical analysis (ANOVA and two-tailed Student's t-tests) was performed on raw data, and the results are expressed as mean ± SD.

## 4.4 Results

Mixed-input BCs were visually selected based on their characteristic bulky flask-shaped somas and position in the outer part of the INL (Stell, 1967). We recorded from 194 cells in the dark-adapted retinal slice of goldfish. We found three physiological classes of BCs which could not be visually distinguished from each other in the living slice preparation. 156 BCs (80%) were depolarizing (ON BCs) (Figure 4.1a), and 17 (9 %) were hyperpolarizing (OFF BCs) to light stimulation throughout the visible spectrum (Figure 4.1b).

In 21 cells (11%), the polarity of the light responses depended on stimulus parameters (wavelength, intensity and/or size), which characterizes them as

opponent mixed-input BCs. The cells depicted in Figure 4.2a and b are two examples, recorded at different light levels. The light responses of these cells were hyperpolarizing at lower intensities (upper row) to 450 and 550 nm, whereas the response to 650 nm was a small depolarization. In both cells, the polarity of the light response to 550 nm reversed at higher light levels (bottom row). The BC in Figure 4.2a completely lost its spectral opponency at higher intensities. The polarity of the light responses of these BCs depends therefore not only on wavelength, but also on intensity. It is important to note here that the stimulus intensities used in these experiments (between -1 and 3 log units) were not extremely bright – opponency was lost before saturation was reached.

What is the mechanism responsible for this opponency? Can center-surround interactions be discarded? As discussed in Chapter 3, mixed-input BCs in the dark-adapted retina are electrically coupled, and with full-field stimulation, surround-mediated responses are negligible. Does this also hold for these

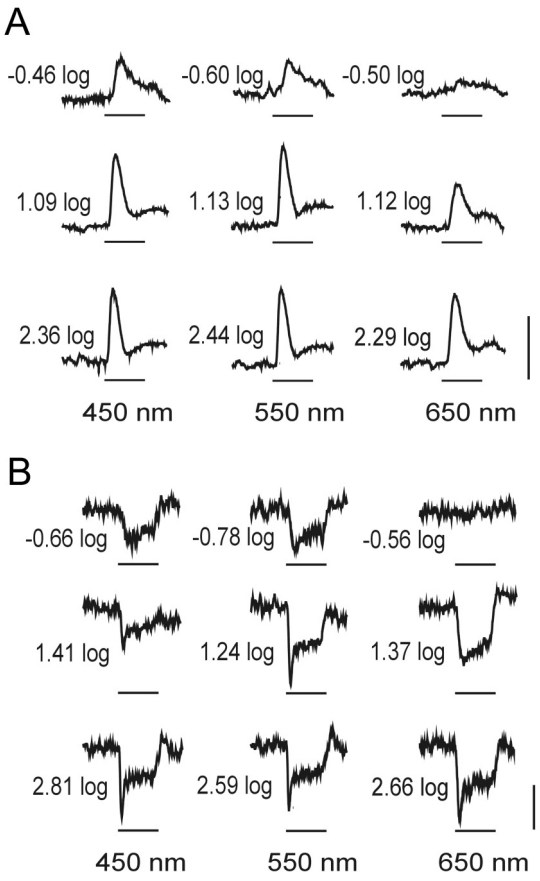


**Figure 4.1:** Non-opponent mixed-input BCs. A) Voltage responses of a non-opponent ON BC to a 100 μm light slit of 450 nm (left), 550 nm (middle) and 650 nm (right) at three different intensity levels (intensity values depicted to the left of the traces). Light responses are depolarizing at all light levels, and the cell is more sensitive (has bigger light responses) to stimulation at 550 nm. Horizontal bars indicate stimulus timing (500 ms) vertical bar = 5 mV. B) Voltage responses of a non-opponent OFF BC to a dim 250 μm light slit of 450 nm (left), 550 nm (middle) and 650 nm (right) at three different intensity levels (intensity values depicted to the left of the traces). Light responses are hyperpolarizing at all light levels, and the cell is more sensitive to stimulation at 550 nm. Horizontal bars indicate stimulus timing (500 ms) vertical bar = 5 mV.

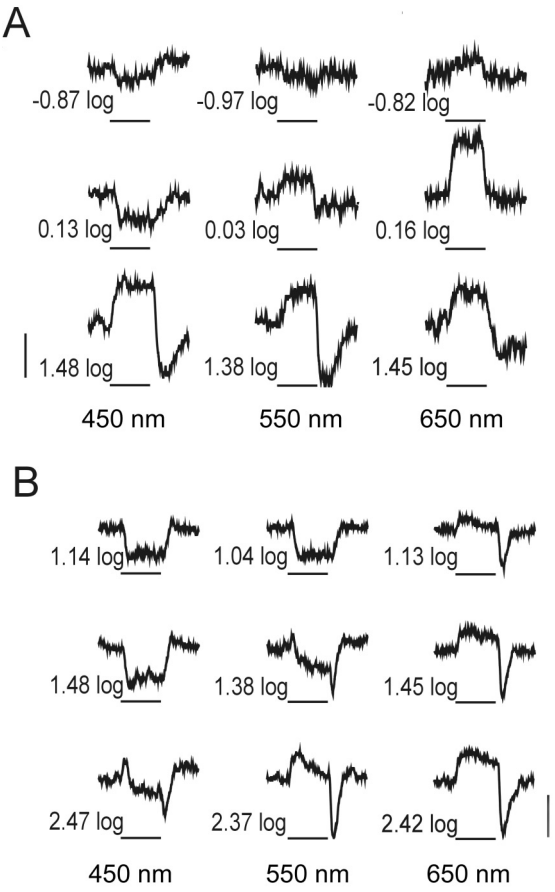


**Figure 4.2:** Opponent BCs. A) Voltage responses of a mixed-input BC to a full-field stimulus of 450 nm (left), 550 nm (middle) and 650 nm (right) at three intensity levels (values depicted to the left of the traces). Upper row: at lower intensities, the cell was spectrally opponent: responses to 450 and 550 nm were hyperpolarizing, whereas for 650 nm the cell depolarized. Middle row: at intermediate light levels, the response to 450 nm was still a hyperpolarization, but the response to 550 nm became depolarizing. Bottom row: at higher intensities, spectral opponency was lost. Horizontal bars represent stimulus timing (500 ms); vertical bar = 2.5 mV. B) Voltage responses of another mixed-input BC to similar stimuli. The polarity of the light response to 550 nm stimulation reversed as intensity was increased, and the response to 450 nm became biphasic (bottom row). Horizontal bars represent stimulus timing (500 ms); vertical bar = 5 mV.

opponent neurons? Figure 4.3 shows the intensity-response relations of an opponent mixed-input BC for stimulation with a 100 µm slit (filled symbols) and with a full field (open symbols) at 450 nm, 550 nm and 650 nm. The relations to large stimuli have in all three cases the same overall shape as the ones for small stimuli, but are shifted towards lower intensities. This leftward shift is consistent with electrical coupling, and not with the activity of surround-mediated processes.

Inner retinal contribution can be excluded as well, since similar opponent responses were recorded from axotomized cells. Additionally, opponency at the BC level was also recorded from retinas bathed in Ringer's solution containing BIC, PTX and STRY, indicating that the underlying process is solely outer retinal. In the following sections, we investigated the photoreceptor input to opponent BCs by comparing their response properties with those of photoreceptors, HCs and non-opponent mixed-input BCs.

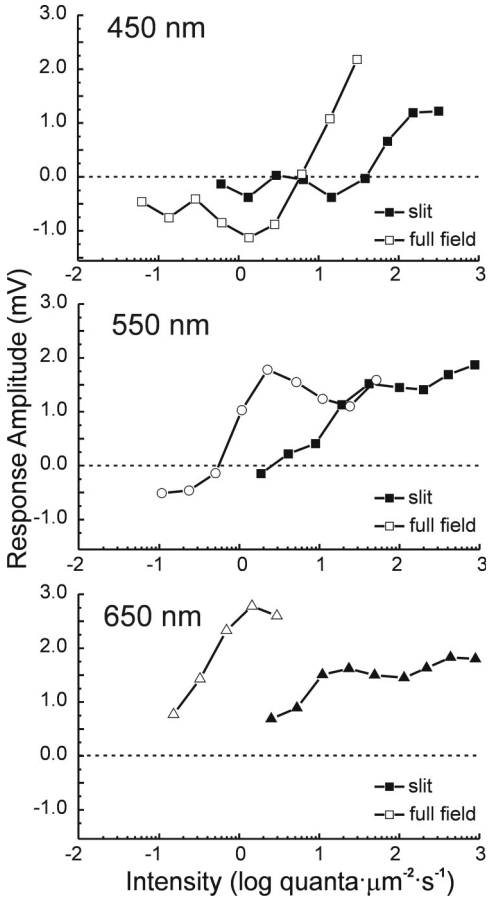


**Figure 4.3:** Opponency is not the result of center-surround interactions. Intensity-response relations of an opponent mixed-input BC to stimulation at 450 nm (upper graph), 550 nm (middle graph) and 650 nm (bottom graph) with a 100 μm slit (filled symbols) and a full field (open symbols). In all graphs, intensity-response relations to full-field stimulation have the same overall shape as the ones for spatially small stimuli, being shifted to lower light levels due to the combined effect of electrical coupling and stray light (as discussed in Chapter 3). The opponency of the light responses depended on intensity for both spatially large and small stimulation: the responses to 450 nm and 550 nm were hyperpolarizing at lower light levels and became depolarizing as stimulus intensity was increased. For 650 nm stimulation, light responses were always depolarizing. This indicates that the intensity-opponent behavior of this BC is not the result of surround-mediated inhibition, but of direct antagonistic photoreceptor inputs.

*Determination of Rod:Cone Input Ratios in Non-Opponent BCs*

The origin of the input to mixed-input BCs (rods, cones or both) can be determined based on the spectral coding and sensitivity of the cells. The majority of ON (153 out of 156, 98.07%) and OFF BCs (8 out of 10, 80 %) recorded were most sensitive to middle-wavelength stimulation (500-550 nm). This indicates that both rods and M-cones could drive their light responses.

To determine the extent of the contribution from each photoreceptor type, one has to compare the BC intensity-response relations with those of the photoreceptors in the same stimulus conditions. Since recording directly from goldfish rods is not feasible due to their diminutive dimensions, we used rod-driven HCs as a measure for rod sensitivity. In order to evaluate the validity of using HC intensity-response relations as representative of photoreceptor sensitivity, we also compared the intensity-response relations of cones and cone-driven HCs.

Figure 4.4a shows the intensity-response relations of 3 S-cones (grey circles), 8 M-cones (grey squares), and 7 L-cones (grey triangles) to stimulation at 550 nm. The dotted and dashed lines are the Hill fits for the intensity-response relations of a rod-driven HC and of a cone-driven HC for full-field stimulation at 550 nm, respectively. Although the intensity-response relations of both HCs have a slope similar to that of a single photoreceptor (for 17 cones, $n$ = 0.91±0.15), their intensity span is very different. The Hill function for the rod-driven HC is shifted to much lower intensities than the range in which cones are active, whereas the curve for the cone-driven HC falls nicely in the cone range.

In Figure 4.4b, a similar comparison is made between the Hill fits for the intensity-response relation of a mixed-input ON BC (dotted line) and of an OFF BC (dashed line) to full-field stimulation at 550 nm. This ON BC is rod-dominated, since its intensity-response relation resembles closely that of a rod-driven HC: it falls outside the cone range and has a slope comparable to that of one single

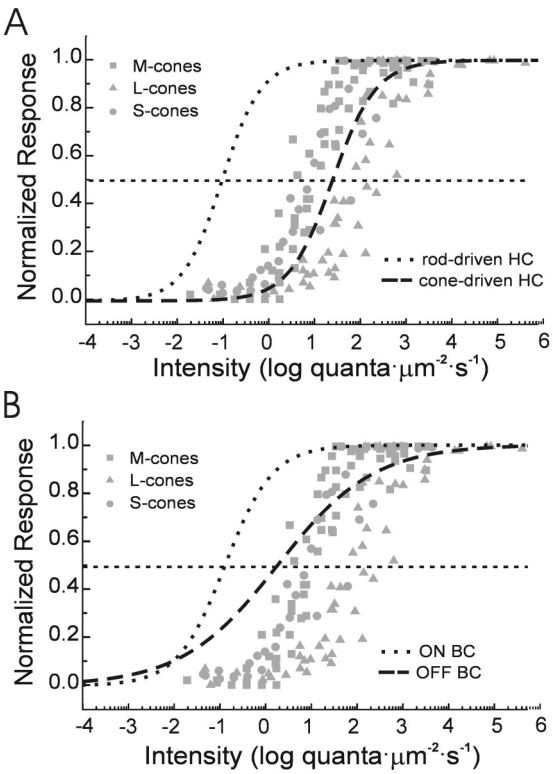


**Figure 4.4:** Sensitivity of the cones and second-order neurons of the goldfish. A) Intensity-response relations of 3 S-cones (circles), 8 M-cones (squares), and 7 L-cones (triangles) to 550 nm stimuli. Responses were normalized to the maximal amplitude in each case. The Hill fits (from Figure 3.3b) for a rod-driven HC (dotted line) and a cone-driven HC (dashed line) to full-field stimulation at 550 nm were normalized and superposed on the cone data to allow comparison. Although the slopes of the curves for the two HCs are similar to that of a single photoreceptor type ($n$ = 0.91 for the cone-driven HC and $n$ = 1.02 for the rod-driven HC), the sigmoidal representing the rod-driven HC lies outside the intensity range in which cones are active ($K$ = -1.02 log), whereas the curve for the cone-driven HC falls within that range ($K$ = 1.38 log). B) The Hill fits (from Figure 3.3c) for the intensity-response relations of two non-opponent mixed-input BCs (ON BC, dotted line; OFF BC, dashed line) to full-field stimulation at 550 nm were normalized and superposed on the cone data. The sigmoidal representing the ON BC is very similar to the one of the rod-driven HC in both slope and sensitivity ($n$ = 0.83, $K$ = -0.88), indicating that this cell receives predominantly rod input. The curve for the OFF BC has a shallower slope ($n$ = 0.41) and its $K$ value ($K$ = 0.26) is in between the ones of the two HC types, suggesting balanced inputs from rods and cones.

photoreceptor. The OFF BC, on the other hand, has a much lower sensitivity and a shallower intensity-response relation. This happens because this cell has a more balanced rod:cone input ratio: the sum of the inputs from rods and cones extends its dynamic range and changes the slope of its intensity-response curve.

Mixed-input BCs are generally more sensitive than the cones, which can be seen by their lower *K* values in Figure 4.5 ($p<0.001$ for ON BCs and $p< 0.001$ for OFF BCs). This does not mean, however, that they receive exclusively rod input in our experimental conditions. The *n* values for the intensity-response relations of OFF BCs (Figure 4.6a) and ON BCs (Figure 4.6b) are smaller than the *n* values of cone intensity-response relations (Figure 4.6c, $p<0.001$), indicating that ON and OFF BCs receive contributions from both types of photoreceptors. OFF BCs tend to have shallower slopes than ON BCs ($p = 0.011$), representing a more balanced proportion of rod and cone inputs.

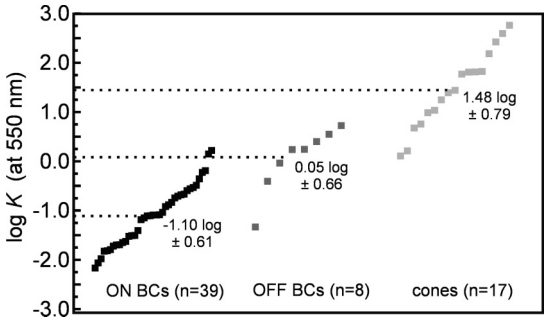


**Figure 4.5:** Mixed-input BCs are more sensitive than cones. The log *K* values of the intensity-response relations of 39 ON BCs (left), 8 OFF BCs (middle) and 17 cones (right) at 550 nm were plotted in ascending order for comparison. Mean ± SD are depicted to the right of the data points. The intensity-response relations of both ON and OFF BCs have lower *K* values (higher sensitivity) than those of goldfish cones, indicating that these BCs receive substantial rod input. OFF BCs tend to be less sensitive than ON BCs, suggesting a more balanced rod:cone input ratio.

Further evidence that the combination of multiple photoreceptor inputs determines the slope of the BC intensity-response relation is shown in Figure 4.7. When one abolishes rod input pharmacologically (in this case, by the application of the group III mGluR agonist DL-AP4), the intensity-response relation of ON BCs becomes steeper, and the sensitivity of the cell decreases, reflecting the contribution of the remaining cone input.

Next, we performed a similar analysis with the intensity-response relation of opponent BCs, in order to determine which photoreceptor types contribute to their light responses.

*Opponent BCs Also Have Varying Rod:Cone Input Ratios*

The intensity-response relations of opponent mixed-input BCs cannot be described by a single Hill function. They can be seen as the combination of, at least, two sigmoidal curves of opposite signs, which originate in different photoreceptor types. Once the component sigmoidals are determined, they can be examined in isolation.

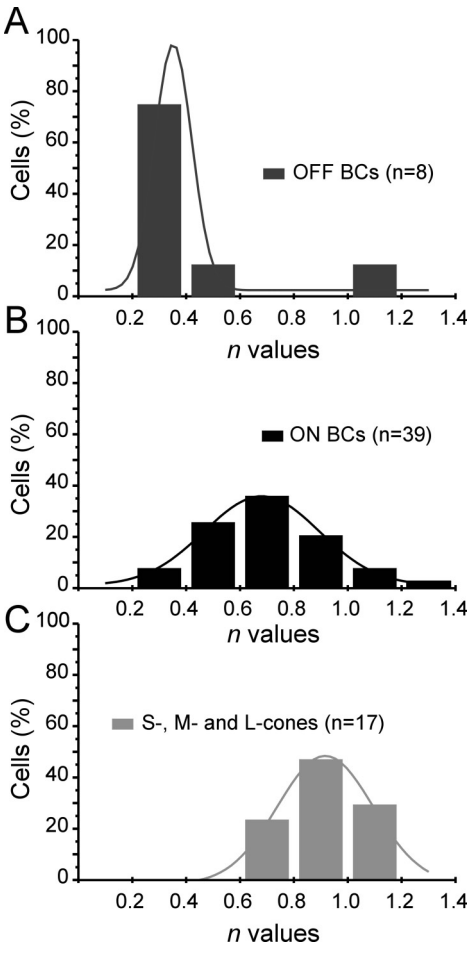


**Figure 4.6:** Mixed-input BCs have varying rod: cone input ratios. The *n* values (slope factors) of the intensity-response relations of 8 OFF BCs (A), 39 ON BCs (B) and 17 cones (C) show distinct distributions. The distribution of *n* values for rod intensity-response relations should be similar to the one for the cones, as can be inferred from rod-driven HC intensity-response relations (as shown in Figure 4.4a). However, the relations of both non-opponent BC types tend to have shallower slopes than the cones, indicating that in addition to rod input, their light responses also receive considerable cone input. The combination of these two inputs decreases the slope of the BC intensity-response relations by extending their dynamic ranges. Mixed-input OFF BCs seem to have a more balanced rod : cone input ratio, as can be inferred by the shallower slope of their intensity-response relations.

Figure 4.8a shows the intensity-response relation of an opponent mixed-input BC to full-field stimulation at 550 nm (open circles). This relation was fitted by the sum of two Hill functions of opposite polarities (continuous line): one depolarizing (dotted line) and one hyperpolarizing (dashed line). Although the linear sum of two sigmoidals is not appropriate to describe quantitatively a non-linear phenomenon such as the interaction between two photoreceptors, it is suitable as a qualitative approximation, and will be used throughout the Chapter as such.

In Figure 4.8b the two components were normalized and superposed on the cone data (already shown in Figure 4.4) to compare the relative sensitivity of the inputs. The depolarizing and hyperpolarizing curves are about 1.36 log apart; the depolarizing input is more sensitive than any of the cones recorded so far, indicating that it originates in rods. The hyperpolarizing curve falls in the cone range.

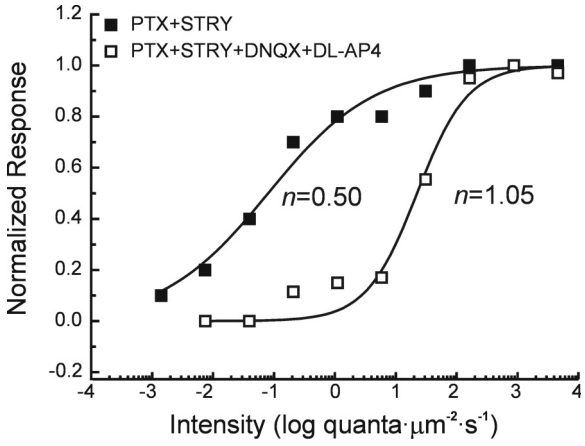


**Figure 4.7:** Photoreceptor input ratio determines the slope of the BC intensity-response relation. Intensity-response relations of a non-opponent ON BC to full-field stimulation at 450 nm in control (closed symbols) and DL-AP4 Ringer's solutions (open symbols). The slope of the relation becomes steeper (*n* values depicted in the figure), and the sensitivity shifts towards higher intensities (in this case, by 2.45 log units) due to the suppression of the rod input to the cell.

Next, we extended the analysis to other wavelengths (450 nm: squares; 550 nm: circles; 650 nm: triangles) in order to determine the spectral sensitivity of the input to this BC (Figure 4.8c). This procedure yields two *K* values (one for each input) for every wavelength. By comparing the *K* values with the action spectra of the various photoreceptor types one can determine which one contributes to the light responses of a particular BC (Figure 4.8d). In this case, the opponent light responses of this mixed-input BC are generated by antagonistic inputs that most closely match the absorption spectra from rods and S-cones (after Mooij and Van den Berg, 1983).

As in the case of non-opponent mixed-input BCs, the rod:cone input ratios of opponent cells varied strongly. Figure 4.9 depicts a cell that receives predominantly cone input. In Figure 4.9a, the intensity-response relations to full-field stimulation at 450 nm (squares) 550 nm (circles) and 650 nm (triangles) are depicted. We measured the responses of this BC twice, with a lapse of about 30 min between measurements. The early responses are at the left (black symbols), and the late ones (higher intensities) are at the right side of the graph (grey symbols). Although the cell slightly changed its adaptive state in between experiments, its intensity-dependent behavior is evident in both sets of data.

We fitted Hill curves to the early intensity-response relations (Figure 4.9b) in order to determine the spectral sensitivity of its inputs. The best fit (continuous lines) was obtained by the sum of two sigmoidals which differed in their *K* values by 0.56 log at 550 nm (Figure 4.9c), both active in the same range as the cones. Although both components were most sensitive to 550 nm (Figure 4.9d), the depolarizing input (squares) has a somewhat broader spectral sensitivity than the hyperpolarizing one (circles), indicating L-cone contribution. At shorter wavelengths, the data points for the depolarizing input deviate from the L-cone absorption spectrum, which can be explained by the larger variation found in the β-bands of L-cone pigments (Mooij and

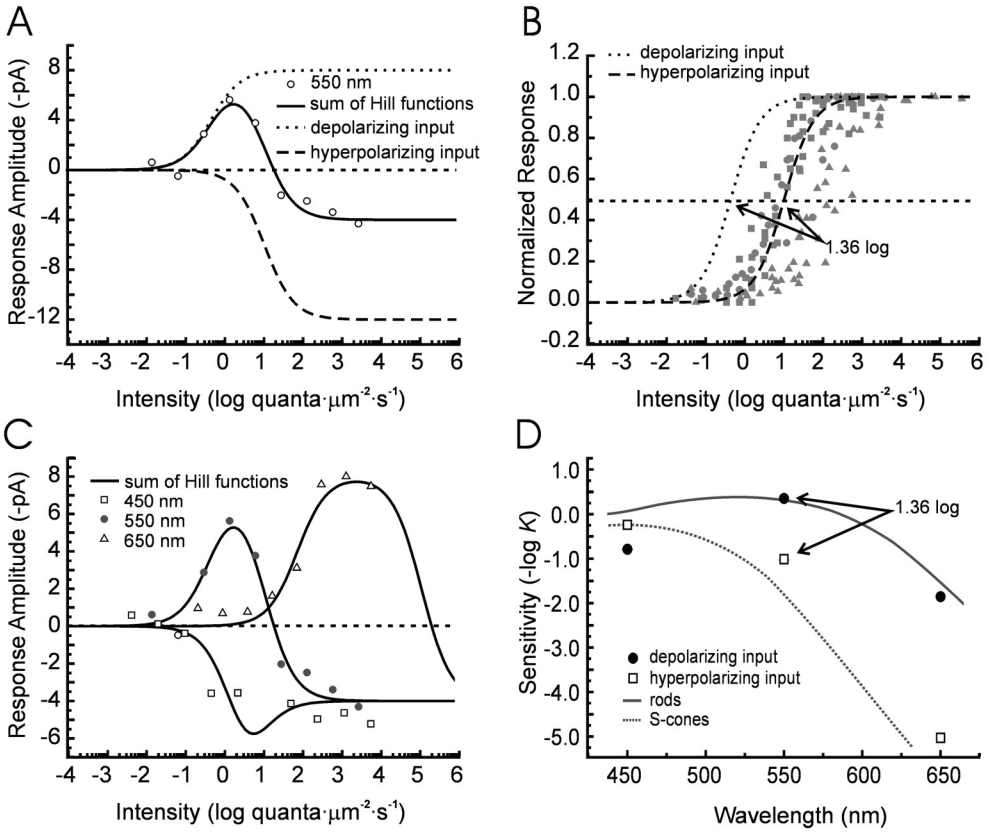


**Figure 4.8:** Rod-cone interactions generate opponent BC responses. A) Intensity-response relation of an opponent mixed-input BC to full-field stimulation at 550 nm (circles). Data points were fit by the sum (continuous line) of two Hill functions of opposite polarities: a depolarizing (dotted line) and a hyperpolarizing (dashed line) component sigmoidals, representing the antagonistic inputs to this cell. B) The two component sigmoidals were normalized (the dashed Hill function representing the hyperpolarizing input was inverted to facilitate comparison) and superposed to the cone intensity-response relations to 550 nm (already shown in Figure 4.4). The depolarizing component (K = -0.36 log) is more sensitive than any of the cones recorded under similar conditions, and there is a 1.36 log unit difference in *K* values between the two inputs. C) The intensity-response relation of this BC to full-field stimulation at 450 nm (squares), 550 nm (circles) and 650 nm (triangles) was fitted by summing two inputs with different light and spectral sensitivities. The best fit (continuous lines) was obtained by the sum of a depolarizing input most sensitive to 550 nm (Figure 4.8d, circles) and a hyperpolarizing input most sensitive to 450 nm (Figure 4.8d, squares). D) Light and spectral sensitivity of the inputs to this opponent BC. The absorption spectra of rods and S-cones (continuous and dotted lines, respectively) were added for comparison (after Mooij and Van den Berg, 1983). The depolarizing component (circles) is most sensitive to 550 nm stimulation and the hyperpolarizing component (squares) is most sensitive to 450 nm light. This, added to the higher sensitivity of the depolarizing input, indicates convergence of antagonistic inputs from rods and S-cones to this BC.

Van den Berg, 1983). A similar mismatch between microspectrophotometric data and electrophysiological measurements can be seen in Figure 1.3.

Taken together, these results indicate that spectral opponency at the BC level can be generated not only by contributions from different spectral types of cones, as suggested previously (Kaneko and Tachibana, 1981; Haverkamp et al., 1999; Kaneko and Tachibana, 1983), but also by antagonistic interactions between rods and cones. We found evidence for opponent interactions between rods and S-cones (Figure 4.8), rods and a mixture of L- and M-cones (BC in Figure 4.3), M- and L-cones (Figure 4.9), and S- and M- cones (not shown).

An extensive analysis of the rod:cone input ratios of opponent mixed-input BCs was not performed due to the brevity and scarcity of the recordings. Nonetheless, the data presented so far suggest that, similarly to what non-opponent mixed-input BCs, opponent mixed-input BCs have varying rod:cone input ratios. The function of their opponent behavior will be addressed in the discussion.

## 4.5 Discussion

Here we show that antagonistic inputs from different photoreceptor types render the sign of the light response of some mixed-input BCs dependent on stimulus wavelength and intensity. These inputs can either originate in rods and cones, or be the result of cone-cone interactions. Further, we also demonstrate that due to our stimulus protocol and to coupling of the BC network, mixed-input BCs of the goldfish retina do not show a pronounced center-surround antagonism in the dark-adapted retina. They are more sensitive to large stimulation than to the presentation of small stimuli at the same wavelength and intensity.

The fact that the polarity of the light response of these mixed-input BCs can change with a variety of parameters such as intensity, wavelength and size has consequences for BC function and information coding in the retina. In the next sections we will address each of these topics separately.

*Glutamate Receptors of Opponent Mixed-Input BCs*

Differently from what happens with HCs, the spectral opponency at the BC level is not a result of the feedback system between HCs and photoreceptors, because BC opponent responses can be evoked with stimuli that are too small to stimulate HCs. Which glutamate receptors could then underlie this opponency?

There is evidence in literature and in this thesis that mixed-input BCs display numerous glutamate receptors whose function is not yet clear. Putative mixed-input ON BCs of the goldfish, for instance, were shown to express at least two mGluRs (mGluR1$\alpha$ Yazulla et al., 2001; Klooster et al., 2001 and mGluR6, this thesis, Chapter 2) and an ionotropic glutamate receptor subunit (GluR2) in their dendrites invaginating into the rod spherules (Klooster et al., 2001). We have also evidence

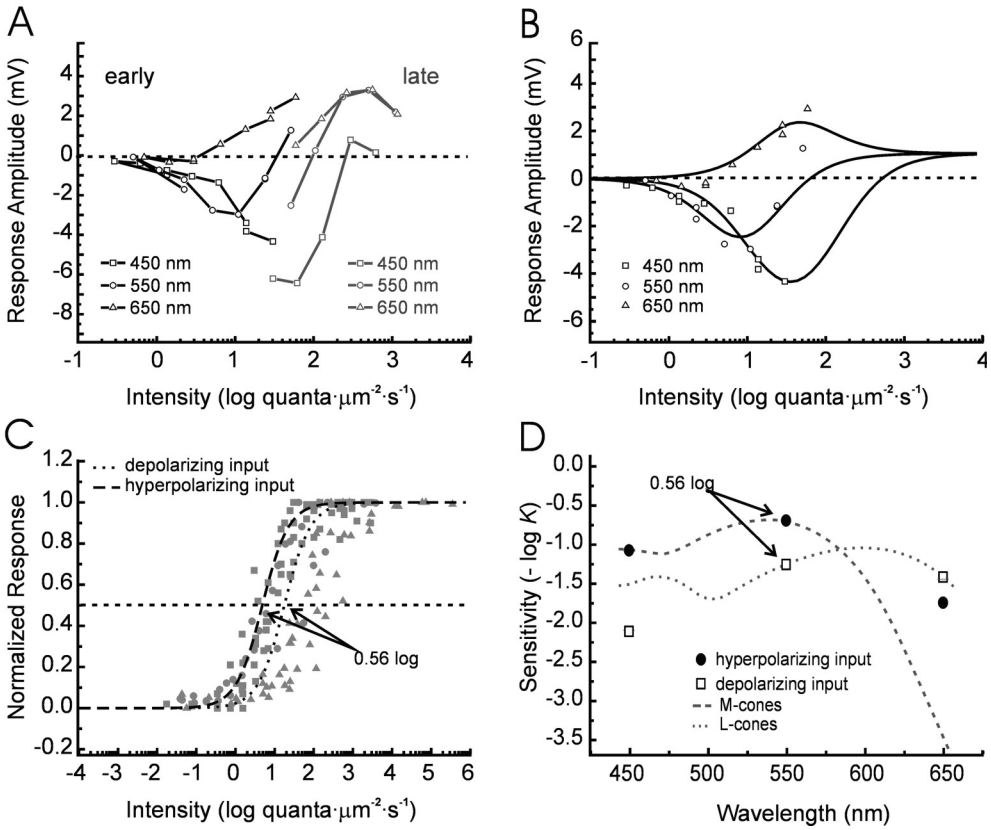


**Figure 4.9:** Opponent BCs have varying rod:cone input ratios. A) Intensity-response relations of an opponent mixed-input BC to full-field stimulation at 450 nm (squares), 550 nm (circles) and 650 nm (triangles) measured at two different moments (in black: early responses; in grey: late responses). Despite a change in adaptive state between the experiments, the cell presented intensity-opponent behavior in both sets of data. B) The early intensity-response relation was fitted by summing two inputs with different light and spectral sensitivities (continuous lines). C) The component sigmoidals for the 550 nm stimulus were normalized and superposed to the cone data. The hyperpolarizing input (dashed line) was inverted to facilitate comparison. Both sigmoidals lie within the intensity range in which cones are active, and the difference in *K* values between them is small (0.56 log), suggesting that this cell received predominantly cone input. D) Light and spectral sensitivity of the inputs to this opponent BC. The absorption spectra of M-cones and L-cones (dashed and dotted lines, respectively) were added for comparison (after Mooij and Van den Berg, 1983). Although both inputs were most sensitive to 550 nm, their spectral sensitivity is somewhat broader at longer wavelengths, consistent with some L-cone contribution. The discrepancy between the L-cone absorption spectrum and the depolarizing input at 450 nm can be ascribed to the larger variation found in the β-bands of the L-cone pigments (Mooij and Van den Berg, 1983).

that dendrites of mixed-input BCs contacting the rod terminals express GluR4 (another iGluR subunit) and EAAT5 (data not shown, but see General Discussion), although we did not perform a systematic double-label EM study to determine which mixed-input BC types express which GluRs. There are at least 5 (Stell, 1967/1976) and maybe 6 (Sherry and Yazulla, 1993) distinct types of mixed-input BCs of the goldfish (two of them stratifying at sublamina a and the rest at sublamina b of the IPL), but we cannot distinguish between them at the EM level.

It is important to remember that these cells also contact cones, and the identity of the GluRs expressed in their dendrites at the cone pedicles is to date unknown. There is pharmacological indication that cones drive predominantly a transporter-like receptor (which could be EAAT5, see Chapters 3, 5 and 6) as well as mGluR6 in mixed-input ON BCs (Grant and Dowling, 1996; Wong et al., 2005b; this thesis, Chapter 2). Also hyperpolarizing responses were shown to be mediated by more than one conductance in the carp (Saito and Kaneko, 1983; Saito et al., 1984).

Taken together, this data indicate that mGluRs, iGluRs and EAATs could participate in the generation of BC opponent responses. Further morphological and pharmacological experiments have to be performed to elucidate the identity of the GluRs involved in generating depolarizing and hyperpolarizing responses in opponent and non-opponent mixed-input BCs of the goldfish.

*Rod-Cone Interactions in the Dark-Adapted Retina*

Previous recordings from GCs and BCs in the goldfish and the closely related carp suggested a complete switch from rod-driven to cone-driven light responses as the retina light adapts (Beauchamp and Daw, 1972; Raynauld, 1972; Shimbo et al., 2000). Our results indicate that although some mixed-input BCs seem to be rod-dominated (as the ON BC in Figure 4.4) or cone-dominated (the opponent BC in Figure 4.9), an abrupt switch does not seem to apply in our experimental conditions.

Mixed-input OFF BCs and some opponent BCs receive balanced input from both rod and cones, and even the so-called rod-dominated ON BCs receive cone input at higher intensities, as one can conclude from the slope and the span of their intensity-response relations. Further, in our preparations both rod- and cone-driven light responses in a given BC were recorded in the same adaptive state, indicating that rod- and cone-driven systems are concomitantly active.

The discrepancy between our data and the other studies might be ascribed to differences in the adaptive state of the retinas and/or in the experimental procedures. For instance, we never worked with adapting backgrounds in order to saturate rods and light adapt the preparation as the other authors did. By working in complete darkness and having long interstimulus intervals, we kept the adaptive state of the preparation constant and demonstrated synergistic and antagonistic interactions between rods and cones in the mesopic range.

*Receptive Field Properties*

In early studies, the BC receptive field organization was assessed by measuring the light responses to spots of increasing diameters, keeping wavelength and intensity fixed (Kaneko, 1973; Kaneko and Tachibana, 1983). The receptive field center was considered to have the same size as the stimulus that yielded the largest response (see Figure 1.6a). From a certain stimulus size on, responses would decrease and even reverse polarity, which was interpreted as an effect of the antagonistic surround.

It is unlikely that spots of increasing diameters can generate surround-induced responses which are bigger than the central ones, because polarization of the central input counteracts the effect of surround-mediated inhibition (Skrzypek and Werblin, 1983; Kraaij et al., 2000). The net effect of simultaneous activation of center- and surround mediated processes in a given cell is a rightward shift of its intensity-response relation as compared to center stimulation only, without a significant effect on the maximal response amplitude (Werblin, 1974).

Although BCs can show clear surround-induced responses when stimulated with light annuli (Werblin and Dowling, 1969; Saito et al., 1981; Kaneko and Tachibana, 1981), our data indicate that the use of increasing stimulus sizes might lead to misinterpretations. In the upper panel of Figure 4.3, for instance, a 100 μm slit around 1.1 log yields a hyperpolarizing response, whereas a full field at the same wavelength and intensity induces a depolarization in that mixed-input opponent BC.

This dependency on stimulus size is not a consequence of the activation of an antagonistic surround by means of large stimuli, but a result of an incomplete activation of a large receptive field center by means of a small stimulus. The electrical coupling of opponent BCs together with stray light, as discussed in Chapter 3, may cause the responses to spatially small and large stimuli at a given wavelength to reverse polarity, giving the false impression of a center-surround organization.

*Function of Opponent Cells*

Figure 4.10a shows that if a BC receives inputs of the same sign from two different photoreceptor types, the resulting intensity-response relation has a shallower slope than the components. Although such a mixed-input BC has a broad dynamic range, it needs large changes in stimulus intensity to change its response amplitude. The non-opponent OFF BC shown in Figure 4.4b has such a shallow intensity-response relation.

On the other hand, a cell that receives inputs of opposite signs from two different photoreceptors has an intensity-response relation with a much steeper slope than any of its components (Figure 4.10b). This BC acts therefore as an ideal intensity change detector: small changes in the stimulus intensity evoke a large change in response amplitude. The opponent inputs transform this BC in a kind of push-pull device, and render it more sensitive to small changes in intensity than either type of photoreceptor alone.

An opponent BC, however, cannot code intensity, since it might give the same response for stimuli at different intensity levels (compare for instance 0.4 and 2.2 log in Figure 4.10b). Therefore, the visual system needs both non-opponent and opponent BCs in order to extract information about the mean luminance and changes in light intensity around this level, respectively.

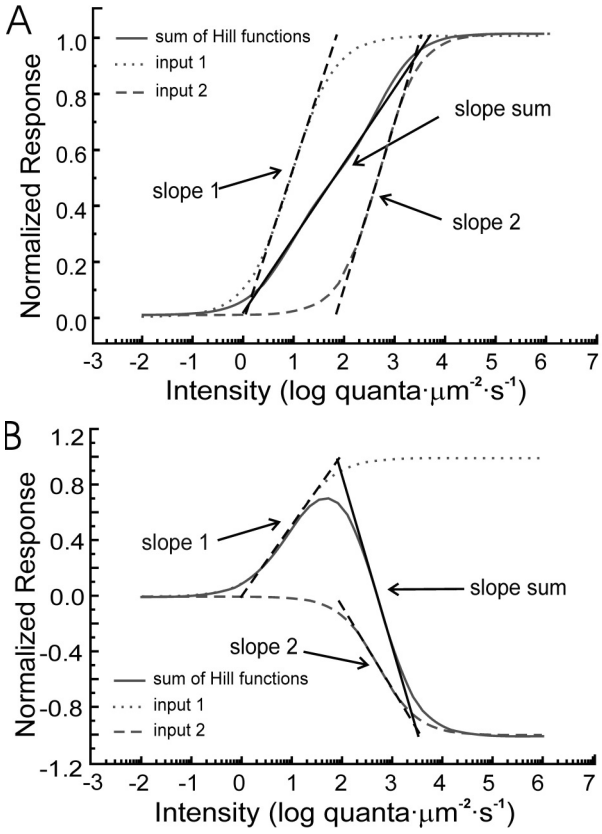


**Figure 4.10:** Opponent BCs have a steeper intensity-response relation. A) Model intensity-response relation of a non-opponent mixed-input BC (based on the OFF BC shown in Figure 3.3c), consisting on the sum of two sigmoidals of the same polarity representing synergistic photoreceptor inputs (dotted and dashed grey lines). The resulting curve (continuous grey line) spans over a broader intensity range than the component sigmoidals, but is shallower. B) Model intensity-response relation of an opponent mixed-input BC (based on a real cell), consisting on the sum of two sigmoidals of opposite signs representing antagonistic photoreceptor inputs (dotted and dashed grey lines). The resulting curve (continuous grey line) is steeper than any of the component sigmoidals (dashed black lines).

*Consequences for the Current Ideas on Visual Information Pathways*

The data presented in this Chapter indicate that the segregation into ON and OFF pathways is not complete at the BC level, since some BCs can present both depolarizing and hyperpolarizing light responses, depending on the intensity or wavelength of the stimulus. For instance, a BC that receives depolarizing inputs from rods and hyperpolarizing inputs from cones (Figure 4.8) is ON at scotopic levels and OFF at photopic levels. According to the concept of ON and OFF pathways, this cell would signal light increments in one situation and light decrements in the other.

Apart from the debate about color vision in lower vertebrates being or not being an opponent process (as discussed in Chapter 1), it is expected that a system subserving the psychophysical experience of color have “neutral points” (reverse its response polarity) in regions of the visible spectrum that correspond to the percept of unique hues (for a review, see Calkins, 2004). For instance, the perception of yellow would need an opponent cell somewhere in the visual system whose neutral point is around 580 nm. Spectrally opponent BCs are not suitable for performing such a task. Their intensity-dependent behavior makes their neutral points shift dramatically, up to the point of abolishing their spectrally opponent character entirely at higher intensities. A similar intensity-dependency was also described in spectrally opponent GCs of the goldfish (Afanador and Adams, 1982) and monkey (de Monasterio et al., 1975a), indicating that this feature is not unique and is transmitted to the forthcoming cells.

BCs and HCs in the teleost may use such a coding strategy to limit redundancy and optimize the use of the available bandwidth, namely via a broadband (non-opponent) and an opponent channel. These retinal channels act in concert to compress and transmit information to the brain (Buchsbaum and Gottschalk, 1983; Schiller et al., 1990a/b), and it seems likely that at the retinal level the different aspects of a visual scene (luminance, color, etc.) are still transmitted together, only to be extracted later (Kingdom and Mullen, 1995; Schiller, 1996; Gegenfurtner and Kiper, 2003).

As to the mixed-input BCs shown in this study, the fact that their response polarities can change with so many parameters suggests that information is not coded by the sign of the response, but by the *response change in relation to a previous situation*. The function of these BCs must lie beyond signaling either darker than background or lighter than background, a role that has been ascribed to ON and OFF BCs previously (Famiglietti and Kolb, 1976; Saito, 1987; Dolan and Schiller, 1994). This idea is supported by studies showing that ON and OFF BCs respond to positive or negative contrasts with the same efficiency (Burkhardt and Fahey, 1998), and show similar kinetics when presented with more physiological stimuli (Armstrong-Gold and Rieke, 2003). Since the convergence of opponent inputs increases BC voltage span and sensitivity to intensity changes, they are suitable for informing the visual system about both increments and decrements around a mean luminance level.

**Acknowledgements**

The authors thank Drs. Colleen Shields, Iris Fahrenfort, Marjelle van Leeuwen and Trijntje Sjoerdsma for helpful comments on earlier versions of the manuscript.

# Chapter 5

# Dendritic Voltage-Gated Potassium Channels: the Rod-Cone Switch in Mixed-Input ON Bipolar Cells of the Goldfish Retina?

*Christina Joselevitch and Maarten Kamermans*
*(To be submitted)*

## 5.1 Abstract

Rod-driven light responses of mixed-input ON BCs are accompanied by a conductance increase mediated by a metabotropic glutamate receptor (mGluR) of the group III. Pharmacological activation of these mGluRs, however, does not seem to modulate the same pathway underlying light responses. Puffs of DL-AP4 induce a linear conductance decrease with a reversal potential ($V_{rev}$) near 0 mV, while rod-driven light responses rectify at positive potentials and do not reverse. The cone-driven light responses of these BCs are accompanied by a conductance decrease with a negative $V_{rev}$, and also rectify at positive potentials. Since both rod- and cone- driven responses rectify, it seems likely that the rectification is a post-synaptic process not related to the glutamate receptor machinery. The rectification of light-driven conductances coincides with the activation of an outwardly rectifying, voltage-gated $K^+$-current ($I_{KV}$). To investigate the relation between voltage-gated and neurotransmitter-elicited currents, a compartmental model of a goldfish mixed-input ON BC was formulated using NEURON. Simulations indicate that, while somatic $I_{KV}$ does not influence light-driven responses, $K^+$ channels localized at the tips of the dendrites shift $V_{rev}$ and increase the rectification considerably. Furthermore, the model illustrates that the high resistance of the dendritic shafts and the homogeneous distribution of glutamate-gated channels along the dendrites allow synaptic inputs and DL-AP4 puffs to yield different *IV* relations. The functions of dendritic $K^+$ channels are manifold. In the scotopic range, they speed up synaptic transmission and generate transience by accelerating BC repolarization. This fast repolarization restores the high gain of the rod-BC synapse, allowing subsequent rod-driven signals to drive the cell efficiently. As light levels increase, tonic suppression of the rod input leads to the opening of many of these voltage-gated channels, shunting the rod pathway and decreasing the gain of the rod-BC synapse.

## 5.2 Introduction

Rod vision near threshold is characterized by a high gain (Ashmore and Falk, 1980). When the retina becomes more light-adapted, cone vision takes over and the gain of the rod pathway decreases (Ashmore and Falk, 1980). Mixed-input BCs receive both rod and cone input and should therefore be able to function optimally in both conditions. This requires special mechanisms to adjust the gain of the rod-BC synapse at different light levels.

Mixed-input ON BCs of the fish retina respond to light via two different mechanisms, a conductance *decrease* with a negative reversal potential ($V_{rev}$) driven by cones and a conductance *increase* with a positive $V_{rev}$ driven by rods (Toyoda, 1973; Kaneko and Shimazaki, 1976; Toyoda et al., 1978). Rod-driven light responses are mediated by mGluR6, which is coupled to a cationic conductance via a pathway involving Go$\alpha$ (Nakajima et al., 1993; Vardi et al., 1993). Recent evidence suggests that cones drive a $Cl^-$ conductance probably mediated by EAAT5 acting as a glutamate receptor (Saito et al., 1979; Arriza et al., 1997; Eliasof et al., 1998a/b; but see General Discussion).

The multiplicity and the characteristics of the photoreceptor inputs to mixed-input ON BCs generate a big paradox at the first synapse. Due to their opposing conductance mechanisms, if rod- and cone-driven pathways are concomitantly active (i.e. in the mesopic range) one might shunt the other (Falk, 1988).

The aim of this study is to characterize the interaction of these inputs and shed light on this controversy. We will show that voltage-gated $K^+$ channels at the tips of the ON BC dendrites provide the morphological substrate for a gain control mechanism in the OPL, allowing mixed-input BCs to operate in a wide range of environmental light conditions.

## 5.3 Material and Methods

*Preparation*

All animal experiments were carried out under the responsibility of the ethical committee of the Royal Netherlands Academy of Arts and Sciences, acting in accordance with the European Communities Council Directive of 24 November 1986 (86/609/EEC). Goldfish (*Carassius auratus)* of 10-15 cm standard body length were kept in aquaria at 18 $^oC$ in a 12 h / 12 h light-dark period. The technique used to prepare retinal slices is a modification of the method described elsewhere (Werblin, 1978). Animals in the light phase of their circadian rhythm were dark-adapted for 5-10 minutes prior to decapitation, and one eye was enucleated under infrared illumination ($\lambda$ > 850 nm). The anterior segment of the eye was removed; the retina was peeled off the pigment epithelium and sclera, and placed receptor-side-up onto a piece of filter paper (Millipore, 13 mm diameter, 8 $\mu$m pore size). Vacuum was

applied to the other side of the filter, in order to suck away the vitreous and attach the isolated retina firmly to the paper. The retina and the filter were cut in slices (100-150 µm thick) that were subsequently positioned on vaseline tracks in a superfusion chamber.

*Solutions*

The composition of the Ringer's solution was (in mM): 102 NaCl, 2.6 KCl, 1 $CaCl_2$, 1 $MgCl_2$, 28 $NaHCO_3$ and 5 glucose (bubbled continuously with 2.5% $CO_2$ and 97.5% $O_2$ for a pH of 7.8, approx. 248 mOsm). Picrotoxin (PTX, 100-500 µM) and strychnine (STRY, 5-18 µM) were added routinely to the control solution in order to block all GABAergic and glycinergic inputs to the BCs. For local drug delivery, DL-AP4 was dissolved in the control Ringer's solution and this solution was used to fill a patch clamp pipette held close to the recorded cell and used for pressure-ejection.

The drug content of the Ringer's solution and the composition of the intracellular solution are given in Table 5.1. Junction potentials for each pipette solution were calculated after Barry and Lynch (1991) and Ng and Barry (1995), and subtracted from the nominal voltage command values before correction for series resistance (see *Data Analysis* section). All chemicals were supplied by Sigma (The Netherlands).

*Optical Stimulator*

The superfusion chamber was mounted on a microscope equipped with infrared ($\lambda$ > 800 nm) differential interference contrast optics (NIKON Eclipse E600-FN, Japan) and the preparation was viewed in a TV monitor by means a 60 x water-immersion objective (N.A. 1.0) and a CCD camera (Philips, The Netherlands).

Two light beams originated from one xenon arc and were separated with a beam splitter (Starna, UK). All set-up configurations were calibrated carefully with a radiometer (Tektronix, 50-245, irradiance head J1812, UK), and later with a photodiode (Siemens BPW34, Germany). Cone light responses to stimulation originating from both channels were used as a control for the calibrations. Both light beams passed through a series of neutral density filters (Schott, Germany), double interference filters (Melles Griot, The Netherlands, peak transmission $\lambda_s$ = 400, 450, 500, 550, 600, 650, 700 nm, 8 nm bandwidth), and circular neutral density wedges (Barr & Strout, UK).

Light stimuli were cast onto the retina via two different optical paths: one light channel was focused through the objective by means of mirrors and lenses and could project small stimuli (slits of 50, 100 and 250 µm interposed on the optical path) onto the preparation; the second channel projected a 3.5 cm field (referred to from now on as "full field") through the microscope condensor. In the isolated retina, one uses spots of light to test the receptive field center of cells with center-surround organization. In slice preparations, light slits directed perpendicularly to the orientation of the slice are equivalent to light spots projected on the photoreceptor

| | Figures | | | | | |
|---|---|---|---|---|---|---|
| **Solutions** | **5.4a** | **5.4c** | **5.5a,b** | **5.5c,d** | **5.6c,d** | **5.7** |
| *KOH* | | | | | 17 | 17 |
| *CsOH* | 18 | 24 | 2 | 22 | | |
| *NaCl* | 34 | | | | | |
| *KCl* | | | | | 10 | 46 |
| *CsCl* | 5 | 47 | 60 | 47 | | |
| *KF* | | | | | 60 | 24 |
| $CH_3O_3SCs$ | | 8 | | 10 | | |
| $MgCl_2$ | | 1 | | 1 | | 1 |
| $CaCl_2$ | 0.1 | 0.1 | | 0.1 | | 0.1 |
| *TEACl* | 20 | | | | | |
| *HEPES* | | 10 | | 20 | | |
| *ATP-Mg* | | | 5 | | | |
| $ATP\text{-}Na_2$ | 10 | | | 10 | | |
| $ATP\text{-}K_2$ | | 10 | | | 10 | 10 |
| $BAPTA\text{-}Na_4$ | 10 | | | | | |
| $BAPTA\text{-}k_4$ | | 10 | 10 | 10 | 10 | 10 |
| *GTP-Na* | 1 | 2 | | | 1 | 1 |
| *GTP-Li* | | | 1 | 1 | | |
| *cAMP* | | 1 | | | | |
| *cGMP-Na* | 1 | 1 | 1 | 1 | 1 | 1 |
| $LY\text{-}K_2$ | 1 | 1 | 1 | 1 | 1 | 1 |
| *[mOsm]* | 204 | 222 | 162 | 228 | 221 | 224 |
| *BIC* | | 200 | | | | |
| *PTX* | 500 | 500 | 500 | 500 | 100* | 500 |
| *STRY* | 18 | 5 | 5 | 5 | 5* | 5 |
| *DNQX* | 50 | | 50 | | | 50** |
| *NBQX* | | | | 20 | | |
| *DL-AP4* | | 250 | | | 20* | 250** |
| *D-AP7* | | | | 250 | | |

**Table 5.1:** Composition (in mM) and osmolarity (in mOsm) of the intracellular solutions used to record from the cells shown in the different Figures, as well as drug content of the Ringer's solution (in μM) in each experiment. TEA: tetraethylammonium; LY: Lucifer Yellow; PTX: picrotoxin; STRY: strychnine; DNQX: 6,7-dinitroquinoxaline-2,3(1H,4H)-dione; NBQX: 1,2,3,4-tetrahydro-6-nitro-2,3-dioxo-benzo[f]quinoxaline-7-sulfonamide; DL-AP4: (±)-2-amino-4-phosphonobutyric acid; D-AP7: D(-)-2-amino-7-phosphono-heptanoate. (*): in Figure 5.6, PTX, STRY and DL-AP4 were added to the Ringer's solution only for the recordings in (B). (**): in Figure 5.7, DL-AP4 and DNQX were added to the Ringer's solution only for the recordings in (B).

side of the retina. The width of the slit on a slice preparation is thus equivalent to the diameter of a spot onto an isolated retina. Given the dimensions of the preparation, the effective diameter of the full field was equivalent to the width of the slices (3-6 mm). Absolute intensity values are given throughout the paper in log quanta·$\mu m^{-2}$·$s^{-1}$.

*Electrodes and Recording Set-up*

Patch pipettes were pulled from borosilicate capillaries (Harvard Apparatus Ltd., UK) with a Brown Flaming Puller (Sutter Instruments, Novato, California) and had impedances between 5 and 15 MΩ when filled with pipette solution and measured in Ringer's solution. Series resistances ranged from 6 to 33 MΩ and were corrected for offline (see next section).

Electrodes were placed in a PCS-5000 micromanipulator (Burleigh Instruments, Inc., Fishers, New York) and connected to an Axopatch 200 Patch Clamp (Axon Instruments, Inc., Union City, California). A second PCS-5000 micromanipulator not connected to the patch-clamp amplifier was used to hold the puffer pipettes (manufactured as described above) and perfuse drugs locally by means of computer-controlled air pressure ejection.

Data acquisition and control of the optical stimulator were made by means of a CED 1401 AD/DA converter (Cambridge Electronic Design Limited, UK) and an MS-DOS-based computer system. Recordings were done in voltage-clamp mode with $V_{hold}$ = -70 mV, unless otherwise stated.

*Data Analysis*

Analyses of current transients were used to calculate the series resistances and the input resistances of the cells. Current relaxations to -10 mV voltage steps from a holding potential of -70 mV for 80 ms were subtracted from the holding current and fit by biexponential functions of the form

$$A_{(t)} = A_0 + A_1 \cdot e^{-t/\tau_1} + A_2 \cdot e^{-t/\tau_2},$$

where $A_0$ is the amplitude of the steady-state current at the end of the voltage step, $A_1$ and $A_2$ are the amplitudes of the two exponentials at the instant of voltage change, and $\tau_1$ and $\tau_2$ are the corresponding time constants of the current decay towards $A_0$. This approach was used because the current relaxations did not follow a monoexponential course (for a detailed explanation of the method and its application, see Mennerick et al., 1997, and Nadeau and Lester, 2000). Fits begun 35-45 µs after the voltage change to avoid contamination by residual system filtering, and extrapolated back to the onset of the voltage step in order to estimate the instantaneous current ($A_0$+$A_1$+$A_2$). The calculated curves were subtracted from the data and the residual plots were used to control the quality of the fits (Ellis and Duggleby, 1978; Mennerick et al., 1997).

Series resistances were then calculated using the equation (Nadeau and Lester, 2000)

$$R_{\text{series}} = \left( \frac{V_{\text{step}}}{A_0 + A_1 + A_2} \right),$$

where $R_{\text{series}}$ is the series resistance, and $V_{\text{step}}$ is the applied voltage clamp step. The voltage error for each recording was calculated offline according to the formula

$$V_{\text{error}} = R_{\text{series}} \cdot A_0,$$

and subtracted from the nominal command voltages subsequently. Input resistances were estimated using the equation

$$R_{\text{in}} = \left( \frac{V_{\text{step}}}{A_0} \right) - R_{\text{series}}.$$

Voltage-gated currents were isolated by means of leak subtraction: the corrected whole-cell *IV* curves were subtracted from linear regressions of the current traces to voltage steps below –70 mV.

*Anatomic Reconstruction*

A retinal slice containing a LY-filled mixed-input ON BC (shown in Figure 5.1) was fixed for 10 minutes at room temperature in 0.1 M phosphate-buffered (pH 6.5) 4% paraformaldehyde solution, washed in PBS for 10 minutes (2x), and blocked in 2% normal goat serum (NGS, Jackson ImmunoResearch Lab, West Grove, PA) in PBS for 20 min. The tissue was mounted on a poly-L-lysine coated slide (Menzel-Gläser, Germany) and incubated overnight with a polyclonal antibody against LY (Chemicon International, Temecula, CA; 1:3000) at 4° C in PBS containing 0.3% Triton X-100 and 5% NGS. After washing (15 min, 3x, in PBS), the section was incubated in the secondary antibody (goat anti-rabbit Cy3 from Jackson ImmunoResearch Lab, West Grove, PA; 1:500) for 30 minutes. The slide was cover-slipped with Vectashield (Vector Labs, Burlingame, CA) and observed on an inverted Zeiss Axiovert 100 M microscope equipped with the LSM 510 META laser scanning confocal module (Zeiss, Germany). Light micrographs were acquired as TIFF files directly from the microscope.

The TIFF files were then examined with the 3D-analysis software Image Pro (Media Cybernetics, Inc., Silver Springs, MD), and the diameters, lengths and 3D coordinates of the different compartments of the mixed-input ON BC were measured by means of a homemade analysis tool (NeuralDraw, written by Koos de Vos, The Netherlands Institute for Brain Research). Because of the diminutive dimensions of the invaginating dendrites contacting rods and cones, estimations of their diameters were made by means of comparing our own EM pictures (Chapter 2) and measurements from literature (Ishida et al., 1980). The parameters obtained from this analysis and used in the model (described in the next section) are listed in Table 5.2.

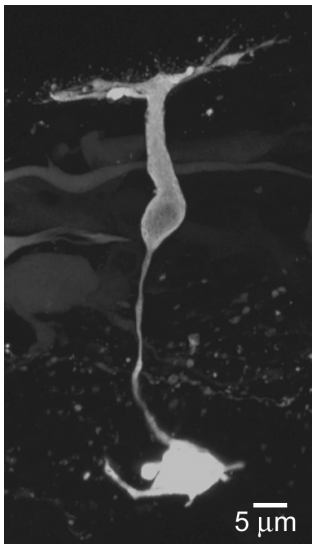


**Figure 5.1:** The LY-filled mixed-input ON BC used to measure the parameters of the model.

| ON BC Structure | Length (μm) | Diameter (μm) |
|---|---|---|
| *Soma* | 32.8 | 5.0 |
| *Axon* | 40.4 | 0.4 |
| *Axon terminal* | 10.0 | 10.0 |
| *Primary Dendrites* | 27.7 | 1.0 |
| *Secondary Dendrites* | 2.5 | variable |
| *Tips at Rod Spherules* | 0.5 | 0.5 |
| *Tips at Cone Pedicles* | 0.1 | 0.1 |

**Table 5.2:** Dimensions of the various regions of the mixed-input ON BC in Figure 5.1.

*Computer Simulations*

All modeling was carried out using NEURON 5.6 (Hines and Carnevale, 1997; Hines and Carnevale, 2000) running on Windows XP machines (an AMD Duron, 800 MHz, and a Pentium *IV*, 2.8 GHz). The integration time step ranged from 0.00625 to 0.025 ms.

The compartmental model for the mixed-input ON BC consisted of a cell with 6 main parts, subdivided in a total of 555 compartments (Figure 5.2): 1) the soma (divided in 10 segments), 2) the axon (10 segments), 3) axon terminal (1 segment), 4) 6 primary dendrites (8 segments each), 5) 54 secondary dendrites (8 segments each), and 6) tips of the secondary dendrites (1 segment). The compartments were much smaller than the electrotonic length constant of each segment; increasing the number of compartments does not change the results described in this Chapter.

Six primary (thick) dendrites sprouted from the mixed-input ON BC soma; each primary dendrite had 9 secondary (thin) dendrites attached to it: 3 contacting cones and 6 contacting rods, with a total of 36 rods and 18 cones projecting to the cell via the tips of the secondary dendrites. A third type of synapse was placed at the base of the secondary dendrites; this synapse was designed in exactly the same manner as the rod-BC synapse, and modulated only in the simulations intended to mimic focal drug (group III mGluR agonists) delivery with a puffer pipette.

Membrane parameters, such as $R_a$, $R_{in}$ and $C_m$ were assumed to be uniform throughout the cell. The passive parameters were $R_a$ = 80 Ω·cm and $C_m$ = 1 μF·cm$^{-2}$, with a passive reversal potential of $E_{leak}$ = -80 mV and a potassium equilibrium

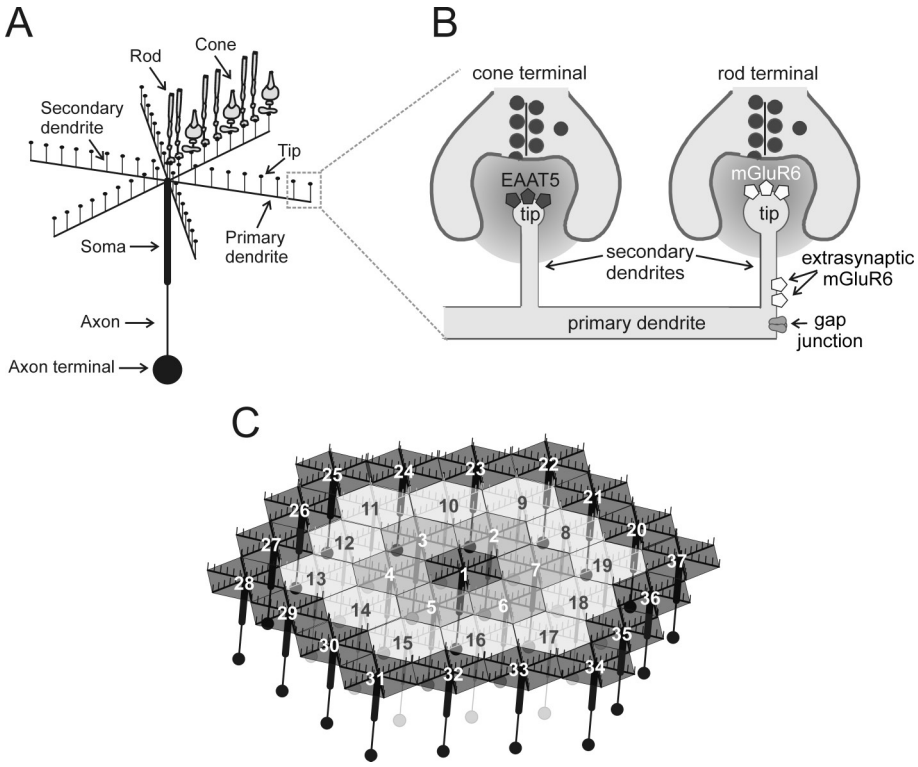


**Figure 5.2:** The model for the ON BC network. A) Schematic drawing of the modeled mixed-input ON BC, showing the main parts: axon terminal, axon, soma, primary dendrites, secondary dendrites and dendritic tips. Each of the 6 primary dendrites has 3 secondary dendrites contacting cones and 6 secondary dendrites contacting rods (to be seen in one of the primary dendrites as an example). B) The area within the dashed square in (A) is enlarged to show the position of the synaptic receptors (at the tips of the dendrites) and the extrasynaptic mGluRs (at the base of the secondary dendrites). Gap junctions are located at the primary dendrites. C) Organization of the coupled syncytium. A central mixed-input ON BC (cell 1) is connected to three rings of cells in a hexagonal lattice. The outer ring is connected to BCs kept at $V_{rest}$.

potential of $E_K$ = -95 mV. The leak conductance density was $g_{leak}$ = 0.15 pS/µm$^2$. Voltage-gated conductances ($I_{KV}$, A-type) were simulated as Hodgkin-Huxley-type ($m^3h$) currents as described in Benison et al. (2001). Since $I_{KV}$ in BCs inactivates very slowly and a sustained current remains (Kaneko and Tachibana, 1985; Tessier-Lavigne et al., 1988; Mao et al., 1998; this Chapter, Figure 5.5), an offset was added to the original current model in order to mimic the non-inactivating part of the current (Figure 5.3). Due to the severe distortion of the *IV* relation and dynamic properties that remote conductances suffer when measured in non-spherical structures such as a BC (Spruston et al., 1993; Hausser and Roth, 1997; Hartline and Castelfranco,

2003; Schaefer et al., 2003), no further attempt was made to match the dynamics of the modeled currents closely to that measured in real cells.

Rods and cones, which provide synaptic input to the BC, were modeled as 3-compartment cells (soma, axon and axon terminal, one segment each) with only passive conductances ($R_a$ = 123 Ω·cm, $C_m$ = 10 µF·cm$^{-2}$, $E_{leak}$ = -50 mV, $g_{leak}$ = 10 pS/µm$^2$). Control of photoreceptor membrane potential was achieved by means of a simulated somatic voltage-clamp. Photoreceptor inputs were built such that rod hyperpolarization would drive a conductance increase in the mixed-input ON BC with $V_{rev}$ = 0 mV, and cone hyperpolarization would drive a conductance decrease with $V_{rev}$ = -60 mV.

Synaptic conductances activated by photoreceptor polarization were arbitrarily simulated such that the rod-driven synaptic conductance density was -125 nA/cm$^2$ in darkness and -300 nA/cm$^2$ in light, and the cone-driven synaptic conductance density was 300 nA/cm$^2$ in darkness and 0 nA/cm$^2$ in light. The extrasynaptic mGluR6 conductance density was -190 nA/cm$^2$ in control and 0 nA/cm$^2$ after puff stimulation.

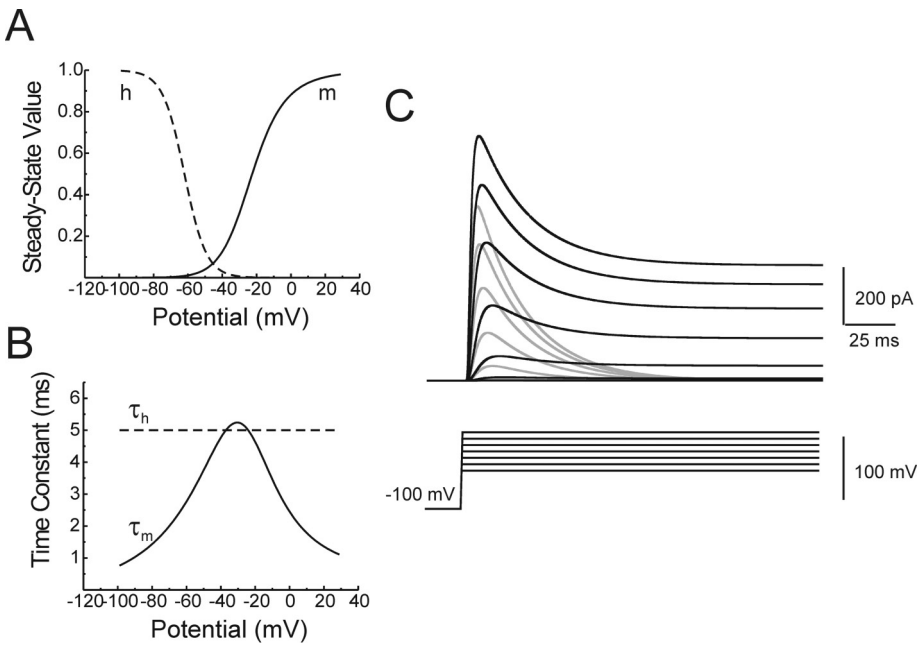


**Figure 5.3:** $I_{K(V)}$. A) Activation (m) and inactivation (h) curves. B) Time constant of activation ($\tau_m$) and inactivation ($\tau_h$). C) Responses to voltage steps from -30 to +20 mV in 10 mV increments from a holding voltage of $V_{hold}$ = -100 mV are shown for the original model (Benison et al., 2001, gray lines) and after the addition of an offset to render the current sustained (black lines). Stimulus timing is depicted at the bottom. In both conditions, $I_{KV}$ conductance density = 100 pS/µm$^2$. The clamped structure was a spherical cell of diameter $D$ = 5 µm, $R_a$ = 80 MΩ, $C_m$ = 1 µF/cm$^2$ and $g_{leak}$ = 0.15 pS/µm$^2$.

In order to study the effects of electrical coupling on BC physiology, the model BC was connected via the primary dendrite to a ring of 6 other BCs, and these BCs were in turn connected to three concentric rows of cells, yielding an hexagonal lattice of 61 cells. This number of coupled cells was chosen such that the receptive field of the central BC was not disturbed by border effects: the BCs in the outer ring were kept at $V_{rest}$, such that only the 37 innermost cells (depicted in Figure 5.2) would effectively be polarized by current injection in the central BC. The gap junctional conductance was simulated using the equation

$$I_{gap} = g_{gap} \cdot (V_j - V_i)$$

where $I_{gap}$ is the gap junctional current flowing from the pre-synaptic cell to the post-synaptic cell, $g_{gap}$ is the gap junctional conductance, $V_i$ is the membrane potential of the post-synaptic cell, and $V_j$ is the membrane potential of the pre-synaptic cell. The total gap junctional current is two times $I_{gap}$, because current flow in electrical synapses is bidirectional.

## 5.4 Results

Mixed-input ON BCs were visually selected based on their characteristic morphology and position in the outer part of the INL (Stell, 1976). Cell type was confirmed by measurements of response properties. LY was routinely included in the pipette solutions and dye-filled cells were observed immediately after the experiment. Data from both intact and axotomized neurons were used. Unless otherwise stated, at least three cells yielded similar results for each experiment reported in the following sections.

*A Voltage-Gated $K^+$ Current Causes Rectification of Light-Driven IV Relations*
Despite all evidence in favor of the mGluR6 cascade being involved in the ON pathway, rod-driven light responses in goldfish mixed-input ON BCs do not reverse at 0 mV in voltage-clamp experiments (Figure 5.4a). Rather, the rod-driven light-induced current in these cells is almost invariably a conductance increase that rectifies at positive potentials (Figure 5.4b). Rectification of the light-induced conductance can also be seen in cone-driven *IV* relations (Figure 5.4c and d), suggesting that this phenomenon is post-synaptic and not directly linked to the GluR machinery responsible for the generation of light responses.

Additional evidence for a post-synaptic origin of the rectification is presented in Figure 5.5. When locally activated by puff delivery of DL-AP4, the mGluRs responsible for the rod pathway could either generate responses with no $V_{rev}$ (Figure 5.5a and b, n = 5), or responses with very linear *IV* relations that would reverse at around 0 mV (Figure 5.5c and d, n = 8), depending on the position of the puffer pipette in relation to the dendritic tree of the BC recorded from. This indicates that the mechanism responsible for the rectification of the light-driven conductance is not

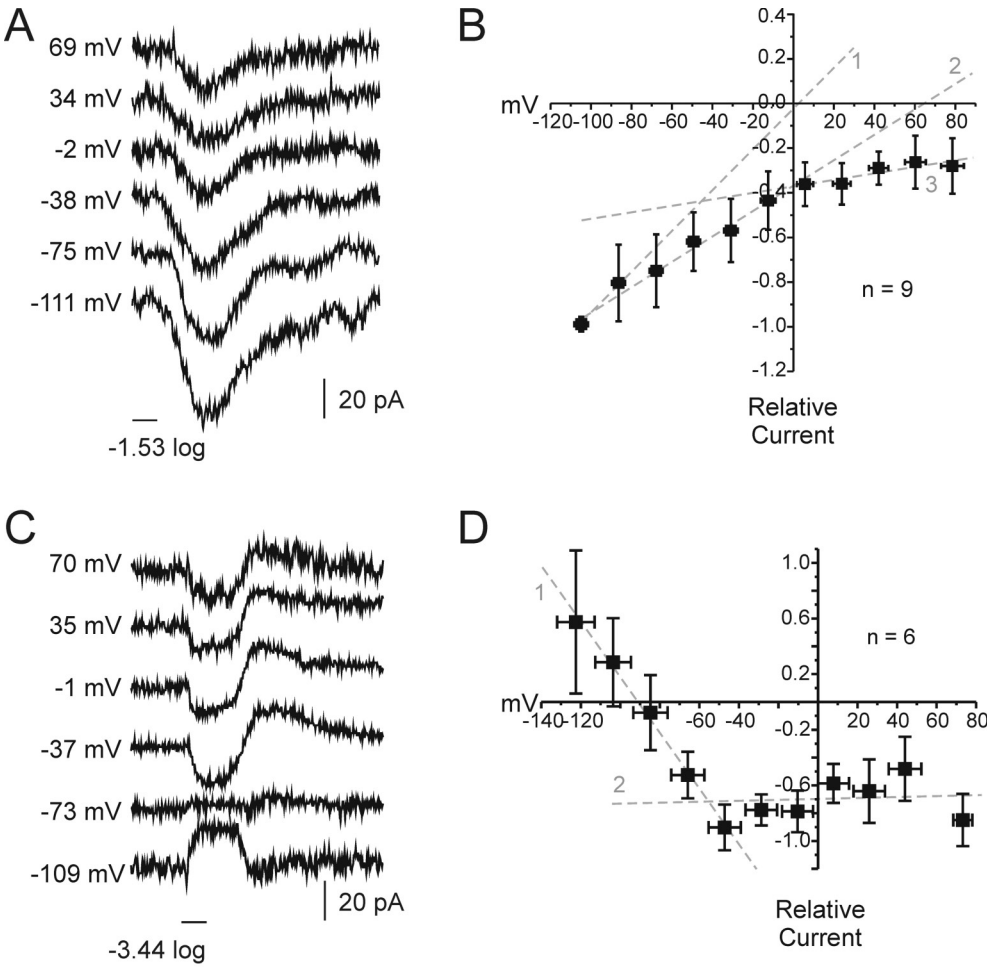


**Figure 5.4:** The light conductance in mixed-input ON BCs rectifies. A) Light responses to full-field stimulation of a mixed-input ON BC clamped at different potentials (values depicted to the left of each trace). Stimulus intensity (-1.53 log) and wavelength (550 nm) were chosen to stimulate rods only. Light responses rectify at positive potentials: the traces at –2 mV, 34 mV and 69 mV have similar amplitudes. Horizontal bar depicts stimulus timing (100 ms). B) Mean relative light-induced *IV* relation of 9 cells stimulated similarly. The most negative current value of each *IV* was scaled to -1. Light responses do not reverse at 0 mV; the *IV* relations rectify at potentials more positive than –20 mV. The three dashed lines are linear regressions through different sets of data points, to show how the slope changes with potential: line (1) is an extrapolation of the points at -104 mV and –86 mV, line (2) is a regression through all negative data points, and line (3) is a regression through all positive data points. C) Light responses of a mixed-input ON BC clamped at different potentials in DL-AP4 Ringer's. At positive potentials, cone-driven light responses also rectify: the traces at –1 mV, 35 mV and 70 mV have similar amplitudes. Light stimulus: 100 µm slit, 550 nm, 3.44 log, 100 ms. D) Mean relative light-induced *IV* relation of 6 cells stimulated similarly. The most negative current value of each *IV* was scaled to -1. The IV relations rectify at potentials more positive than –40 mV. Line (1) is an extrapolation of the 5 most negative data points; line (2) is a regression through the points positive to -40 mV.

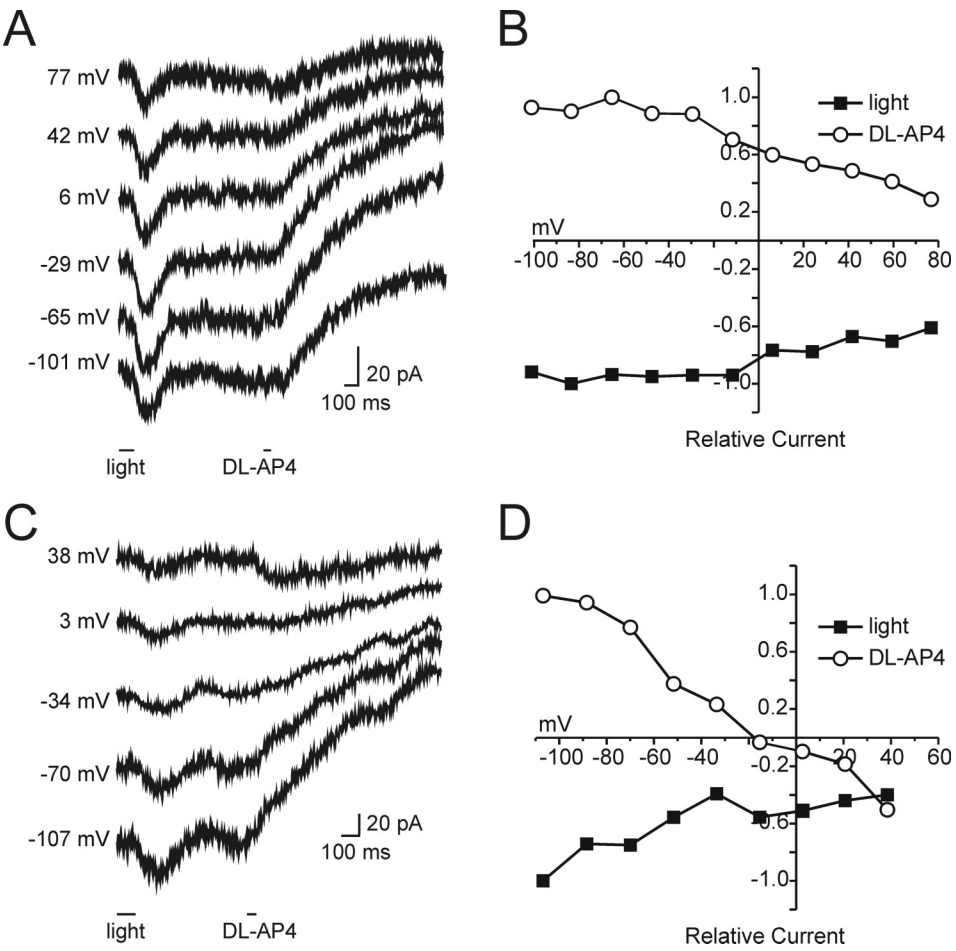


**Figure 5.5:** Compartmentalization of voltage-gated conductances in mixed-input ON BCs. A) Responses of a mixed-input ON BC clamped at different potentials (values depicted to the left of each trace) to light flashes (100 μm slit, 550 nm, 0.64 log, 100 ms) and to puff application of DL-AP4 (250 μM, 50 ms) at the OPL. Neither light nor puff responses reverse with increasing potentials, suggesting that the glutamate release of the photoreceptors and the drug act on the same cell compartment(s). B) The relative *IV* relations for the peak light responses (filled symbols) and for the puff responses (open symbols, measured 150-200 ms after drug delivery) are almost mirror images of each other. The most positive data points of the puff-induced *IVs* were scaled to 1, and the most negative data points of the light-induced *IVs* were scaled to -1. C) Responses of another cell clamped at different potentials (values depicted to the left of each trace) to light flashes (100 μm slit, 550 nm, 0.64 log, 100 ms) and puff application of DL-AP4 (250 μM, 50 ms) at the OPL. Light responses do not reverse, but puff responses become inward at positive potentials. D) Relative *IV* relations for the peak light responses (filled symbols) and for the puff responses (open symbols, measured 150-200 ms after drug delivery). The most positive data points of the puff-induced *IVs* were scaled to 1, and the most negative data points of the light-induced *IVs* were scaled to -1. While light responses rectify at potentials positive to –40 mV, puff responses reverse close to 0 mV. This indicates that photoreceptors and the puffer pipette are reaching different compartments of the cell with distinct distributions of $K^+$ channels and glutamate receptors.

homogeneously distributed throughout the cell membrane, but confined to regions of the BC dendrites closely related to the sites of synaptic input. Despite the ubiquity of mGluR6-IR in the cell membrane (Chapter 2, Figure 2.11), we did not find evidence for active somatic receptors: DL-AP4 puffs directed towards the cell soma and/or axon terminals did not elicit responses in any of the mixed-input ON BCs tested (n =18).

We subsequently investigated BC membrane properties that could account for the rectification of light- and agonist-induced currents in mixed-input ON BCs. The whole-cell *IV* relations of mixed-input ON BCs are fairly linear (Figure 5.6a). When one fits linear regressions through the negative data points and subtract these from the whole *IV* relations, one can observe the non-linear components of the membrane conductances (Figure 5.6b). At potentials positive to -60 mV, an outwardly rectifying voltage-gated current activates. The maximal amplitude of this current is around 300 pA at 0 mV. Depolarization produces a quick time-dependent increase in outward current, which has a fast transient component (Figure 5.6c), and a sustained component (Figure 5.6d). This outward current was shown to be carried mainly by $K^+$ ions in BCs of the goldfish (Kaneko and Tachibana, 1985), axolotl (Tessier-Lavigne et al., 1988) and salamander (Mao et al., 1998). Rectification of rod- (Figure 5.7a, filled symbols) and cone-driven (Figure 5.7b, filled symbols) *IV* relations becomes prominent when this voltage-gated $K^+$ current ($I_{KV}$, open symbols) activates. The similarity in the voltage range of *IV* rectification and activation of $I_{KV}$ indicates that the opening of voltage-gated $K^+$ channels at positive potentials might interfere with the measurement of synaptic currents.

*$K^+$ Channels Are Localized to Dendritic Tips*

To investigate the influence of the localization of $I_{KV}$ on the rod-driven *IV* relations of mixed-input ON BCs, four conditions were simulated: 1) $K^+$ channels localized only to the soma (Figure 5.8a), 2) $K^+$ channels localized only to the primary dendrites (Figure 5.8b), 3) $K^+$ channels localized only to the secondary dendrites (Figure 5.8c), and 4) $K^+$ channels localized only at the tips of the secondary dendrites (Figure 5.8d). In all cases, exclusively synaptic mGluRs were modulated.

When $I_{KV}$ was located at the soma (Figure 5.8a) or on the primary dendrites (Figure 5.8b), the whole-cell leak-subtracted *IV* relations (left panels) reached physiological values already at very low $I_{KV}$ densities, due to the large membrane area of these compartments. The *IV* relations of the light-driven conductance (right panels) in these conditions remained nonetheless linear, suggesting that somatic $K^+$ channels do not contribute to the rectification of light-induced currents. Only when $K^+$ channels were localized to the secondary dendrites and/or to the very tips of the dendrites was rectification achieved for physiological values of leak-subtracted *IV* relations. The largest rectification was observed when $I_{KV}$ was confined to the tips of the dendrites (Figure 5.8d), suggesting that great part of these channels must be in close apposition to the sites of synaptic input.

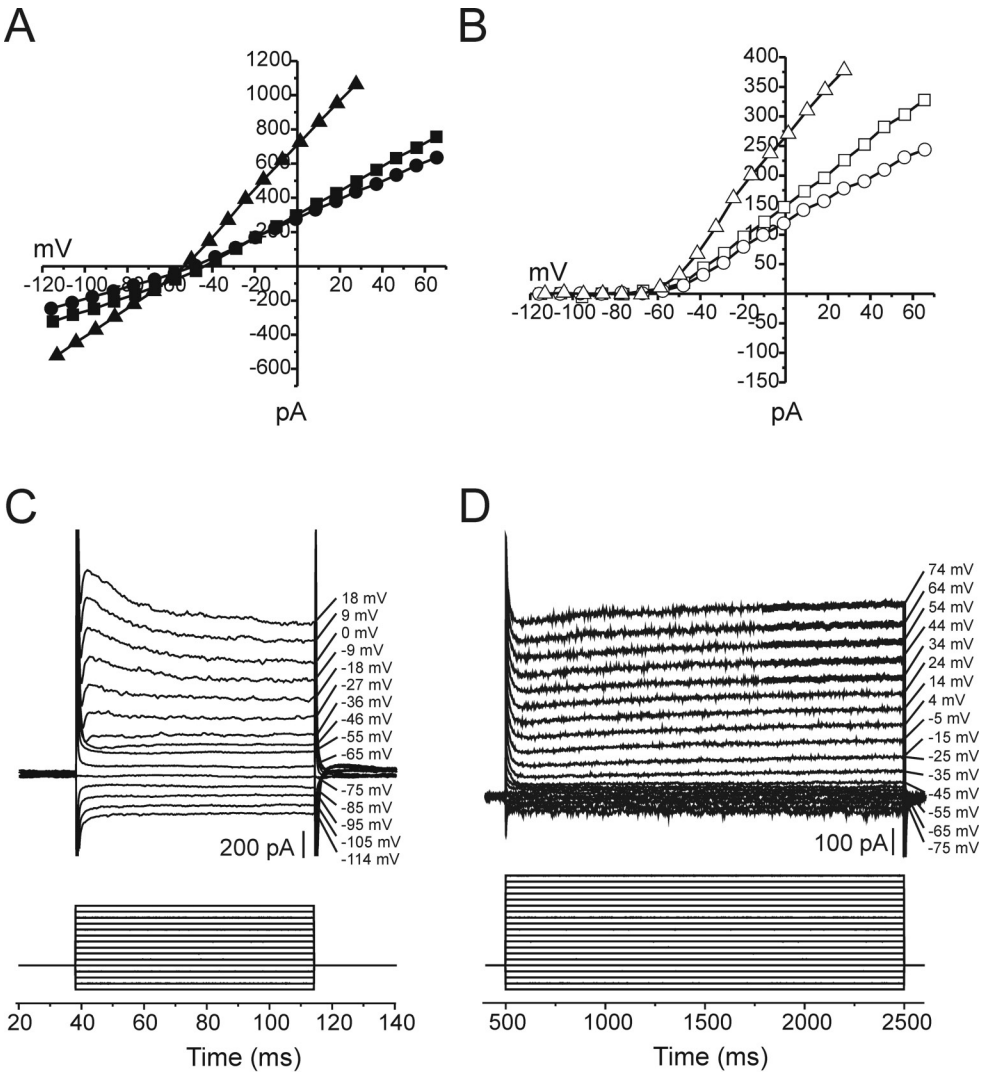


**Figure 5.6:** Voltage-gated currents of mixed-input ON BCs. A) Whole-cell *IV* relations of three mixed-input ON BCs, voltage-clamped for 80 ms to different potentials from a $V_{hold}$ of -75 mV and measured 60-65 ms after $V_{step}$. Relations are linear and whole-cell currents vary between 200 pA and 800 pA at 0 mV (see also Figure 3.10a). B) Leak-subtracted whole-cell *IV* relations for the three cells in (A). In all cases, an outwardly rectifying voltage-gated current activates at -60 mV. This conductance is relatively small when compared to whole-cell currents: its maximal amplitude is around 300 pA at 0 mV. C) The cell was voltage-clamped for 80 ms to different potentials (shown beside each trace) from a $V_{hold}$ of -75 mV. In this fast time scale, a transient outward current is activated at potentials more positive than -60 mV. This current has a fast onset and does not inactivate completely. D) A similar experiment with the same cell in (A), this time with a longer $V_{step}$ (2000 ms). In this slow time base the sustained component of the voltage-gated current is evident. Traces in (D) were leak-subtracted on line. Stimulus timing depicted at the bottom of the figure.

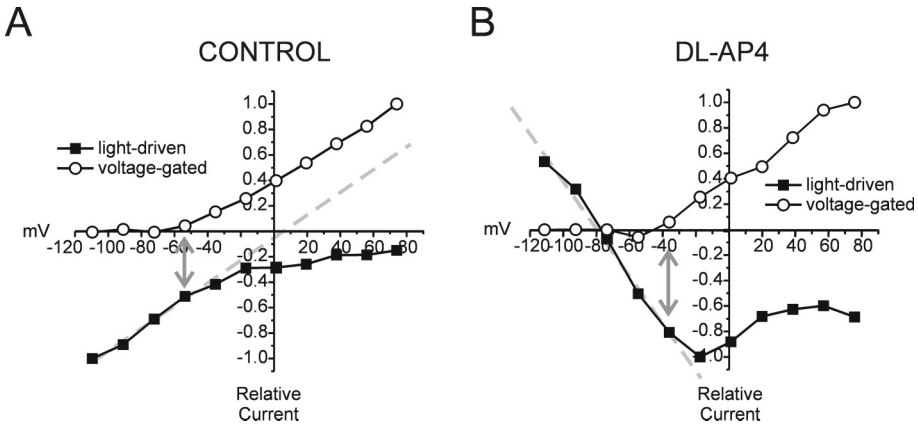


**Figure 5.7:** Relation between the rectification of *IV* curves for the light-driven conductance and the activation range of voltage-gated currents. A) *IV* relations for the light-driven conductance (filled symbols) and leak-subtracted whole-cell currents (open symbols) of the same cell in control Ringer's. The most positive data points of the leak-subtracted *IVs* were scaled to 1, and the most negative data points of the light-induced *IVs* were scaled to -1. A linear regression through the four most negative data points is shown in grey. The light conductance starts deviating from linearity at the same potential (around -60 mV, arrow) in which $I_{KV}$ activates. Light stimulus: full field, 550 nm, -0.10 log, 100 ms. B) *IV* relations for the light-driven conductance (filled symbols) and leak-subtracted whole-cell currents (open symbols) of the same cell in (A) in DL-AP4 Ringer's. The most positive data points of the leak-subtracted *IVs* were scaled to 1, and the most negative data points of the light-induced *IVs* were scaled to -1. A linear regression through the four most negative data points is shown in grey. Similarly to what happens in (A), the light conductance starts deviating from linearity at the same potential (in this case around -40 mV, arrow) in which $I_{KV}$ activates. Note that the slope of the light-driven conductance even becomes positive at more depolarized potentials. Light stimulus: full field, 550 nm, 3.31 log, 100 ms.

Similarly to what happened in the case of rod-driven light responses, when $K^+$ channels were confined to the soma (Figure 5.9a) or primary dendrites (Figure 5.9b), cone-driven *IV* relations (right panels) remained linear, even though the magnitude of the whole-cell leak-subtracted currents (left panels) was comparable to that recorded from real cells (compare these graphs with Figure 5.6b). Light-induced currents only rectified when $I_{KV}$ was localized to the secondary dendrites and to the tips of the secondary dendrites contacting cones (Figure 5.9c and d). In some simulations, the slope of the light-induced current even became positive at more depolarized levels, as sometimes observed in our recordings (see Figure 5.6b). This happens because at these potentials the voltage-gated currents are much larger than the light-modulated conductance.

Cone-driven light responses rectified the most when voltage-gated $K^+$ channels were localized to the tips of the secondary dendrites. However, because considerable rectification was already achieved with small values of $I_{KV}$ at the secondary dendrites, the confinement of voltage-gated conductances to the dendritic terminations might not be as critical for the cone pathway as for the rod pathway.

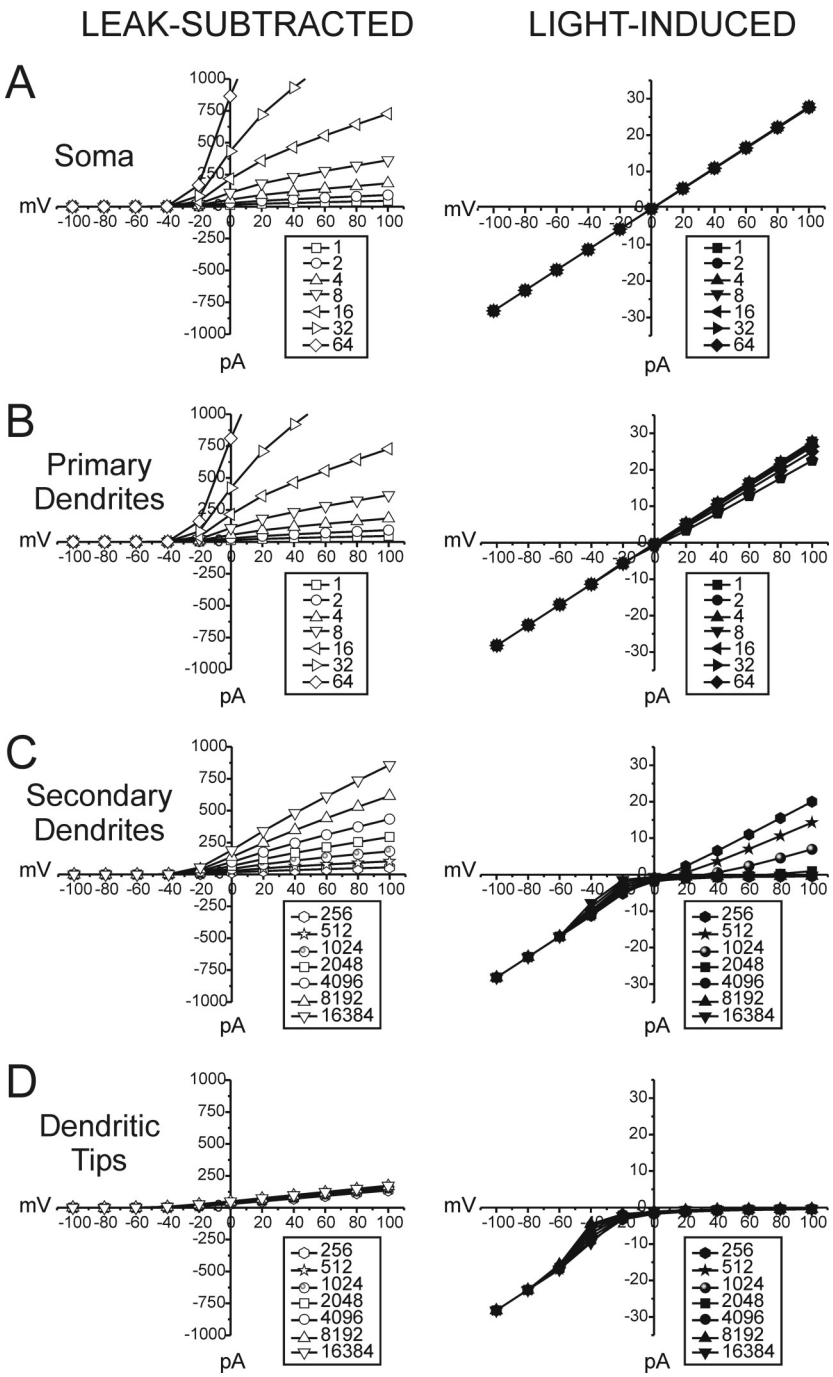
LEAK-SUBTRACTED
LIGHT-INDUCED
A
Soma
B
Primary Dendrites
C
Secondary Dendrites
D
Dendritic Tips
mV
pA
1
2
4
8
16
32
64
256
512
1024
2048
4096
8192
16384

**Figure 5.8 (opposite page):** The effect of compartmentalization of $K^+$ channels on light-induced (rod-driven) *IV* relations. A) $I_{KV}$ confined to the soma; B) $I_{KV}$ confined to the primary dendrites; C) $I_{KV}$ confined to the secondary dendrites; D) $I_{KV}$ confined to the tips of the secondary dendrites. Left panels (open symbols) depict leak-subtracted whole-cell IV relations for increasing $I_{KV}$ densities (values in pS/μm$^2$ at the bottom of the graphs). Right panels (closed symbols) show the light-induced *IV* relations in each condition for all values of $I_{KV}$. Somatic (A) and dendritic (B) $I_{KV}$ do not contribute to the rectification of light-induced currents. Only when the voltage-gated $K^+$ channels are restricted to the secondary dendrites (C) or to the tips of the secondary dendrites (D) rectification is achieved with $I_{KV}$ values in the physiological range. The largest amount of rectification is observed when voltage-gated $K^+$ channels are concentrated at the tips of the dendrites, in the vicinity of the mGluR6-driven channels. In this condition, light-driven *IV* relations rectify considerably even when the leak-subtracted currents are very small. Diameter of the secondary dendrites = 0.01 μm.

*Diameter of the Secondary Dendrites is Crucial for Rectification*

In order to investigate how the morphology of the dendrites influences the behavior of the light-driven conductances, we changed the diameter of the secondary dendrites. Varying the diameter of the dendritic shafts in the model affects the shape of light-driven *IV* relations. The amount of rectification of rod-driven (Figure 5.10b) and cone-driven (Figure 5.10c) conductances is inversely related to the diameter of the secondary dendrites. As shown in Figure 5.11, similar results can be obtained with very thin dendrites and low $I_{KV}$ densities, or with broader shafts and larger $I_{KV}$ densities. Note that the simulations in Figures 5.10 and 5.11 are not intended to yield absolute values for the diameter of the secondary dendrites or for the $I_{KV}$ density at the dendritic tips, but only to show the interdependency of these two parameters.

The diameter of the secondary dendrites influences the shape of light-driven conductances because it determines the resistance between the somatic compartment and the site of synaptic input. Thin shafts have high resistances, which cause a voltage drop when current flows from the soma to the tips in a voltage-clamp experiment. The voltage reaching the site of input is therefore much smaller than the one actually applied at the soma. As a consequence, the smaller the secondary dendrite, the smaller $I_{KV}$ needs to be to induce rectification of the light-induced conductances. Broadening the dendritic shafts decreases the resistance of the secondary dendrites, diminishing the voltage drop along the dendrites as current flows along the cable. Because broader dendrites allow better control of the voltage at the tips of the dendrites, more $I_{KV}$ is needed to generate rectifying light-driven *IV* relations.

*Puff Responses Versus Light Responses*

Figure 5.12 illustrates that the separation of synaptic and extrasynaptic mGluRs by the high resistance of the secondary dendrites generates the differences observed between puff-evoked responses and the light-induced modulation of photoreceptor glutamate release (shown in Figure 5.5). When voltage-gated $K^+$ channels are distributed along the secondary dendrites, conductances located proximally in the secondary dendrites (the extrasynaptic mGluRs, Figure 5.12d) do not rectify, whereas those located distally (the synaptic mGluRs, Figure 5.12c) show

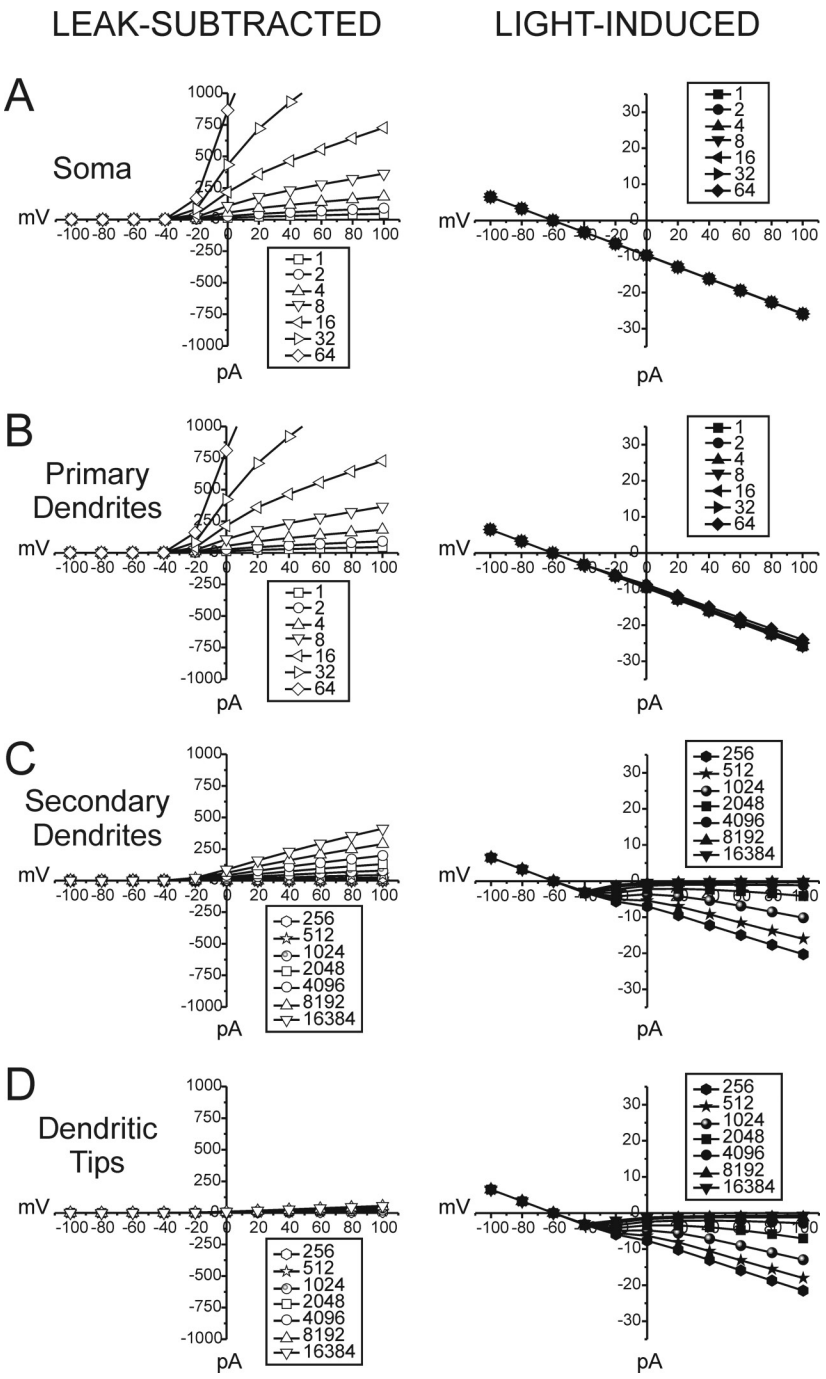
LEAK-SUBTRACTED
LIGHT-INDUCED
A
Soma
B
Primary Dendrites
C
Secondary Dendrites
D
Dendritic Tips
mV
pA
1
2
4
8
16
32
64
256
512
1024
2048
4096
8192
16384

**Figure 5.9 (opposite page):** The effect of compartmentalization of $K^+$ channels on light-induced (cone-driven) *IV* relations. A) $I_{KV}$ confined to the soma; B) $I_{KV}$ confined to the primary dendrites; C) $I_{KV}$ confined to the secondary dendrites; D) $I_{KV}$ confined to the tips of the secondary dendrites. Left panels (open symbols) depict leak-subtracted whole-cell IV relations for increasing $I_{KV}$ densities (values in pS/μm$^2$ at the bottom of the graphs). Right panels (closed symbols) show the light-induced IV relations in each condition for all values of $I_{KV}$. Somatic (A) and dendritic (B) $I_{KV}$ do not contribute to the rectification of light-induced currents. Only when the voltage-gated $K^+$ channels are restricted to the secondary dendrites (C) or to the tips of the secondary dendrites (D) rectification is achieved with $I_{KV}$ values in the physiological range. The largest amount of rectification is observed when voltage-gated $K^+$ channels are concentrated at the tips of the dendrites, in the vicinity of the EAAT5-driven channels. In this condition, light-driven *IV* relations rectify considerably even when the leak-subtracted currents are very small. Diameter of the secondary dendrites = 0.01 μm.

pronounced rectification. For the cone-driven pathway this large resistance is also necessary to generate rectification, but $K^+$ channels do not need to be confined to the tips of the dendrites.

In summary, these simulations suggest that $K^+$ channels located at the tips of thin dendrites of mixed-input ON BCs can account for the non-linearity of the light-induced *IV* relations. Currents located proximally to this high resistance (i.e. extrasynaptic mGluRs) are not affected by the voltage attenuation along the dendrites and can be accurately clamped.

*Electrical Coupling Increases Rectification*

The simulations shown so far were performed in uncoupled cells. Real mixed-input ON BCs are however electrically coupled, as shown in Chapter 3. In order to investigate the influence of electrical coupling in the behavior of light-induced currents, we built an hexagonal network of 61 cells, distributed in 4 concentric rings (see methods). The single gap junctional conductances ($g_{gap}$) used in the model are summarized in Table 5.3, as well as the corresponding $R_{in}$ of the central cell for each $g_{gap.}$ These $g_{gap}$ values were chosen such as to yield a receptive field diameter of approximately 370 μm, which is close to the lower values reported in literature for carp mixed-input ON BCs (from 300 μm to 1 mm, Saito and Kujiraoka, 1988s), and for salamander ON BCs (from 345 to 662 μm, Borges and Wilson, 1987).

$R_{in}$ decreases as $g_{gap}$ increases, and this has many consequences for BC physiology, as described below. The amount of coupling that yields the proper BC receptive field size, however, is relatively small. For instance, the diameter of the receptive field in goldfish HCs, which are strongly coupled, is at least one order of magnitude larger (Kamermans et al., 1996).

The spatial integration in the BC network is illustrated in Figure 5.13a, in which the somatic membrane potential of cells in the different rings of the BC lattice are depicted for a voltage step of 100 mV applied to the soma of the central BC. Neighboring cells are polarized to a smaller extent by the $V_{step}$ applied to the central BC, and the amount of polarization is proportional to $g_{gap.}$ Consequently, as shown in Figure 5.13b, electrical coupling leads to an increase in the amplitude of BC whole-

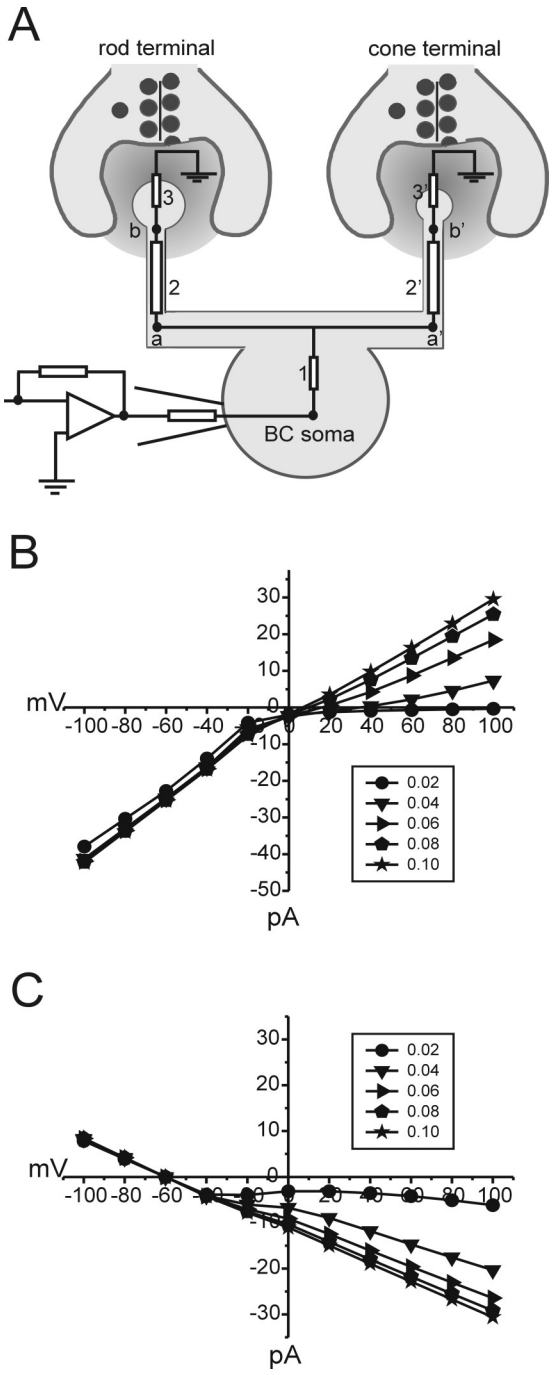


**Figure 5.10:** Increasing the diameter of the secondary dendrites linearizes light-induced currents. A) Schematic drawing of the circuit involved in the rectification of the light-driven conductance of mixed-input ON BCs. Due to their small diameter, the resistance of the secondary dendrites contacting rods (2) and cones (2') is large. Current flowing from the soma (1) to the tips of the dendrites (3 and 3') induces a voltage drop between the somatic compartment (as measured in the nodes a and a') to the tips (measured in nodes b and b'). The residual voltage that reaches the tips causes the voltage-gated $K^+$ channels located at the tips to open, and due to this opening voltage control of the dendritic tips is lost. B) Simulations of the changes in the rod-driven *IV* relation of a mixed-input ON BC induced by varying the diameter of the secondary dendrites projecting to rod spherules. Values of the secondary dendrites (in µm) are depicted in the picture. For this simulation, $I_{KV}$ = 1 nS/µm$^2$. C) Simulations of the changes in the cone-driven *IV* relation of a mixed-input ON BC induced by varying the diameter of the secondary dendrites projecting to cone pedicles. Values of the secondary dendrites (in µm) are depicted in the picture. $I_{KV}$ = 10 nS/µm$^2$.

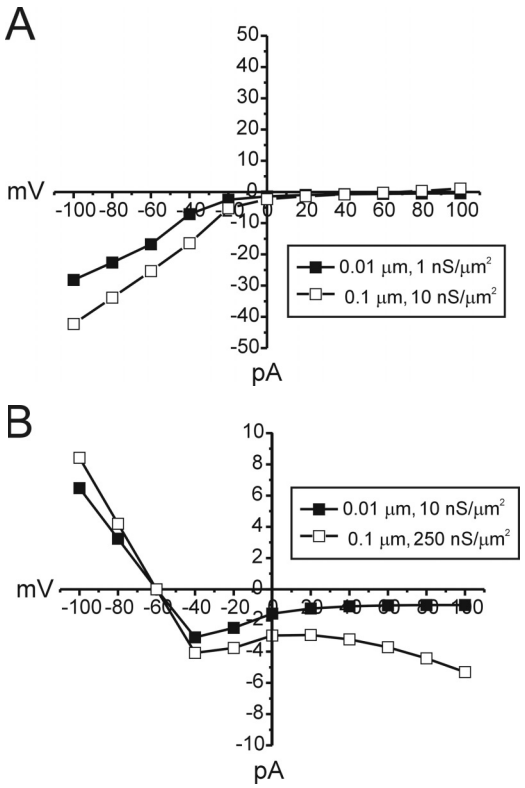


**Figure 5.11:** The interdependency of the diameter of the secondary dendrites and $I_{KV}$ density at the dendritic tips. A) Model simulations of rod-driven *IV* relations in two different conditions: thin secondary dendrites and low $I_{KV}$ density (closed symbols, parameter values depicted in the figure), and thicker dendrites with larger $I_{KV}$ density (open symbols, parameter values depicted in the figure). In both cases, the light-induced current rectifies. B) Model simulations of cone-driven *IV* relations in two different conditions: thin secondary dendrites and low $I_{KV}$ density (closed symbols, parameter values depicted in the figure), and thicker dendrites with larger $I_{KV}$ density (open symbols, parameter values depicted in the figure). Similarly to what happens in (A), the light-induced current rectifies in both cases.

cell currents. The $V_{rev}$ of all whole-cell currents is around -40 mV, because this is the resting membrane potential of the cells in the BC network. When the recorded BC is clamped at this potential, no current will flow through the gap junctions.

Figure 5.13c shows that electrical coupling shifts the $V_{rev}$ of the light-induced *IV* relation to more positive potentials, due to the fact that the neighboring cells are not clamped to the same extent as the central BC. The slope of the light-induced *IV* relations becomes steeper as the strength of coupling augments. This happens because the total light-induced *IV* relation measured in the central BC is the sum of the *IV* relations of the central cell and the relations originating from neighboring cells, which are smaller and slightly shifted in the voltage axis. The same argument holds for the cone-driven conductance (Figure 5.13d).

When $K^+$ channels are placed at the tips of the dendrites of all cells in the coupled syncytium (Figure 5.14), the activation of these channels in both the central BC and in the coupled BCs enlarges the voltage difference between the somatic compartments of the central cell and its neighbors. In this condition, the effects of coupling will become very asymmetrical: at more depolarized potentials, the

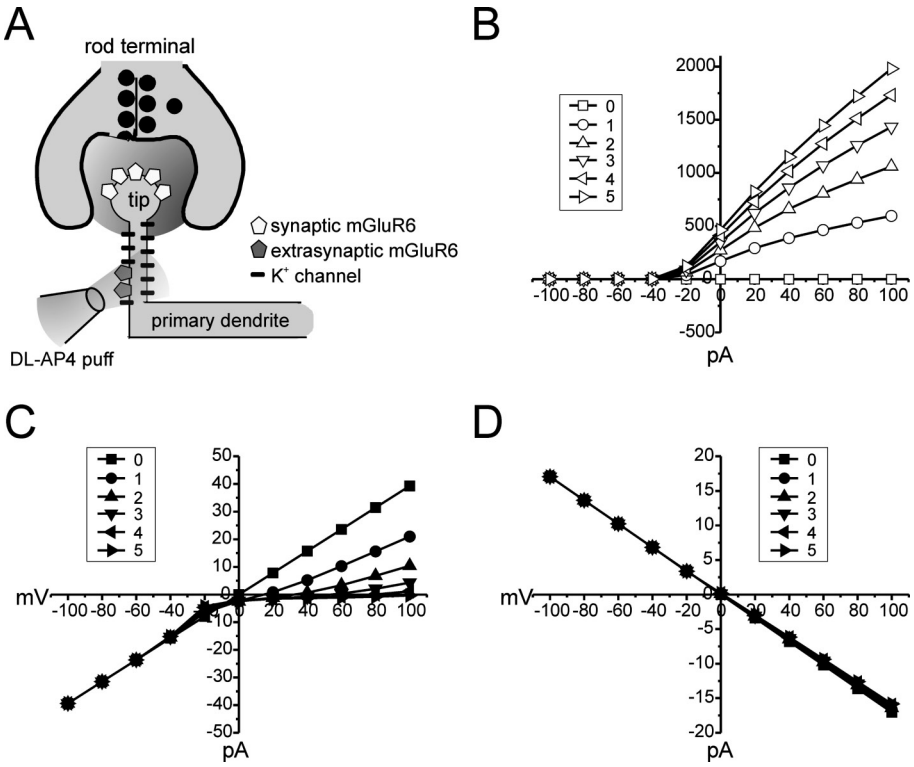


**Figure 5.12:** $I_{KV}$ in the secondary dendrites does not induce rectification of the extrasynaptic mGluR-driven conductance. A) Schematic drawing of the simulations shown in (B), (C) and (D). Voltage-gated $K^+$ channels were placed in the secondary dendrites, between the extrasynaptic and synaptic conductances. B) Leak-subtracted whole-cell *IV* relations of the model BC for different $I_{KV}$ densities (values in nS/µm$^2$ depicted in the figure). C) Light-driven *IV* relations for each $I_{KV}$ density. The amount of rectification at positive potentials increases with the strength of the voltage-gated conductance. D) *IV* relations for the focal delivery of DL-AP4, for each $I_{KV}$ density. Because the extrasynaptic mGluRs modulated by the drug puff are located proximally in the secondary dendrites, their conductance is not affected by $I_{KV}$ density. In these simulations, diameter of the secondary dendrites = 0.025 µm.

activation of $I_{KV}$ in the neighboring cells will lead to an increase in the rectification of both rod- (Figure 5.14a) and cone-driven (Figure 5.14b) *IV* relations. Also here, the slope of the total light-induced *IV* relations changes with the strength of coupling, because it results from the sum of many *IV* relations slightly displaced in the voltage axis. These curves strongly resemble the *IV* relations of Figure 5.4. Taken together, these simulations suggest that although electrical coupling between mixed-input ON BCs does not induce rectification of light-driven conductances *per se*, it does increase the effects of dendritic $K^+$ channels on rod- and cone-driven *IV* relations.

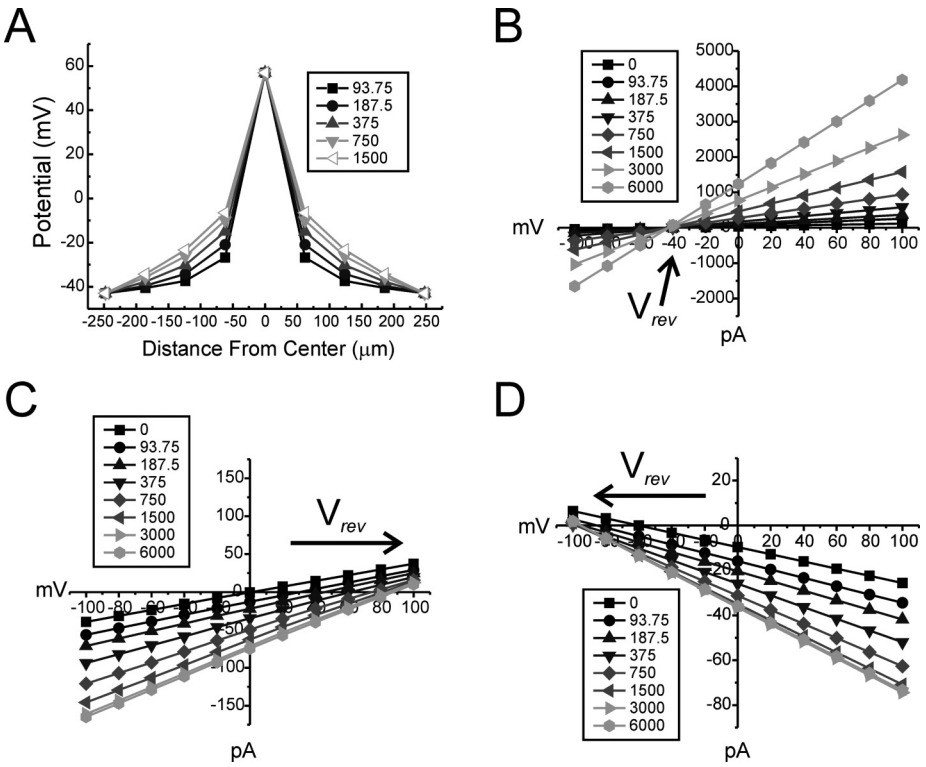


**Figure 5.13:** The influence of electrical coupling in the physiology of mixed-input ON BCs. A) Electrical coupling increases the size of the BC receptive field. Somatic membrane potentials of cells in different rings of the coupled syncytium when the central BC (BC1) was stepped from $V_{rest}$ (-43 mV) to 57 mV. The amount of polarization of the neighboring cells increases with the strength of coupling (values of $g_{gap}$ in pS depicted in the picture). This means that currents originating from photoreceptor inputs to the central cell will also be shared by the coupled lattice, and the amount of current escape will depend on $g_{gap}$. B) Electrical coupling increases whole-cell currents. Whole-cell *IV* relations of the central BC when clamped at a $V_{hold}$ of -70 mV and stepped from -100 to 100 mV for different strengths of coupling (values of $g_{gap}$ in pS depicted in the picture). As the strength of coupling increases, $R_{in}$ decreases and as a result whole-cell currents are augmented. C) Electrical coupling shifts the apparent $V_{rev}$ of the rod-driven *IV* relations. Light-induced *IV* curves measured in the central BC when clamped at a $V_{hold}$ of -70 mV and stepped from -100 to 100 mV for different strengths of coupling (values of $g_{gap}$ in pS depicted in the picture). The apparent $V_{rev}$ shifts proportionally towards more positive values as coupling is increased, but no rectification is induced. D) Electrical coupling shifts the apparent $V_{rev}$ of the cone-driven IV relations. Light-induced IV curves measured in the central BC when clamped at a $V_{hold}$ of -70 mV and stepped from -100 to 100 mV for different strengths of coupling (values of $g_{gap}$ in pS depicted in the picture). The apparent $V_{rev}$ shifts proportionally towards more negative values as coupling is increased, but no rectification is induced.

## 5.5 Discussion

In this Chapter we show that rod- and cone-driven light responses of mixed-input ON BCs rectify at positive potentials. This rectification is the combined result of

| $g_{gap}$ (pS) | $R_{in}$ (MΩ) | $R_c$ (MΩ) | $R_{in}$: $R_c$ |
|---|---|---|---|
| 93.75 | 459 | 889 | 0.52 |
| 187.5 | 301 | 444 | 0.68 |
| 375 | 203 | 222 | 0.91 |
| 750 | 140 | 111 | 1.26 |
| 1500 | 90 | 56 | 1.62 |
| 3000 | 54 | 28 | 1.94 |
| 6000 | 33 | 14 | 2.39 |

**Table 5.3:** Electrical properties of the coupled BC syncytium. $g_{gap}$: single gap junctional conductances used in the model; $R_{in}$: input resistances of the modeled BC for each junctional conductance; $R_c$: coupling resistances for each value of single gap junctional conductance.

the presence of dendritic voltage-gated $K^+$ channels at the tips of the dendrites contacting the photoreceptors, the high resistance of the dendritic shafts, and mild electrical coupling between neighboring BCs. Next, we will discuss the function of this organization in visual processing.

*The Validity of the Model*

The model presented in this Chapter aims at a qualitative description of the light-induced conductance in mixed-input ON BCs. As any model will do, this deviates in some aspects from a real cell, especially in being less complex in terms of morphology, inputs and membrane properties. Since we did not reconstruct the fine details of the dendritic compartments, we made conservative choices regarding the number and dimensions of these compartments (54 secondary dendrites per BC, each about 2.5 µm long). These values are probably underestimates (see Table 3.2). If the model were to be extended such as to match the intricate dendritic morphology described in literature (Scholes, 1975; Stell, 1978; Stell and Lightfoot, 1979; Ishida et al., 1980), similar results would be obtained, because the rectification is not due to the number of inputs, but rather due to the relation between $I_{KV}$, the glutamate-induced conductance and the resistance of the dendrites. For instance, no data is currently available on the length of the secondary dendrites, which influences the flow of current between somato- and dendritic compartments. Longer secondary dendrites would make light-induced *IV* relations rectify for even smaller $I_{KV}$ densities.

Another critical factor is the density of the $K^+$ channels at the tips of the BC dendrites. As shown in Figure 5.11, similar results can be obtained with different settings of parameters, and therefore a quantitative analysis demands a finer tuning of the geometry of the model BC to that of a real cell. Before we can convert these $K^+$ currents into channel densities, the specific subunit composition of these dendritic $K^+$

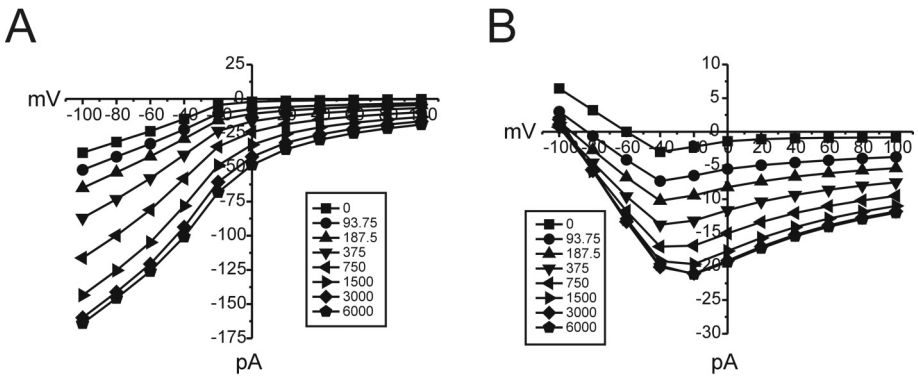


**Figure 5.14:** Influence of electrical coupling in the rectification of the light-driven conductance in mixed-input BCs. A) Simulations of the changes in the rod-driven *IV* relation of a mixed-input ON BC for full-field stimulation induced by varying the gap junctional conductance (values in pS depicted in the figure) when $K^+$ channels are placed at the dendritic tips. Inward currents increase more at negative potentials, because the activation of dendritic $K^+$ channels in both the central and neighboring cells increases space clamp problems at depolarized levels. This way, electrical coupling increases the rectification induced by $I_{KV}$. For this simulation, $I_{KV}$ at the dendritic tips = 1 nS/µm$^2$ and diameter of the secondary dendrites = 0.025 µm. B) Simulations of the changes in the cone-driven *IV* relation of a mixed-input ON BC for full-field stimulation induced by varying the gap junctional conductance (values in pS depicted in the figure). For this simulation, $I_{KV}$ at the dendritic tips = 1 nS/µm$^2$ and diameter of the secondary dendrites = 0.01 µm. Again, inward currents are smaller at positive potentials due to the activation of dendritic $K^+$ channels in both the central and neighboring cells, impairing clamp quality even further. At hyperpolarized potentials, the change in the slope of the *IV* relations results from the sum of the cone-driven *IV* relations of all the cells in the lattice. This way, electrical coupling increases rectification due to $I_{KV}$ also in the cone pathway.

channels must be determined. The single unit conductance of delayed rectifier-type $K^+$ channels can vary by more than ten fold, and their density in different tissues can change up to more than 100 fold (Hille, 1992; Coetzee et al., 1999). This means that an $I_{KV}$ of 1 nS/µm$^2$ could be interpreted as anything between 2500 channels of 4 pS single unit conductance per µm$^2$ and 250 channels of 40 pS per µm$^2$. A similar line of thought can be applied to the $g_{gap}$ values used in the coupling simulations, due to the huge gamma of single unit conductances of the various connexin types (Dermietzel et al., 2000).

*Are Mixed-Input ON BCs Isopotential?*

The data and simulations in this Chapter suggest that mixed-input ON BCs are not isopotential. Due to the nature of the synaptic inputs, the dendritic tips contacting rods might be slightly more depolarized than the cell soma, while the dendrites contacting cones would be slightly more hyperpolarized than the soma (not shown). This inhomogeneity has important functional consequences (see next sections), because it leads to a larger activation of dendritic $K^+$ channels at the sites of rod synaptic input as compared to the sites of cone input.

Most arguments about BCs being isopotential come from experiments conducted on isolated cells (Lasater et al., 1984; Attwell et al., 1987). In these experiments, one assumes that the isolation procedure does not amputate peripheral dendrites, and that the active conductances are homogeneously distributed throughout the membrane. Yet these assumptions might not hold (Kaneko and Tachibana, 1985; Schultz et al., 2001). For instance, the high percentage of cells in these preparations that lack responses to glutamate (Lasater et al., 1984) and GABA (Kaneko et al., 1991) indicates that the dendritic tips and shafts are lost, since most glutamate receptors are concentrated in this region (Hack et al., 1999; Haverkamp et al., 2001; Klooster et al., 2001; Schultz et al., 2001; this thesis, Chapter 2), and GABAc receptor subunits are located at the primary and secondary dendrites (Klooster et al., 2004).

Our results show that even small neurons can be anisopotential. This is surprising, because anisopotentiality is usually thought of as a property of large CNS neurons, such as pyramidal neurons (Hausser and Roth, 1997). What makes this happen? The first factor making small BCs anisopotential is a non-uniform distribution of active conductances, in this case $I_{KV}$. Although this is an electrophysiological and model study, morphological support for our conclusions can be found in literature. Some voltage-gated $K^+$ channel subunits are preferentially expressed at the dendritic tips of murine rod BCs (Klumpp et al., 1995; Pinto and Klumpp, 1998), voltage-gated $Na^+$ channels were identified in goldfish cone-driven BC dendrites and somas (Zenisek et al., 2001), and large $Ca^{2+}$, $Ca^{2+}$-dependent $K^+$ and $Cl^+$ currents originate in the giant synaptic terminals of goldfish mixed-input ON BCs (Kaneko and Tachibana, 1985; Kaneko et al., 1991; Tachibana et al., 1993; Okada et al., 1995; Burrone and Lagnado, 1997; Sakaba et al., 1997; Zenisek and Matthews, 1997). The second factor is the high resistance of the secondary dendrites. The funneling of the dendritic shafts in relation to the dendritic tips can lead to a further increase in this resistance difference. Such a dendritic morphology was described in mixed-input ON BCs of the smooth dogfish (Witkovsky and Stell, 1973), goldfish (Stell, 1978; Ishida et al., 1980; Klooster et al., 2001) and rudd (Scholes, 1975), as well as in rod BCs of the guinea pig and rabbit retinas (Ladman, 1958; Sjostrand, 1998a/b).

*The $K^+$ Currents of Mixed-Input ON BCs*

BCs have large outwardly rectifying $K^+$ currents (Kaneko and Tachibana, 1985; Attwell et al., 1987; Tessier-Lavigne et al., 1988), which is consistent with our results. However, some authors argue that these currents are not active at physiological membrane potentials and therefore should not shape BC light responses (Attwell et al., 1987; Spiridon et al., 1998). Our work shows that this is not necessarily the case. First of all, since the BCs are anisopotential, the $K^+$ channels located at the tips of the dendrites can experience a more depolarized membrane potential than that measured at the soma. This might be the reason for our finding that $I_{K(V)}$ activates in the working range of mixed-input ON BCs. This is consistent with other studies

showing that these conductances play an important role in adaptive mechanisms involved in controlling the dynamics and gain of BC light responses (Mao et al., 1998/2002): the light-induced depolarization of the BC membrane activates delayed-rectifier-like currents that induce band-pass behavior in these cells.

The identity of the $K^+$ channels responsible for the generation of these outwardly rectifying currents in mixed-input ON BCs is still unknown. KV1.1, KV1.2 and KV2.1 were described, with slightly different subcellular distributions (Yazulla and Studholme, 1998). In this study, KV1.2-IR was found in putative mixed-input ON BC dendrites invaginating into the cone pedicles, but not in the rod spherules, suggesting that the dendrites of the same cell would express different KV subunits depending on the type of synaptic contact. In mouse rod-driven ON BCs, KV1.3 was found to be concentrated at the tips of the BC dendrites contacting rods (Klumpp et al., 1995; Pinto and Klumpp, 1998), making this subunit a likely candidate for generating the rectifying light-driven *IV* relations reported here.

*Dendritic Potassium Channels as a Gain Control Mechanism*

As discussed in Chapter 3, the rod-BC synapse has a very high gain in order to allow large threshold responses at the BC level in the scotopic range, when only a few photons are available for a few rods (Ashmore and Falk, 1980; Capovilla et al., 1987; Falk, 1988; Copenhagen et al., 1990). Such an amplification at the rod-BC synapse is necessary because rod voltage responses at threshold are extremely small (Fain, 1975; Copenhagen and Owen, 1976; Fain et al., 1976), slow, and buried in noise (Taylor and Smith, 2004; Field et al., 2005).

Amplification of single-photon rod signals increases the responses of second-order neurons, but it also implies in amplification of noise levels (Taylor and Smith, 2004; Field et al., 2005). Such amplification in signal is however not necessary for light intensities that generate sizeable responses from rods and that stimulate cones. The gain of the rod-BC cell synapse is therefore not static and changes with stimulus intensity and/or background light levels (Ashmore and Falk, 1980; Yang and Wu, 1997): the more photons available, the lower the gain.

One of the mechanisms responsible for the high gain of the rod-BC synapse and for eliminating some of its noise is the mGluR6 cascade itself (Falk, 1988; Shiells, 1994; Shiells and Falk, 1995; Sampath and Rieke, 2004). The mechanism responsible for the gain decrease at higher light levels is unknown. We propose that one of the mechanisms for such gain control is the activation of voltage-gated $K^+$ currents in the vicinity of synaptic input sites.

The proposed mechanism works as follows. In the dark, the mGluR6 pathway is activated in a sustained manner, keeping the cation channels in the mixed-input ON BC membrane almost closed. Since in this condition the tips of the dendrites are relatively hyperpolarized, $I_{KV}$ is hardly activated. This makes the resistance of the tips of the dendrites high. In this condition, a small modulation of the mGluR6 pathway will lead to signal transmission to the soma, since the resistance of the tip is balanced to the resistance of the secondary dendrite.

At higher light levels, the mGluR6 pathway will be less activated, and the tips of the dendrites will depolarize. This will in turn activate $I_{KV}$, and the overall result will be a reduction of the resistance of the tips. Because in this condition the balance between the resistance of the tips and the resistance of the secondary dendrites is lost, the signals from rods to the mixed-input ON BC will be transmitted with low gain. This system will modify the gain during light and dark adaptation. Consistent with this idea are the findings that voltage-gated $K^+$ conductances in mixed-input ON BCs are enhanced by dopamine (Fan and Yazulla, 1999a/b; Yazulla et al., 2001; Fan and Yazulla, 2001; Connaughton and Warndorf, 2005), and that dopamine levels are higher in the light-adapted retina (Witkovsky and Dearry, 1991; Djamgoz and Wagner, 1992).

This system has additional intriguing features. The gain of the rod-BC synapse at rod threshold is such that a few photons falling onto a few rods will lead to a large modulation of the mGluR6 pathway in the mixed-input ON BC, potentially saturating its response. The proposed mechanism, however, will quickly change the gain of the synapse of the stimulated rods by activating $I_{KV}$ only at those dendrites, allowing signals from other rods to activate the mixed-input BC with the highest possible gain. A consequence of this is that the responses become shorter than the rod response itself. In fact, rod-driven ON BC responses are much faster than rod light responses in both lower vertebrates and mammals (Field et al., 2005).

**Acknowledgements**

The authors thank Drs. Leon Lagnado, Robert G. Smith and Henrique von Gersdorff for helpful discussions.

# Chapter 6

# General Discussion

In the previous Chapters, several properties of mixed-input BCs were analyzed, such as their mGluR palette, electrical coupling, the interaction between their many inputs in the mesopic state, and their dendritic $K^+$ channels. These features enable mixed-input BCs to function optimally not only under mesopic conditions, but in a wide range of intensity levels and adaptive states. Many questions regarding the architecture and function of the photoreceptor-BC synapse and its downstream properties, however, still remain unanswered. This final Chapter will address some of these open issues.

## 6.1 Glutamate Receptors in the Photoreceptor-BC Synapse

*Pre-Synaptic Receptors*

The presence of mGluR4 (a group III mGluR) in the rod spherules of the goldfish (Chapter 2) made us wonder whether this receptor could be involved in regulating photoreceptor glutamate release, as in other parts of the central nervous system (Takahashi et al., 1996; Wu and Saggau, 1997; Cochilla and Alford, 1998; Anwyl, 1999). Although we did not find mGluR4 in cone pedicles, mGluR8 (which is a member of the same group) was found in mammalian rods and cones (Duvoisin et al., 1995), and there is evidence that the cone glutamate release is reduced by bath application of group III agonists in many species (rat: Koulen et al., 1999; carp: Hirasawa et al., 2002; newt: Hosoi et al., 2005). Two different mechanisms for the suppression of glutamate release were proposed: either an inhibition of $I_{Ca}$ (Koulen et al., 1999; Hosoi et al., 2005) or the activation of a 4-AP-sensitive $K^+$ current (Daniel and Crepel, 2001; Hirasawa et al., 2002). As a consequence, the light responses of HCs and BCs are suppressed (Hirasawa et al., 2002; Hosoi et al., 2005).

In order to verify whether a pre-synaptic action of DL-AP4 could account for a suppression of the light responses in mixed-input ON BCs, we investigated the effect of DL-AP4 in rod-driven and cone-driven HCs. If DL-AP4 would decrease photoreceptor glutamate release, we would expect to see both HC types hyperpolarize and their light response amplitudes should decrease. While this was the case in rod-driven HCs (Figure 6.1a), this effect was too small to account for the loss of light responses in mixed-input ON BCs. The fact that rod-driven HC responses were not completely abolished means that the photoreceptor glutamate release was still being modulated by light during the treatment, and therefore ON BCs should be able to respond as well. Furthermore, a decrease in the glutamate release of the rods would make mixed-input ON BC *depolarize*, and would *increase*

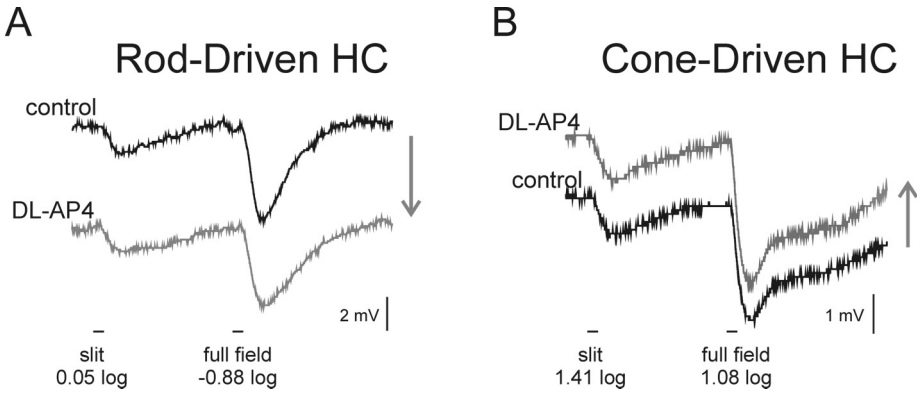


**Figure 6.1:** Effect of DL-AP4 in HCs. A: Light responses of a rod-driven HC to stimulation at 550 nm (stimulus intensity depicted in the figure) in control Ringer's (with 500 µM PTX and 20 µM STRY) and in the presence of 250 µM DL-AP4. The group III mGluR agonist hyperpolarized the cell about 6 mV (arrow) and decreased slightly the response amplitude. The horizontal bar depicts stimulus timing (100 ms). B: Light responses of a monophasic cone-driven HC to stimulation at 550 nm (stimulus intensity depicted in the figure) in control Ringer's (with 500 µM PTX and 20 µM STRY) and in the presence of 250 µM DL-AP4. The group III mGluR agonist depolarized the cell about 1.5 mV (arrow) and increased slightly the response amplitude. The horizontal bar depicts stimulus timing (100 ms).

$I_{hold}$ in a voltage-clamp experiment. In contrast to this prediction, bath application of DL-AP4 (n = 45) or ACPT-I (n = 4) *hyperpolarized* mixed-input ON BCs by 6-10 mV and *decreased* $I_{hold}$ by approximately 100-200 pA, consistent with a predominant post-synaptic effect of the drugs.

The effect of DL-AP4 on cone-driven HCs is also not consistent with a pre-synaptic effect. In both cells tested, the amplitude of the light responses increased. The cell in Figure 6.1a depolarized slightly, while the other cell tested hyperpolarized. These effects could be explained by a direct action of DL-AP4 on cone-driven HCs, since they also express group III mGluRs (Chapter 2). Since we used a saturating dose of DL-AP4 in these experiments, it is unlikely that the mild effects obtained in HCs would reflect an incomplete activation of the (pre- or post-synaptic) receptors. Direct effects of DL-AP4 onto cone-driven HC light responses in the goldfish were reported previously (Nawy et al., 1989; Takahashi and Copenhagen, 1992).

These results, though preliminary, do not support a strong suppression of photoreceptor glutamate release by group III mGluRs. Rather, they point to either mild pre-synaptic effects on the rod spherules, and/or mild post-synaptic effects on HCs themselves.

*Post-Synaptic Receptors*

There are at least 5 or 6 mixed-input BC types (Stell, 1978; Ishida et al., 1980; Sherry and Yazulla, 1993), and at least 9 cone-driven BCs in the goldfish (Sherry and Yazulla, 1993). Within these two main morphological classes, BCs subdivide

further into ON and OFF cells (Kaneko, 1970), and within the ON and OFF groups, there are neurons whose light responses present spectral coding (Saito et al., 1979; Sakakibara and Mitarai, 1982; Shimbo et al., 2000). Given the existence of cells that can both hyperpolarize and depolarize to light, and the variety of iGluR subunits and mGluRs at BC dendrites, it seems logical to assume that some of these receptors co-localize. Table 6.1 summarizes what is known so far about the localization of iGluR subunits and the mGluR composition in BCs of the teleost retina. The immunocytochemical techniques used in these studies, however, do not allow an unambiguous identification of the neurons labeled, nor can tell whether there is co-localization.

In Chapters 2, 3 and 5 we discussed the evidence for mGluR6 mediating rod-driven light responses in mixed-input ON BCs. We also showed that cone-driven depolarizing light responses are insensitive to agonists of mGluRs of the group III, such as DL-AP4 and ACPT-I. At least in the salamander (Hensley et al., 1993; Maple et al., 1999), mixed-input OFF BC responses are mediated by iGluRs. Evidence for co-localization of different GluRs in goldfish mixed-input BCs is presented in Figure 6.2, in which the light responses of a cell are shown in control (upper traces) and after bath application of DNQX and DL-AP4. This BC was spectrally coded in control Ringer's; the hyperpolarizing responses were abolished in the presence of the drugs, and a DL-AP4-insensitive depolarization appeared. These results indicate that at least in this cell, AMPA-KA receptors were involved in generating the hyperpolarizing light responses, whereas the depolarizing responses were not mediated by mGluR6.

The receptor responsible for the cone-driven light responses of these cells remains to some extent a mystery. There is evidence both in favor and against a role of EAAT5 in the generation of these light responses. The cone-driven pathway in fish BCs can be partly mediated by mGluR6 (Wong et al., 2005) and partly by a receptor that modulates either a $K^+$ or a $Cl^-$ conductance (Saito et al., 1978; Saito et al., 1979; Nawy and Copenhagen, 1987/1990; Grant and Dowling, 1995/1996). The receptor seems to have a transporter-like pharmacology: it needs the presence of extracellular $Na^+$ to induce a current, and it can be partially inhibited by glutamate

| article | GluR | cell type |
|---|---|---|
| *Peng et al., 1995*[1] | GluR2, GluR2/3 | mixed-input ON BCs |
| *Schultz et al., 1997*[1] | GluR4 | putative OFF BCs |
| *Yazulla and Studholme, 1999*[1] | GluR4 | OFF BCs |
| *Gafka et al., 1999*[2] | mGluR1α, mGluR5, mGluR2/3, mGluR6 | BCs |
| *Vandenbranden et al., 2000*[1] | GluR1, GluR4 | BCs |
| *Schultz et al., 2001*[3] | GluR2/3, GluR4, GluR5-7 | OFF BCs (all ), mixed-input ON BCs (GluR2/3) |
| *Klooster et al., 2001*[1] | GluR2, mGluR1α | mixed-input ON BCs |
| *Yazulla and Studholme, 2001*[4] | GluR4, mGluR1α | OFF BCs (GluR4), mixed-input ON BCs (mGluR1α) |
| *This thesis, Chapter 2*[1] | mGluR1α, mGluR6 | mixed-input ON BCs |

**Table 6.1:** Morphological localization of AMPA-KA iGluR subunits (GluR 1-7) and mGluRs in BCs of the teleost retina. [1]: goldfish; [2]: catfish; [3]: carp; [4]: zebrafish.

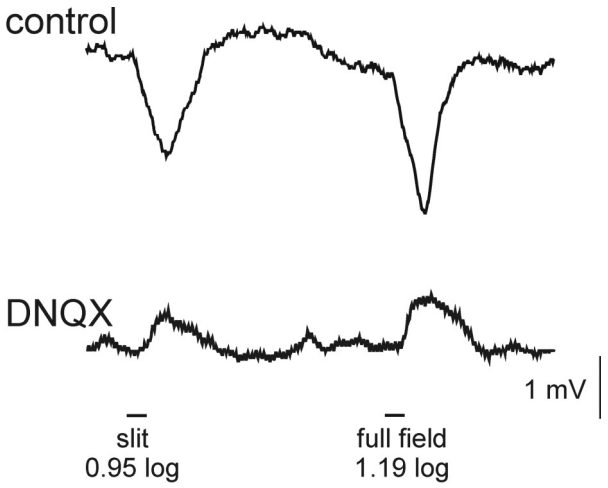


**Figure 6.2:** Evidence for the colocalization of multiple glutamatergic conductances in mixed-input BCs. A: Light responses of a spectrally opponent mixed-input BC to stimulation at 650 nm (stimulus intensity depicted in the figure) in control Ringer's (with 500 µM PTX, 5 µM STRY and 250 µM DL-AP4) and in the presence of 50 µM DNQX. The iGluR antagonist hyperpolarized the cell about 7 mV and abolished completely the hyperpolarizing light responses. The depolarizing light response, which in control conditions could only be evoked at shorter wavelengths, remained. The horizontal bar depicts stimulus timing (100 ms).

uptake blockers (Grant and Dowling, 1995; Grant and Dowling, 1996).

The cloning and characterization of EAAT5, a glutamate transporter that mobilizes a large $Cl^-$ conductance, as well as the finding that it is expressed in the retinal BCs (Arriza et al., 1997; Eliasof et al., 1998b) made it tempting to conclude that this transporter might mediate cone-driven depolarizing light responses in fish ON BCs (Arriza et al., 1997; Wong et al., 2005). However, although this transporter-like conductance is only found in cone-driven BC responses of the fish retina, EAAT5 is not exclusively expressed in the fish retina, nor is it restricted to cone-driven BC dendrites. It is also present in Müller cells of the salamander retina (Eliasof et al., 1998b), in rod- and cone-driven BCs and photoreceptors of the rat retina (Pow and Barnett, 2000), as well as in photoreceptors of the rabbit and macaque (Pow et al., 2000).

Figure 6.3 shows the ultrastructural localization of EAAT5 in the cone pedicles (Figure 6.3a) and in the rod spherules (Figure 6.3b) of the goldfish retina. In the cone terminals, invaginating processes that could belong to BC dendrites are labeled. These processes sometimes terminate at the position of cone-driven ON BC dendrites (arrows), or end at a certain distance from the synaptic ribbons, as the dendrites of mixed-input ON BCs do. In the rod spherule, the EAAT5 antibody labels elongated invaginating dendrites that terminate in close apposition to the synaptic ribbon. These positive processes resemble those of mixed-input ON BCs in position and cytological appearance (see Chapter 2).

If EAAT5 is present in both rod- and cone-driven dendrites of mixed-input ON BCs, and if EAAT5 mediates light responses, then at least part of the rod-driven light responses of these cells should be mediated by EAAT5 as well. However, we have no evidence for EAAT5-mediated rod-driven depolarizations in mixed-input ON BCs of the goldfish. The rod-driven light responses of these neurons could always be

blocked by DL-AP4 (n = 45) or ACPT-I (n = 4). This raises the question as to whether EAAT5 is really the “mystery cone-driven ON receptor”. There is recent evidence that, at least in the axon terminals of mixed-input ON BCs of the goldfish, EAAT5 might be related to local feedback circuits (Palmer et al., 2003).

One could argue that maybe EAAT5 has distinct functions in different compartments of mixed-input ON BCs, modulating cone-driven light responses at dendrites contacting cones, and uptaking glutamate in dendrites contacting rods and in the axon terminals, without generating sizeable responses. Alternatively, other EAATs could be involved in mixed-input ON BC light responses. All of the 5 cloned EAATs have a thermodynamically uncoupled $Cl^-$ conductance, (Wadiche et al., 1995; Fairman et al., 1995), and show similar dependence to $Na^+$ and sensitivity to glutamate (Eliasof et al., 1998b). EAAT2 (also called GLT-1) is also expressed in BCs (goldfish: Vandenbranden et al., 2000; salamander: Eliasof et al., 1998a/b; rat: Rauen and Kanner, 1994; Rauen et al., 1996; monkey: Rauen and Kanner, 1994), although it seems to be concentrated at the axon terminals.

But are these three glutamate receptor types – AMPA/KA for hyperpolarizing responses, and mGluR6 and the transporter-like receptor for depolarizing responses – the only ones responsible for mixed-input BC light-driven conductances? Probably not. A fourth type of light response was described in BCs of the carp retina (Saito and Kaneko, 1983; Saito et al., 1984; Shimbo et al., 2000): a hyperpolarization induced by a conductance decrease with a negative $V_{rev}$. This conductance could also be driven by a transporter-like receptor, provided it is expressed in cells with different values of $E_{Cl}$. In cells that hyperpolarize to light, $E_{Cl}$ would have to be *more positive*

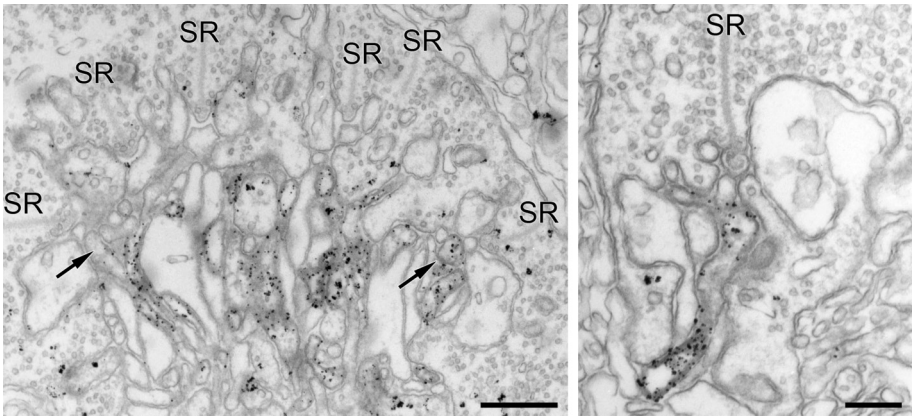


**Figure 6.3:** Ultrastructural localization of EAAT5 in the OPL. A: In the cone pedicles, invaginating structures are positively labeled. These elements are never found in close apposition to the presynaptic ridge (SR), indicating they may belong to ON BCs. The lateral and central elements of the triad are unlabeled. Scale bar = 0.5 µm. B: In the rod spherules, invaginating dendrites are also labeled. These elements are found either in close apposition to the presynaptic ridge (SR) or a little away from it. Scale bar = 0.25 µm.

than $V_{rest}$, whereas in cells that depolarize to light, $E_{Cl}$ would have to be *more negative* than $V_{rest}$. Studies in mouse (Satoh et al., 2001) indicate that ON BCs tend to have a slightly more positive $E_{Cl}$ than OFF BCs, although $E_{Cl}$ in ON BCs was shown to vary in according to $V_{rest}$ (Billups and Attwell, 2002).

In spite of the confusing picture in literature, the data in Figure 6.4 suggests that the two types of conductance decrease can be expressed concomitantly in the BC, irrespective of $V_{rest}$. This BC was rod-dominated and only depolarized to light in control conditions, but became spectrally opponent after application of DL-AP4. Ionotropic GluRs could not contribute to the light-driven outward currents due to the presence of DNQX in the bath, and mGluR6 could not contribute to the light-driven inward currents. We recorded from 9 such cells (Table 6.2), and the facts that the majority of them lacked axonal terminations and that PTX and STRY were present in the bath suggests that these hyperpolarizing light responses are arising in the outer retina due to direct photoreceptor input. Further, the data indicates that these cone-driven conductances cannot be mediated by the same transporter-like receptor, unless BCs keep different $Cl^-$ concentrations in individual dendrites.

The reason for this multitude of glutamatergic conductances in mixed-input BCs remains a puzzle. The difference in their sensitivity to light, however, suggests that they might be active under different adaptive states. In the carp retina, chromatic adaptation (Saito et al., 1981) or light adaptation (Shimbo et al., 2000) can both

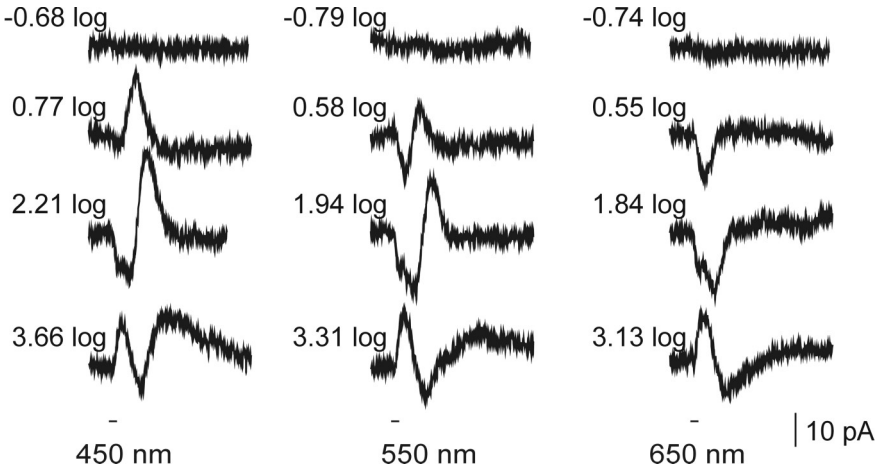


**Figure 6.4:** Evidence for additional cone-driven glutamate receptors in mixed-input ON BCs. Light-evoked currents of a mixed-input ON BC in DL-AP4 Ringer's to full-field stimulation at 450 nm, 550 nm and 650 nm and four different intensity levels. The complex waveforms and change in response polarity as light intensity increases indicate that there is more than one conductance being modulated by the light flashes. These conductances must be a result of direct photoreceptor input, because this cell did not have an axon terminal, and GABAergic inputs and HC activity were blocked pharmacologically. Drug content of the Ringer's solution (μM): 250 DL-AP4, 500 PTX, 5 STRY, 50 DNQX. Horizontal bars depict stimulus timing (100 ms).

| Drug Treatment | Presence of Axon Terminal | | |
|---|---|---|---|
| | yes | no | ? |
| *DNQX+PTX+STRY+DNQX+ACPT-I* | | 1 | |
| *DNQX+PTX+STRY+DL-AP4* | | 4 | |
| *PTX+STRY+DL-AP4* | 1 | 2 | 1 |

**Table 6.2:** Mixed-input ON BCs that became spectrally opponent upon application of DL-AP4. Most of the cells had lost their axonal terminations due to the slicing procedure. This, added to the presence of PTX+STRY (and in some cases DNQX as well) indicates that the opponent responses originated from direct glutamatergic inputs at the OPL.

render mixed-input ON BCs spectrally opponent. This is consistent with our results. We proposed in Chapter 5 that the tonic activation of voltage-gated $K^+$ channels in the dendrites expressing mGluR6 could lead to a decrease in the gain of the rod-BC synapse. Light adaptation would therefore favor these cone-driven light responses. Since both depolarizing and hyperpolarizing cone-driven responses are conductance decreases, they would not be affected by dendritic $I_{KV}$ the same way.

Lastly, the change in response properties (from only depolarizing to spectrally coded) induced by the suppression of the mGluR6 conductance indicates that these cells would be optimized for light detection in the dark-adapted state, and for light intensity changes around a mean level in the light-adapted state, as discussed in Chapter 4. Similar adaptive changes were described in GCs of the goldfish (Beauchamp and Daw, 1972; Raynauld, 1972), which would suggest that many physiological properties of GCs arise already at the first synapse.

## 6.2 Trade-Offs In Retinal Organization

The visual system most likely evolved such as to code visual information optimally. This means transmitting a maximum amount of information using a minimum amount of energy. But some physiological requirements can be conflicting. For instance, high spatial resolution requires a large number of nerve fibers with small receptive fields, whereas high sensitivity requires a small number of fibers with large receptive fields. The same trade-off between specificity and sensitivity exists when it comes to color vision (Barlow and Mollon, 1982).

Additionally, the high metabolic cost of keeping a large number of optic nerve fibers (Laughlin, 2001) and the mechanical constraints imposed by the eye movements led to the evolution of a thin optic nerve (Meister, 1996). One of the solutions that evolved is a strong convergence of many photoreceptors onto a second-order neuron. This convergence increases the sensitivity of the system, but might decrease resolution. In the next paragraphs, we will discuss the costs

and benefits of large, overlapping receptive fields for spatial resolution and visual sensitivity.

*Costs for Visual Acuity…*

The spatial resolution of the visual system is limited by a number of factors, starting with the optics of the eye itself (Cornsweet, 1970; Barlow and Mollon, 1982; Pettigrew et al., 1986). Once projected onto the retina, the image is sampled by photoreceptors and the resulting acuity will depend on the spacing between photoreceptors and the neuronal wiring, which differs for scotopic and photopic vision (Barlow and Mollon, 1982). The fovea lacks rods (Cornsweet, 1970), and foveal cones project to BCs and BCs to GCs on a one-to-one basis (Dowling, 1987; Rodieck, 1998). In the peripheral retina, neither the rod- nor the cone-driven pathways have such "exclusive lines", and this means that the receptive fields of second- and third- order neurons are larger than in the fovea (Kier et al., 1995). The fact that the foveal region has the highest visual acuity (Barlow and Mollon, 1982) led scientists to conclude that there must be a relation between receptive field size and spatial resolution (Pettigrew et al., 1986). Further, the absence of a foveal region in many species would imply that in these species visual acuity should necessarily be poor (Pettigrew et al., 1986). But how much does a GC layer with large receptive fields limit the spatial resolution of the eye? To answer this, one needs to understand how these receptive fields are generated, and how different receptive fields from different cells interact.

There are two main determinants of receptive field size. First, receptive field centers of second- and third- order neurons are primarily dependent on the extension of their dendritic trees. In both mammals (Kier et al., 1995) and fish (Hitchcock and Easter, 1986), the dendritic trees of GCs enlarge towards the retinal periphery. Throughout the retina, the dendritic trees of (non-foveal) GCs are much larger than those of BCs (Hitchcock and Easter, 1986), which means that considerable convergence takes place as signals flow from the outer to the inner retina (Stell and Lightfoot, 1975; Copenhagen et al., 1990; Taylor and Smith, 2004). In the goldfish, for instance, mixed-input OFF BCs contact around 30 photoreceptors (Stell, 1978; Ishida et al., 1980; this thesis, Table 3.2), while wide-field OFF GCs collect signals from around 35 mixed-input OFF BCs and 100 ACs (Hitchcock, 1989). This convergence of inputs, which is larger for the rod than for the cone system (Johns and Easter, 1977), would alone yield large sampling areas at the GC level, even in the absence of lateral interactions.

Another factor that influences the extension of retinal receptive field centers is electrical coupling. As shown in Chapters 3, 4 and 5 of this thesis, mixed-input BCs are electrically coupled, and as a result the BC receptive field center extends beyond the dimensions of its dendritic tree. But BCs are not the only retinal neurons which integrate signals laterally. There is both morphological and electrophysiological evidence that gap junctional coupling between homologous neurons is present at all levels in the retina (Table 6.3), maybe as a way to spare retinal hardwiring and

to improve signal-to-noise-ratio and temporal resolution (Lamb and Simon, 1976; Laughlin, 2002; Discussion in Chapter 3). As a result of coupling, receptive fields increase further from the outer to the inner retina.

If one expects visual acuity to be strictly related to receptive field center sizes, both neural convergence and electrical coupling would blur the neural image considerably. Although surround-mediated interactions help shrink receptive field centers (Stell and Kock, 1984), spatial summation at the GC level can still be considerable, even in cells with center-surround organization (Daw, 1968; Afanador and Adams, 1976). There are however strategies that can help the visual system retrieve higher spatial resolution despite this progression from small to large functional receptive fields as one advances from the photoreceptor to the GC layer. One of these strategies is to increase the overlap between these receptive fields (Fischer, 1973; Meister, 1996). Color vision, for instance, benefits from this same strategy: few photoreceptors with largely overlapping spectral sensitivities. This allows us to discriminate about 200 hues within a 300 nm interval (Barlow and Mollon, 1982).

In fact, psychophysical estimates of visual acuity in a number of species indicate that photoreceptor densities are the limiting factors for spatial resolution, regardless of the sizes of individual GC receptive fields. In the goldfish, for instance, while spatial summation areas of some GC receptive field centers would predict a spatial resolution of 3 to 30° depending on the adaptive state of the retina, behavioral studies found values as high as 0.15°, which corresponds roughly to the resolution limit imposed by cone density (for reviews, see Stell and Kock, 1984 and Neumeyer, 2003). In the bullfrog, the size of the rod network alone would predict a scotopic visual acuity of about 10° (Fain et al., 1976) which is much lower than the actual scotopic acuity measured in anurans (Aho et al., 1993; Aho, 1997).

There is evidence for considerable divergence of signals from one photoreceptor onto many second-order neurons in fish (Stell and Kock, 1984) and primate (Grünert et al., 1994) retinas. A single rod spherule in the goldfish has approximately 5 to 8 post-synaptic processes contacting the ribbon, of which at least 3 are BCs (Stell and Lightfoot, 1979; Stell and Kock, 1984). Occasionally, rods with two synaptic ribbons are also found (Figure 6.5), and in these terminals divergence is even larger. Though less frequent in the goldfish, such rods are present in a number of species (Migdale et al., 2003; Thoreson et al., 2004). In the cone-driven pathway, divergence is also significant: cyprinid cones can have up to 25 ribbons, depending on spectral type (Figure 6.2a, Downing and Djamgoz, 1989).

The ratio between the total number of cones and GCs in the adult goldfish retina seems to be only 2:1 or even less (Neumeyer, 2003), which suggests that the high acuity measured behaviorally might reflect this relation. This ratio, however, pools all types of GCs. Unfortunately, little is known about how many GC types there are, how they are connected to the outer retina, and how their outputs are compared later. These are critical factors to determine what the final spatial resolution will

| Cell Type | Morphology | Physiology | Animal |
|---|---|---|---|
| *rods* | Raviola and Gilula, 1973 | | monkey |
| | Witkovsky et al., 1974 | | carp |
| | Fain et al., 1976 | Fain, 1975 | toad |
| | | Detwiler et al., 1978 | turtle |
| | Marc et al., 1988 | | goldfish |
| | Zhang and Wu, 2004 | Attwell and Wilson, 1980 | salamander |
| *cones* | | Baylor et al., 1971 | turtle |
| | Raviola and Gilula, 1973 | | monkey, rabbit |
| | Witkovsky et al., 1974 | | carp |
| | Marc et al., 1988 | | goldfish |
| | | DeVries et al., 2002 | ground squirrel |
| | O'Brien et al., 2004 | | bass |
| *HCs* | | Norton et al., 1968 | carp |
| | | Dowling and Ripps, 1971 | skate |
| | | Kaneko, 1971 | dogfish |
| | | Marchiafava and Pasino, 1973 | tench |
| | Witkovsky et al., 1979 | | pikeperch |
| | Marc et al., 1988 | | goldfish |
| *BCs* | Witkovsky and Stell, 1973 | | smooth dogfish |
| | Wong-Riley, 1974 | Borges and Wilson, 1987 | salamander |
| | Marc et al., 1988 | | goldfish |
| | Cuenca et al., 1993 | Kujiraoka and Saito, 1986 | carp |
| | Umino et al., 1994 | Umino et al., 1994 | black bass, dace, carp |
| *ACs* | Marc et al., 1988 | | goldfish |
| | Vaney, 1991 | | cat, rabbit |
| | Xin and Bloomfield, 1997 | Xin and Bloomfield, 1997 | rabbit |
| | | Bloomfield and Volgyi, 2004 | mouse, rabbit |
| *GCs* | | Mastronarde, 1983 | cat |
| | Vaney, 1991 | | cat, rabbit |
| | Xin and Bloomfield, 1997 | Xin and Bloomfield, 1997 | rabbit |
| | Schubert et al., 2005 | | mouse |

**Table 6.3:** Morphological and physiological evidence for gap junctional coupling at all levels in the retina of different vertebrates.

be. At least 4 morphological types were described in the goldfish (Hitchcock and Easter, 1986) and 11 in the rabbit (Rockhill et al., 2002), but their physiology and connectivity patterns are not well understood. Although the adaptive state of the retina determines which physiological GC types are recruited to convey light-driven signals (Northmore, 1977), even the receptive field centers of the same GC types overlap to some extent (Kock and Reuter, 1978; Peichl and Wässle, 1979; Macy and

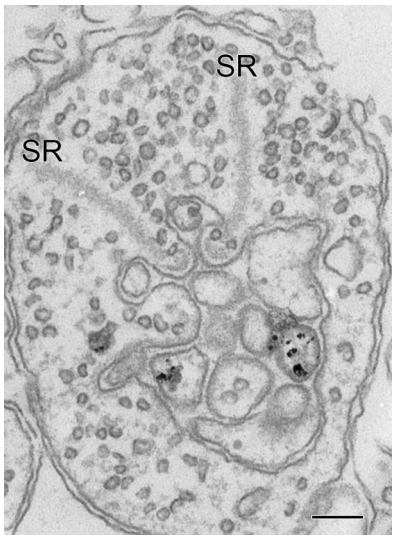


**Figure 6.5:** Divergence in the rod-driven pathway. Electron micrograph of a goldfish rod with two synaptic ribbons (SR). The number of invaginating elements in the vicinity of these ridges is larger than in the case of terminals containing single ribbons. Scale bar = 0.25 µm.

Easter, 1981).

In conclusion, although large receptive fields might look detrimental for visual acuity at a first glance, they can actually help improve spatial resolution. Depending on how the retina is hardwired (i.e. how many parallel channels there are and what their coverage factor of the retina is) and how retinal signals are compared downstream in the visual system, spatial resolution could be improved by the overlap of receptive fields of GCs sampling from slightly similar areas and collecting from roughly the same photoreceptors (Meister, 1996).

*… And Benefits for Sensitivity?*

Rod-driven cells collect from more photoreceptors than cone-driven cells, and this larger sampling area helps increase their threshold sensitivity (Barlow and Mollon, 1982). The progressive increase in convergence throughout the retinal layers coincides with an amplification of light-driven signals as they advance through the retina (Capovilla et al., 1987; Copenhagen et al., 1990). While single-photon responses in rods might be in the µV range (Fain, 1975; Fain et al., 1976), rod-driven light responses in BCs, HCs and GCs have a much higher gain (in mV/Rh*, Copenhagen et al., 1990). This increase in both spatial summation and voltage gain led some authors to speculate about a causal relation between both (Capovilla et al., 1987; Copenhagen et al., 1990; Taylor and Smith, 2004). It was also speculated that convergence could increase the half-maximal sensitivity (log $K^{-1}$) of second-order neurons (Copenhagen et al., 1990; Taylor and Smith, 2004), due to the combination of this higher voltage gain and larger summation area of second-order neurons.

Although this view may sound intuitively correct, having many rods (or

cones) converge onto a second-order neuron does not per se increase the voltage gain of the system. Convergence increases in the fish eye as the animals grow, because the formation of new rod photoreceptors outnumbers that of BCs and GCs throughout life (Johns and Easter, 1977; Kock, 1982; Stell and Kock, 1984). The extension of BC dendritic trees (Stell and Kock, 1984; Bloomfield and Hitchcock, 1991) and of GC receptive fields (Macy and Easter, 1981) also increases with the age and size of the fish, due to the decrease in second-order neuron densities with retinal stretching. In spite of this increase in convergence, there is no evidence for response amplitude differences between BCs or GCs from fish of different sizes.

As far as sensitivity is concerned, a distinction between half-maximal sensitivity and threshold sensitivity must be made. Provided the gain of the photoreceptor-BC-GC synapses is high enough to allow responses to single photons in BCs, threshold sensitivity can indeed benefit from a larger sampling area, simply because it increases the probability of a photon being absorbed within the receptive field of a cell being recorded from. The half-maximal sensitivity of a BC to a given stimulus, on the other hand, depends on a number of factors, such as its glutamate receptor composition and number, the kinds of photoreceptors (rods, L-, M-, S- or UV cones) that synapse onto it, and the ratios of these inputs rather than the absolute number.

Furthermore, second-order neurons need to produce dendritic membrane to accommodate new synapses as photoreceptor are added (Kier et al., 1995), and this newly produced membrane contains both transmitter-controlled and non-synaptic ion channels. This means that the total conductance of the post-synaptic cells could increase with convergence and with age, and therefore the influence of a single photoreceptor onto second-order neurons could decrease proportionally (Ashmore and Falk, 1980; Falk, 1988). Depending on the relation between the total conductance of the cell, the conductance of a synapse and the number of new synapses, the sensitivity of single cells throughout life could be kept rather constant no matter the degree of convergence.

The same may hold for the whole animal: because the whole eye, the pupil aperture and the magnification factor of the lens also increases with age (Easter et al., 1977; Macy and Easter, 1981; Powers et al., 1988), it is likely that either the visual angle subtended by the growing GC receptive fields or the overlap between these fields remains constant with growth (Macy and Easter, 1981). Although absolute thresholds measured in large fish tend to be slightly lower than in small animals (about 0.25 log units), this increase in sensitivity is not proportional to the change in rod:GC ratio (Powers et al., 1988). Furthermore, other factors such as attention also change with development, and might play a role in setting the sensitivity of the visual system during growth.

But what is the role of convergence then? One could speculate that convergence spares retinal wiring and avoids redundancy. “Exclusive lines” such as the foveal pathways have a high metabolic cost. Further, convergence could

increase signal-to-noise ratio by reducing the influence a single photoreceptor exerts onto second-order neurons (Ashmore and Falk, 1980; Falk, 1988). Similarly to what happens when there is electrical coupling (see Discussion Chapter 3), spontaneous events would be averaged out at the synapse, and only the correlated activity of a group of photoreceptors would be transmitted to the forthcoming neurons. Finally, to allow high sensitivity in the rod pathway, signal amplification and gain control would remain largely dependent on the post-synaptic machinery, as addressed in Chapters 3 and 5.

### 6.3 General Comments

Although we know more about the retina now than we did 50 years ago, there are still major questions which wait to be answered. The final goal of vision research is to find out how molecules relate to morphology, how morphology relates to physiology, and how physiology relates to function. Hopefully this thesis has added some small pieces to this puzzle.

# References


Abe, T.; Sugihara, H.; Nawa, H.; Shigemoto, R.; Mizuno, N.; and Nakanishi, S. (1992) Molecular characterization of a novel metabotropic glutamate receptor mGluR5 coupled to inositol phosphate/$Ca^{2+}$ signal transduction. *J. Biol. Chem.* **267**: 13361-13368.

Adly, M.A.; Spiwoks-Becker, I.; and Vollrath, L. (1999) Ultrastructural changes of photoreceptor synaptic ribbons in relation to time of day and illumination. *Invest. Ophthalmol. Vis. Sci.* **40**: 2165-2172.

Afanador, A.J. and Adams, A.J. (1976) Spatial summation properties of goldfish ganglion cells. *Am. J. Optom. Physiol. Opt.* **53**: 177-181.

Afanador, A.J. and Adams, A.J. (1982) Early visual adaptation in color opponent goldfish ganglion cells. *Am. J. Optom. & Physiol. Opt.* **59**: 642-652.

Aho, A.C. (1997) The visual acuity of the frog (*Rana pipiens*). *J. Comp. Physiol. A* **180**: 19-24.

Aho, A.C.; Donner, K.; Helenius, S.; Larsen, L.O.; and Reuter, T. (1993) Visual performance of the toad (*Bufo bufo*) at low light levels: retinal ganglion cell responses and prey-catching accuracy. *J. Comp. Physiol. A* **172**: 671-682.

Akazawa, C.; Ohishi, H.; Nakajima, Y.; Okamoto, N.; Shigemoto, R.; Nakanishi, S.; and Mizuno, N. (1994) Expression of mRNAs of L-AP4-sensitive metabotropic glutamate receptors (mGluR4, mGluR6, mGluR7) in rat retina. *Neurosci. Lett.* **171**: 52-54.

Anwyl, R. (1999) Metabotropic glutamate receptors: electrophysiological properties and role in plasticity. *Brain Res. Brain Res. Rev.* **29**: 83-120.

Armstrong-Gold, C.E. and Rieke, F. (2003) Bandpass filtering at the rod to second-order cell synapse in salamander (*Ambystoma tigrinum*) retina. *J. Neurosci.* **23**: 3796-3806.

Arriza, J.L.; Eliasof, S.; Kavanaugh, M.P.; and Amara, S.G. (1997) Excitatory amino acid transporter 5, a retinal glutamate transporter coupled to a chloride conductance. *Proc. Natl. Acad. Sci. U.S.A.* **94**: 4155-4160.

Ashmore, J.F. and Falk, G. (1980) Response of rod bipolar cells in the dark-adapted retina of the dogfish, *Scyliorhinus canicula*. *J. Physiol. (Lond.)* **300**: 115-150.

Attwell, D.; Mobbs, P.; Tessier-Lavigne, M.; and Wilson, M. (1987) Neurotransmitter-induced currents in retinal bipolar cells of the axolotl, *Ambystoma mexicanum*. *J. Physiol. (Lond.)* **387**: 125-161.

Attwell, D. and Wilson, M. (1980) Behaviour of the rod network in the tiger salamander retina mediated by membrane properties of individual rods. *J. Physiol. (Lond.)* **309**: 287-315.

Awatramani, G.B. and Slaughter, M.M. (2001) Intensity-dependent, rapid activation of presynaptic metabotropic glutamate receptors at a central synapse. *J. Neurosci.* **21**: 741-749.

Barlow, H.B.; Fitzhugh, R.; and Kuffler, S.W. (1957) Dark adaptation, absolute threshold and Purkinje shift in single units of the cat's retina. *J. Physiol. (Lond.)* **137**: 327-337.

Barlow, H.B. and Mollon, J.D. (1982) *The senses.* Cambridge: Cambridge University Press.

Barry, P.H. and Lynch, J.W. (1991) Liquid junction potentials and small cell effects in patch-clamp analysis. *J. Membr. Biol.* **121**: 101-117.

Baylor, D.A. and Fuortes, M.G.F. (1970) Electrical responses of single cones in the retina of turtle. *J. Physiol. (Lond.)* **207**: 77-92.

Baylor, D.A.; Fuortes, M.G.F.; and O'Bryan, P.M. (1971) Receptive fields of cones in the retina of the turtle. *J. Physiol. (Lond.)* **214**: 265-294.

Beauchamp, R.D. and Daw, N.W. (1972) Rod and cone input to single goldfish optic nerve fibers. *Vision Res.* **12**: 1201-1212.

Beauchamp, R.D.; Rowe, J.S.; and O'Reilly, L.A. (1979) Goldfish spectral sensitivity: identification of the three cone mechanisms in heart-rate conditioned fish using colored adapting backgrounds. *Vision Res.* **19**: 1295-1302.

Behrens, U.D.; Kasten, P.; and Wagner, H.-J. (1998) Adaptation-dependent plasticity of rod bipolar cel axon terminal morphology in the rat retina. *Cell Tissue Res.* **294**: 243-251.

Behrens, U.D. and Wagner, H.J. (1996) Adaptation-dependent changes of bipolar cell terminals in fish retina: effects on overall morphology and spinule formation in Ma and Mb cells. *Vision Res.* **36**: 3901-3911.

Belgum, J.H. and Copenhagen, D.R. (1988) Synaptic transfer of rod signals to horizontal and bipolar cells in the retina of the toad (*Bufo marinus*). *J. Physiol. (Lond.)* **396**: 225-245.

Benison, G.; Keizer, J.; Chalupa, L.M.; and Robinson, D.W. (2001) Modeling temporal behavior of postnatal cat retinal ganglion cells. *J. Theor. Biol.* **210**: 187-199.

Berntson, A. and Taylor, W.R. (2000) Response characteristics and receptive field widths of ON-bipolar cells in the mouse retina. *J. Physiol. (Lond.)* **524**: 879-889.

Bevans, C.G. and Harris, A.L. (1999) Direct high affinity modulation of connexin channel activity by cyclic nucleotides. *J. Biol. Chem.* **274**: 3720-3725.

Billups, D. and Attwell, D. (2002) Control of intracellular chloride concentration and GABA response polarity in rat retinal ON bipolar cells. *J. Physiol. (Lond.)* **545**: 183-198.

Bloomfield, S.A. and Dacheux, R.F. (2001) Rod vision: pathways and processing in the mammalian retina. *Prog. Retin. Eye Res.* **20**: 351-384.

Bloomfield, S.A. and Hitchcock, P.F. (1991) Dendritic arbors of large-field ganglion cells show scaled growth during expansion of the goldfish retina: a study of morphometric and electrotonic properties. *J. Neurosci.* **11**: 910-917.

Bloomfield, S.A. and Volgyi, B. (2004) Function and plasticity of homologous coupling between AII amacrine cells. *Vision Res.* **44**: 3297-3306.

Bloomfield, S.A. and Xin, D. (1997) A comparison of receptive-field and tracer-coupling size of amacrine and ganglion cells in the rabbit retina. *Vis. Neurosci.* **14**: 1153-1165.

Borges, S. and Wilson, M. (1987) Structure of the receptive fields of bipolar cells in the salamander retina. *J. Neurophysiol.* **58**: 1275-1291.

Boycott, B.B. and Wässle, H. (1999) Parallel processing in the mammalian retina: the Proctor Lecture. *Invest. Ophthalmol. Vis. Sci.* **40**: 1313-1327.

Brakeman, P.R.; Lanahan, A.A.; O'Brien, R.; Roche, K.; Barnes, C.A.; Huganir, R.L.; and Worley, P.F. (1997) Homer: a protein that selectively binds metabotropic glutamate receptors. *Nature* **386**: 284-288.

Brandstätter, J.H.; Koulen, P.; Kuhn, R.; and Wässle, H. (1998) The metabotropic glutamate receptor -mGluR8- in the rat retina: localization and possible function. *Invest. Ophthal. Vis. Sci. Suppl.* **39**: S412.

Buchsbaum, G. and Gottschalk, A. (1983) Trichromacy, opponent colours coding and optimum colour information transmission in the retina. *Proc. R. Soc. Lond., B, Biol. Sci.***220**: 89-113.

Burkhardt, D.A. and Fahey, P.K. (1998) Contrast enhancement and distributed encoding by bipolar cells in the retina. *J. Neurophysiol.* **80**: 1070-1081.

Burrone, J. and Lagnado, L. (1997) Electrical resonance and $Ca^{2+}$ influx in the synaptic terminal of depolarizing bipolar cells from the goldfish retina. *J. Physiol. (Lond.)* **505**: 571-584.

Burt, J.M. and Spray, D.C. (1988) Inotropic agents modulate gap junctional conductance between cardiac myocytes. *Am. J. Physiol.* **254**: H1206-H1210.

Byzov, A.L.; Golubtzov, K.V.; and Trifonov, J.A. (1977) The model of mechanism of feedback between horizontal cells and photoreceptors in vertebrate retina. In: Barlow, H.B. and Fatt, P. (eds.) *Vertebrate photoreception*. London: Academic Press.

Cai, W. and Pourcho, R.G. (1999) Localization of metabotropic glutamate receptors mGluR1a and mGluR2/3 in the cat retina. *J. Comp. Neurol.* **407**: 427-437.

Calkins, D.J. (2004) Linking retinal circuits to color opponency. In: Chalupa, L.M. and Werner, J.S. (eds.) *The visual neurosciences*. Cambridge: The MIT Press.

Calkins, D.J. and Sterling, P. (1999) Evidence that circuits for spatial and color vision segregate at the first retinal synapse. *Neuron* **24**: 313-321.

Calkins, D.J.; Tsukamoto, Y.; and Sterling, P. (1996) Foveal cones form basal as well as invaginating junctions with diffuse ON bipolar cells. *Vision Res.* **36**: 3373-3381.

Capovilla, M.; Hare, W.A.; and Owen, W.G. (1987) Voltage gain of signal transfer from retinal rods to bipolar cells in the tiger salamander. *J. Physiol. (Lond.)* **391**: 125-140.

Cervetto, L. and MacNichol, E.F. (1972) Inactivation of horizontal cells in turtle retina by glutamate and aspartate. *Science* **178**: 767-768.

Chaytor, A.T.; Marsh, W.L.; Hutcheson, I.R.; and Griffith, T.M. (2000) Comparison of glycyrrhetinic acid isoforms and carbenoxolone as inhibitors of EDHF-type relaxations mediated via gap junctions. *Endothelium* **7**: 265-278.

Cochilla, A.J. and Alford, S. (1998) Metabotropic glutamate receptor-mediated control of neurotransmitter release. *Neuron* **20**: 1007-1016.

Coetzee, W.A.; Amarillo, Y.; Chiu, J.; Chow, A.; Lau, D.; McCormack, T.; Moreno, H.; Nadal, M.S.; Ozaita, A.; Pountney, D.; Saganich, M.; Vega-Saenz, d.M.; and Rudy, B. (1999) Molecular diversity of $K^+$ channels. *Ann. N.Y. Acad. Sci.* **868**: 233-285.

Connaughton, V.P. and Nelson, R. (2000) Axonal stratification patterns and glutamate-gated conductance mechanisms in zebrafish retinal bipolar cells. *J. Physiol. (Lond.)* **524**: 135-146.

Connaughton, V.P. and Warndorf, M. (2005) D1- and D2-like dopamine receptor activity enhance outward $K^+$ currents in zebrafish retinal bipolar cells. *Invest. Ophthal. Vis. Sci.* **46**: E-Abstract 1195.

Copenhagen, D.R. and Green, D.G. (1987) Spatial spread of adaptation within the cone network of the turtle retina. *J. Physiol. (Lond.)* **393**: 763-776.

Copenhagen, D.R.; Hemilä, S.; and Reuter, T. (1990) Signal transmission through the dark-adapted retina of the toad (*Bufo marinus*) Gain, convergence and signal/noise. *J. Gen. Physiol.* **95**: 717-732.

Copenhagen, D.R. and Owen, W.G. (1976) Functional characteristics of lateral interaction between rods in the retina of the snapping turtle. *J. Physiol. (Lond.)* **259**: 251-282.

Cornsweet, T.N. (1970) *Visual perception.* London: Academic Press, Inc.

Cuenca, N.; Fernandez, E.; Garcia, M.; and De Juan, J. (1993) Dendrites of rod dominant ON-bipolar cells are coupled by gap junctions in carp retina. *Neurosci. Lett.* **162**: 34-38.

Daniel, H. and Crepel, F. (2001) Control of $Ca^{2+}$ influx by cannabinoid and metabotropic glutamate receptors in rat cerebellar cortex requires $K^+$ channels. *J. Physiol. (Lond.)* **537**: 793-800.

Daw, N.W. (1967) Goldfish retina: organization for simultaneous color contrast. *Science* **158**: 942-944.
Daw, N.W. (1968) Colour-coded ganglion cells in the goldfish retina: extension of their receptive fields by means of new stimuli. *J. Physiol. (Lond.)* **197**: 567-592.
Daw, N.W. and Beauchamp, R.D. (1972) Unusual units in the goldfish optic nerve. *Vision Res.* **12**: 1849-1856.
de Groot, J.R.; Veenstra, T.; Verkerk, A.O.; Wilders, R.; Smits, J.P.; Wilms-Schopman, F.J.; Wiegerinck, R.F.; Bourier, J.; Belterman, C.N.; Coronel, R.; and Verheijck, E.E. (2003) Conduction slowing by the gap junctional uncoupler carbenoxolone. *Cardiovasc. Res.* **60**: 288-297.
de Monasterio, F.M.; Gouras, P.; and Tolhurst, D.J. (1975a) Concealed colour opponency in ganglion cells of the rhesus monkey retina. *J. Physiol. (Lond.)* **251**: 217-229.
de Monasterio, F.M.; Gouras, P.; and Tolhurst, D.J. (1975b) Trichromatic colour opponency in ganglion cells of the rhesus monkey retina. *J. Physiol. (Lond.)* **251**: 197-216.
Dermietzel, R.; Kremer, M.; Paputsoglu, G.; Stang, A.; Skerrett, I.M.; Gomes, D.; Srinivas, M.; Janssen-Bienhold, U.; Weiler, R.; Nicholson, B.J.; Bruzzone, R.; and Spray, D.C. (2000) Molecular and functional diversity of neural connexins in the retina. *J. Neurosci.* **20**: 8331-8343.
Detwiler, P.B. and Hodgkin, A.L. (1979) Electrical coupling between cones in turtle retina. *J. Physiol. (Lond.)* **291**: 75-100.
Detwiler, P.B.; Hodgkin, A.L.; and McNaughton, P.A. (1978) A surprising property of electrical spread in the network of rods in the turtle's retina. *Nature* **274**: 562-565.
DeValois, R.L.; Abramov, I.; and Mead, W.R. (1967) Single cell analysis of wavelength discrimination at the lateral geniculate nucleus in the macaque. *J. Neurophysiol.* **30**: 415-433.
DeVries, S.H. (2000) Bipolar cells use kainate and AMPA receptors to filter visual information into separate channels. *Neuron* **28**: 847-856.
DeVries, S.H.; Qi, X.; Smith, R.; Makous, W.; and Sterling, P. (2002) Electrical coupling between mammalian cones. *Curr. Biol.* **12**: 1900-1907.
DeVries, S.H. and Schwartz, E.A. (1999) Kainate receptors mediate synaptic transmission between cones and OFF bipolar cells in a mammalian retina. *Nature* **397**: 157-160.
Dhein, S. (1998) Gap junction channels in the cardiovascular system: pharmacological and physiological modulation. *Trends Pharmacol. Sci.* **19**: 229-241.
Dhein, S. (2004) Pharmacology of gap junctions in the cardiovascular system. *Cardiovasc. Res.* **62**: 287-298.
Dhingra, A.; Jiang, M.; Wang, T.L.; Lyubarsky, A.; Savchenko, A.; Bar-Yehuda, T.; Sterling, P.; Birnbaumer, L.; and Vardi, N. (2002) Light response of retinal ON bipolar cells requires a specific splice variant of Ga(o). *J. Neurosci.* **22**: 4878-4884.
Dhingra, A.; Lyubarsky, A.; Jiang, M.; Pugh, E.N., Jr.; Birnbaumer, L.; Sterling, P.; and Vardi, N. (2000) The light response of ON bipolar neurons requires Ga(o). *J. Neurosci.* **20**: 9053-9058.
Dixon, D.B.; Takahashi, K.-I.; and Copenhagen, D.R. (1993) L-glutamate suppresses HVA calcium current in catfish horizontal cells by raising intracellular proton concentration. *Neuron* **11**: 267-277.
Djamgoz, M.B.; Petruv, R.; Yasui, S.; Furukawa, T.; and Yamada, M. (1998) Modulation of chromatic difference in receptive field size of H1 horizontal cells in carp retina: dopamine- and APB-sensitive mechanisms. *Neurosci. Res.* **30**: 13-24.
Djamgoz, M.B.A. and Wagner, H.-J. (1992) Localization and function of dopamine in the adult vertebrate retina. *Neurochem. Int.* **20**: 139-191.
Dolan, R.P. and Schiller, P.D. (1994) Effect of ON channel blockade with 2-amino-4-phosphonobytyrate (APB) on brightness and contrast perception in monkeys. *Vis. Neurosci.* **11**: 23-32.
Dong, C.J. and McReynolds, J.S. (1989) APB increases apparent coupling between horizontal cells in mudpuppy retina. *Vision Res.* **29**: 541-544.
Dong, C.J. and McReynolds, J.S. (1991) The relationship between light, dopamine release and horizontal cell coupling in the mudpuppy retina. *J. Physiol. (Lond.)* **440**: 291-309.
Dorr, S. and Neumeyer, C. (1997) Simultaneous color contrast in goldfish. A quantitative study. *Vision Res.* **37**: 1581-1593.
Dowling, J.E. (1986) Dopamine: a retinal neuromodulator? *Trends Neurosci.* **9**: 236-240.
Dowling, J.E. (1987) *The retina. An approachable part of the brain*. Cambridge: Belknap Press.
Dowling, J.E. and Ehinger, B. (1978) The interplexiform cell system. I. Synapses of the dopaminergic neurons of the goldfish retina. *Proc. R. Soc. Lond., B, Biol. Sci.* **201**: 7-26.
Dowling, J.E. and Ripps, H. (1971) S-potentials in the skate retina. Intracellular recordings during light and dark adaptation. *J. Gen. Physiol.* **58**: 163-189.
Downing, J.E.G. and Djamgoz, M.B.A. (1989) Quantitative analysis of cone photoreceptor-horizontal cell connectivity patterns in the retina of a cyprinid fish: electron microscopy of functionally identified and HRP-labelled horizontal cells. *J. Comp. Neurol.* **289**: 537-553.
Duvoisin, R.M.; Zhang, C.; and Ramonell, K. (1995) A novel metabotropic glutamate receptor expressed in the retina and olfactory bulb. *J. Neurosci.* **15**: 3075-3083.
Easter, S.S.; Johns, P.A.; and Baumann, L.R. (1977) Growth of the adult goldfish eye. I: Optics. *Vision Res.* **17**: 469-477.

Ebrey, T. and Koutalos, Y. (2001) Vertebrate photoreceptors. *Prog. Retin. Eye Res.* **20**: 49-94.
Eccles, J.C. and McGeer, P.L. (1979) Ionotropic and metabotropic neurotransmission. *Trends Neurosci.* **2** : 39-40.
Elfgang, C.; Eckert, R.; Lichtenberg-Frate, H.; Butterweck, A.; Traub, O.; Klein, R.A.; Hulser, D.F.; and Willecke, K. (1995) Specific permeability and selective formation of gap junction channels in connexin-transfected HeLa cells. *J. Cell Biol.* **129**: 805-817.
Eliasof, S.; Arriza, J.L.; Leighton, B.H.; Amara, S.G.; and Kavanaugh, M.P. (1998a) Localization and function of five glutamate transporters cloned from the salamander retina. *Vision Res.* **38**: 1443-1454.
Eliasof, S.; Arriza, J.L.; Leighton, B.H.; Kavanaugh, M.P.; and Amara, S.G. (1998b) Excitatory amino acid transporters of the salamander retina: identification, localization, and function. *J. Neurosci.* **18**: 698-712.
Ellis, K.J. and Duggleby, R.G. (1978) What happens when data are fitted to the wrong equation? *Biochem. J.* **171**: 513-517.
Euler, T.; Schneider, H.; and Wässle, H. (1996) Glutamate responses of bipolar cells in a slice preparation of the rat retina. *J. Neurosci.* **16**: 2934-2944.
Fahrenfort, I.; Habets, R.L.; Spekreijse, H.; and Kamermans, M. (1999) Intrinsic cone adaptation modulates feedback efficiency from horizontal cells to cones. *J. Gen. Physiol.* **114**: 511-524.
Fain, G.L. (1975) Quantum sensitivity of rods in the toad retina. *Science* **187**: 838-841.
Fain, G.L.; Gold, G.H.; and Dowling, J.E. (1976) Receptor coupling in the toad retina. *Cold Spring Harb. Symp. Quant. Biol.* **40**: 547-561.
Fairman, W.A.; Vandenberg, R.J.; Arriza, J.L.; Kavanaugh, M.P.; and Amara, S.G. (1995) An excitatory amino-acid transporter with properties of a ligand-gated chloride channel. *Nature* **375**: 599-603.
Falk, G. (1988) Signal transmission from rods to bipolar and horizontal cells: a synthesis. *Prog. Retinal Res.* **8**: 255-279.
Famiglietti, E.V.; Kaneko, A.; and Tachibana, M. (1977) Neuronal Architecture of ON and OFF pathways to ganglion cells in carp retina. *Science* **198**: 1267-1269.
Famiglietti, E.V. and Kolb, H. (1976) Structural basis for ON-and OFF-center responses in retinal ganglion cells. *Science* **194**: 193-195.
Fan, S.F. and Yazulla, S. (1999a) Modulation of voltage-dependent $K^+$ currents ($I_{KV}$) in retinal bipolar cells by ascorbate is mediated by dopamine D1 receptors. *Vis. Neurosci.* **16**: 923-931.
Fan, S.F. and Yazulla, S. (1999b) Suppression of voltage-dependent $K^+$ currents in retinal bipolar cells by ascorbate. *Vis. Neurosci.* **16**: 141-148.
Fan, S.F. and Yazulla, S. (2001) Dopamine depletion with 6-OHDA enhances dopamine D1-receptor modulation of potassium currents in retinal bipolar cells. *Vis. Neurosci.* **18**: 327-337.
Field, G.D. and Rieke, F. (2002) Nonlinear signal transfer from mouse rods to bipolar cells and implications for visual sensitivity. *Neuron* **34**: 773-785.
Field, G.D.; Sampath, A.P.; and Rieke, F. (2005) Retinal processing near absolute threshold: from behavior to mechanism. *Annu. Rev. Physiol.* **67**: 491-514.
Fischer, B. (1973) Overlap of receptive field centers and representation of the visual field in the cat's optic tract. *Vision Res.* **13**: 2113-2120.
Francis, D.; Stergiopoulos, K.; Ek-Vitorin, J.F.; Cao, F.L.; Taffet, S.M.; and Delmar, M. (1999) Connexin diversity and gap junction regulation by pHi. *Dev. Genet.* **24**: 123-136.
Fratzer, C.; Dorr, S.; and Neumeyer, C. (1994) Wavelength discrimination of the goldfish in the ultraviolet spectral range. *Vision Res.* **34**: 1515-1520.
Fuortes, M.G.F. and Simon, E.J. (1974) Interactions leading to horizontal cell responses in the turtle retina. *J. Physiol. (Lond.)* **240**: 177-198.
Fyk-Kolodziej, B.; Qin, P.; and Pourcho, R.G. (2003) Identification of a cone bipolar cell in cat retina which has input from both rod and cone photoreceptors. *J. Comp. Neurol.* **464**: 104-113.
Gafka, A.C.; Vogel, K.S.; and Linn, C.L. (1999) Evidence of metabotropic glutamate receptor subtypes found on catfish horizontal and bipolar retinal neurons. *Neuroscience* **90**: 1403-1414.
Gegenfurtner, K. (2001) Color in the cortex revisited. *Nat. Neurosci.* **4**: 339-340.
Gegenfurtner, K.R. and Kiper, D.C. (2003) Color vision. *Annu. Rev. Neurosci.* **26**: 181-206.
Getting, P.A. (1974) Modification of neuron properties by electrotonic synapses. I. Input resistance, time constant, and integration. *J. Neurophysiol.* **37**: 846-857.
Goldberg, G.S.; Moreno, A.P.; Bechberger, J.F.; Hearn, S.S.; Shivers, R.R.; MacPhee, D.J.; Zhang, Y.C.; and Naus, C.C. (1996) Evidence that disruption of connexon particle arrangements in gap junction plaques is associated with inhibition of gap junctional communication by a glycyrrhetinic acid derivative. *Exp. Cell Res.* **222**: 48-53.
Goldberg, G.S.; Valiunas, V.; and Brink, P.R. (2004) Selective permeability of gap junction channels. *Biochim. Biophys. Acta* **1662**: 96-101.
Grabowski, S.K.; Pinto, L.H.; and Pak, W.L. (1972) Adaptation in retinal rods of axolotl: intracellular recordings. *Science* **176**: 1240-1243.
Grant, G.B. and Dowling, J.E. (1995) A glutamate-activated chloride current in cone-driven ON bipolar cells of the white perch retina. *J. Neurosci.* **15**: 3852-3862.

Grant, G.B. and Dowling, J.E. (1996) On bipolar cell responses in the teleost retina are generated by two distinct mechanisms. *J. Neurophysiol.* **76**: 3842-3849.
Greferath, U.; Grünert, U.; and Wässle, H. (1990) Rod bipolar cells in the mammalian retina show protein kinase C-like immunoreactivity. *J. Comp. Neurol.* **301**: 433-442.
Grünert, U.; Martin, P.R.; and Wässle, H. (1994) Immunocytochemical analysis of bipolar cells in the macaque monkey retina. *J. Comp. Neurol.* **348**: 607-627.
Hack, I.; Peichl, L.; and Brandstätter, J.H. (1999) An alternative pathway for rod signals in the rodent retina: rod photoreceptors, cone bipolar cells, and the localization of glutamate receptors. *Proc. Natl. Acad. Sci. U.S.A.* **96**: 14130-14135.
Hare, W.A. and Owen, W.G. (1990) Spatial organization of the bipolar cell's receptive field in the retina of the tiger salamander. *J. Physiol. (Lond.)* **421**: 233-245.
Harosi, F.I. (1976) Spectral relations of cone pigments in goldfish. *J. Gen. Physiol.* **68**: 65-80.
Harosi, F.I. and MacNichol, E.F. (1974) Visual Pigments of goldfish cones. Spectral properties and dichroism. *J. Gen. Physiol.* **63**: 279-304.
Hartline, D.K. and Castelfranco, A.M. (2003) Simulations of voltage clamping poorly space-clamped voltage-dependent conductances in a uniform cylindrical neurite. *J. Comput. Neurosci.* **14**: 253-269.
Hartline, H.K. (1938) The response of single optic nerve fibers of the vertebrate eye to illumination of the retina. *Am. J. Physiol.* **121**: 400-415.
Hausser, M. and Roth, A. (1997) Estimating the time course of the excitatory synaptic conductance in neocortical pyramidal cells using a novel voltage jump method. *J. Neurosci.* **17**: 7606-7625.
Haverkamp, S.; Grünert, U.; and Wässle, H. (2001) The synaptic architecture of AMPA receptors at the cone pedicle of the primate retina. *J. Neurosci.* **21**: 2488-2500.
Haverkamp, S.; Mockel, W.; and Ammermüller, J. (1999) Different types of synapses with different spectral types of cones underlie color opponency in a bipolar cell of the turtle retina. *Vis. Neurosci.* **16**: 801-809.
Hawryshyn, C.W. (1991) Light-adaptation properties of the ultraviolet-sensitive cone mechanism in comparison to the other receptor mechanisms of goldfish. *Vis. Neurosci.* **6**: 293-301.
Hawryshyn, C.W. and Beauchamp, R.D. (1985) Ultraviolet photosensitivity in goldfish: an independent U.V. retinal mechanism. *Vision Res.* **25**: 11-20.
Hedden, W.L. and Dowling, J.E. (1978) The interplexiform cell system. II. Effects of dopamine on goldfish retinal neurones. *Proc.R.Soc.Lond., B, Biol.Sci.* **201**: 27-55.
Heidelberger, R. and Matthews, G. (1992) Calcium influx and calcium current in single synaptic terminals of goldfish retinal bipolar neurons. *J. Physiol. (Lond.)* **447**: 235-256.
Hensley, S.H.; Yang, X.-L.; and Wu, S.M. (1993) Identification of glutamate receptor subtypes mediating inputs to bipolar cells and ganglion cells in the tiger salamander retina. *J. Neurophysiol.* **69**: 2099-2107.
Hering, E. (1964) *Outlines of a theory of the light sense*. Cambridge: Harvard University Press.
Heuss, C. and Gerber, U. (2000) G-protein-independent signaling by G-protein-coupled receptors. *Trends Neurosci.* **23**: 469-475.
Higgs, M.H.; Romano, C.; and Lukasiewicz, P.D. (2002) Presynaptic effects of group III metabotropic glutamate receptors on excitatory synaptic transmission in the retina. *Neuroscience* **115**: 163-172.
Hille, B. (1992) *Ionic channels of excitable membranes*. Sunderland: Sinauer Associates, Inc.
Hines, M.L. and Carnevale, N.T. (1997) The NEURON simulation environment. *Neural Comput.* **9**: 1179-1209.
Hines, M.L. and Carnevale, N.T. (2000) Expanding NEURON's repertoire of mechanisms with NMODL. *Neural Comput.* **12**: 995-1007.
Hirasawa, H.; Shiells, R.; and Yamada, M. (2002) A metabotropic glutamate receptor regulates transmitter release from cone presynaptic terminals in carp retinal slices. *J. Gen. Physiol.* **119**: 55-68.
Hitchcock, P.F. (1989) Morphology and distribution of synapses onto a type of large field ganglion cell in the retina of the goldfish. *J. Comp. Neurol.* **283**: 177-188.
Hitchcock, P.F. and Easter, S.S. (1986) Retinal ganglion cells in goldfish: a qualitative classification into four morphological types, and a quantitative study of the development of one of them. *J. Neurosci.* **6**: 1037-1050.
Hopkins, J.M. and Boycott, B.B. (1997) The cone synapses of cone bipolar cells of primate retina. *J. Neurocytol.* **26**: 313-325.
Hosoi, N.; Arai, I.; and Tachibana, M. (2005) Group III metabotropic glutamate receptors and exocytosed protons inhibit L-type calcium currents in cones but not in rods. *J. Neurosci.* **25**: 4062-4072.
Houamed, K.M.; Kuijper, J.L.; Gilbert, T.L.; Haldeman, B.A.; O'Hara, P.J.; Mulvihill, E.R.; Almers, W.; and Hagen, F.S. (1991) Cloning, expression, and gene structure of a G protein-coupled glutamate receptor from rat brain. *Science* **252**: 1318-1321.
Hurvich, L.M. (1985) Opponent-colours theory. In: Ottoson, D. and Zeki, S. (eds.) *Central and peripheral mechanisms of color vision.* Wenner-Gren Center International Symposium Series vol. 43. Houndsmill: McMillan Press.
Hurvich, L.M. and Jameson, D. (1957) An opponent-process theory of color vision. *Psychol. Rev.* **64**: 384-404.
Ishida, A.T.; Stell, W.K.; and Lightfoot, D.O. (1980) Rod and cone inputs to bipolar cells in goldfish retina. *J. Comp. Neurol.* **191**: 315-335.

Itzhaki, A. and Perlman, I. (1987) Light adaptation of red cones and L1-horizontal cells in the turtle retina: effect of the background spatial pattern. *Vision Res.* **27**: 685-696.
Johns, P.A. and Easter, S.S. (1977) Growth of the adult goldfish eye. II. Increase in retinal cell number. *J. Comp. Neurol.* **176**: 331-342.
Kamermans, M.; Fahrenfort, I.; Schultz, K.; Janssen-Bienhold, U.; Sjoerdsma, T.; and Weiler, R. (2001) Hemichannel-mediated inhibition in the outer retina. *Science* **292**: 1178-1180.
Kamermans, M.; Haak, J.; Habraken, J.B.A.; and Spekreijse, H. (1996) The size of the horizontal cell receptive fields adapts to the stimulus in the light adapted goldfish retina. *Vision Res.* **36**: 4105-4120.
Kamermans, M.; Kraaij, D.A.; and Spekreijse, H. (1998) The cone/horizontal cell network: a possible site for color constancy. *Vis. Neurosci.* **15**: 787-797.
Kamermans, M. and Spekreijse, H. (1995) Spectral behavior of cone-driven horizontal cells in teleost retina. *Prog. Ret. Eye Res.* **14**: 313-360.
Kamphuis, W.; Klooster, J.; and Dijk, F. (2003) Expression of AMPA-type glutamate receptor subunit (GluR2) in ON-bipolar neurons in the rat retina. *J. Comp. Neurol.* **455**: 172-186.
Kaneko, A. (1970) Physiological and morphological identification of horizontal, bipolar and amacrine cells in goldfish retina. *J. Physiol. (Lond.)* **207**: 623-633.
Kaneko, A. (1971a) Electrical connexions between horizontal cells in the dogfish retina. *J. Physiol. (Lond.)* **213**: 95-105.
Kaneko, A. (1971b) Physiological studies of single retinal cells and their morphological identification. *Vision Res. Suppl.* **3**: 17-26.
Kaneko, A. (1973) Receptive field organization of bipolar and amacrine cells in the goldfish retina. *J. Physiol. (Lond.)* **235**: 133-153.
Kaneko, A. (1987) The functional role of retinal horizontal cells. *Jpn. J. Physiol.* **37**: 341-358.
Kaneko, A. and Hashimoto, H. (1969) Electrophysiological study of single neurons in the inner nuclear layer of the carp retina. *Vision Res.* **9**: 37-55.
Kaneko, A. and Saito, T. (1983) Ionic mechanisms underlying the response of OFF-center bipolar cells in the carp retina. II. Study on responses evoked by transretinal current stimulation. *J. Gen. Physiol.* **81**: 603-612.
Kaneko, A. and Shimazaki, H. (1976) Synaptic transmission from photoreceptors to bipolar and horizontal cells in the carp retina. *Cold Spring Harb. Symp. Quant. Biol.* **40**: 537-546.
Kaneko, A.; Suzuki, S.; Pinto, L.H.; and Tachibana, M. (1991) Membrane currents and pharmacology of retinal bipolar cells: a comparative study on goldfish and mouse. *Comp. Biochem. Physiol.* **98C**: 115-127.
Kaneko, A. and Tachibana, M. (1978) Convergence of rod and cone signals to single bipolar cells in the carp retina. *Sens. Processes* **2**: 383-387.
Kaneko, A. and Tachibana, M. (1981) Retinal bipolar cells with double colour-opponent receptive fields. *Nature* **293**: 220-222.
Kaneko, A. and Tachibana, M. (1983) Double color-opponent receptive fields of carp bipolar cells. *Vision Res.* **23**: 381-388.
Kaneko, A. and Tachibana, M. (1985) A voltage-clamp analysis of membrane currents in solitary bipolar cells dissociated from *Carassius auratus*. *J. Physiol. (Lond.)* **358**: 131-152.
Kaneko, A. and Tachibana, M. (1987) GABA mediates the negative feedback from amacrine to bipolar cells. *Neurosci. Res. Suppl.* **6**: S239-S252.
Kato, A.; Ozawa, F.; Saitoh, Y.; Fukazawa, Y.; Sugiyama, H.; and Inokuchi, K. (1998) Novel members of the Vesl/Homer family of PDZ proteins that bind metabotropic glutamate receptors. *J. Biol. Chem.* **273**: 23969-23975.
Kier, C.K.; Buchsbaum, G.; and Sterling, P. (1995) How retinal microcircuits scale for ganglion cells of different size. *J. Neurosci.* **15**: 7673-7683.
Kingdom, F.A. and Mullen, K.T. (1995) Separating colour and luminance information in the visual system. *Spat. Vis.* **9**: 191-219.
Klooster, J.; Nunes, C.B.; Yazulla, S.; and Kamermans, M. (2004) Postsynaptic localization of gamma-aminobutyric acid transporters and receptors in the outer plexiform layer of the goldfish retina: an ultrastructural study. *J. Comp. Neurol.* **474**: 58-74.
Klooster, J.; Studholme, K.M.; and Yazulla, S. (2001a) Localization of the AMPA glutamate receptor subunit 2 (GluR2) in cone horizontal cell dendrites of the fish retina. *Invest. Ophthal. Vis. Sci. Suppl.* **42**: S727.
Klooster, J.; Studholme, K.M.; and Yazulla, S. (2001b) Localization of the AMPA subunit GluR2 in the outer plexiform layer of goldfish retina. *J. Comp. Neurol.* **441**: 155-167.
Klumpp, D.J.; Song, E.J.; Ito, S.; Sheng, M.H.; Jan, L.Y.; and Pinto, L.H. (1995) The Shaker-like potassium channels of the mouse rod bipolar cell and their contributions to the membrane current. *J. Neurosci.* **15**: 5004-5013.
Kock, J.H. (1982) Neuronal addition and retinal expansion during growth of the crucian carp eye. *J. Comp. Neurol.* **209**: 264-274.
Kock, J.H. and Reuter, T. (1978) Retinal ganglion cells in the crucian carp (*Carassius carassius*). II. Overlap, shape, and tangential orientation of dendritic trees. *J. Comp. Neurol.* **179**: 549-568.
Kolb, H. and Famiglietti, E.V. (1976) Rod and cone pathways in the retina of the cat. *Invest. Ophthal.* **15**: 935-945.

Kolb, H. and Lipetz, L.E. (1991) The anatomical basis for colour vision in the vertebrate retina. In: Gouras, P. (ed.) *The perception of colour*. London: Macmillan Press.

Kolb, H.; Zhang, L.; and Dekorver, L. (1993) Differential staining of neurons in the human retina with antibodies to protein kinase C isozymes. *Vis. Neurosci.* **10**: 341-351.

Koulen, P.; Kuhn, R.; Wässle, H.; and Brandstätter, J.H. (1997) Group I metabotropic glutamate receptors mGluR1a and mGluR5a: localization in both synaptic layers of the rat retina. *J. Neurosci.* **17**: 2200-2211.

Koulen, P.; Kuhn, R.; Wässle, H.; and Brandstätter, J.H. (1999) Modulation of the intracellular calcium concentration in photoreceptor terminals by a presynaptic metabotropic glutamate receptor. *Proc. Natl. Acad. Sci. U.S.A.* **96**: 9909-9914.

Koulen, P.; Malitschek, B.; Kuhn, R.; Wässle, H.; and Brandstätter, J.H. (1996) Group II and group III metabotropic glutamate receptors in the rat retina: distributions and developmental expression patterns. *Eur. J. Neurosci.* **8**: 2177-2187.

Kraaij, D.A.; Spekreijse, H.; and Kamermans, M. (2000) The nature of surround induced depolarizing responses in goldfish cones. *J. Gen. Physiol.* **115**: 1-14.

Krizaj, D.; Owen, W.G.; and Witkovsky, P. (1998) Dopamine D2 receptor-mediated modulation of rod-cone coupling in the *Xenopus* retina. *J. Comp. Neurol.* **398**: 529-538.

Kujiraoka, T. and Saito, T. (1986) Electrical coupling between bipolar cells in carp retina. *Proc. Natl. Acad. Sci. U.S.A.* **83**: 4063-4066.

Kwak, B.R.; Hermans, M.M.; De Jonge, H.R.; Lohmann, S.M.; Jongsma, H.J.; and Chanson, M. (1995) Differential regulation of distinct types of gap junction channels by similar phosphorylating conditions. *Mol. Biol. Cell* **6**: 1707-1719.

Ladman, A.J. (1958) The fine structure of the rod-bipolar cell synapse in the retina of the albino rat. *J. Biophys. Biochem. Cytol.* **4**: 459-466.

Lamb, T.D. and Simon, E.J. (1976) The relation between intercellular coupling and electrical noise in turtle photoreceptors. *J. Physiol. (Lond.)* **263**: 257-286.

Land, E.H.; Hubel, D.H.; Livingstone, M.S.; Perry, S.H.; and Burns, M.M. (1983) Colour-generating interactions across the corpus callosum. *Nature* **303**: 616-618.

Lasater, E.M. and Dowling, J.E. (1982) Carp horizontal cells in culture respond selectively to L- glutamate and its agonists. *Proc. Natl. Acad. Sci. U.S.A.* **79**: 936-940.

Lasater, E.M. and Dowling, J.E. (1985) Dopamine decreases conductance of the electrical junctions between cultured retinal horizontal cells. *Proc. Natl. Acad. Sci. U.S.A.* **82**: 3025-3029.

Lasater, E.M.; Dowling, J.E.; and Ripps, H. (1984) Pharmacological properties of isolated horizontal and bipolar cells from the skate retina. *J. Neurosci.* **4**: 1966-1975.

Laughlin, S.B. (2001) Energy as a constraint on the coding and processing of sensory information. *Curr. Opin. Neurobiol.* **11**: 475-480.

Laughlin, S.B. (2002) Retinal function: coupling cones clarifies vision. *Curr. Biol.* **12**: R833-R834.

Laurie, D.J.; Schoeffter, P.; Wiederhold, K.H.; and Sommer, B. (1997) Cloning, distribution and functional expression of the human mGlu6 metabotropic glutamate receptor. *Neuropharmacology* **36**: 145-152.

Li, W.; Keung, J.W.; and Massey, S.C. (2004) Direct synaptic connections between rods and OFF cone bipolar cells in the rabbit retina. *J. Comp. Neurol.* **474**: 1-12.

Linn, C.L. and Gafka, A.C. (1999) Activation of metabotropic glutamate receptors modulates the voltage-gated sustained calcium current in a teleost horizontal cell. *J. Neurophysiol.* **81**: 425-434.

Luo, F.J. and Liang, P.J. (2003) Metabotropic glutamate receptor-mediated hetero-synaptic interaction of red- and green-cone inputs to LHC of carp retina. *Brain Res. Bull.* **60**: 67-71.

MacNichol, E.F. and Svaetichin, G. (1958) Electric responses from the isolated retinas of fishes. *Am. J. Ophthalmol.* **46**: 26-46.

Macy, A. and Easter, S.S. (1981) Growth-related changes in the size of receptive field centers of retinal ganglion cells in goldfish. *Vision Res.* **21**: 1497-1504.

Mangel, S.C. and Dowling, J.E. (1985) Responsiveness and receptive field size of carp horizontal cells are reduced by prolonged darkness and dopamine. *Science* **229**: 1107-1109.

Mao, B.Q.; MacLeish, P.R.; and Victor, J.D. (1998) The intrinsic dynamics of retinal bipolar cells isolated from tiger salamander. *Vis. Neurosci.* **15**: 425-438.

Mao, B.Q.; MacLeish, P.R.; and Victor, J.D. (2002) Relation between potassium-channel kinetics and the intrinsic dynamics in isolated retinal bipolar cells. *J. Comput. Neurosci.* **12**: 147-163.

Maple, B.R.; Gao, F.; and Wu, S.M. (1999) Glutamate receptors differ in rod- and cone-dominated OFF-center bipolar cells. *NeuroReport* **10**: 3605-3610.

Marc, R.E.; Liu, W.-L.S.; and Muller, J.F. (1988) Gap junctions in the inner plexiform layer of the goldfish retina. *Vision Res.* **28**: 9-24.

Marchiafava, P.L. (1978) Horizontal cells influence membrane potential of bipolar cells in the retina of the turtle. *Nature* **275**: 141-142.

Marchiafava, P.L. and Pasino, E. (1973) The spatial dependent characteristics of the fish S-potential evoked by brief flashes. *Vision Res.* **13**: 1355-1365.
Mariani, A.P. (1983) Giant bistratified bipolar cells in monkey retina. *Anat. Rec.* **206**: 215-220.
Mastronarde, D.N. (1983) Interactions between ganglion cells in cat retina. *J. Neurophysiol.* **49**: 350-364.
Masu, M.; Iwakabe, H.; Tagawa, Y.; Miyoshi, T.; Yamashita, M.; Fukuda, Y.; Sasaki, H.; Hiroi, K.; Nakamura, Y.; and Shigemoto, R. (1995) Specific deficit of the ON response in visual transmission by targeted disruption of the mGluR6 gene. *Cell* **80**: 757-765.
Masu, M.; Tanabe, Y.; Tsuchida, K.; Shigemoto, R.; and Nakanishi, S. (1991) Sequence and expression of a metabotropic glutamate receptor. *Nature* **349**: 760-765.
Meister, M. (1996) Multineuronal codes in retinal signaling. *Proc. Natl. Acad. Sci. U.S.A.* **93**: 609-614.
Mennerick, S.; Zenisek, D.; and Matthews, G. (1997) Static and dynamic membrane properties of large-terminal bipolar cells from goldfish retina: experimental test of a compartment model. *J. Neurophysiol.* **78**: 51-62.
Migdale, K.; Herr, S.; Klug, K.; Ahmad, K.; Linberg, K.; Sterling, P.; and Schein, S. (2003) Two ribbon synaptic units in rod photoreceptors of macaque, human, and cat. *J. Comp. Neurol.* **455**: 100-112.
Miller, J.L.; Picones, A.; and Korenbrot, J.I. (1994) Differences in transduction between rod and cone photoreceptors: an exploration of the role of calcium homeostasis. *Curr. Opin. Neurobiol.* **4**: 488-495.
Mitarai, G.; Goto, T.; and Takagi, S. (1978) Receptive field arrangement of color opponent bipolar and amacrine cells in the carp retina. *Sens. Processes* **2**: 375-382.
Mitropoulou, G. and Bruzzone, R. (2003) Modulation of perch connexin35 hemi-channels by cyclic AMP requires a protein kinase A phosphorylation site. *J. Neurosci. Res.* **72**: 147-157.
Miyachi, E.I. and Murakami, M. (1989) Decoupling of horizontal cells in carp and turtle retinae by intracellular injection of cyclic AMP. *J. Physiol. (Lond.)* **419**: 213-224.
Miyachi, E.I. and Murakami, M. (1991) Synaptic inputs to turtle horizontal cells analyzed after blocking of gap junctions by intracellular injection of cyclic nucleotides. *Vision Res.* **31**: 631-635.
Mooij, J.E.M. and Van den Berg, T.J.T.P. (1983) The spectral shape of A2 visual pigments. *Vision Res.* **23**: 701-705.
Murakami, M.; Ohtsu, K.; and Ohtsuka, T. (1972) Effects of chemicals on receptors and horizontal cells in the retina. *J. Physiol. (Lond.)* **227**: 899-913.
Nadeau, H. and Lester, H.A. (2000) Two-compartment model for whole-cell data analysis and transient compensation. *J. Neurosci. Methods* **99**: 25-35.
Naka, K.I. (1972) The horizontal cells. *Vision Res.* **12**: 573-588.
Naka, K.I. and Nye, P.W. (1971) Role of horizontal cells in organization of the catfish retinal receptive field. *J. Neurophysiol.* **34**: 785-801.
Naka, K.I. and Witkovsky, P. (1972) Dogfish ganglion cell discharge resulting from extrinsic polarization of the horizontal cells. *J. Physiol. (Lond.)* **223**: 449-460.
Nakajima, Y.; Iwakabe, H.; Akazawa, C.; Nawa, H.; Shigemoto, R.; Mizuno, N.; and Nakanishi, S. (1993) Molecular characterization of a novel retinal metabotropic glutamate receptor mGluR6 with a high agonist selectivity for L-2-amino-4-phosphonobutyrate. *J. Biol. Chem.* **268**: 11868-11873.
Nawy, S. (1999) The metabotropic receptor mGluR6 may signal through G(o), but not phosphodiesterase, in retinal bipolar cells. *J. Neurosci.* **19**: 2938-2944.
Nawy, S. and Copenhagen, D.R. (1987) Multiple classes of glutamate receptor on depolarizing bipolar cells in retina. *Nature* **325**: 56-58.
Nawy, S. and Copenhagen, D.R. (1990) Intracellular cesium separates two glutamate conductances in retinal bipolar cells of goldfish. *Vision Res.* **30**: 967-972.
Nawy, S.; Sie, A.; and Copenhagen, D.R. (1989) The glutamate analog 2-amino-4-phosphonobutyrate antagonizes synaptic transmission from cones to horizontal cells in the goldfish retina. *Proc. Natl. Acad. Sci. U.S.A.* **86**: 1726-1730.
Negishi, K.; Kato, S.; and Teranishi, T. (1988) Dopamine cells and rod bipolar cells contain protein kinase C-like immunoreactivity in some vertebrate retinas. *Neurosci. Lett.* **94**: 247-252.
Neumeyer, C. (1984) On spectral sensitivity in the goldfish. Evidence for neural interactions between different 'cone mechanisms'. *Vision Res.* **24**: 1223-1231.
Neumeyer, C. (1985) An ultraviolet Receptor as a fourth receptor type in goldfish color vision. *Naturwissenschaften* **72**: 162-163.
Neumeyer, C. (1986) Wavelength discrimination in the goldfish. *J. Comp. Physiol. A* **158**: 203-213.
Neumeyer, C. (2003) Wavelength dependence of visual acuity in goldfish. *J. Comp. Physiol. A* **189**: 811-821.
Neumeyer, C. and Arnold, K. (1989) Tetrachromatic color vision in the goldfish becomes trichromatic under white adaptation light of moderate intensity. *Vision Res.* **29**: 1719-1727.
Ng, B. and Barry, P.H. (1995) The measurement of ionic conductivities and mobilities of certain less common organic ions needed for junction potential corrections in electrophysiology. *J. Neurosci. Methods* **56**: 37-41.
Nicholson, B.J.; Weber, P.A.; Cao, F.; Chang, H.; Lampe, P.; and Goldberg, G. (2000) The molecular basis of selective permeability of connexins is complex and includes both size and charge. *Braz. J. Med. Biol. Res.* **33**: 369-378.

Nomura, A.; Shigemoto, R.; Nakamura, Y.; Okamoto, N.; Mizuno, N.; and Nakanishi, S. (1994) Developmentally regulated postsynaptic localization of a metabotropic glutamate receptor in rat rod bipolar cells. *Cell* **77**: 361-369.

Northmore, D.P. (1977) Spatial summation and light adaptation in the goldfish visual system. *Nature* **268**: 450-451.

Norton, A.L.; Spekreijse, H.; Wolbarsht, M.L.; and Wagner, H.G. (1968) Receptive field organization of the S-potential. *Science* **160**: 1021-1022.

O'Brien, J.; Nguyen, H.B.; and Mills, S.L. (2004) Cone photoreceptors in bass retina use two connexins to mediate electrical coupling. *J. Neurosci.* **24**: 5632-5642.

Okada, T.; Horoguchi, H.; and Tachibana, M. (1995) $Ca^{2+}$-dependent $Cl^-$ current at the presynaptic terminals of goldfish retinal bipolar cells. *Neurosci. Res.* **23**: 297-303.

Okamoto, N.; Hori, S.; Akazawa, C.; Hayashi, Y.; Shigemoto, R.; Mizuno, N.; and Nakanishi, S. (1994) Molecular characterization of a new metabotropic glutamate receptor mGluR7 coupled to inhibitory cyclic AMP signal transduction. *J. Biol. Chem.* **269**: 1231-1236.

Osborne, N.N.; Broyden, N.J.; Barnett, N.L.; and Morris, N.J. (1991) Protein kinase C (a and b) immunoreactivity in rabbit and rat retina: effect of phorbol esters and transmitter agonists on immunoreactivity and the translocation of the enzyme from cytosolic to membrane compartments. *J. Neurochem.* **57**: 594-604.

Palacios, A.G.; Varela, F.J.; Srivastava, R.; and Goldsmith, T.H. (1998) Spectral sensitivity of cones in the goldfish, *Carassius auratus*. *Vision Res.* **38**: 2135-2146.

Palmer, M.J.; Hull, C.; Vigh, J.; and Von Gersdorff, H. (2003a) Synaptic cleft acidification and modulation of short-term depression by exocytosed protons in retinal bipolar cells. *J. Neurosci.* **23**: 11332-11341.

Palmer, M.J.; Taschenberger, H.; Hull, C.; Tremere, L.; and Von Gersdorff, H. (2003b) Synaptic activation of presynaptic glutamate transporter currents in nerve terminals. *J. Neurosci.* **23**: 4831-4841.

Peichl, L. and Wässle, H. (1979) Size, scatter and coverage of ganglion cell receptive field centers in the cat retina. *J. Physiol. (Lond.)* **291**: 117-141.

Peng, Y.-W.; Blackstone, C.D.; Huganir, R.L.; and Yau, K.W. (1995) Distribution of glutamate receptor subtypes in the vertebrate retina. *Neuroscience* **66**: 483-497.

Peracchia, C. (2004) Chemical gating of gap junction channels; roles of calcium, pH and calmodulin. *Biochim. Biophys. Acta* **1662**: 61-80.

Pettigrew, J.D.; Sanderson, K.J.; and Levick, W.R. (1986) *Visual neuroscience*. Cambridge: Cambridge University Press.

Piccolino, M.; Neyton, J.; and Gerschenfeld, H.M. (1984) Decrease of GAP junction permeabiltiy induced by dopamine and cyclic adenosine 3':5'-monophosphate in horizontal cells of turtle retina. *J. Neurosci.* **4**: 2477-2488.

Picones, A. and Korenbrot, J.I. (1995) Permeability and interaction of $Ca^{2+}$ with cGMP-gated channels differ in retinal rod and cone photoreceptors. *Biophys. J.* **69**: 120-127.

Pinto, L.H. and Klumpp, D.J. (1998) Localization of potassium channels in the retina. *Prog. Retin. Eye Res.* **17**: 207-230.

Pottek, M.; Hoppenstedt, W.; Janssen-Bienhold, U.; Schultz, K.; Perlman, I.; and Weiler, R. (2003) Contribution of connexin26 to electrical feedback inhibition in the turtle retina. *J. Comp. Neurol.* **466**: 468-477.

Pow, D.V. and Barnett, N.L. (2000) Developmental expression of excitatory amino acid transporter 5: a photoreceptor and bipolar cell glutamate transporter in rat retina. *Neurosci. Lett.* **280**: 21-24.

Pow, D.V.; Barnett, N.L.; and Penfold, P. (2000) Are neuronal transporters relevant in retinal glutamate homeostasis? *Neurochem. Int.* **37**: 191-198.

Powers, M.K.; Bassi, C.J.; Rone, L.A.; and Raymond, P.A. (1988) Visual detection by the rod system in goldfish of different sizes. *Vision Res.* **28**: 211-221.

Poznanski, R.R. (1999) Electrophysiology of a leaky cable model for coupled neurones. *J. Austral. Math. Soc. B* **40**: 59-71.

Pugh, E.N. and Lamb, T.D. (1990) Cyclic GMP and calcium: the internal messengers of excitation and adaptation in vertebrate photoreceptors. *Vision Res.* **30**: 1923-1948.

Purkinje, J.E. (1825) *Neue Beiträge zur Kenntniss des Sehens in subjektiver Hinsicht*. Berlin: G. Beimer.

Rauen, T. and Kanner, B.I. (1994) Localization of the glutamate transporter GLT-1 in rat and macaque monkey retinae. *Neurosci. Lett.* **169**: 137-140.

Rauen, T.; Rothstein, J.D.; and Wässle, H. (1996) Differential expression of three glutamate transporter subtypes in the rat. *Cell Tissue Res.* **286**: 325-336.

Raviola, E. and Gilula, N.B. (1973) Gap junctions between photoreceptor cells in the vertebrate retina. *Proc. Natl. Acad. Sci. U.S.A.* **70**: 1677-1681.

Raynauld, J.P. (1972) Goldfish retina: sign of the rod input in opponent color ganglion cells. *Science* **177**: 84-85.

Rebrik, T.I. and Korenbrot, J.I. (1998) In intact cone photoreceptors, a $Ca^{2+}$-dependent, diffusible factor modulates the cGMP-gated ion channels differently than in rods. *J. Gen. Physiol.* **112**: 537-548.

Rebrik, T.I. and Korenbrot, J.I. (2004) In intact mammalian photoreceptors, $Ca^{2+}$-dependent modulation of cGMP-gated ion channels is detectable in cones but not in rods. *J. Gen. Physiol* **123**: 63-75.

Ribelayga, C.; Wang, Y.; and Mangel, S.C. (2002) Dopamine mediates circadian clock regulation of rod and cone input to fish retinal horizontal cells. *J. Physiol. (Lond.)* **544**: 801-816.

Rockhill, R.L.; Daly, F.J.; MacNeil, M.A.; Brown, S.P.; and Masland, R.H. (2002) The diversity of ganglion cells in a mammalian retina. *J. Neurosci.* **22**: 3831-3843.
Rodbell, M. (1980) The role of hormone receptors and GTP-regulatory proteins in membrane transduction. *Nature* **284**: 17-22.
Rodieck, R.W. (1998) *The first steps in seeing*. Sunderland: Sinauer Associates.
Rorig, B.; Klausa, G.; and Sutor, B. (1996) Intracellular acidification reduced gap junction coupling between immature rat neocortical pyramidal neurones. *J. Physiol. (Lond.)* **490 ( Pt 1)**: 31-49.
Rossum, M.C.W. and Smith, R.G. (1998) Noise removal at the rod synapse of mammalian retina. *Vis. Neurosci.* **15**: 809-821.
Rouach, N.; Segal, M.; Koulakoff, A.; Giaume, C.; and Avignone, E. (2003) Carbenoxolone blockade of neuronal network activity in culture is not mediated by an action on gap junctions. *J. Physiol. (Lond.)* **553**: 729-745.
Saito, T. (1987) Physiological and morphological differences between ON- and OFF- center bipolar cells in the vertebrate retina. *Vision Res.* **27**: 135-142.
Saito, T. and Kaneko, A. (1983) Ionic mechanisms underlying the responses of OFF-center bipolar cells in the carp retina. I. Studies on responses evoked by light. *J. Gen. Physiol.* **81**: 589-601.
Saito, T.; Kondo, H.; and Toyoda, J.I. (1978) Rod and cone signals in the ON-center bipolar cell: their different ionic mechanisms. *Vision Res.* **18**: 591-595.
Saito, T.; Kondo, H.; and Toyoda, J.I. (1979) Ionic mechanisms of two types of ON-center bipolar cells in the carp retina. I. The responses to central illumination. *J. Gen. Physiol.* **73** : 73-90.
Saito, T.; Kondo, H.; and Toyoda, J.I. (1981) Ionic mechanisms of two types of ON-center bipolar cells in the carp retina. II. The responses to annular illumination. *J. Gen. Physiol.* **78**: 569-589.
Saito, T. and Kujiraoka, T. (1982) Physiological and morphological identification of two types of ON-center bipolar cells in the carp retina. *J. Comp. Neurol.* **205**: 161-170.
Saito, T. and Kujiraoka, T. (1988) Characteristics of bipolar-bipolar coupling in the carp retina. *J. Gen. Physiol.* **91**: 275-287.
Saito, T.; Kujiraoka, T.; and Toyoda, J.I. (1984) Electrical and morphological properties of OFF-center bipolar cells in the carp retina. *J. Comp. Neurol.* **222**: 200-208.
Saito, T.; Kujiraoka, T.; and Yonaha, T. (1983) Connections between photoreceptors and horseradish peroxidase-injected bipolar cells in the carp retina. *Vision Res.* **23**: 352-362.
Saito, T.; Kujiraoka, T.; Yonaha, T.; and Chino, Y. (1985) Re-examination of photoreceptor-bipolar connectivity patterns in carp retina: HRP-EM and Golgi-EM studies. *J. Comp. Neurol.* **236**: 141-160.
Sakaba, T.; Ishikane, H.; and Tachibana, M. (1997) $Ca^{2+}$ -activated $K^+$ current at presynaptic terminals of goldfish retinal bipolar cells. *Neurosci. Res.* **27**: 219-228.
Sakai, H.M. and Naka, K.I. (1983) Synaptic organization involving receptor, horizontal and ON- and OFF-center bipolar cells in the catfish retina. *Vision Res.* **23**: 339-351.
Sakakibara, M. and Mitarai, G. (1982) Chromatic properties of bipolar cells in the carp retina. *Color Res. Appl.* **7**: 178-181.
Sampath, A.P. and Rieke, F. (2004) Selective transmission of single photon responses by saturation at the rod-to-rod bipolar synapse. *Neuron* **41**: 431-443.
Sasaki, T. and Kaneko, A. (1996) L-glutamate-induced responses in OFF-type bipolar cells of the cat retina. *Vision Res.* **36**: 787-795.
Satoh, H.; Kaneda, M.; and Kaneko, A. (2001) Intracellular chloride concentration is higher in rod bipolar cells than in cone bipolar cells of the mouse retina. *Neurosci. Lett.* **310**: 161-164.
Saugstad, J.A.; Kinzie, J.M.; Mulvihill, E.R.; Segerson, T.P.; and Westbrook, G.L. (1994) Cloning and expression of a new member of the L-2-amino-4-phosphonobutyric acid-sensitive class of metabotropic glutamate receptors. *Mol. Pharmacol.* **45**: 367-372.
Schaefer, A.T.; Helmstaedter, M.; Sakmann, B.; and Korngreen, A. (2003) Correction of conductance measurements in non-space-clamped structures: 1. Voltage-gated $K^+$ channels. *Biophys. J.* **84**: 3508-3528.
Schiller, P.D.; Logothetis, N.K.; and Charles, E.R. (1990a) Role of the color-opponent and broadband channels in vision. *Vis. Neurosci.* **5**: 321-346.
Schiller, P.H. (1991) The colour-opponent and broadband channels of the primate visual system. In: Valberg, A. and Lee, B.B. (eds.) *Pigments to perception*. New York: Plenum Press.
Schiller, P.H. (1992) The ON and OFF channels of the visual system. *Trends Neurosci.* **15**: 86-92.
Schiller, P.H. (1996) On the specificity of neurons and visual areas. *Behav. Brain Res.* **76**: 21-35.
Schiller, P.H.; Logothetis, N.K.; and Charles, E.R. (1990b) Functions of the colour-opponent and broad-band channels of the visual system. *Nature* **343**: 68-70.
Schmitz, F.; Kirsch, M.; and Wagner, H.-J. (1989) Calcium modulated synaptic ribbon dynamics in cone photoreceptors: a pharmacological and electron spectroscopic study. *Eur. J. Cell Biol.* **49**: 207-212.
Schneeweis, D.M. and Schnapf, J.L. (1995) Photovoltage of rods and cones in the macaque retina. *Science* **268**: 1053-1056.
Schneeweis, D.M. and Schnapf, J.L. (1999) The photovoltage of macaque cone photoreceptors: adaptation, noise, and kinetics. *J. Neurosci.* **19**: 1203-1216.

Schoepp, D.D.; Jane, D.E.; and Monn, J.A. (1999) Pharmacological agents acting at subtypes of metabotropic glutamate receptors. *Neuropharmacology* **38**: 1431-1476.
Scholes, J.H. (1975) Colour receptors, and their synaptic connexions, in the retina of a cyprinid fish. *Philos. Trans. R. Soc. Lond., B, Biol. Sci.* **270**: 61-118.
Scholes, J.H. and Morris, J. (1973) Receptor-bipolar connectivity patterns in fish retina. *Nature* **241** : 52-54.
Schubert, T.; Degen, J.; Willecke, K.; Hormuzdi, S.G.; Monyer, H.; and Weiler, R. (2005) Connexin36 mediates gap junctional coupling of a-ganglion cells in mouse retina. *J. Comp. Neurol.* **485**: 191-201.
Schultz, K.; Goldman, D.J.; Ohtsuka, T.; Hirano, J.; Barton, L.; and Stell, W.K. (1997) Identification and localization of an immunoreactive AMPA-type glutamate receptor subunit (GluR4) with respect to identified photoreceptor synapses in the outer plexiform layer of goldfish retina. *J. Neurocytol.* **26**: 651-666.
Schultz, K.; Janssen-Bienhold, U.; and Weiler, R. (2001) Selective synaptic distribution of AMPA and kainate receptor subunits in the outer plexiform layer of the carp retina. *J. Comp. Neurol.* **435**: 433-449.
Schultze, M. (1866) Zur Anatomie und Physiologie der Retina. *Arch. Mikr. Anat.* **2**: 175-286.
Sherry, D.M. and Yazulla, S. (1993) Goldfish bipolar cells and axon terminal patterns: a Golgi study. *J. Comp. Neurol.* **329**: 188-200.
Shiells, R.A. (1994) Glutamate receptors for signal amplification. *Curr. Biol.* **4**: 917-918.
Shiells, R.A. and Falk, G. (1995) Signal transduction in retinal bipolar cells. *Prog. Retin. Eye Res.* **14**: 223-247.
Shiells, R.A.; Falk, G.; and Naghshineh, S. (1981) Action of glutamate and aspartate analogues on rod horizontal and bipolar cells. *Nature* **294**: 592-594.
Shimbo, K.; Toyoda, J.I.; Kondo, H.; and Kujiraoka, T. (2000) Color-opponent responses of small and giant bipolar cells in the carp retina. *Vis. Neurosci.* **17**: 609-621.
Sjostrand, F.S. (1998a) Structure determines function of the retina, a neural center. 1. The synaptic ribbon complex. *J. Submicrosc. Cytol. Pathol.* **30**: 1-29.
Sjostrand, F.S. (1998b) Structure determines function of the retina, a neural center. 2. The second, third and fourth circuits. *J. Submicrosc. Cytol. Pathol.* **30**: 193-206.
Skrzypek, J.A.C.F. and Werblin, F.S. (1983) Lateral interactions in absence of feedback to cones. *J. Neurophysiol.* **49**: 1007-1016.
Slaughter, M.M. and Miller, R.F. (1981) 2-amino-4-phosphonobutyric acid: a new pharmacological tool for retinal research. *Science* **211**: 182-185.
Slaughter, M.M. and Miller, R.F. (1983) The role of excitatory amino acid transmitters in the mudpuppy retina: an analysis with kainic acid and N-methyl aspartate. *J. Neurosci.* **3**: 1701-1711.
Sohl, G. and Willecke, K. (2004) Gap junctions and the connexin protein family. *Cardiovasc. Res.* **62**: 228-232.
Spiridon, M.; Kamm, D.; Billups, B.; Mobbs, P.; and Attwell, D. (1998) Modulation by zinc of the glutamate transporters in glial cells and cones isolated from the tiger salamander retina. *J. Physiol. (Lond.)* **506**: 363-376.
Spruston, N.; Jaffe, D.B.; Williams, S.H.; and Johnston, D. (1993) Voltage- and space-clamp errors associated with the measurement of electrotonically remote synaptic events. *J. Neurophysiol.* **70**: 781-802.
Steinberg, T.H.; Civitelli, R.; Geist, S.T.; Robertson, A.J.; Hick, E.; Veenstra, R.D.; Wang, H.Z.; Warlow, P.M.; Westphale, E.M.; and Laing, J.G. (1994) Connexin43 and connexin45 form gap junctions with different molecular permeabilities in osteoblastic cells. *EMBO J.* **13**: 744-750.
Stell, W.K. (1967) The structure and relationships of horizontal cells and photoreceptor-bipolar synaptic complexes in goldfish retina. *Am. J. Anat.* **121**: 401-424.
Stell, W.K. (1976) Functional polarization of horizontal cell dendrites in goldfish retina. *Invest. Ophthalmol.* **15**: 895-908.
Stell, W.K. (1978) Inputs to bipolar cell dendrites in goldfish retina. *Sens. Processes* **2**: 339-349.
Stell, W.K. (1980) Photoreceptor-specific synaptic pathways in goldfish retina: a world of colour, a wealth of connections. In: Verriest, G. (ed.) *Colour Vision Deficiencies vol. 5.* Bristol: Adam Hilger.
Stell, W.K. and Harosi, F.I. (1976) Cone structure and visual pigment content in the retina of the goldfish. *Vision Res.* **16**: 647-657.
Stell, W.K.; Ishida, A.T.; and Lightfoot, D.O. (1977) Structural basis for ON- and OFF-center responses in retinal bipolar cells. *Science* **198**: 1269-1271.
Stell, W.K. and Kock, J.H. (1984) Structure, development and visual acuity in the goldfish retina. In: Robert Hilfer, S. and Sheffield, J.B. (eds.) *Molecular and cellular basis of visual acuity*. New York: Springer-Verlag New York Inc.
Stell, W.K. and Lightfoot, D.O. (1975) Color-specific interconnections of cones and horizontal cells in the retina of the goldfish. *J. Comp. Neurol.* **159**: 473-502.
Stell, W.K. and Lightfoot, D.O. (1979) Computer-aided reconstruction and analysis of goldfish rod synapses. *Seitai Kagaku* **30**: 173-177.
Stell, W.K.; Lightfoot, D.O.; Wheeler, T.G.; and Leeper, H.F. (1975) Goldfish retina: functional polarization of cone horizontal cell dendrites and synapses. *Science* **190**: 989-990.
Stergiopoulos, K.; Alvarado, J.L.; Mastroianni, M.; Ek-Vitorin, J.F.; Taffet, S.M.; and Delmar, M. (1999) Hetero-domain interactions as a mechanism for the regulation of connexin channels. *Circ. Res.* **84**: 1144-1155.
Suchyna, T.M.; Nitsche, J.M.; Chilton, M.; Harris, A.L.; Veenstra, R.D.; and Nicholson, B.J. (1999) Different ionic selectivities for connexins 26 and 32 produce rectifying gap junction channels. *Biophys. J.* **77**: 2968-2987.

Suzuki, S. and Kaneko, A. (1990) Identification of bipolar cell subtypes by protein kinase C-like immunoreactivity in the goldfish retina. *Vis. Neurosci.* **5**: 223-230.

Szente, M.; Gajda, Z.; Said, A.K.; and Hermesz, E. (2002) Involvement of electrical coupling in the in vivo ictal epileptiform activity induced by 4-aminopyridine in the neocortex. *Neuroscience* **115**: 1067-1078.

Tachibana, M. and Kaneko, A. (1987) Gamma-aminobutyric acid exerts a local inhibitory action on the axon terminal of bipolar cells: evidence for a negative feedback from amacrine cells. *Proc. Natl. Acad. Sci. U.S.A.* **84**: 3501-3505.

Tachibana, M.; Okada, T.; Arimura, T.; Kobayashi, K.; and Piccolino, M. (1993) Dihydropyridine-sensitive calcium current mediates neurotransmitter release from bipolar cells of the goldfish retina. *J. Neurosci.* **13**: 2898-2909.

Takahashi, K.-I. and Copenhagen, D.R. (1992) APB suppresses synaptic input to retinal horizontal cells in fish: A direct action on horizontal cells modulated by intracellular pH. *J. Neurophysiol.* **67**: 1633-1642.

Takahashi, K.-I.; Dixon, D.B.; and Copenhagen, D.R. (1993) Modulation of a sustained calcium current by intracellular pH in horizontal cells of fish retina. *J. Gen. Physiol.* **101**: 695-714.

Takahashi, T.; Forsythe, I.D.; Tsujimoto, T.; Barnes-Davies, M.; and Onodera, K. (1996) Presynaptic calcium current modulation by a metabotropic glutamate receptor. *Science* **274**: 594-597.

Tanabe, Y.; Masu, M.; Ishii, T.; Shigemoto, R.; and Nakanishi, S. (1992) A family of metabotropic glutamate receptors. *Neuron* **8**: 169-179.

Tanabe, Y.; Nomura, A.; Masu, M.; Shigemoto, R.; Mizuno, N.; and Nakanishi, S. (1993) Signal transduction, pharmacological properties, and expression patterns of two rat metabotropic glutamate receptors, mGluR3 and mGluR4. *J. Neurosci.* **13**: 1372-1378.

Taylor, W.R. and Smith, R.G. (2004) Transmission of scotopic signals from the rod to rod-bipolar cell in the mammalian retina. *Vision Res.* **44:** 3269-3276.

Teranishi, T.; Negishi, K.; and Kato, S. (1983) Dopamine modulates S-potential amplitude and dye-coupling between external horizontal cells in carp retina. *Nature* **301**: 243-246.

Tessier-Lavigne, M.; Attwell, D.; Mobbs, P.; and Wilson, M. (1988) Membrane currents in retinal bipolar cells of the axolotl. *J. Gen. Physiol.* **91**: 49-72.

Thoreson, W.B. and Miller, R.F. (1993) Membrane currents evoked by excitatory amino acid agonists in ON bipolar cells of the mudpuppy retina. *J. Neurophysiol.* **70**: 1326-1338.

Thoreson, W.B.; Rabl, K.; Townes-Anderson, E.; and Heidelberger, R. (2004) A highly $Ca^{2+}$-sensitive pool of vesicles contributes to linearity at the rod photoreceptor ribbon synapse. *Neuron* **42**: 595-605.

Thoreson, W.B. and Ulphani, J.S. (1995) Pharmacology of selective and non-selective metabotropic glutamate receptor agonists at L-AP4 receptors in retinal ON bipolar cells. *Brain Res.* **676**: 93-102.

Tian, N. and Slaughter, M.M. (1995) Functional properties of a metabotropic glutamate receptor at dendritic synapses of ON bipolar cells in the amphibian retina. *Vis. Neurosci.* **12**: 755-765.

Tomita, T. (1965) Electrophysiological study of the mechanisms subserving color coding in the fish retina. *Cold Spring Harb. Symp. Quant. Biol.* **30**: 559-566.

Tornqvist, K.; Yang, X.-L.; and Dowling, J.E. (1988) Modulation of cone horizontal cell activity in the teleost fish retina. III. Effects of prolonged darkness and dopamine on electrical coupling between horizontal cells. *J. Neurosci.* **8**: 2279-2288.

Toyoda, J. (1973) Membrane resistance changes underlying the bipolar cell response in the carp retina. *Vision Res.* **13**: 283-294.

Toyoda, J.I.; Saito, T.; and Kondo, H. (1978) Three types of horizontal cells in the stingray retina: their morphology and physiology. *J. Comp. Neurol.* **179**: 569-580.

Toyoda, J.I. and Tonosaki, K. (1978) Studies on the mechanisms underlying horizontal-bipolar interaction in the carp retina. *Sens. Processes* **2**: 359-365.

Trexler, E.B.; Bukauskas, F.F.; Bennett, M.V.; Bargiello, T.A.; and Verselis, V.K. (1999) Rapid and direct effects of pH on connexins revealed by the connexin46 hemichannel preparation. *J. Gen. Physiol.* **113**: 721-742.

Tsin, A.T.C.; Liebman, P.A.; Beatty, D.D.; and Drzymala, R. (1981) Rod and cone visual pigments in the goldfish. *Vision Res.* **21**: 943-946.

Tsukamoto, Y.; Morigiwa, K.; Ueda, M.; and Sterling, P. (2001) Microcircuits for night vision in mouse retina. *J. Neurosci.* **21**: 8616-8623.

Tu, J.C.; Xiao, B.; Yuan, J.P.; Lanahan, A.A.; Leoffert, K.; Li, M.; Linden, D.J.; and Worley, P.F. (1998) Homer binds a novel proline-rich motif and links group 1 metabotropic glutamate receptors with IP3 receptors. *Neuron* **21**: 717-726.

Ueda, Y.; Iwakabe, H.; Masu, M.; Suzuki, M.; and Nakanishi, S. (1997) The mGluR6 5' upstream transgene sequenc directs a cell-specific and developmentally regulated expression in retinal rod and ON-type cone bipolar cells. *J. Neurosci.* **17**: 3014-3023.

Umino, O.; Maehara, M.; Hidaka, S.; Kita, S.; and Hashimoto, Y. (1994) The network properties of bipolar-bipolar cell coupling in the retina of teleost fishes. *Vis. Neurosci.* **11**: 533-548.

Uyama, N.; Shimahara, Y.; Okuyama, H.; Kawada, N.; Kamo, S.; Ikeda, K.; and Yamaoka, Y. (2003) Carbenoxolone inhibits DNA synthesis and collagen gene expression in rat hepatic stellate cells in culture. *J. Hepatol.* **39**: 749-755.

Van den Pol, A.N. and Gorcs, T. (1988) Glycine and glycine receptor immunoreactivity in brain and spinal cord. *J. Neurosci.* **8**: 472-492.

Vandenbranden, C.A.; Yazulla, S.; Studholme, K.M.; Kamphuis, W.; and Kamermans, M. (2000a) Immunocytochemical localization of the glutamate transporter GLT-1 in goldfish (*Carassius auratus*) retina. *J. Comp. Neurol.* **423**: 440-451.

Vandenbranden, C.A.V.; Kamphuis, W.; Nunes Cardozo, J.J.; and Kamermans, M. (2000b) Expression and localization of ionotropic glutamate receptor subunits in the goldfish retina - an *in situ* hybridization and immunocytochemical study. *J. Neurocytol.* **29**: 729-742.

Vaney, D.I. (1991) Many diverse types of retinal neurons show tracer coupling when injected with biocytin or neurobiotin. *Neurosci. Lett.* **125**: 187-190.

Vaquero, C.F.; Velasco, A.; and De la Villa, P. (1997) Quantitative measurement of protein kinase C immunoreactivity in rod bipolar cells of the goldfish retina. *Brain Res.* **773**: 208-212.

Vardi, N. (1998) a subunit of Go localizes in the dendritic tips of ON bipolar cells. *J. Comp. Neurol.* **395**: 43-52.

Vardi, N.; Duvoisin, R.; Wu, G.; and Sterling, P. (2000) Localization of mGluR6 to dendrites of ON bipolar cells in primate retina. *J. Comp. Neurol.* **423**: 402-412.

Vardi, N.; Matesic, D.F.; Manning, D.R.; Liebman, P.A.; and Sterling, P. (1993) Identification of a G-protein in depolarizing rod bipolar cells. *Vis. Neurosci.* **10**: 473-478.

Vardi, N. and Morigiwa, K. (1997) ON cone bipolar cells in rat express the metabotropic receptor mGluR6. *Vis. Neurosci.* **14**: 789-794.

Vardi, N.; Morigiwa, K.; Wang, T.L.; Shi, Y.J.; and Sterling, P. (1998) Neurochemistry of the mammalian cone 'synaptic complex'. *Vision Res.* **38**: 1359-1369.

Vargas, G.; Yeh, T.Y.; Blumenthal, D.K.; and Lucero, M.T. (1999) Common components of patch-clamp internal recording solutions can significantly affect protein kinase A activity. *Brain Res.* **828**: 169-173.

Verweij, J.; Hornstein, E.P.; and Schnapf, J.L. (2003) Surround antagonism in macaque cone photoreceptors. *J. Neurosci.* **23**: 10249-10257.

Vollrath, L. and Spiwoks-Becker, I. (1996) Plasticity of retinal ribbon synapses. *Microsc. Res. Tech.* **35**: 472-487.

Wadiche, J.I.; Amara, S.G.; and Kavanaugh, M.P. (1995) Ion fluxes associated with excitatory amino acid transport. *Neuron* **15**: 721-728.

Wagner, H.-J. (1973) Darkness-induced reduction of the number of synaptic ribbons in fish retina. *Nature New Biol.* **246**: 53-55.

Wagner, H.-J. (1980) Light-dependent plasticity of the morphology of horizontal cell terminals in cone pedicles of fish retinas. *J. Neurocytol.* **9**: 573-590.

Weiler, R. (1994) Spinules: a case for synaptic plasticity. *Trends Neurosci.* **17**: 6.

Weiler, R.; Kolbinger, W.; and Kohler, K. (1989) Reduced light responsiveness of the cone pathway during prolonged darkness does not result from an increase of dopaminergic activity in the fish retina. *Neurosci. Lett.* **99**: 214-218.

Weiler, R. and Wagner, H.-J. (1984) Light-dependent change of cone-horizontal cell interactions in carp retina. *Brain Res.* **298**: 1-9.

Werblin, F.S. (1974) Control of retinal sensitivity. II. Lateral interactions at the outer plexiform layer. *J. Gen. Physiol.* **63**: 62-87.

Werblin, F.S. (1978) Transmission along and between rods in the tiger salamander retina. *J. Physiol. (Lond.)* **280**: 449-470.

Werblin, F.S. and Dowling, J.E. (1969) Organization of the retina of the muddpuppy, *Necturus maculosus*. II. Intracellular recording. *J. Neurophysiol.* **32**: 339-355.

Wiesel, T.N. and Hubel, D.H. (1966) Spatial and chromatic interactions in the lateral geniculate body of the rhesus monkey. *J. Neurophysiol.* **29**: 1115-1156.

Willecke, K.; Eiberger, J.; Degen, J.; Eckardt, D.; Romualdi, A.; Guldenagel, M.; Deutsch, U.; and Sohl, G. (2002) Structural and functional diversity of connexin genes in the mouse and human genome. *Biol. Chem.* **383**: 725-737.

Witkovsky, P.; Burkhardt, D.A.; and Nagy, A.R. (1979) Synaptic connections linking cones and horizontal cells in the retina of the pikeperch (*Stizostedion vitreum*). *J. Comp. Neurol.* **186**: 541-560.

Witkovsky, P. and Dearry, A. (1991) Functional roles of dopamine in the vertebrate retina. *Prog. Retinal Res.* **11**: 247-292.

Witkovsky, P.; Shakib, M.; and Ripps, H. (1974) Interreceptoral junctions in the teleost retina. *Invest. Ophthalmol.* **13**: 996-1009.

Witkovsky, P. and Stell, W.K. (1973a) Retinal structure in the smooth dogfish *Mustelus canis*: electron microscopy of serially sectioned bipolar cell synaptic terminals. *J. Comp. Neurol.* **150**: 147-167.

Witkovsky, P. and Stell, W.K. (1973b) Retinal structure in the smooth dogfish, *Mustelus canis*: Light microscopy of bipolar cells. *J. Comp. Neurol.* **148**: 47-60.

Wong, K.Y.; Adolph, A.R.; and Dowling, J.E. (2005a) Retinal bipolar cell input mechanisms in giant danio. I. Electroretinographic analysis. *J. Neurophysiol.* **93**: 84-93.

Wong, K.Y.; Cohen, E.D.; and Dowling, J.E. (2005b) Retinal bipolar cell input mechanisms in giant danio. II. Patch-clamp analysis of on bipolar cells. *J. Neurophysiol.* **93**: 94-107.

Wong-Riley, M.T. (1974) Synaptic organization of the inner plexiform layer in the retina of the tiger salamander. *J. Neurocytol.* **3**: 1-33.
Wu, L.G. and Saggau, P. (1997) Presynaptic inhibition of elicited neurotransmitter release. *Trends Neurosci.* **20**: 204-212.
Wu, S.M.; Gao, F.; and Maple, B.R. (2000) Functional architecture of synapses in the inner retina: segregation of visual signals by stratification of bipolar cell axon terminals. *J. Neurosci.* **20**: 4462-4470.
Wu, S.M. and Yang, X.-L. (1988) Electrical coupling between rods and cones in the tiger salamander retina. *Proc. Natl. Acad. Sci. U.S.A.* **85**: 275-278.
Xia, Y. and Nawy, S. (2003) The gap junction blockers carbenoxolone and 18beta-glycyrrhetinic acid antagonize cone-driven light responses in the mouse retina. *Vis. Neurosci.* **20**: 429-435.
Xin, D. and Bloomfield, S.A. (1997) Tracer coupling pattern of amacrine and ganglion cells in the rabbit retina. *J. Comp. Neurol.* **383**: 512-528.
Yager, D. (1967) Behavioral measures and theoretical analysis of spectral saturation in the goldfish *Carassius auratus*. *Vision Res.* **7**: 707-727.
Yager, D. (1968) Behavioural measures of the spectral sensitivity of the dark-adapted goldfish. *Nature* **220**: 1052-1053.
Yager, D. (1969) Behavioral measures of spectral sensitivity in the goldfish following chromatic adaptation. *Vision Res.* **9**: 179-186.
Yamada, M. and Saito, T. (1988) Effects of dopamine on bipolar cells in the carp retina. *Biomed. Res.* **2**: 125-130.
Yamada, M. and Saito, T. (1997) Dual component in receptive field centre of bipolar cells in carp retina. *Vision Res.* **37**: 2331-2338.
Yamashita, M. and Wässle, H. (1991) Responses of rod bipolar cells isolated from the rat retina to the glutamate agonist 2-amino-4-phosphonobutyric acid (APB). *J. Neurosci.* **11**: 2372-2382.
Yang, X.-L.; Tornqvist, K.; and Dowling, J.E. (1988a) Modulation of cone horizontal cell activity in the teleost fish retina. I. Effects of prolonged darkness and background illumination on light responsiveness. *J. Neurosci.* **8**: 2259-2268.
Yang, X.-L.; Tornqvist, K.; and Dowling, J.E. (1988b) Modulation of cone horizontal cell activity in the teleost fish retina. II. Role of interplexiform cells and dopamine in regulating light responsiveness. *J. Neurosci.* **8**: 2269-2278.
Yang, X.-L. and Wu, S.M. (1989) Effects of CNQX, APB, PDA and kynurenate on horizontal cells of the tiger salamander retina. *Vis. Neurosci.* **3**: 207-212.
Yang, X.-L. and Wu, S.M. (1997) Response sensitivity and voltage gain of the rod- and cone-bipolar cell synapse in dark-adapted tiger salamander retina. *J. Neurosci.* **78**: 2662-2673.
Yazulla, S. (1976) Cone input to bipolar cells in the turtle retina. *Vision Res.* **16**: 737-744.
Yazulla, S. and Studholme, K.M. (1992) Light-dependent plasticity of the synaptic terminals of Mb bipolar cells in goldfish retina. *J. Comp. Neurol.* **320**: 521-530.
Yazulla, S. and Studholme, K.M. (1998) Differential distribution of Shaker-like and Shab-like $K^+$-channel subunits in goldfish retina and retinal bipolar cells. *J. Comp. Neurol.* **396**: 131-140.
Yazulla, S. and Studholme, K.M. (1999) Co-localization of Shaker A-type $K^+$ channel (Kv1.4) and AMPA-glutamate receptor (GluR4) immunoreactivities to dendrites of OFF-bipolar cells of goldfish retina. *J. Neurocytol.* **28**: 63-73.
Yazulla, S. and Studholme, K.M. (2001) Neurochemical anatomy of the zebrafish retina as determined by immunocytochemistry. *J. Neurocytol.* **30**: 551-592.
Yazulla, S.; Studholme, K.M.; Fan, S.F.; and Mora-Ferrer, C. (2001) Neuromodulation of voltage-dependent $K^+$ channels in bipolar cells: immunocytochemical and electrophysiological studies. *Prog. Brain Res.* **131**: 201-213.
Yazulla, S.; Studholme, K.M.; McIntosh, H.H.; and Fan, S.F. (2000) Cannabinoid receptors on goldfish retinal bipolar cells: electron- microscope immunocytochemistry and whole-cell recordings. *Vis. Neurosci.* **17**: 391-401.
Yazulla, S.; Studholme, K.M.; and Wu, J.Y. (1987) GABAergic input to the synaptic terminals of mb1 bipolar cells in the goldfish retina. *Brain Res.* **411**: 400-405.
Zeki, S. (1983a) Colour coding in the cerebral cortex: the responses of wavelength-selective and colour-coded cells in monkey visual cortex to changes in wavelength composition. *Neuroscience* **9**: 767-781.
Zeki, S. (1983b) The relationship between wavelength and color studied in single cells of monkey striate cortex. *Prog. Brain Res.* **58**: 219-227.
Zenisek, D.; Henry, D.; Studholme, K.; Yazulla, S.; and Matthews, G. (2001) Voltage-dependent sodium channels are expressed in nonspiking retinal bipolar neurons. *J. Neurosci.* **21**: 4543-4550.
Zenisek, D. and Matthews, G. (1997) Calcium action potentials in retinal bipolar neurons. *Vis. Neurosci.* **15**: 69-75.
Zhang, J. and Wu, S.M. (2003) Goa labels ON bipolar cells in the tiger salamander retina. *J. Comp. Neurol.* **461**: 276-289.
Zhang, J. and Wu, S.M. (2004) Connexin35/36 gap junction proteins are expressed in photoreceptors of the tiger salamander retina. *J. Comp. Neurol.* **470**: 1-12.
Zhou, Z.J.; Fain, G.L.; and Dowling, J.E. (1993) The excitatory and inhibitory amino acid receptors on horizontal cells isolated from the white perch retina. *J. Neurophysiol.* **70**: 8-19.

# Summary

Once projected onto the retina, the image of our world stimulates photoreceptors and thereby initiates a cascade of processes that culminates in visual perception. The absorption of photons at the photoreceptor layer is signaled to bipolar cells (BCs), and transmitted from BCs to ganglion cells (GCs), which ultimately form the output of the eye to the brain. Before reaching the brain, however, this visual signal has to be compressed such as to transmit a maximum of information with a minimum of wiring.

BCs are not mere relay stations between photoreceptors and GCs. Complex calculations already take place at the photoreceptor-BC synapse, which enable the visual system to perform optimally from dusk to dawn, when light levels change dramatically. Among the many BC types, mixed-input BCs are specially suited for bridging the gap between high scotopic and high photopic levels, due to the fact that they receive signals from both rods and cones. These cells and their mechanisms for coding visual signals in the twilight zone are the object of study of this thesis.

In **Chapter 1**, a brief review of literature data concerning retinal anatomy and physiology is presented. Emphasis is given to the different mixed-input BC types and the visual tasks these cells are thought to participate in, such as the segregation of visual signals in two complementary channels (the ON- and OFF- pathways), chromatic processing, and light-dark adaptation.

In **Chapter 2**, the localization of metabotropic glutamate receptors (mGluRs) in the goldfish outer plexiform layer (OPL) is studied. The receptor responsible for rod-driven light responses in ON BCs, mGluR6 (a group III mGluR), is not the only one found at BC dendrites invaginating into rod spherules. Processes of putative mixed-input ON BCs in this synapse are also positively labeled for mGluR1$\alpha$, whose function remains obscure. Lateral elements in the rod triads, probably belonging to rod-driven horizontal cells (HCs), are sometimes immunoreactive for mGluR1$\alpha$ and mGluR6 as well. In the cone pedicles, mGluRs of all three groups are found at horizontal cell (HC) dendrites, but none is found at BC processes. The function of these mGluRs at the HC level is unknown. They might be involved in shaping light responses, since the light-driven conductance in HCs is mediated by AMPA/KA receptors. Finally, mGluR4 (another group III mGluR) is found in about 80% of the rods, and in no cones. This pre-synaptic localization of mGluR4 points to a possible function in controlling glutamate release, a hypothesis that is further investigated in **Chapter 6**.

In **Chapter 3**, electrical coupling is demonstrated in both mixed-input ON and OFF BCs. This lateral integration of signals makes the receptive field center of these cells much larger than their dendritic trees. As a consequence, light responses to spatially small stimuli that do not cover the whole receptive field are less sensitive than those to full-field stimulation. Further, coupling decreases the input resistance

($R_{in}$) of BCs dramatically, limits effective dialysis with the pipette solution and shifts the apparent reversal potential ($V_{rev}$) of light-driven conductances. The gap junctions responsible for this electrical communication are neither permeable to Lucifer Yellow (LY), nor are they sensitive to pH manipulations or to commonly used gap junction blockers. This indicates that the connexins forming these gap junctions are distinct from those responsible for electrical coupling at the HC level. The function of coupling as a mechanism to improve signal-to-noise ratio at the expense of some loss in sensitivity is discussed. The costs that these large receptive fields might represent for visual acuity are dealt with in **Chapter 6**.

In **Chapter 4**, spectral opponency in mixed-input BCs is shown to be a result of antagonistic interactions between rods and cones, or between different spectral types of cones. Because the polarity of these spectrally coded responses also changes with the intensity of the stimulus, it cannot be the underlying mechanism for color vision, which does not show the same intensity dependency. Rather, these BCs seem to be ideal intensity change detectors. The antagonist inputs make the intensity-response relations of opponent BCs much steeper than those of photoreceptors. As a consequence, small changes in stimulus intensity evoke a large change in response amplitude in these cells. These results indicate that goldfish BCs seem to use the same coding scheme as cone-driven HCs to compress information, via a non-opponent, broadband channel (the non-opponent mixed-input ON and OFF BCs), and opponent channels. Which glutamate receptors could be responsible for such intensity-dependent behavior is discussed in **Chapter 6**.

In **Chapter 5**, the presence and function of voltage-gated $K^+$ channels at the tips of the dendrites of mixed-input ON BCs is investigated through electrophysiological experiments and model simulations using NEURON. The anatomy of the dendritic terminals and the selective distribution of voltage-gated channels in these dendritic boutons lead to the rectification of light-driven *IV* relations, and can serve as a gain control mechanism at the rod-BC synapse. In the scotopic range, they can speed up synaptic transmission and generate transience by accelerating BC repolarization. This fast repolarization restores the high gain of the rod-BC synapse, allowing subsequent rod-driven signals to drive the cell efficiently. As light levels increase, tonic suppression of the rod input leads to the opening of many of these voltage-gated channels, shunting the rod pathway and decreasing the gain of the rod-BC synapse. Under this condition, the transmission of cone-driven signals is favored, and the balance between rod- and cone-driven signals at the BC level shifts from rod-dominated to cone-dominated.

In **Chapter 6**, unsolved issues such as the function of such a multitude of glutamatergic receptors at the first synapse, as well as the costs and benefits of large spatial summation for visual acuity and sensitivity are addressed.

# Resumo

Ao ser projetada sobre a retina, a imagem do mundo exterior estimula os fotorreceptores e inicia um processo que culmina em percepção visual. Há na retina dois tipos de fotorreceptores: cones e bastonetes, em cujos terminais ocorre a transmissão sináptica para neurônios de segunda ordem. Esses fotorreceptores diferenciam-se principalmente na sua sensibilidade à luz. A absorção de fótons na camada dos fotorreceptores é comunicada a células bipolares (BCs), que retransmitem a informação visual às células ganglionares (GCs). Os axônios dessas últimas formam o nervo óptico, que conduz os sinais visuais ao cérebro. Todavia, esses sinais necessitam ser comprimidos ante de atingir o nervo óptico, para que uma quantidade máxima de informação seja transmitida com um mínimo de conexões.

BCs não são simples estações intermediárias na retina. Processos complexos ocorrem na sinapse entre os fotorreceptores essas células que possibilitam ao sistema visual funcionar de maneira adequada em condições luminosas distintas. Dentre os muitos tipos de BCs, as BCs de entrada mista são ideais para fazer a ponte entre os níveis escotópico e fotópico, por receber estímulos de ambas as classes de fotorreceptores. Essas células e seus mecanismos de codificação de sinais visuais no crepúsculo são os temas desta tese.

O **Capítulo 1** fornece uma revisão dos dados de literatura referentes à anatomia e fisiologia retinianas, com ênfase nos vários tipos de BCs. Esses neurônios executam várias tarefas, tais como segregar a informação visual em duas vias complementares de transmissão (os canais ON e OFF), oponência espectral, e adaptação a níveis distintos de luminosidade. As células bipolares ON (ON BCs) despolarizam ao início de um estímulo luminoso, enquanto as células OFF (OFF BCs) despolarizam à cessação do estímulo.

O **Capítulo 2** descreve a localização ultraestrutural dos receptores metabotrópicos glutamatérgicos (mGluRs) na retina externa do peixe dourado. Esses receptores dividem-se em três grupos principais com características farmacológicas distintas. O receptor envolvido nas respostas induzidas pelos bastonetes em ON BCs, mGluR6 (pertencente ao grupo III), não é o único presente nos dendritos dessas células. Processos de prováveis ON BCs de entrada mista são também positivos para mGluR1$\alpha$, embora a função desse receptor nessas células seja uma incógnita. Elementos laterais nos terminais sinápticos dos bastonetes, provavelmente oriundos de células horizontais (HCs), são também positivos para mGluR1$\alpha$ e mGluR6 em alguns casos. Nos pedículos dos cones, mGluRs dos três grupos são encontrados em dendritos pertencentes a HCs, enquanto os processos das BCs são negativos. A função desses receptores em HCs é obscura. Eles poderiam estar ligados à modulação das respostas à luz, uma vez que a geração destas em HCs se dá via receptores do tipo AMPA/KA. Por fim, mGluR4 (um outro

receptor do grupo III) é encontrado em 80% dos bastonetes, estando ausente em cones. Essa localização pré-sináptica indica uma possível função desse receptor no controle da liberação de glutamato pelos bastonetes, hipótese testada no **Capítulo 6**.

O **Capítulo 3** mostra que tanto as ON BCs quanto as OFF BCs de entrada mista são acopladas eletricamente. Há dois tipos de transmissão sináptica: a) transmissão química, discutida nos capítulos anteriores, e b) transmissão elétrica, efetuada através de junções comunicantes. A integração lateral obtida por meio de tais junções torna o campo receptivo das BCs maior do que o diâmetro de suas arborizações dendríticas. Como conseqüência, a sensibilidade a estímulos que não cobrem todo o centro do campo receptivo é menor do que para estimulação completa da retina. Além disso, o acoplamento elétrico diminui a resistência de entrada das BCs, evita a diálise efetiva com a solução do eletrodo e desloca o potencial de inversão aparente das condutâncias induzidas pela luz. As junções comunicantes dessas células não são permeáveis a Lucifer Yellow (LY), e são insensíveis a manipulações de pH e a drogas bloqueadoras normalmente utilizadas. Esses resultados indicam que as conexinas responsáveis pela formação dessas junções são diferentes daquelas envolvidas na comunicação elétrica entre HCs. A função do acoplamento elétrico como um mecanismo para melhorar a relação sinal-ruído às custas da sensibilidade é discutida nesse capítulo, enquanto as conseqüências de tais campos receptivos extensos para a acuidade visual são tratadas no **Capítulo 6**.

O **Capítulo 4** descreve a oponência espectral em BCs de entrada mista como uma conseqüência de interações entre cones e bastonetes, ou entre tipos espectrais distintos de cones. Como essas respostas oponentes dependem da intensidade do estímulo luminoso, é improvável que elas sejam o mecanismo subjacente à visão de cores. Ao invés disso, essas células poderiam funcionar eficientemente como detectores de mudanças na intensidade luminosa, uma vez que a interação antagônica das suas entradas produz nessas BCs uma curva *V(logI)* mais íngreme do que a curva *V(logI)* dos fotorreceptores. Como resultado, pequenas mudanças na intensidade do estímulo luminoso provocam grandes mudanças na amplitude de resposta das BCs oponentes. Juntos, esses resultados sugerem que, para comprimir informação, BCs usam um esquema de codificação semelhante àquele encontrado em outros neurônios retinianos como as HCs: um canal de banda larga e não oponente (como as BCs ON e OFF de entrada mista) e canais oponentes. No **Capítulo 6**, os receptores glutamatérgicos responsáveis por essas respostas oponentes são discutidos.

O **Capítulo 5** estuda, através de experimentos eletrofisiológicos e de simulações matemáticas (em NEURON), a presença e função de canais de $K^+$ dependentes de voltagem na extremidade dos dendritos de ON BCs de entrada mista. A anatomia dos dendritos e a distribuição específica desses canais levam à retificação das relações corrente-voltagem, e podem atuar como um mecanismo de

controle de amplificação na sinapse entre bastonetes e BCs. Em níveis escotópicos, esse arranjo pode acelerar a transmissão sináptica e tornar as respostas à luz mais transientes. Essa repolarização rápida restabelece o alto ganho da sinapse entre bastonetes e BCs, garantindo que sinais subseqüentes sejam transmitidos eficientemente. Quando a iluminação ambiente aumenta (como, por exemplo, no crepúsculo), a supressão contínua da liberação de glutamato na fenda sináptica induz a abertura de vários desses canais dependentes de voltagem, pondo o sistema dos bastonetes em derivação e diminuindo o ganho dessa sinapse. Nessa situação, a transmissão de sinais oriundos dos cones é favorecida e as ON BCs deixam de ser dominadas pelos bastonetes, passando a ser predominantemente dirigidas por cones.

O **Capítulo 6** discute temas pouco compreendidos, como a função da ampla gama de receptores glutamatérgicos na primeira sinapse do sistema visual, bem como as vantagens e desvantagens da existência de campos receptivos extensos para a sensibilidade e acuidade visuais.

# Samenvatting

Eenmaal geprojecteerd op het netvlies, stimuleert het beeld van de wereld om ons heen de fotoreceptoren en daardoor begint er een serie van processen die eindigt in visuele perceptie. Er zijn twee soorten fotoreceptoren: staafjes en kegeltjes. In het kegel- en staafvoetje vindt de synaptische overdracht plaats. Na absorptie van fotonen in de fotoreceptor-laag wordt het signaal doorgegeven aan de bipolaire cellen (BC's), waarna de BC's het signaal doorgeven aan de ganglioncellen (GC's). Via de *nervus opticus* geven de GC's het signaal weer door aan de hersenen. Echter, dit visuele signaal moet gecomprimeerd worden voordat het naar de hersenen gaat, zodat een maximale hoeveelheid informatie met minimale bedrading wordt overgebracht.

BC's zijn geen simpele tussenstations in het netvlies. Er vinden complexe processen in de fotoreceptor-BC synaps plaats die het visuele systeem in staat stellen om onder verschillende lichtomstandigheden optimaal te functioneren. Van de vele soorten BC's zijn mixed-input BC's het meest geschikt om het verschil tussen hoog-scotopische (maanlicht) en hoog-fotopische (daglicht) niveaus te overbruggen, omdat zij van zowel staafjes als kegeltjes signalen ontvangen. Deze cellen en hun mechanismen voor het coderen van visuele signalen in de schemering zijn de onderwerpen van dit proefschrift.

In **Hoofdstuk 1** wordt een kort overzicht gegeven van de literatuurgegevens over retinale anatomie en fysiologie. Aandacht wordt besteed aan de verschillende BC-typen. BC's hebben verschillende taken zoals de segregatie van visuele signalen in complementaire ON- en OFF-pathways, kleurcodering, en licht-donker adaptatie. ON-cellen depolariseren wanneer het licht aan gaat, terwijl OFF-cellen depolariseren wanneer het licht uit gaat.

**Hoofdstuk 2** geeft een overzicht van de lokalisatie van metabotropische glutamaat-receptoren (mGluRs) in de buitenste laag van de goudvis-retina. Er zijn drie groepen metabotropische receptoren met verschillende farmacologische eigenschappen. De receptor verantwoordelijk voor de staaf-gestuurde lichtresponsen van ON-BC's, de mGluR6 receptor (een groep III mGluR), is niet de enige die aanwezig is op de BC-dendrieten. Processen van mogelijke mixed-input ON-BC's zijn ook positief voor mGluR1$\alpha$, echter de functie van mGluR1$\alpha$ blijft onduidelijk. Laterale elementen in de staafvoetjes, die mogelijkerwijs bij staaf-horizontale cellen (HC's) horen, zijn soms ook immunopositief voor mGluR1$\alpha$ en mGluR6. In de kegelvoetjes worden mGluRs van alle drie de groepen aangetoond op HC-dendrieten, terwijl BC-processen negatief zijn. De functie van deze mGluRs in HC's is onbekend. Zij zouden een rol bij het moduleren van lichtresponsen kunnen spelen, aangezien de licht-geïnduceerde conductantie in deze cellen door AMPA/KA receptoren tot stand komt. Tenslotte, blijkt mGluR4 (een andere groep III mGluR) in ongeveer 80% van de staafjes te worden aangetroffen, en afwezig te

zijn in de kegelvoetjes. Deze pre-synaptische lokalisatie van mGluR4 zou mogelijk een rol kunnen spelen in de controle van de glutamaat-afgifte in de staafjes. Deze hypothese wordt in **Hoofdstuk 6** verder onderzocht.

In **Hoofdstuk 3** wordt elektrische koppeling aangetoond tussen mixed-input ON- zowel als in mixed-input OFF-BC's. Er zijn twee soort van overdracht: een chemische synaps, besproken in de voorafgaande hoofdstukken, en een andere vorm van overdracht, de elektrische synaps. Elektrische koppeling wordt veroorzaakt door gap-junctions. Door de laterale integratie van signalen wordt het centrum van het receptieve veld van de BC's veel groter dan hun dendritische vertakkingen. Het gevolg van een en ander is dat lichtresponsen voor kleine stimuli die het receptieve veld niet volledig bedekken minder gevoelig zijn dan die voor ruimtelijk uitgebreide lichtstimulatie. Daarnast zorgt elektrische koppeling voor vermindering van de input-weerstand, voor verhindering van effectieve dialyse met de pipet-oplossing en voor een verschuiving van de schijnbare omkeer-potentiaal van de licht-geïnduceerde conductanties. De voor deze communicatie verantwoordelijke gap-junctions laten Lucifer Yellow (LY) niet door en zijn bovendien ongevoelig voor pH-manipulaties en voor verschillende gap-junction blokkers. Dit laat zien dat de connexines die zulke gap-junctions vormen van een andere soort zijn dan degene die in elektrische communicatie tussen HC's betrokken zijn. De functie van koppeling als een mechanisme om de signaal-ruis verhouding te verbeteren ten koste van gevoeligheid wordt bediscussieerd. De gevolgen van deze grote receptieve velden voor gezichtsscherpte worden behandeld in **Hoofdstuk 6**.

**Hoofdstuk 4** beschrijft de spectrale opponentie in mixed-input BC's als consequentie van antagonistische interacties tussen staafjes en kegeltjes of de interacties tussen verschillende spectrale soorten kegeltjes. Omdat deze spectraal gecodeerde lichtresponsen afhankelijk zijn van de intensiteit van de stimulus, kunnen zij niet het onderliggende mechanisme voor kleurwaarneming zijn. Echter, deze BC's blijken wel goede detectoren voor intensiteitsveranderingen te zijn. De antagonistische inputs veroorzaken een intensiteit-respons relatie van deze cellen die veel steiler is dan die van fotoreceptoren. Dit heeft als gevolg dat kleine verschillen in lichtintensiteit tot grote veranderingen in respons-amplitudes leiden. Tezamen suggereren de resultaten dat BC's hetzelfde coderingschema als HC's gebruiken om informatie te comprimeren, namelijk een breedbandig, niet-opponent kanaal (de niet-opponente mixed-input ON- en OFF-BC's), en opponente kanalen. De vraag welke glutamaat-receptoren zulke opponente responsen mogelijk maken wordt besproken in **Hoofdstuk 6**.

In **Hoofdstuk 5** wordt de aanwezigheid en functie van spanningsafhankelijke $K^+$-kanalen in de uitlopers van de dendrieten van mixed-input ON-BC's bestudeerd door elektrofysiologische experimenten in combinatie met modelsimulaties (NEURON). De anatomie van de dendrieten en de selectieve distributie van spanningsafhankelijke kanalen in deze dendritische uitlopers leiden tot rectificatie van de licht-geïnduceerde *IV* relaties, en kunnen werken als een mechanisme

voor de regulering van de versterking in de staaf-BC synaps. In het scotopische gebied kunnen zij door het sneller repolariseren van BC's voor een versnelling van synaptische overdracht en de generatie van transiënte responsen zorgen. Deze snelle repolarisatie herstelt de hoge versterking in de staaf-BC synaps, en zorgt ervoor dat staaf-geïnduceerde signalen de cel efficiënt kunnen beïnvloeden. Naarmate het lichter wordt, veroorzaakt ononderbroken suppressie van de staaf-input het open gaan van vele van zulke kanalen, wat tot een shunt van het staaf-systeem en een afname van de versterking in de staaf-BC synaps leidt. In deze toestand wordt de overdracht van kegel-geïnduceerde signalen bevorderd, en de balans tussen staaf- en kegelsignalen op het BC niveau verschuift van staaf-gedomineerd naar kegel-gedomineerd.

In **Hoofdstuk 6** worden onopgeloste thema's zoals de functie van de vele verschillende typen glutamaat-receptoren in de fotoreceptor-terminal, en de voor- en nadelen van grote receptieve velden voor gezichtsscherpte en gevoeligheid bediscussieerd.

# List of Abbreviations

| | |
|---|---|
| $\lambda$ | wavelength |
| $\lambda_{max}$ | wavelength of peak absorption |
| $\Omega$ | ohm |
| 4-AP | 4-aminopyridine |
| A | ampere |
| AC | amacrine cell |
| ACPT-I | (1S,3R,4S)-1-aminocyclopentane-1,3,4-tricarboxylic acid |
| AMPA | $\alpha$-amino-3-hydroxy-5-methyl-4-isoxazolepropionic acid |
| BAPTA | 1,2-bis(2-aminophenoxy)ethane-N,N,N',N'-tetraacetic acid |
| BC | bipolar cell |
| BIC | bicuculline methobromide |
| B/W | black and white |
| cAMP | adenosine 3',5'-cyclic monophosphate |
| CBX | carbenoxolone |
| cGMP | guanosine 3',5'-cyclic monophosphate |
| CK | creatine phosphokinase |
| $C_m$ | specific membrane capacitance |
| CNS | central nervous system |
| Cy3 | sodium1-[5-(N-succinimidyloxycarbonyl)-pent-1-yl]-2-[3-(3,3-dimethyl-1-ethyl-5-sulfonato-indolin-2-ylidene)-1-propen-1-yl]-3,3-dimethyl-3H-indolium-5-sulfonate |
| Cx | connexin |
| DAB | diaminobenzidine |
| D-AP7 | (-)-2-amino-7-phosphono-heptanoate |
| DAPI | 4',6-diamidino-2-phenylindole |
| DL-AP4 | (±)-2-amino-4-phosphonobutyric acid |
| DNQX | 6,7-dinitroquinoxaline-2,3(1H,4H)-dione |
| EAAT | excitatory amino acid transporter |
| $E_{Cl}$ | equilibrium potential for chloride ions |
| EGTA | ethylene glycol-bis(2-aminoethylether)-N,N,N',N'-tetraacetic acid |
| EM | electron microscopy |
| $E_K$ | reversal potential of the potassium conductance |
| $E_{leak}$ | reversal potential of the leak conductance |
| ERG | electroretinogram |
| F | farad |
| FITC | fluorescein isothiocyanate |
| $g$ | conductance |
| GABA | $\gamma$-aminobutyric acid |
| GC | ganglion cell |
| GCL | ganglion cell layer |
| $g_{gap}$ | gap junctional conductance |
| $g_{leak}$ | leak conductance density |
| GluR | glutamate receptor |
| Go$\alpha$ | G-protein (other), subunit $\alpha$ |
| GTP | guanosine 5'-triphosphate |
| HC | horizontal cell |
| HEPES | 4-(2-hydroxyethyl)piperazine-1-ethanesulfonic acid |
| HRP | horseradish peroxidase |
| $I_{Ca}$ | voltage-gated $Ca^{2+}$ current |
| $I_{gap}$ | gap junctional current |
| iGluR | ionotropic glutamate receptor |
| $I_{hold}$ | holding current |
| $I_{KV}$ | voltage-gated potassium current |
| INL | inner nuclear layer |
| IPL | inner plexiform layer |
| IR | immunoreactivity |
| $IV$ | current-voltage relation |
| $K$ | light intensity for half-maximal response |
| KA | kainate |
| KGlu | D-gluconic acid (potassium gluconate) |
| KO | knock-out |
| L-cone | long-wavelength-sensitive cone |
| LGN | lateral geniculate nucleus |
| LSM | laser scanning microscopy |
| LY | Lucifer Yellow |
| M-cone | middle-wavelength-sensitive cone |
| mGluR | metabotropic glutamate receptor |
| $n$ | slope factor for Hill functions |
| NBQX | 1,2,3,4-tetrahydro-6-nitro-2,3-dioxo-benzo[f]quinoxaline-7-sulfonamide |
| NGS | normal goat serum |
| OFF BC | hyperpolarizing bipolar cell |
| ON BC | depolarizing bipolar cell |
| ONL | outer nuclear layer |
| OPL | outer plexiform layer |
| PAGE | polyacrylamide gel electrophoresis |
| PB | phosphate buffer |
| PBS | sodium phosphate buffer |
| PC | phosphocreatine |
| PKA | protein kinase A |
| PKC$\alpha$ | protein kinase C, isoenzyme $\alpha$ |
| PMA | phorbol 12-myristate 13-acetate |
| PTX | picrotoxin |
| $R_a$ | axial resistance |
| $R_c$ | coupling resistance |
| $R_{in}$ | input resistance |
| $R_m$ | membrane resistance |
| $R_{seal}$ | seal resistance |
| $R_{series}$ | series resistance |
| S | siemens |
| S-cone | short-wavelength-sensitive cone |
| SDS | sodium dodecyl sulphate |
| STRY | strychnine |
| TEA | tetraethylammonium |
| UV cone | UV-sensitive cone |
| V | volt |
| $V_{error}$ | voltage error |
| $V_{hold}$ | holding potential |
| $V_{rest}$ | resting membrane potential |
| $V_{rev}$ | reversal potential |
| $V_{step}$ | voltage step |
| $X$ | light intensity (in Hill functions) |
| $Y$ | response (in Hill functions) |
| $Y_{max}$ | maximal response (in Hill functions) |

# Acknowledgements

I started this Ph.D. project in October 1999 with the naivety and the enthusiasm of the beginners. Since this fresh start, I learned many lessons and encountered some difficulties, like all Ph.D. students do. Expressions such as Ohm's Law, Kirchoff's Law and Murphy's Law were incorporated to my vocabulary, not to mention a large number of Dutch curse words. And, most important of all, many nice people crossed my way and helped me when I needed. It is these people I would like to acknowledge here.

In the first place, I am grateful to my advisor, Maarten Kamermans, for his patience and support. Working with such a clever person is very challenging and can sometimes be pretty hard for one's vanity. But it is most of all great fun. I know that if I have Maarten as a model to follow I will always be walking forward in life (and hopefully in science too).

Second, I would like to thank my paranymphs and ex-room mates, Marjelle van Leeuwen and Mieke Struik, for the great atmosphere they created in the lab. Their talent for human relationships turned our room into a cheerful and pleasant place to be, and made some of the darkest days much lighter.

Third, my colleagues Yvonne Claassen-Rombout, Joris Coppens, Frederike Dijk, Iris Fahrenfort, Willem Kamphuis, Jan Klooster, Bob Nunes-Cardozo, Ton Put, Colleen Shields, Trijntje Sjoerdsma, Tom van den Berg and Ben Willekens deserve my gratitude for helping me such a great deal, for very exciting scientifical discussions and great group work. Henk Bosveld and Bertus Hendriks from the AMC machine shop and Robert Numan were also very important to keep the set-up going. Luuk Fransen, Adriaan Klop, Maarten Prins and Marcel Timmerman were at the right place at the right time. And my dear friend and great artist Carol Leticia Quaini Sousa gets a big fat 'thank you' for making such a beautiful cover for this book, as well as some very funny drawings of bipolar cells which are *not* in this book.

I read once in a friend's thesis that it is important to acknowledge not only those that helped you keep on working, but also the people that kept you from only working. In this sense I owe a great deal of my emotional stability to (meanwhile my husband) Thomas Reiter, whose love, patience, dedication, energy and social demands sometimes exceeded the limits of feasibility. My parents Carmen and Leon Joselevitch (valeu, mãe! valeu, pai!) also supported me unconditionally in words, deeds and tons of Brazilian coffee, which I used up to the very last microgram.

Lastly, I am indebted to the *Conselho Nacional de Pesquisa* (CNPq, Brazil) and the Netherlands Ophthalmic Research Institute for making it possible for me to come to the Netherlands. I may not be as ingenuous as when I started this project, but I am still in love with the visual system, and still willing to find the universal that is contained in the particular.